Role of calcium mobilising messengers in cardiac arrhythmias



Razik Bin Abdul Mu-u-min

St-Hugh's College

University of Oxford

A thesis submitted for degree of

Doctor of Philosophy

Hilary 2019

Abstract

Nicotinic acid adenine dinucleotide phosphate (NAADP) is the most potent calcium ion (Ca^{2+}) activating second messenger due to its ability to release Ca^{2+} from intracellular acidic stores at nanomolar concentrations. NAADP has been known to play an important role in controlling excitation-contraction coupling in the heart. The ADP-ribosyl cyclase (ARC) CD38, is believed to be responsible for the production of NAADP in the heart.

The first part of the thesis assesses the role of NAADP pathway in calcium handling of cardiac atrial tissues by genetically (*CD38*$^{-/-}$ mice) and pharmacologically (bafilomycin A1) impairing NAADP pathway. Optical mapping techniques were used to observe the calcium transients and action potentials of mouse atrial tissues. At baseline conditions (without the activation of β-adrenoceptors), no contribution of the NAADP signalling pathway was observed in cardiac atria with respect to its calcium handling, action potential characteristics and resting heart rate. However, under the effect of the β-adrenoceptor agonist isoprenaline, *CD38*$^{-/-}$ mouse atria and bafilomycin A1 treated wildtype mouse atria showed a blunted increase in calcium transient amplitudes and heart rate as compared to control wildtype atria.

The second part of the thesis focuses on understanding the association of NAADP signalling pathway with the sarcoplasmic reticulum (SR), using a Ca^{2+} indicator to directly observe the SR Ca^{2+} content. NAADP was observed to increase the Ca^{2+} content of the SR in wildtype and *CD38*$^{-/-}$ mice ventricular cardiomyocytes in a bafilomycin A1 sensitive manner. Moreover, stimulating β-adrenergic response using cyclic adenosine monophosphate (cAMP) showed a reduced effect on SR Ca^{2+} increase in *CD38*$^{-/-}$ myocytes as compared to wildtype myocytes and disruption of lysosomes using bafilomycin A1 in wildtype myocytes also reduced the SR Ca^{2+} increase in response to cAMP. These observations provide further evidence that the NAADP signalling pathway has a prominent role in β-adrenergic response in the heart.

Although CD38 has been suggested as an enzyme that can produce both NAADP and cyclic adenosine diphosphate ribose (cADPR), several studies have attributed a non-CD38 ARC to catalyse the production of cADPR in the heart. The third part of the thesis, therefore, attempted to characterise the ARC present in sheep cardiac SR membrane preparations (SRMP). Functional and molecular biology experiments in this thesis strongly suggests that the ARC found in sheep SRMP is CD38.

Finally, in the last section of this thesis, a protocol for combining optical mapping with optogenetic pacing is discussed to study intracellular Ca^{2+} transients in atrial tissues of mice genetically modified to express channelrhodopsin 2 (ChR2) on phenylethanolamine N-methyltransferase (Pnmt)-derived cardiomyocytes (PdCMs). On optogenetic pacing, a shift in primary pacemaker sites could be seen towards the left atrium where the PdCMs were localised with minimal disturbance on the Ca^{2+} handling properties of the atrial tissue. Although this cell type-specific optogenetic pacing strategy targeting PdCMs as candidates for biopacemaking is still at an early stage of development, it could potentially lay foundation for an exciting prospect of clinical applications in treating heart rhythm disorders in the future.

Acknowledgements

The opportunity to pursue my DPhil in the prestigious University of Oxford was an overwhelming and greatly rewarding experience. This major milestone of my life would undoubtedly not have been possible without the love, support and guidance that I received from my family, friends and colleagues.

I would first like to thank my supervisor Prof. Derek Terrar for his continuous support, kindness and encouragement. I will forever be grateful to him for all the knowledge and wisdom he imparted to me and for his trust and patience throughout the course of my DPhil studies. I would also like to express sincere gratitude to my co-supervisor Prof. Ming Lei for welcoming me to his lab and for his unwavering support and generosity during this course.

I must thank my dearest of friends from the Ming, Sitsapesan and Paolo labs for their love and support that helped me maintain a strong and positive attitude as I moved towards the goal of completing my DPhil in a meaningful way. Special gratitude goes to Abbie, Alastair, Alexander, Ali, Babis, Chris, Claire, Dr Elisa, Dr Faizzan, Lara, Kathryn, Ria, Roshan, Dr Sam and Tianyi for their companionship and for all the smiles throughout this long journey. I wish them all the very best in life!

I would like to take this moment to thank my mentor Dr Christian Bollensdorff for believing in me and pushing me to achieve greater things in life. I thank him from the bottom of my heart for always being there for a chat to guide me during this difficult phase.

I gratefully acknowledge the funding I received towards my DPhil from Qatar Foundation (QF) through the Qatar Research Leadership Programme (QRLP). Special thanks to Dr Ayman for being our voice to the QF management and for all his support and assistance to make this course a successful one. I am proud to be a part of the Qatar Foundation family and look forward to being integrated into the growing scientific research community of Qatar.

My heartfelt gratitude goes out to my mother Nazim who was my first teacher and my greatest strength. I dedicate this thesis to her for sacrificing her best years to make me the person I am today. I thank my father Abdul Mu-u-min who taught me to be humble in my victories, gracious in my defeats and to always keep striving forward. Special appreciation goes to my siblings and to my ever-supportive in-laws for encouraging me to follow my dreams.

Most importantly, I thank my beautiful wife Razia for making this dream possible. Thank you for holding a bright torch and showing me the way whenever I felt lost in life. Thank you for all the patience and love you showered on me whenever I felt my goals were unattainable. Thank you for being there for me to complete this DPhil by putting your own life on hold. Thank you for pushing me to become the best version of myself.

Thank you.

Abbreviations

ADPR	ADP ribose
ADPRP	ADP-ribose 2'-phosphate
AM	acetoxymethyl ester
ANF	atrial natriuretic factor
Ang-II	angiotensin II
ANOVA	analysis of variance
ARC	ADP- ribosyl cyclase
Asp	aspartic acid
AVN	atrio-ventricular node
BNP	brain natriuretic peptide
BSA	bovine serum albumin
BST-1	bone marrow stromal cell antigen-1
BZ194	3-carboxy-1-octylcarbamoylmethylpyridinium bromide
Ca2+	calcium ions
CaD	Ca^{2+} transient durations
cADPR	cyclic adenosine diphosphate ribose
CaMKII	Ca^{2+}/calmodulin-dependent protein kinase II
cAMP	cyclic adenosine monophosphate
Cav1.3	calcium channel, voltage-dependent, L type, alpha 1D subunit
cGDPR	cyclic GDP- ribose
ChR2	channelrhodopsin 2
CIB1	calcium and integrin-binding protein 1
CICR	calcium-induced-calcium-release
cIDPR	cyclic inosine diphosphate-ribose
CPVT	catecholaminergic polymorphic ventricular tachycardia
Cu^{2+}	copper ions
Cys	cysteine
DAD	delayed afterdepolarisation
DAG	diacylglycerol
DHAB	2,2'-dihydroxyazobenzene
DMSO	dimethyl sulphoxide
DTT	dithiothreitol
EAD	early afterdepolarisation
EDTA	ethylenediaminetetraacetic acid
EPAC	exchange factor directly activated by cAMP
ER	endoplasmic reticulum
ES	embryonic stem cells
GAPDH	glyceraldehyde-3-phosphate dehydrogenase

GCPR	G protein-coupled receptors	**K+**	potassium ions
GDP	guanosine diphosphate	**K_d**	dissociation constant
GDP	guanosine diphosphate	**KO**	knockout
Glu	glutamic acid	**LAMP-2**	lysosome-membrane associated protein 2
Gly	glycine	**LC-MS**	liquid chromatography-mass spectrometry
GPN	Gly-Phe-β-naphthylamide	**LSR**	light sarcoplasmic reticulum (fraction)
G_s	stimulatory G-protein	**LTCC**	L-type Ca^{2+} channels
H^+	hydrogen ions	**MEF**	mouse embryonic fibroblasts
HSR	heavy sarcoplasmic reticulum (fraction)	**Mg^{2+}**	magnesium ions
ICA	intrinsic cardiac adrenergic	**mPTP**	mitochondrial permeability transition pores
i_{Ca}	inward Ca^{2+} currents	**NA**	nicotinic acid
I_f	funny' current	**Na+**	sodium ions
iNa	first inward current	**NAADP**	nicotinic acid adenine dinucleotide phosphate
IP_3	inositol 1,4,5-triphosphate	**NAD**	nicotinamide adenine dinucleotide
IP_3R	IP_3 receptor	**NADP**	nicotinamide adenine dinucleotide phosphate
IR	ischaemia/reperfusion	**NCX**	Na^+- Ca^{2+} exchanger
i_{to}	transient outward current	**NGD**	nicotinamide guanine dinucleotide
IVC	inferior vena cava	**NHD**	nicotinamide hypoxanthine dinucleotide

NMN	nicotinamide mononucleotide	**SAP**	sino-atrial preparation
PBS	phosphate-buffered saline	**SEM**	standard error of mean
PdCM	Pnmt derived cardiomyocytes	**SERCA**	sarco-endoplasmic reticular ATPase pump
PDMS	polydimethylsiloxane	**siRNA**	small interfering RNA
Phe	phenylalanine	**SND**	sinus node dysfunction
PI(3,5)P2	phosphatidylinositol 3,5-bisphosphate	**SR**	sarcoplasmic reticulum
PIP_2	phosphatidylinositol 4,5-bisphosphate	**SRMP**	sarcoplasmic reticulum- enriched membrane preparation
PKA	protein kinase A	**SVC**	superior vena cava
PKC	protein kinase C	**T_m**	melting temperature
PLB	phospholamban	**TPC**	two-pore channels
Pnmt	phenylethanolamine N-methyltransferase	**Trp**	tryptophan
PSEN	presenilin 1	**TRPML1**	transient receptor potential mucolipin-1 channel
RNA	ribonucleic acid	**TRPML2**	transient receptor potential mucolipin-2 channel
RT-PCR	reverse transcription polymerase chain reaction	**UV**	ultraviolet
RyR	ryanodine receptors	**Val**	valine
SAN	sino-atrial node	**Zn^{2+}**	zinc ions

Table of contents

1. Introduction 1

1.1 General Introduction 2

1.2 Cardiomyocyte structure 3

1.3 Cardiac excitation-contraction coupling 6

1.3.1 Cardiac action potential 6

1.3.2 Calcium-induced-calcium-release (CICR) and cardiac contraction 11

1.4 β-adrenergic signalling in the heart 15

1.5 CD38/ ADP-ribosyl cyclase 17

1.5.1 History 17

1.5.2 Catalytic function and biological distribution of CD38 18

1.5.3 Homologues of CD38 21

1.5.4 Enzymatic structure and activity of CD38 22

1.5.4.1 Catalytic residues of CD38 22

1.5.4.2 Cysteine residues of ARCs 23

1.5.4.3 Glycosylations of CD38 25

1.5.4.4 Oligomerisations of CD38 26

1.5.4.5 CD38 activity and pH 27

1.5.5 Topological paradox of CD38 29

1.5.6 CD38 in cardiac physiology 31

1.5.6.1 CD38 in cardiac development 31

1.5.6.2 Physiological function of CD38 in the heart 32

1.5.7 CD38 in cardiac pathology 35

1.5.8 Other ARCs in mammalian tissue 38

1.6 Nicotinic acid adenine dinucleotide phosphate (NAADP) 39

1.6.1 Introduction 39

1.6.2 NAADP dependent calcium release 40

1.6.3 Intracellular targets of NAADP 44

1.6.4 Two- Pore channels (TPCs) as NAADP receptors 47
1.6.5 Effects of NAADP in non- cardiac tissues 51
1.6.6 Effect of NAADP in cardiac physiology 54
1.6.7 Effect of NAADP in cardiac pathology 58
1.7 Other calcium mobilising molecules 60
1.7.1 Inositol 1,4,5-triphosphate (IP_3) 60
1.7.2 Cyclic adenosine diphosphate ribose (cADPR) 63
1.8 Specific aims of this thesis 65
2. Methods and Materials 67
2.1 Animals 68
2.2 Mouse atrial preparation 69
2.3 Mouse ventricular myocyte isolation 70
2.4 Sheep sarcoplasmic reticulum-enriched membrane preparation 73
2.5 Mouse mixed membrane preparation 75
2.6 Reverse Transcription Polymerase Chain Reaction (RT-PCR) 75
2.7 Detection of ADP-ribosyl cyclase activity using NGD assay 77
2.8 Drug docking 78
2.9 Western blotting 79
2.10 Immunoprecipitation 80
2.11 Mass spectrometry 82
2.12 Fluorescence imaging 83
2.12.1 Mouse atrial preparation Ca^{2+} and transmembrane voltage (V_m) dye loading and optical imaging 84
2.12.2 Mouse ventricular cardiomyocyte sarcoplasmic reticulum Ca^{2+} dye loading and imaging 87
2.13 Recipes for solution 89
2.14 Suppliers of drugs and chemicals 89
2.15 Statistics 90
2.15 Experimental design 90

2.15 Group sizes for experiments 91

3. Contribution of NAADP signalling pathway on calcium handling at rest and during β-adrenoceptor activation in murine atria 94

3.1 Background 95

3.2 Methods 99

3.3 Results 101

3.3.1 Intrinsic activity of the NAADP pathway in murine cardiac atria 101

3.3.1.1 No differences were observed in the Ca2+ transient amplitudes of electrically stimulated atria at resting conditions between wildtype and CD38-/- mice. 101

3.3.1.2 Wildtype and *CD38*$^{-/-}$ mice had comparable resting heart rates 101

3.3.1.3 No significant differences observed between the Ca^{2+} transient durations and action potential durations in isolated atria at resting conditions between wildtype and *CD38*$^{-/-}$ mice. 102

3.3.1.4 The conduction velocity at resting conditions were not significantly different in electrically stimulated atria of wildtype and *CD38*$^{-/-}$ mice. 103

3.3.1.5 Bafilomycin A1 had no effect on the Ca^{2+} transient amplitudes and resting heart rates of isolated atria from wildtype and *CD38*$^{-/-}$ mice at resting conditions. 103

3.3.2 Effect of NAADP pathway in murine cardiac atria during β-adrenoreceptor activation 104

3.3.2.1 The effect of isoprenaline on calcium transient amplitudes and heart beating rate were blunted in *CD38*$^{-/-}$ mice as compared to wildtype mice. 104

3.3.2.2 The effect of isoprenaline on calcium transient amplitudes and heart beating rate were reduced in wildtype mice in the presence of bafilomycin A1 105

3.3.2.3 Bafilomycin A1 had no effect on the Ca^{2+} transient amplitudes and heart beating rate in *CD38*$^{-/-}$ mice treated with isoprenaline 106

3.4 Discussion 124

3.4.1 Does NAADP pathway have an intrinsic activity in murine atria when β-adreneroceptors are not stimulated? 124

3.4.2 Does NAADP pathway play a role in Ca^{2+} handling during β-adrenergic stimulation murine atria?.....129

4. The effect of NAADP signalling pathway on sarcoplasmic reticulum calcium content in isolated mouse ventricular myocytes 133

4.1 Background..... 134

4.2 Methods 139

4.3 Results..... 141

4.3.1 Successful SR Ca^{2+} indicator loading and the effect of permeabilisation on the lysosomes 141

4.3.2 Wildtype and *CD38*$^{-/-}$ mice had comparable SR Ca^{2+} levels at baseline conditions 142

4.3.3 Bafilomycin A1 had no effect on the SR Ca^{2+} in wildtype and *CD38*$^{-/-}$ mice ventricular myocytes at baseline conditions..... 142

4.3.4 NAADP increased the SR Ca^{2+} levels in wildtype and *CD38*$^{-/-}$ mice ventricular myocytes 143

4.3.5 Bafilomycin A1 blunted the effect of NAADP on the SR Ca^{2+} levels in wildtype and *CD38*$^{-/-}$ mice ventricular myocytes..... 143

4.3.6 The effect of cAMP on SR Ca^{2+} was reduced in *CD38*$^{-/-}$ mice ventricular myocytes as compared to wildtype mice myocytes. 145

4.3.7 The effect of cAMP on SR Ca^{2+} was reduced by bafilomycin A1 in wildtype mice ventricular myocytes..... 145

4.3.8 Bafilomycin A1 had no effect on SR Ca^{2+} levels in *CD38*$^{-/-}$ mice ventricular cardiomyocytes in the presence of cAMP. 146

4.3.9 SAN4825 had no effect on SR Ca^{2+} levels in wildtype mice ventricular cardiomyocytes in the presence of cAMP. 146

4.4 Discussion..... 160

4.4.1 Loading Ca^{2+} indicator into the SR of mouse ventricular myocytes: General considerations..... 160

4.4.2 Does the activation of the NAADP pathway increase the SR Ca^{2+} load in murine ventricular myocytes? 162

4.4.3 Does SAN4825 inhibit the increases in SR Ca^{2+} load in murine ventricular myocytes under β-adrenoceptor stimulation?..... 163

4.4.4 Probable mechanism of the NAADP pathway in Ca^{2+} handling of the heart under β-adreneroceptor stimulation..... 165

4.4.5 Limitations of the SR Ca^{2+} dye loading technique 169

5. Presence of CD38 in sarcoplasmic reticulum-enriched membrane preparation from sheep hearts 172

5.1 Background..... 173

5.2 Methods 176

5.3 Results..... 178

5.3.1 Sheep heart showed an expressed CD38 gene but no functional CD157 gene.....178

5.3.2 In silico evidence suggested Kuromanin binding to the active sites of human CD38 178

5.3.3 Sheep cardiac SRMP showed ARC cyclase activity and was inhibited by the CD38 inhibitor Kuromanin 179

5.3.4 Western Blotting suggested the presence of CD38 in sheep cardiac SRMP.....180

5.3.5 Purification of CD38 from SRMP by Immunoprecipitation 180

5.3.6 Mass spectrometry analysis of the purified protein from immunoprecipitation.....181

5.4 Discussion..... 191

5.4.1 Does a functional CD38 gene exist in sheep heart? 191

5.4.2 Would SR be a suitable place for CD38? 192

5.4.3 Is there evidence for the existence of CD38 in the SRMP from sheep hearts?..... 194

6. A protocol for optical mapping of murine sinoatrial preparation with optogenetic pacing...... 200

6.1 Background..... 201

6.2 Methods 204

6.3 Results..... 206

6.3.1 Optogenetic pacing of sino-atrial preparations from Pnmt-cre/ChR2 mice 206

6.3.2 Optogenetic pacing of PdCMs can create a novel leading pacemaker site in a murine SAP 207

6.3.3 Optogenetic pacing of PdCMs has only minor impact on calcium dynamics……..208

6.4 Discussion 214

6.4.1 Does optogenetic pacing disturb the normal conduction and Ca^{2+} handling properties of murine SAP? ……..214

6.4.2 Can the technique of optogenetic pacing of PdCMs be applied to study sinoatrial dysfunctions?……..……..214

7. Conclusion and future work 217

7.1 Conclusion 218

7.2 Future work 224

References 227

List of figures

Figure 1.1:	Ventricular action potential in humans and contributing channels	8
Figure 1.2:	Ca^{2+} cycling in a ventricular myocyte	12
Figure 1.3:	Enzymatic activities catalysed by CD38	20
Figure 1.4:	Structure of CD38	24
Figure 1.5:	Roles of CD38 in the heart	33
Figure 3.1:	Imaging set-up for the optical mapping of Rhod-2 and Di-4-ANBDQPQ in murine isolated atrial tissues.	108
Figure 3.2:	Baseline calcium transient amplitudes of electrically stimulated isolated left atria of wildtype and *CD38*$^{-/-}$ mice.	109
Figure 3.3:	Resting heart rate of spontaneously beating isolated right atria of wildtype and *CD38*$^{-/-}$ mice	110
Figure 3.4:	Calcium transient durations (CaD10, CaD50, CaD80) of electrically stimulated isolated left atria of wildtype and *CD38*$^{-/-}$ mice at resting conditions.	111
Figure 3.5:	Baseline conduction velocity of electrically stimulated isolated left atria of wildtype and *CD38*$^{-/-}$ mice.	112
Figure 3.6:	Action potential durations (APD10, APD50, APD90) of spontaneously beating isolated right atria of wildtype and *CD38*$^{-/-}$ mice at resting conditions.	113
Figure 3.7:	Baseline calcium transient amplitudes of electrically stimulated isolated left atria of wildtype and *CD38*$^{-/-}$ mice in the presence of Bafilomycin A1.	114
Figure 3.8:	Resting heart rate of spontaneously beating isolated right atria of wildtype and *CD38*$^{-/-}$ mice in the presence of bafilomycin A1.	115
Figure 3.9:	Percentage change in calcium transient amplitudes of electrically stimulated isolated left atria of wildtype and *CD38*$^{-/-}$ mice during activation of β–adrenoreceptors.	116
Figure 3.10:	Percentage change in calcium transient amplitudes of electrically stimulated isolated left atria of wildtype mice during activation of β–adrenoreceptors in the presence of Bafilomycin A1 (5 μM).	117
Figure 3.11:	Percentage change in calcium transient amplitudes of electrically stimulated isolated left atria of *CD38*$^{-/-}$ mice during activation of β–adrenoreceptors in the presence of Bafilomycin A1 (5 μM).	118
Figure 3.12:	Summary of percentage change in calcium transient amplitudes of electrically stimulated isolated left atria of wildtype and *CD38*$^{-/-}$ mice during activation of β–adrenoreceptors in the presence of Bafilomycin A1 (5 μM).	119
Figure 3.13:	Percentage change in heart rate of spontaneously beating isolated right atria of wildtype and *CD38*$^{-/-}$ mice during activation of β–adrenoreceptors.	120

Figure 3.14:	Percentage change in heart rate of spontaneously beating isolated right atria of wildtype mice during activation of β–adrenoreceptors in the presence of Bafilomycin A1 (5 μM).	121
Figure 3.15:	Percentage change in heart rate of spontaneously beating isolated right atria of *CD38*$^{-/-}$ mice during activation of β–adrenoreceptors in the presence of Bafilomycin A1 (5 μM).	122
Figure 3.16:	Summary of percentage change in heart rate of spontaneously beating isolated right atria of wildtype and *CD38*$^{-/-}$ mice during activation of β–adrenoreceptors in the presence of Bafilomycin A1 (5 μM).	123
Figure 4.1:	Examples of Mag-fluo-4, AM loading in permeabilised and non-permeabilised murine ventricular cardiomyocytes	147
Figure 4.2:	Mag-fluo-4, AM loading characteristics in murine ventricular cardiomyocytes	148
Figure 4.3:	Permeabilisation by 0.005% saponin does not affect the lysosomes of murine ventricular myocytes	149
Figure 4.4:	SR calcium content of ventricular cardiomyocytes of wildtype and *CD38*$^{-/-}$ mice at resting conditions.	150
Figure 4.5:	SR calcium content of ventricular cardiomyocytes of wildtype and *CD38*$^{-/-}$ mice preincubated with bafilomycin A1.	151
Figure 4.6:	Percentage change in SR calcium levels of ventricular cardiomyocytes from wildtype mice in the presence of NAADP.	152
Figure 4.7:	Percentage change in SR calcium levels of ventricular cardiomyocytes from *CD38*$^{-/-}$ mice in the presence of NAADP.	153
Figure 4.8:	Percentage change in SR calcium levels of bafilomycin A1 preincubated ventricular cardiomyocytes from wildtype mice in the presence of NAADP.	154
Figure 4.9:	Percentage change in SR calcium levels of bafilomycin A1 preincubated ventricular cardiomyocytes from *CD38*$^{-/-}$ mice in the presence of NAADP.	155
Figure 4.10:	Percentage change in SR calcium levels of ventricular cardiomyocytes from wildtype and *CD38*$^{-/-}$ mice in the presence of cAMP.	156
Figure 4.11:	Percentage change in SR calcium levels of bafilomycin A1 preincubated ventricular cardiomyocytes from wildtype mice in the presence of cAMP.	157
Figure 4.12:	Percentage change in SR calcium levels of bafilomycin A1 preincubated ventricular cardiomyocytes from *CD38*$^{-/-}$ mice in the presence of cAMP.	158
Figure 4.13:	Percentage change in SR calcium levels of SAN4825 preincubated ventricular cardiomyocytes from wildtype mice in the presence of cAMP.	159
Figure 5.1:	Presence of functional CD38 gene in sheep hearts (detected by RT-PCR)	183

Figure 5.2:	*In silico* evidence of Kuromanin binding to the active sites of human *CD38*	184
Figure 5.3:	cGDPR production by sheep cardiac SRMP is inhibited by Kuromanin	185
Figure 5.4:	Western blot showing the presence of CD38 in sheep cardiac SRMP	186
Figure 5.5:	Coomassie Brilliant blue staining of SDS-PAGE gel run with products obtained after Immunoprecipitation of CD38 from sheep cardiac SRMP.	187
Figure 6.1:	Representative murine cardiac Sino-Atrial Preparation (SAP) and the schematic of the optical imaging apparatus	209
Figure 6.2:	Effect of optical pacing on Ca^{2+} transients in murine cardiac SAP.	210
Figure 6.3:	Shift of leading pacemaker site during optogenetic pacing	211
Figure 6.4:	Effect of optogenetic pacing on tissue activation and conduction velocity in SAP.	212
Figure 6.5:	Effect of optogenetic pacing on rise time and Ca^{2+} transient durations in SAP.	213
Figure 7.1:	Schematic for the proposed mechanism for the NAADP pathway in response to β-adrenergic stimulation in cardiomyocytes.	222

List of Tables

Table 2.1:	Conditions for RT-PCR	92
Table 2.2:	List of solutions	93
Table 5.1:	List of top 15 matched uncharacterised sheep proteins obtained from mass spectrometry and their % similarity to human and bovine CD38 protein sequences.	188
Table 5.2:	List of top 15 matches of bovine proteins of similar molecular weight as CD38 against sheep cardiac SRMP purified by immunoprecipitation and analysed by mass spectrometry.	189
Table 5.3:	List of top 15 matches of human proteins of similar molecular weight as CD38 against sheep cardiac SRMP purified by immunoprecipitation and analysed by mass spectrometry.	190

Chapter 1

Introduction

1.1 General Introduction

The circulatory system is composed of the heart and blood vessels, including arteries, veins, and capillaries. The body has two circulatory systems: The pulmonary circulation and the systemic circulation. The pulmonary circulation system sends deoxygenated blood from the heart to the lungs, where the blood is oxygenated and returned to the heart. The systemic circulation system sends the newly-oxygenated blood to all parts of the body and returns it to the heart.

The heart is a well-developed muscular pump that circulates blood around the body. This enables every cell in the body to be supplied with nutrients and oxygen and, also remove waste products for excretion. Each pumping cycle of the heart can be split into two phases, namely the diastole and the systole. During diastole, the heart relaxes and is filled with blood. During systole, a coordinated contraction results in the ejection of blood into the arteries. The coordination of the contraction-relaxation cycle is achieved using electrical signals. The electrical signals originate from the major pacemaker region of the heart, the Sino-atrial node (SAN). The signal spreads throughout the atria resulting in its contraction and, thereby, blood re-filling of the ventricles. Electrically insulated tissue between the atria and the ventricles ensures that the signal is unable to pass directly from the atria to the ventricles. A specific conduction pathway transports the electrical impulse from the atria to the ventricles. Atrio-ventricular node (AVN), a component of this pathway, delays the impulse from the atria by approximately 100 ms (depending on species) to allow atrial contraction before the ventricles. The electrical signal then passes through the bundle of His to the Purkinje fibres, which transmit the stimulus to the apex of the heart. This ensures that contraction of the ventricles begins at the apex so that blood is pushed

towards the exit vessels. The electrical signal spreads between myocytes through gap junctions that electrically connect cells of the heart so that the whole organ functions as an electrical syncytium.

Calcium ions (Ca^{2+}) play a central role in both electrical excitation of the heart and the generation of mechanical force of contraction. Subcellular pathways that control and regulate Ca^{2+} concentration and movement are complex and have been studied for decades. Deeper understanding of these pathways can direct us to develop better therapeutic strategies towards pathological circumstances arising from abnormal calcium regulation.

1.2 Cardiomyocyte structure

The human cardiomyocyte is of a rectangular flat slab (ventricular cardiomyocytes) or cylindrical (atrial cardiomyocytes) shape with a length of 50-100 μm and a diameter of 10-20 μm (Levick 2010). They are connected to adjacent cardiomyocytes via end-to-end intercalated discs. The intercalated discs consist of two distinct junctions: the desmosome and gap junction, which are responsible for providing the cardiomyocytes with mechanical strength and electrical conduction, respectively. The gap junction consists of hollow tubes consisting of six subunits of the protein connexin to form a connexon. Pairs of connexons from adjacent myocytes are joined end-to-end to form a continuous channel across the myocytes. Due to the presence of the gap junction, ions can flow from one myocyte to the next and thus stay electrically connected allowing them to contract near simultaneously (Rohr 2004). The desmosomes, containing the transmembrane glycoprotein cadherin, rivet the myocytes together providing it mechanical strength. They

span between a 25 nm space between cardiomyocytes. Additionally, desmin filaments anchored to the desmosomes run through the myocyte and are responsible for the cell's tensile strength (Kowalczyk and Green 2013).

Cardiomyocytes have a distinct striated pattern due to the presence of alternating thick and thin contracting filaments called the 'A bands' and 'I bands', respectively. A set of A band and I band, called a sarcomere, forms the basic unit of the cardiac contractile machinery. The A bands consists of thick filaments containing around 400 myosin molecules each. The I bands contain thin actin filaments that are interposed between the A bands. The resting length of a sarcomere is approximately 2 μm (Levick 2010). A sarcomere is arranged between two Z-lines which runs perpendicular to the axis of the cell and is made up of the protein α-actinin. Actin filaments are anchored to the α-actinin of the Z-lines and run perpendicular to it (parallel to the axis of the cell). The actin filaments are arranged as a two-stranded helix and the groove of the helix contains a regulatory protein, tropomyosin. A regulatory complex consisting of troponins are also attached to the tropomyosin. The troponin complex consists of three units: the inhibitory protein Troponin-I, the Ca^{2+}-binding protein Troponin-C, and the tropomyosin binding protein Troponin-T. Myosin filaments are bound to the protein titin which in turn, is anchored to α-actinin on the Z-line and runs perpendicular to it. Myosin filaments contain a fibrous tail and a globular head, which can bind to actin. Tropomyosin covers the myosin binding sites of the actin filaments. Ca^{2+} bind to the troponin complex and alters the structure of tropomyosin, thereby revealing the cross-bridge binding site of actin. This ensues the bind of myosin heads to actin, following which the contraction of the filaments occurs (Levick 2010).

The plasma membranes of ventricular myocytes have deep invaginations into the intracellular space that run along the Z-lines and are known as transverse (T)-tubules. The T-tubules contain key ion channels which are important for the function of contraction machinery of the cardiomyocyte. The presence of T-tubules allows Ca^{2+} entry into the centre of the cell, thereby, allowing a homogenous rise in intracellular Ca^{2+} when the myocyte is electrically stimulated (Hong and Shaw 2017). However, T-tubules in atrial myocytes are either lacking or are sparsely developed. This results in an increase in Ca^{2+} at the periphery of the myocyte initially before it propagates to the centre of the cell (Dibb et al. 2013; Maxwell and Blatter 2017).

The sarcoplasmic reticulum (SR) is a large membrane-bound intracellular compartment within a cardiomyocyte. The SR is 20-60 nm wide and is at close proximity to the T-tubules. The SR is a store containing a large concentration of Ca^{2+} which are released into the cytoplasm when the myocyte is excited and leads to its contraction. The SR has two functional regions; the junctional SR and the non-junctional SR. The junctional SR is approximately 15 nm from the T-tubules and forms a 'diad' where ryanodine receptors (RyRs) on the SR form extensions from the SR towards the T-tubules (Eisner et al. 2017). The formation of diads helps in calcium-induced-calcium-release (CICR), which will be discussed in more detail in the next section. The non-junctional SR comprises of sarco-endoplasmic reticular ATPase pumps (SERCA) which are responsible for the refilling of Ca^{2+} into the SR from the cytoplasm after the CICR (Bers 2002).

The cardiac cell is also densely packed with mitochondria which are located between the sarcomeres and also below the plasma membrane. Since cardiomyocytes solely depend on aerobic metabolism as their energy source, such high levels of mitochondria are

important in the cardiac cells. The abundance and strategic positioning of mitochondria in cardiomyocytes allow efficient localised ATP delivery system to support contraction, ion homeostasis and metabolism (Gustafsson and Gottlieb 2008).

1.3 Cardiac excitation-contraction coupling

1.3.1 Cardiac action potential

The intracellular resting potential of a cardiomyocyte is between -80 mV and -90 mV. Cardiomyocytes have a high intracellular potassium ion (K^+) concentration (140 mM) as compared to the extracellular concentration (4 mM). On the contrary, the intracellular concentration of sodium ion (Na^+) (4-16 mM) is much lower than the extracellular concentration (140 mM) (Bers, Barry, and Despa 2003). In resting cardiomyocytes, the inward rectifier channel (K_{ir}) allows K^+ to leak out of the cell due to the concentration gradient but do not allow Na^+ and other ions to pass inwards due to its selectiveness for K^+ ions. This leaves the cell negatively charged relative to the extracellular space. However, the chemical force which leads to the outward leak of K^+ ions is equilibrated by an electrical force attracting K^+ ions into the cell. The voltage at which this equilibrium, called the 'Potassium equilibrium potential', occurs is calculated by the Nernst equation to be -94 mV. Physiologically, the resting membrane potential is slightly more positive than that obtained from the Nernst equation. This is due to the low inward flow of Na^+ ions (1/10- 1/100th of that of K^+ flow). These ions are pumped out of the cell via a Na^+/K^+ pump, leading to an inflow of K^+ ions. This results in a net resting membrane potential between -80 mV and -90 mV.

A depolarising current from adjacent cells through the gap junctions leads to the initiation of the action potential in a cardiomyocyte. This current slightly increases the membrane potential to the trigger potential of approximately -60 mV. At this potential, voltage gated sodium channels open causing an abrupt increase in plasma membrane conductivity. This allows for the 'first inward current' (i_{Na}), which is a rapid influx of Na^+ ions into the cell resulting in a depolarising overshoot of the membrane potential to positive potential of +20 mV to +30 mV. These Na^+ channels are time-dependent and inactivate shortly after the depolarisation leaving the overshoot as a brief phenomenon. This sudden rise of membrane potential is known as phase 0 of the action potential (Levick 2010).

Following the phase 0 of the cardiac action potential, the membrane goes through a brief but rapid partial repolarisation, marked as phase 1. The membrane potential drops down to +10 mV - -10 mV. This is due to a 'transient outward current' (i_{to}), where there is an outflow of K^+ ions through voltage-gated potassium channels. These channels open as a response to the rapid depolarisation of membrane potential and like the fast Na^+ channels in phase 0, these channels are time-dependent, resulting in transient opening and quick inactivation. The i_{to} is also contributed by an inward flow of the negative chloride ions through chloride channels. The i_{to} enhances the electrochemical gradient for Ca^{2+} and controls the action potential duration. Epicardial cardiomyocytes express more transient outward K^+ channels and therefore have a shorter action potential than endocardial cardiomyocytes (Whalley, Wendt, and Grant 1995). During phase 1 of the action potential, the Na^+- Ca^{2+} exchanger (NCX) can function in reverse mode. At membrane potentials higher than the combined reversal potential for Na^+ and Ca^{2+} (E_{Na-Ca}), NCX generates a brief outward current by transporting three sodium ions out of the cell and one calcium ion into the cell (Eisner and Lederer 1985; Kohajda et al. 2016).

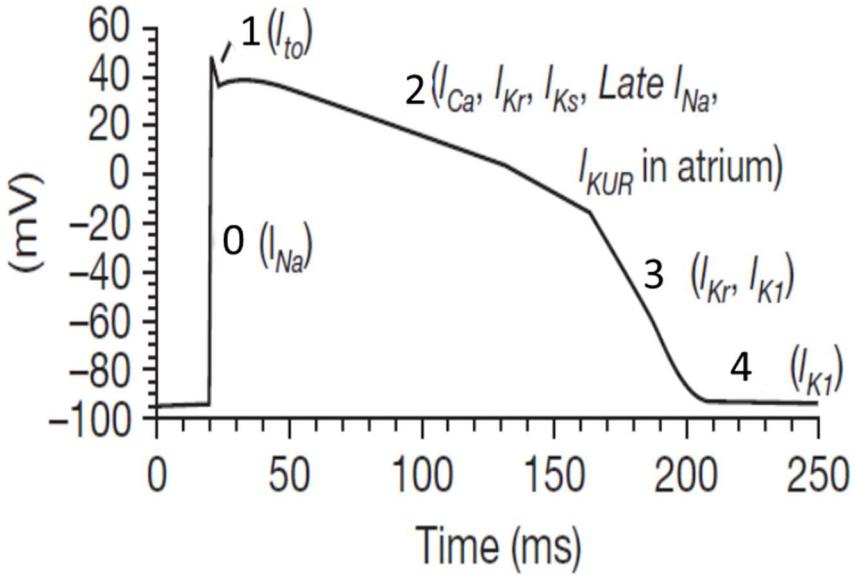


Figure 1.1: Ventricular action potential in humans and contributing channels.

The different phases of the action potential is labelled as phase 0, 1, 2, 3 and 4. I_{Na}: Na^+ current, I_{to}: Transient outward K^+ current, I_{Ca}: Ca^{2+} current, I_{Kr}: rapid activating K^+ current, I_{Ks}: Slow activating K^+ current, I_{kur}: Ultra-rapid activating K^+ current, I_{K1}: Inward rectifier K^+ current. Figure modified from (Eldstrom and Fedida 2011).

The next phase of the action potential, namely the phase 2, gives the cardiac action potential its unique feature, the plateau. This phase of the action potential lasts for 200-400 ms. The major component of phase 2 is the long lasting 'inward Ca^{2+} currents' (i_{Ca}). The i_{Ca} prevents the rapid repolarisation of the cardiomyocyte unlike in skeletal muscle fibres or nerve axons. The inward flow of Ca^{2+} is through the voltage-gated long-opening or L-type Ca^{2+} channels (LTCC). These channels are abundantly present in the T-tubules and are activated by the rapid depolarisation of the membrane potential in phase 0. The

i_{Ca} peaks at 2-7 ms after activation but flows for a long time since the LTCC inactivates slowly and therefore maintains the depolarisation of the membrane. The conduction of K_{ir} reduces with increases in membrane potential and the small outward K^+ counterbalances the i_{Ca} and preserves the plateau phase for hundreds of milliseconds (Levick 2010). Cardiac contraction occurs due to events occurring in phase 2 of the action potential. Ca^{2+} flowing in through the LTCC activate adjacent RyRs on the SR, resulting in a larger Ca^{2+} release from the SR which leads to cardiomyocyte contraction. (Bers 2002; Whalley, Wendt, and Grant 1995). The later parts of the plateau are attributed to the closing of the LTCCs and an inward flow of Na^+ ions through NCX. The electrogenic NCX pumps in three Na^+ ions in exchange of one Ca^{2+} ion extruded out from the myocyte resulting in a net inward current. The NCX is affected by membrane potential and ion concentrations and can also work in a 'reverse mode' briefly during the phase 0 of the action potential (Eisner and Lederer 1985).

Towards the end of the phase 2 of the cardiac action potential, conductance through gradual opening of K^+ channels, leads to the 'delayed rectifier currents' (I_{Kr}, I_{Ks}). This plays an important role in phase 3 of the action potential. The outward K^+ current is slowly increased by the rectifier current I_{Ks} until the late plateau inward currents are surpassed after which repolarisation occurs until the I_{Kr} is restored. Resting transmembrane ionic concentration gradients are restored by returning Na^+ and Ca^{2+} ions to the extracellular environment (or intracellular stores), and K^+ ions to the cell interior and achieving the resting membrane potential (Nerbonne and Kass 2005; Levick 2010). The phases 0-3 are repeated throughout the lifespan of the heart. A schematic diagram for an action potential and its contributing channels are given in Figure 1.1.

The SAN cells, however, have a slightly different and unique profile for their action potential. This uniqueness is due to a slow spontaneous depolarisation of the membrane potential towards its action potential threshold during the diastole, thereby lacking a stable resting potential. At the end of the repolarisation of SAN cells (approximately -60mV), phase 4 begins as slow and inward Na^+ channels open leading to the generation of an inward '"funny" current' (I_f). As the membrane potential approaches -50 mV, transient or 'T-type Ca^{2+} channels' open resulting in an inward Ca^{2+} current which in turn depolarises the membrane potential more. Further depolarisation is achieved by the opening of the LTCC at -40 mV which leads the membrane potential to the threshold of the action potential (-30 mV). Calcium channel, voltage-dependent, L type, alpha 1D subunit (Cav1.3) is also known to contribute to the late stage of diastolic depolarisation (Zhang et al. 2002; Capel and Terrar 2015). The phase 0 depolarisation of the SAN action potential is caused by opening of more LTCC during which the I_f and the T-type Ca^{2+} currents decline. Phase 0 depolarisation in SAN cells is much slower than atrial or ventricular cardiomyocytes due to the slower movement of Ca^{2+} through the LTCC. The phase 3 repolarisation occurs as K^+ channels open leading to an outward hyperpolarising current, as the LTCCs gets inactivated (DiFrancesco and Borer 2007; Klabunde 2012). Precise mechanisms of pacemaker activity of the sinus node is not entirely understood and is a subject of extensive discussion. Controversy arise as research groups attribute the timing events in the surface membrane (membrane clock) or the uptake and release of Ca^{2+} from the SR (calcium clock) as the dominant mechanism for pacemaker activity of the sinus node. The hyperpolarisation activated I_f is believed to be an important aspect of the membrane clock. 'Local Ca^{2+} release events' and NCX activity have been considered important for the calcium clock of the pacemaker activity. Under normal conditions, a

combined interaction between the membrane and calcium clocks might be responsible for the pacemaker activity of the sinus node (Capel and Terrar 2015).

1.3.2 Calcium-induced-calcium-release (CICR) and cardiac contraction

The electrical activation of the plasma membrane of cardiomyocytes leads to contraction. Ca^{2+} is key to this phenomenon and thereby plays a central role in cardiac contraction. CICR forms the basic mechanism of cardiac contraction wherein depolarisation of the plasma membrane enables Ca^{2+} entry into the myocyte and triggers a larger release of Ca^{2+} from the sarcoplasmic reticulum, leading to activation of the myofilaments and evoking their shortening, hence, myocyte contraction (Bers 2002; Fabiato 1983). Corruption of the excitation-contraction system through the mismanagement of Ca^{2+} has been implicated in dysfunction of the contractile apparatus and arrhythmias (Pogwizd et al. 2001; Landstrom, Dobrev, and Wehrens 2017).

During phase 2 of the cardiac action potential, opening of the LTCC on the T-tubules of the plasma membranes leads to the inward Ca^{2+} currents (I_{Ca}). LTCC has a single pore-forming protein, the α1 subunit, and is assisted by several regulatory subunits. The α1 subunit has four domains, each with six transmembrane loops. A charged voltage sensor on the fourth transmembrane segment (S4) of the α1 unit confers the LTCC with its voltage sensitivity. The Ca^{2+} selectivity of the channel is due to glutamate residues on the pore-lining P loop. Inactivation of the LTCC is enhanced through the Ca^{2+} binding protein calmodulin that enables the closure of the channel in an intracellular Ca^{2+}-dependent manner. The β subunits of the LTCC can be phosphorylated by protein kinase A (PKA)

and may increase channel activity during β-adrenergic stimulation (Kamp and Hell 2000; Levick 2010; Zuhlke et al. 1999; Reuter, Kokubun, and Prod'hom 1986).

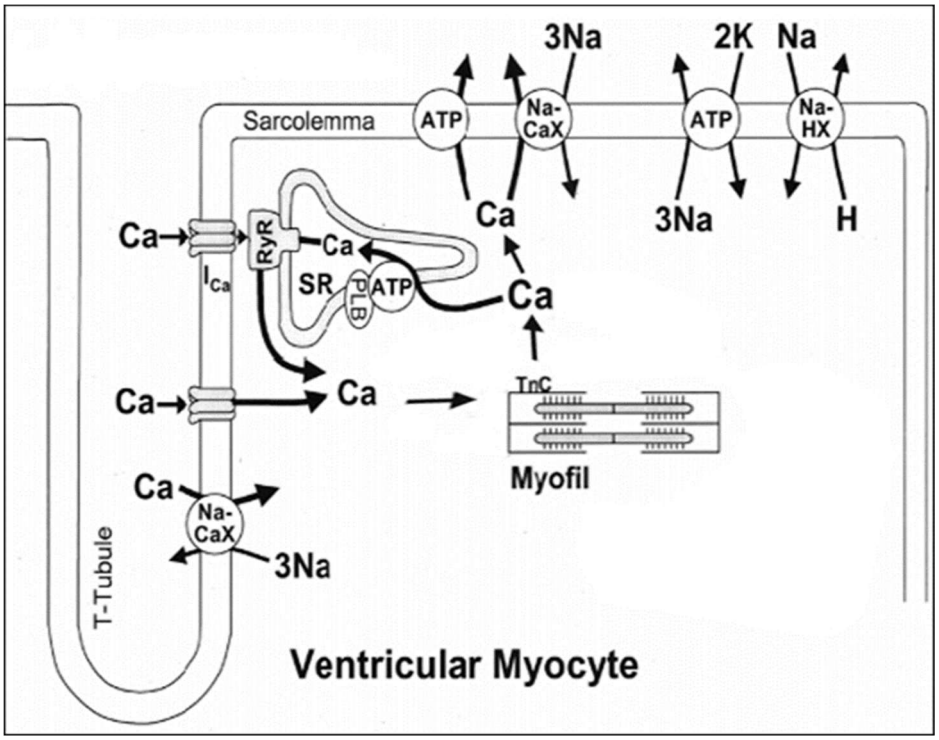


Figure 1.2: Ca^{2+} cycling in a ventricular myocyte.

Ca^{2+} enters the cell through voltage activated Ca^{2+} channels (I_{Ca}) on the T-tubule and triggers Ca^{2+} release from the SR via RyRs. This leads to contraction of the myocyte after which Ca^{2+} reuptake into the SR takes place and the remaining Ca^{2+} is extruded from the cell via the NCX. Figure modified from (Bers 2002).

Following the entry of Ca^{2+} into the myocyte through the LTCC, further release of Ca^{2+} from the SR is facilitated through the RyRs on the SR membrane. Mammalian tissues can express three subtypes of ryanodine receptors, RyR1, RyR2 and RyR3. RyR1 and RyR2 are majorly expressed in skeletal tissues while RyR2 is expressed mainly in cardiac

tissues. RyR2 exist as tetramers with each subunit having a molecular mass of 565 kDa (Otsu et al. 1990). The junctional SR forms a diad with the T-tubules such that the RyRs come in close proximity to the LTCC (approximately 15 nm), thereby RyR activation is tightly coupled to the Ca^{2+} entry through the LTCC (Fawcett and McNutt 1969; Eisner et al. 2017). Ca^{2+} entry through a single LTCC can activate a cluster of 6-20 RyRs. Myocyte-wide Ca^{2+} release from the SR due to simultaneous firing of LTCCs activated RyRs increases the cytoplasmic Ca^{2+} concentration from 100 nM to nearly 1 μM. The Ca^{2+} released from the SR rapidly diffuses into the sarcomere to initiate contraction. The release of Ca^{2+} from the SR through the RyRs is regulated by Ca^{2+}. A larger influx of Ca^{2+} through the LTCC leads to a larger release from the SR. However, at much higher levels of Ca^{2+}, RyRs are inactivated and might perhaps be the mechanism for the termination of Ca^{2+} release from the SR before diastole (Fabiato 1985). Additional regulation of RyR can also be through SR luminal Ca^{2+} concentration. Higher luminal Ca^{2+} concentrations lead to higher and longer Ca^{2+} releases from the SR while lower levels of luminal Ca^{2+} leads to RyR inactivation (Gyorke and Gyorke 1998; Ching, Williams, and Sitsapesan 2000).

During diastole, troponin-I is bound to actin in such a way that myosin binding sites on the actin filaments are blocked. As the cytoplasmic Ca^{2+} concentration increases as a result of Ca^{2+} release from the SR, Ca^{2+} binds to troponin-C, thereby increasing the affinity of troponin-C for troponin-I. The tight binding of troponin-C to troponin-I releases the latter from the actin filaments. The troponin-tropomyosin complex moves deeper into the groove on actin such that the myosin binding sites of the actin filaments become exposed. This enables the myosin head to bind to actin and form cross-bridges. The myosin heads pull itself along the actin filament by repeated binding, rotating and

dissociating from the actin filaments (called the power stroke) and is powered by ATP hydrolysis. The myosin advances by 5-10 nm during each power stroke and leads to sarcomere shortening and cardiomyocyte contraction (Levick 2010; Bers 2002; Landstrom, Dobrev, and Wehrens 2017). Sarcomere shortening in cardiomyocytes is dependent on the release of Ca^{2+} from the SR. The higher the release of Ca^{2+} from the SR, more troponin complexes are formed and consequently more myosin binding sites are revealed, resulting in stronger contractions.

Relaxation of the cardiomyocyte after contraction occurs is achieved by the extrusion of Ca^{2+} from the cytoplasm. Ca^{2+} is removed from the cytosol by two mechanisms: Ca^{2+} reuptake into the SR by SERCA and Ca^{2+} extrusion into the extracellular environment by the NCX. 75-90% of the Ca^{2+} is transported into the SR by SERCA while 10-25% of the Ca^{2+} is transported to the extracellular space by the NCX. SERCA is a P-type ion pump located on the non-junctional SR with ten transmembrane spanning domains, an ATP binding site, a phosphorylation site, a β-strand domain and a hinge region (MacLennan et al. 1985). The cardiac isoform of SERCA is SERCA2a, while the skeletal muscle isoform is SERCA1a. SERCA transports two Ca^{2+} ions into the SR for every molecule of ATP consumed. The function of SERCA is regulated by the inhibitory protein phospholamban (PLB). Dephosphorylated PLB binds to SERCA2a and inhibits its function by slowing down Ca^{2+} transport into the SR (Tada et al. 1982; Reddy et al. 1996). However, phosphorylation of PLB by PKA at Ser-16 or Ca^{2+}/calmodulin-dependent protein kinase II (CaMKII) at Thr-17 removes the inhibitory effect of PLB on SERCA resulting in enhanced transport of Ca^{2+} into the SR (Kirchberger, Tada, and Katz 1974; Le Peuch et al. 1979). The NCX is an exchange pump on the plasma membrane and transports three Na^{+} ions across the membrane for one Ca^{2+} ion. Though the NCX can work in forward

and reverse directions during the action potential depending on the membrane voltage, Ca^{2+} extrusion is its primary function (Frank et al. 1992). A small proportion of cytosolic Ca^{2+} is also extruded into the extracellular space by the sarcolemmal calcium ATPase. A schematic diagram for the Ca^{2+} transport events during one contraction cycle is given in Figure 1.2.

1.4 β-adrenergic signalling in the heart

The 'fight-or-flight' response is a physiological reaction that occurs in response to acute stress or exercise. Under this response, the heart can rapidly increase its output to nearly five-fold. This is mediated through the sympathetic nervous system and acts on the cardiomyocytes via the β-adrenergic signalling system. The two major elicitors that trigger the β-adrenergic signalling are the catecholamines adrenaline and noradrenaline (El-Armouche and Eschenhagen 2009). Adrenaline is produced by adrenal medulla and noradrenaline is produced by the adrenal medulla as well as postganglionic neurons. These mediators circulate throughout the body and act on the β-adrenergic receptors (β-ARs) on the heart when needed resulting in increased heart rate, contractility, conduction velocity and relaxation (de Lucia, Eguchi, and Koch 2018).

The β-adrenergic receptors are members of G protein-coupled receptors (GCPR) superfamily of receptors. Currently, three subtypes of β-ARs have been characterised, namely, β_1-ARs, β_2-ARs and β_3-ARs (Zhu et al. 2011). In the cardiovascular system, β_1-ARs and β_2-ARs are present as central regulators of cardiac performance along with very low expression of β_3-ARs (Brodde, Bruck, and Leineweber 2006). Cardiomyocytes show

an abundance of β_1-ARs and non-cardiomyocytes (e.g.: endothelial cells) express β_2-ARs and β_3-ARs (de Lucia, Eguchi, and Koch 2018). The β-ARs, like other GCPRs, are characterised by a core structure with extracellular amino terminus, intracellular carboxyl terminus and seven transmembrane α-helices, connected by three extracellular and intracellular loops (Rockman, Koch, and Lefkowitz 2002). Initiation of the β-adrenergic signalling begins with ligand binding to the β-ARs. The receptors undergo a conformational change that evokes an exchange of guanosine diphosphate (GDP) for guanosine triphosphate (GTP) leading to the dissociation of the stimulatory G-protein (G_s) into its active subunit $G_{\alpha s}$ and sets in motion a cascade of downstream events. The $G_{\alpha s}$ subunit activates adenylyl cyclase (AC), which in turn catalyses the conversion of adenosine triphosphate (ATP) to cyclic adenosine monophosphate (cAMP). The increase in levels of cAMP activate cAMP-dependent PKA. Activated PKA phosphorylates a variety of effectors to elicit a functional response. These include troponin I, LTCC, and PLB, among others, resulting in chronotropic, lusitropic, dromotropic and inotropic effects in the heart (Freedman and Lefkowitz 2004).

The β-adrenergic pathway has been implicated to play a role in the initiation and maintenance of arrhythmias. One of the main mechanisms involved in arrhythmias is afterdepolarisations. Afterdepolarisations are abnormal depolarisations that occur during phase 2,3 or 4 of the cardiac action potential. Afterdepolarisations occurring during phase 2 or 3 of the action potential is called early afterdepolarisation (EAD) and are caused by dysfunctional Ca^{2+} or Na^{+} channels. Afterdepolarisation occurring from the resting potential is known as delayed afterdepolarisation (DAD) and are caused by abnormal Na^{+} or chloride channels (Johnson and Antoons 2018). A strong link between β-adrenergic pathway and arrhythmias has been demonstrated in catecholaminergic polymorphic

ventricular tachycardia (CPVT) mouse models. CPVT is a condition with an RyR or calsequestrin mutation that leads to increased open probability of RyR or abnormal SR Ca^{2+} buffering. In CPVT mouse models, higher rate of DADs was observed under the influence of catecholamines (Liu et al. 2006). This was attributed to increased RyR sensitisation to catecholamines thereby leading to lowered threshold for SR for Ca^{2+} waves and enhanced Ca^{2+} loading of the SR (Fernandez-Velasco et al. 2009). Under excessive Ca^{2+} load, DADs and EADs are also reported to appear simultaneously. A study by Johnson et al. showed that on exposure to isoprenaline, occurrence of DADs resulted in beat-to-beat variability of repolarisation and EADs. DADs increased the duration of the subsequent action potential mediated by an increase in LTCC current resulting in generation of Ca^{2+} waves before the end of the repolarisation, thereby, inducing EADs (Johnson et al. 2013). Other studies using knockout mice have also reported that total deficiency of adrenoreceptors resulted in reduction of atrial and ventricular arrhythmias (Stockigt et al. 2012). Understanding the β-adrenergic signalling in the heart and the factors that affect it is critical to finding therapeutic targets for cardiac arrhythmias.

1.5 CD38/ ADP-ribosyl cyclase

1.5.1 History

The enzyme CD38 was first discovered in 1980 by E.L. Reinherz and S.F Scholssman in their attempt to identify and characterise cell-surface markers with monoclonal antibodies to search for molecules for immunophenotyping of T cells (Reinherz et al. 1980). Further studies by Greaves Lab revealed that the gene encoding human CD38 is located at chromosome 4 (Katz et al. 1983). Isolation of the cDNA of this gene was performed by

Jackson and Bell (Jackson and Bell 1990). A polypeptide consisting of a short N-terminal cytoplasmic tail (21 residues), a single transmembrane segment and a carboxyl-terminal extracellular domain carrying the four potential N-linked glycosylation sites around 32 kDa.

1.5.2 Catalytic function and biological distribution of CD38

CD38 is considered as a multifunctional enzyme due to its ability to catalyse multiple enzymatic reactions. CD38 catalyses the synthesis of nicotinic acid adenine dinucleotide phosphate (NAADP) from the substrates nicotinic acid (NA) and nicotinamide adenine dinucleotide phosphate (NADP). This is achieved by a base-exchange reaction where the nicotinamide group of the NADP is replaced with NA. This reaction is heavily favoured at acidic pH. Also, at acidic pH, CD38 can convert NAADP to ADP-ribose 2'-phosphate (ADPRP) by functioning as a hydrolase. CD38 is also known to hydrolyse NADP to ADPRP at neutral pH or in the absence of NA (Aarhus et al. 1995; Graeff et al. 2006). To date, the base-exchange reaction has been the only reported method of generating NAADP and the ability of CD38 to catalyse this reaction has only been detected in vitro. In vitro experiments in several tissues required a functional CD38 to produce NAADP. Studies in lymphokine-activated killer cells and hepatic stellate cells showed that NAADP levels were unaffected by angiotensin and interleukin-8 in *CD38*$^{-/-}$ mice, indicating a requirement of CD38 for endogenous NAADP production (Kim, Cho, and Kim 2010; Rah et al. 2010). Similar results were seen in pancreatic acinar cells, where cholecystokinin-induced increases in NAADP levels were absent in *CD38*$^{-/-}$ mice (Cosker et al. 2010). However, contradicting studies were published by groups wherein NAADP levels were comparable in wild-type and *CD38*$^{-/-}$ mice, both at basal levels and upon β-

adrenergic stimulation (Gul et al. 2016; Soares et al. 2007). The inconsistency in the results might be due to the complications in reliably measuring the minute amounts of endogenous NAADP using the current techniques (Lewis et al. 2007; Graeff and Lee 2002).

Another important catalytic function of CD38 is in the form of an ADP- ribosyl cyclase (ARC). CD38 has been observed to catalyse the cyclisation of nicotinamide adenine dinucleotide (NAD) to the cyclic product, cyclic adenosine diphosphate ribose (cADPR). CD38 can also hydrolyse NAD and cADPR to ADP ribose (ADPR) (Kim, Jacobson, and Jacobson 1993; Lee and Aarhus 1991). *In vitro* and *in vivo* studies have confirmed the role of CD38 in the cyclisation NAD. Tissues from *CD38*$^{-/-}$ mice were observed to have a reduced endogenous amount of cADPR as compared to wild-type (Partida-Sanchez et al. 2001). Mixed membrane preparations from wildtype mice were shown to synthesise cADPR while the *CD38*$^{-/-}$ mice lacked this ability (Lin et al. 2017). Moreover, activation of receptors by isoprenaline, acetylcholine and glucose increased the level of cADPR in various tissues in a CD38 dependent manner (Gul et al. 2016; Fukushi et al. 2001; Kato et al. 1999). A schematic diagram showing the different reactions catalysed by CD38 is given in Figure 1.3.

CD38 was first identified by monoclonal antibody typing of lymphocytes and was considered a lymphocyte-specific antigen (Reinherz et al. 1980). Further research revealed that CD38 was ubiquitously expressed in multiple tissues. Numerous researches have shown the presence of CD38 in organs including, but not limited to, heart, bone, brain, eye, pancreas, and the gut (Fernandez et al. 1998; Lin et al. 2017; Malavasi et al. 2008; Meszaros, Bak, and Chu 1993). Initially believed to be a surface antigen, CD38

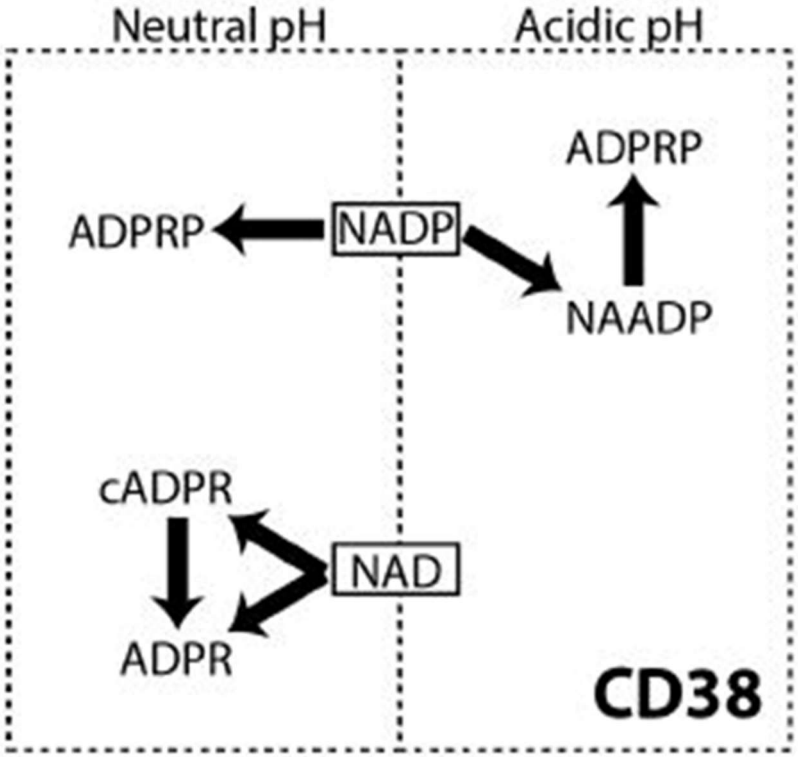


Figure 1.3: Enzymatic activities catalysed by CD38.

Black arrows represent the reactions catalysed by CD38. CD38 favours the conversion of NADP to NAADP at acidic pH. It can also hydrolyse NAADP to ADPRP. CD38 can also catalyse the cyclisation of NAD into cADPR at neutral pH. Hydrolysis of cADPR into ADPR can also be catalysed by CD38.

was later observed to be expressed in several intracellular organs including the nucleus, ribosome, mitochondria and endoplasmic reticulum (Adebanjo et al. 1999; Sun et al. 2002; Yalcintepe et al. 2005; Yamada et al. 1997). The enzymatic products of CD38, NAADP and cADPR, are active Ca^{2+} messengers that play important roles in cellular functions of microbial, plant and animal kingdoms (Lee 2006). The widespread cellular

functions they regulate include T-cell activation, chemotaxis, fertilization, cell proliferation, neurite growth, cardiac response to stress, long-term synaptic depression, among others (Brailoiu et al. 2006; Churchill et al. 2003; Gasser, Bruhn, and Guse 2006; Guse et al. 1999; Lin et al. 2017; Reyes-Harde et al. 1999). The synthesis and degradation of NAADP and cADPR by CD38 makes it a unique multifunctional enzyme.

1.5.3 Homologues of CD38

Aplysia cyclase, an ADP-ribosyl cyclase from the ovotestis of the sea mollusc Aplysia was the first enzyme found to be able to cyclise the linear molecule, NAD, to the cyclic product, cADPR (Lee and Aarhus 1991). A sequence similarity of 86 of 256 residues of CD38 and Aplysia cyclase indicated the cyclase activity of CD38 (States, Walseth, and Lee 1992). The Aplysia cyclase was a soluble protein in contrast to the CD38 which was a glycosylated transmembrane protein. A third member was added to the ADP-ribosyl cyclase family as CD157 (or bone marrow stromal cell antigen-1, BST-1), a GPI-anchored antigen of 42- 45 kDa (Itoh et al. 1994). Also, CD157 is the only known mammalian homologue of CD38. In 2005, another GPI-anchored antigen was found in *Schistosoma mansoni*, a human parasite (Goodrich et al. 2005). All the four ARCs shared a 20-30% in their protein sequences (Lee 2006). Interestingly, a stretch of nine residues, TLEDTLLGY (also known as TLED domain), found around the centre of the CD38 protein sequence, is highly conserved among the four homologues. Moreover, ten cysteine residues necessary for the conserved intra-disulphide bonds for the activity of the enzyme were found to be conserved across the four ARC homologues (Goodrich et al. 2005; Prasad et al. 1996).

Though some enzyme characteristics were different among the four ARCs, all the enzymes were capable of synthesising the hydrolysis resistant and fluorescent cyclic GDP- ribose (cGDPR) from Nicotinamide guanine dinucleotide (NGD), a substrate analog of NAD (Graeff et al. 1994). Also, barring CD157, all the other homologues were able to catalyse the base- exchange reaction of NA and NADP to form NAADP (Goodrich et al. 2005; Higashida et al. 2017; Malavasi et al. 2008).

1.5.4 Enzymatic structure and activity of CD38

1.5.4.1 Catalytic residues of CD38

In 2000, Lee's group discovered five important amino acid residues important for the activity of human CD38. Mutations in the tryptophan Trp125 and Trp189 resulted in reduced activity of the enzyme, suggesting a substrate positioning function for these residues. Substitution of the aspartate residue Asp155 with a glutamic acid, asparagine or glutamine, resulted in a multi-fold increase in GDP (guanosine diphosphate)-ribosyl cyclase activity. Substituting the glutamic acid Glu146 with valine and leucine repressed the activity of the enzyme. Perhaps most importantly, alteration of Glu226 by substitution by other residues like aspartic acid, asparagine, glutamine, leucine or glycine rendered the enzyme completely ineffective suggesting a very important role for the residue in the catalytic activity of CD38 (Munshi et al. 2000).

Further studies by Lee's group in the form of X-ray crystallography of CD38 and nicotinamide mononucleotide (NMN), a substrate analog of NAADP, showed that the complex was in close proximity to Glu146 and Asp155. Site directed mutagenesis of these

residues with uncharged residues eliminated the strong pH dependence of CD38 and enabled the base exchange reaction even at alkaline pH (Graeff et al. 2006; Lee 2006).

The specificity of the two acidic residues was further demonstrated by changing the adjacent Asp147 to Val, which had minimal effect on the pH dependence. Crystallography confirmed that Asp147 was situated and directed away from the bound substrate. Synthesis of NAADP catalysed by CD38 is known to have strong preference for acidic pH, suggesting that Glu146 and Asp155 are also critical determinants (Graeff et al. 2006). As Glu146 and Asp155 are negatively charged at neutral pH, it was proposed that the electrostatic repulsion between the negatively charged residues and the charged NA group of NAADP would prevent the substrate binding to the active site and, therefore, hindering its hydrolysis. This was shown to be the case by mutagenesis. Glu146 was found to be responsible for controlling the pH dependence of NAADP synthesis by the cyclase (Graeff et al. 2006).

Additionally, the ring of Trp189 in CD38 was shown to be parallel to and stacked with the nicotinamide ring of NMN, supporting that this residue is critical in managing the binding of substrates (Graeff et al. 2006).

1.5.4.2 Cysteine residues of ARCs

Ten cysteine residues of CD38 were found to be conserved and aligned in the protein sequences with the other ARC homologues (Tohgo et al. 1994). The Bruzzone lab showed

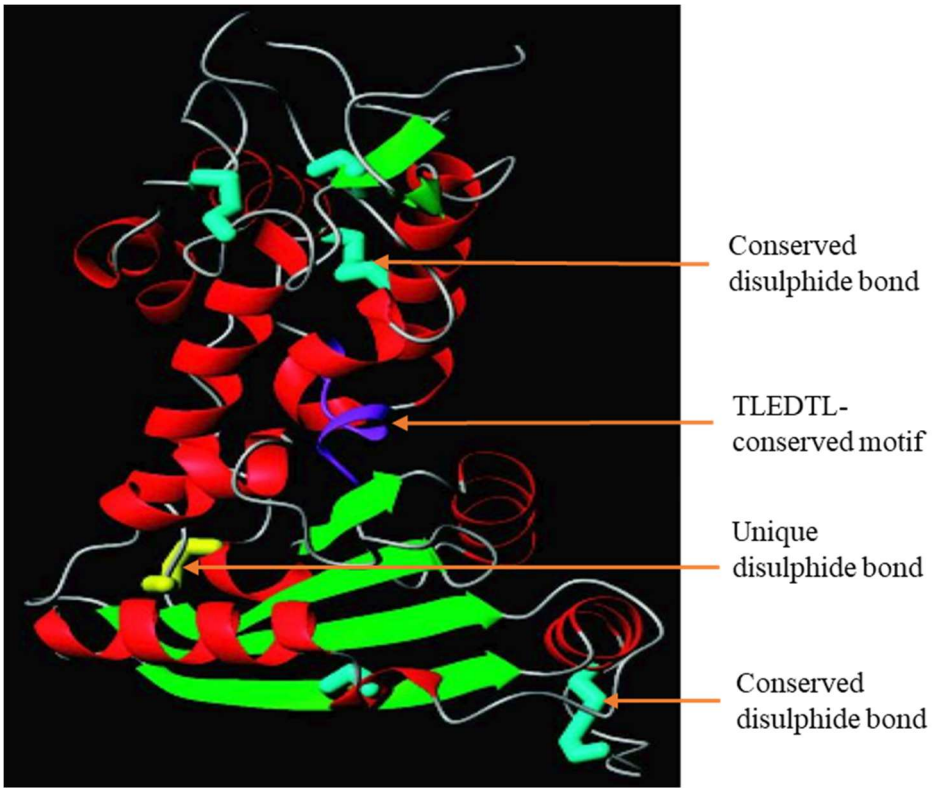


Figure 1.4: Structure of CD38.

A ribbon diagram illustrating the structure of CD38. The cyan regions show the conserved disulphide bonds of CD38. The purple region shows the conserved TLEDTL motif that CD38 shares with other ARCs. The yellow region shows the unique disulphide bond of CD38. Illustration modified from (Lee 2006)

that the conserved cysteine residues were not critical in the enzymatic activities of CD38 and *Aplysia* cyclase. Thiol-modifying and thiol-oxidising agents such as N-ethylmaleimide, iodoacetamide, and hydrogen peroxide did not affect the cyclase activity of CD38 and Aplysia cyclase. Interestingly, β-mercaptoethanol, a chemical with disulphide bond reducing properties, was able to impair the cyclase activity of CD38 in a dose dependant manner but not that of Aplysia cyclase. It was suggested that the

inactivation of CD38 was due to its oligomerisation by β-mercaptoethanol and that four leucine zipper-like sequences on the ecto-cellular portion of CD38 may be involved in the oligomerisation process. It was also suggested that even though the disulphide bonds reactive to β-mercaptoethanol do not possess catalytic activity, they might be responsible for the stability of the protein and the maintenance of its active structure (Guida et al. 1995; Zocchi et al. 1995).

CD38 functions as a cyclase in the formation of cADPR, and as a hydrolase to catalyse the hydrolysis of cADPR into ADPR. However, the *Aplysia* cyclase is known only to possess the cyclase activity (Aarhus et al. 1995). Tohgo and co-workers found that the two cysteine residues cys119 and cys201 were responsible for the hydrolase activity of CD38. Site directed mutagenesis of these cysteine residues resulted in the loss of hydrolase functionality of CD38. Moreover, introduction of cysteine residues into the corresponding sites of Aplysia cyclase presented it with hydrolase properties (Tohgo et al. 1994).

1.5.4.3 Glycosylations of CD38

N-linked glycosylation is considered to play an important role in accurate folding and translocation of a nascent protein to the membranes and also in post-translational modification (Rajan et al. 1995; Tifft, Proia, and Camerini-Otero 1992). Early work by Jackson and Bell on isolated cDNA of human CD38 revealed four potential N-linked glycosylation sites within the carboxy-terminal of CD38 (Jackson and Bell 1990). Deglycosylation of a recombinant CD38 protein (from rat cDNA) (42-46 kDa) using N-glycosidase F reduced its molecular weight to 33 kDa. Kinetic analysis of the deglycosylated CD38 revealed an increase in Km and a reduction in Vmax. This showed

the importance of N-linked glycosylation in the catalytic activity of CD38 (Chidambaram and Chang 1998). Similar results were found by Muller-Steffner and co-workers on using a deglycosylated recombinant CD38 from bovine cDNA (Muller-Steffner et al. 2010). A study by Gao and Mehta revealed that in the presence of an N-linked glycosylation inhibitor, CD38 produced cross-linked oligomers suggesting that N-linked glycosylation plays a crucial role in maintaining its structural stability and preventing inter-molecular cross-links (Gao and Mehta 2007).

Multiple studies by Zhao and co-workers have suggested the presence of an unglycosylated type -III human CD38. Contrary to previous observations, this form of CD38 has been observed to maintain its enzymatic activity (Liu et al. 2017; Zhao, Lam, and Lee 2012; Zhao et al. 2011; Zhao et al. 2015).

1.5.4.4 Oligomerisations of CD38

Crystallographic and biochemical studies have revealed that Aplysia cyclase and BST-1 exist in a non-covalent dimeric form (Munshi et al. 1998; Sato et al. 1999). CD38, on the other hand, was observed to exist in different oligomeric forms from a plethora of studies. Bruzzone and co-workers reported that human CD38 reconstituted in proteoliposomes and transfected HeLa cells is observed as a mixture of monomers, homodimers and homotetramers. Other studies also reported similar observations (Bruzzone et al. 1998; Franco et al. 1998; Mallone et al. 1998). CD38 purified from porcine heart microsomes treated with an antiserum to recombinant rat CD38 revealed a series of bands ranging from 45 to 285 kDa under non-reducing conditions in a protein immunoblot analysis. Under reducing conditions, only the 45 kDa band was seen. The oligomers at higher molecular weights were found to be very stable at high concentrations of SDS in the

sample buffer and also at low temperatures. It was also observed that the oligomers had higher cyclase activity than the monomers (Chidambaram, Wong, and Chang 1998). CD38 induced by retinoic acid in human myeloid (HL-60) leukaemia cells was observed to be in a tetrameric form. This form of CD38 was observed to be a more potent cyclase while its hydrolase activity was inferior as compared to the monomeric form. The authors suggested that post-translational modifications might be responsible for the different catalytic activities of this tetramer (Umar, Malavasi, and Mehta 1996). A study by Hara-Yokoyama et al revealed that mouse CD38 formed tetramers by dimerization of dimers. They suggested that this form of CD38 was critical for its catalytic activity and membrane localisation (Hara-Yokoyama et al. 2012).

1.5.4.5 CD38 activity and pH

The enzymatic activity of CD38 has a critical pH dependency. This is evident in the production of NAADP from the base-exchange reaction of NA and NADP, and to a lesser extent, in the cyclisation of NAD to for cADPR (Aarhus et al. 1995; Graeff et al. 2006; Lin et al. 2017).

Aarhus et al. observed that in the presence of CD38, the cyclisation of NAD to form cADPR was seen to be more efficient at a neutral pH rather than at the acidic pH of 4. An approximately two-fold increase in the production of cADPR was observed when the pH was changed from 4 to 7. In another experiment, they incubated CD38 (and *Aplysia* cyclase) with substrates NADP (1 mM) and NA (30 mM), at varying pH. They observed that at acidic pH, formation of NAADP was predominant. The production of NAADP was maximal between pH 4 and 5 and a 22-fold decrease in rate of the NAADP

production was observed at pH 7. They also noted that the rate of formation of ADPRP was twice as fast at pH 7 than at pH 4 (Aarhus et al. 1995).

With respect to the formation of ADPRP, contradictory results were published by Graeff and co-workers wherein they observed that hydrolysis of NAADP was maximal at pH 5. They observed that the hydrolysis of NAADP by CD38 was over 65 % more efficient at pH 4 than at pH 7 (Graeff et al. 2006). This discrepancy among the results of the two groups perhaps might be due to the different experimental conditions employed. Since Aarhus et al. incubated NA and NADP and observed the formation of ADPRP, there might very well be a hindrance in the formation of ADPRP due to the production of NAADP as different substrates could compete for the active site of CD38. In the study by Graeff et al., NAADP was the substrate for which ADPRP formation was observed, thereby, production of NAADP does not confound the rate of ADPRP formation.

There are reports that hypothesised the formation of NAADP in compartmentalised, acidic stores like the acidic endolysosome which favourably agrees with the acidic pH dependency of CD38 to form NAADP (Cosker et al. 2010; Davis et al. 2008). However, the half-maximal effective concentration of NAADP in mobilising Ca^{2+} is as little as 30 nM in sea-urchin egg homogenates (Aarhus et al. 1995). Studies on cardiomyocytes have also shown the effectiveness of concentrations of NAADP at the nanomolar range (Macgregor, Rakovic, et al. 2007). Therefore, a very low production of NAADP at neutral or alkaline pH must be able to activate appropriate signalling responses.

1.5.5 Topological paradox of CD38

Topology of membrane proteins are classified based on their orientation in the cell membrane and the peptide sequences (topogenic sequences) that are essential for their membrane targeting. Type I proteins are targeted to the endoplasmic reticulum (ER) by an N-terminal signal sequence and is then anchored to the cell membrane by a stop-transfer sequence. Unlike Type I, types II and III have only a single topogenic sequence responsible for both its insertion and anchoring. Type II proteins are targeted to the endoplasmic reticulum (ER) and subsequently to the extracellular space with its C-domain while the same is achieved by type III proteins with its N-domain (Spiess 1995).

Early studies, predominantly in lymphocytes, suggested CD38 to be an ecto-enzyme present on the cell surface as a type II single spanning membrane protein with its active C-terminal facing outwards of the cell while the N-terminal was facing the cytosol (Jackson and Bell 1990; Malavasi et al. 1994). This orientation of CD38 posed an interesting question as of how CD38 can produce NAADP and cADPR, both of which, along with their substrates, were intracellular messengers. Franco and co-workers hypothesised that a connexin (Cx43) -mediated release of NAD occurs to the outside of the cell. CD38 mediated production of cADPR occurs and the cADPR is transported back into the cell, hence completing an autocrine loop (Franco et al. 2001; Bruzzone et al. 2001). A study by Davis et al. proposed that the functionally active ARCs are sequestered in intracellular acidic organelles and transporters potentiate the movement of substrates and products to and from organelles, respectively (Davis et al. 2008).

An alternative suggestion was proposed in the form of a type III topology for CD38, wherein, the active C-terminal domain of the enzyme was facing the cytoplasm while the N-terminal domain faced the extracellular matrix (Zhao, Lam, and Lee 2012). The "positive inside rule" for single-pass membrane proteins suggests that the higher positively charged terminal of the protein should face the cytosol (von Heijne 1989). The N-terminal of CD38 has three positive charges while the C-terminal has a net positive charge of two. This is consistent with the ecto-enzyme configuration of CD38 as observed in earlier studies. However, noting the small difference in charges between the two terminals, it was suggested that a type III orientation could also be feasible since proteins with small charge differences between its terminals were known to exist in more than one orientation (von Heijne 2006). This was confirmed in later studies which observed type III configurations of CD38 in HL60 cells after differentiation with retinoic acid, U937 monocytic cells activated by interferon γ and in peripheral blood mononuclear cells (Zhao, Lam, and Lee 2012). Clarification was needed about type III CD38 in terms of the stability and activity of the catalytically active domain in the reducing environments of the cytoplasm. A soluble form of CD38 when made to be expressed in the cytoplasm was observed to be active as it increased the cellular cADPR. Also, monoclonal antibodies directed at the disulphide bridges of CD38, critical for its activity and stability, was shown to be intact, thereby, further confirming its activity (Zhao et al. 2011). A recent study observed that type III was functionally active and its activity was modulated through its interaction with calcium and integrin-binding protein 1 (CIB1) (Liu et al. 2017). Mutating four positive residues to negative from the N-terminal side led to complete expression of type III CD38 (Zhao, Lam, and Lee 2012; Zhao et al. 2015). Additionally, mutating three serine residues from the N-terminal to aspartate (equivalent of stimulating endogenous

phosphorylation) showed a heightened expression of CD38. This might suggest a mechanism of regulation of the CD38 orientations through endogenous phosphorylation of serine in the nascent polypeptide (Lee 2014). Zhao et al. hypothesised that type II and type III can operate hand in hand in cells. For fast cellular responses, such as stimulation by hormonal agonists, type III CD38 might be invoked. For slower and long-term responses such as cell differentiation, type II CD38 might be more suitable (Zhao et al. 2015).

1.5.6 CD38 in cardiac physiology

1.5.6.1 CD38 in cardiac development

CD38 has been implicated in the cardiac system as early as the development of the heart. The role of CD38 in cardiac development in mouse embryonic stem cells (ES) was studied by Wei et al. (Wei et al. 2012). In vitro cardiomyocyte differentiation initiated by embryoid body formation gave rise to more abundant and earlier beating cells in CD38 knockdown ES cells as compared to controls ES cells. Through FACS analysis, they observed that troponin-positive cardiomyocytes were more copious in CD38 knockdown colonies or those treated with the cADPR antagonist 8-bromo-cADPR, suggesting a role for the cADPR dependant Ca^{2+} pathway in cardiac development. Although cardiomyocytes differentiated from normal ES cells and CD38 knockdown ES cells were functionally similar, RT-PCR and western blot analysis reported that several cardiac markers showed increased expression in the CD38 knockdown ES. These included the alpha myosin light chain α-MLC, the transcription factor GAT4A, myocyte enhancer factor 2C MEF2C, and the cardiac homeobox protein NKX2.5 and. Moreover,

overexpression of CD38 in mouse ES cells showed a decrease in cardiomyocyte differentiation. The authors also showed that the FGF4-Erk1/2 cascade, which is important for cardiac differentiation, was supressed by the CD38-cADPR pathway. Wei et al. proposed that CD38-cADPR-Ca^{2+} cascade antagonises the cardiogenesis of mouse ES cells (Wei et al. 2012).

1.5.6.2 Physiological function of CD38 in the heart

The two enzymatic products of CD38, namely cADPR and NAADP, are the most potent Ca^{2+} releasing second messengers (Lee 2001). Nearly three decades of studies on these second messengers has uncovered a wealth of knowledge on its function in different cell types.

Early evidence of cADPR action on the heart was studied by Iino et al., wherein they showed that the application of the cADPR increased contraction strengths and calcium transient amplitudes in electrically stimulated isolated guinea-pig ventricular cardiomyocytes and were inhibited by the cADPR antagonist, 8-amino-cADPR. Suppression of SR function using ryanodine and thapsigargin also prevented these effects suggesting the activity of cADPR through an SR mediated manner (Iino et al. 1997; Rakovic et al. 1999; Prakash et al. 2000). Further studies supported this proposal as photorelease of a caged-cADPR in guinea-pig and rat cardiomyocytes slowly increased the frequency of calcium sparks and amplitudes of Ca^{2+} transients and was abolished in the presence of 8-amino-cADPR. The authors suggested that the slow effect of cADPR on cardiomyocyte might indicate existence of complex interactions in the pathways rather than direct activation of RyRs by cADPR (Cui, Galione, and Terrar 1999). The β-

adrenergic pathway may also be influenced by cADPR. In hearts from mouse and guinea-pigs, isoprenaline was observed to raise the levels of cADPR (Gul et al. 2016; Lewis et al. 2012). Gul et al. reported that isoprenaline induced a sustained Ca^{2+} increase, which

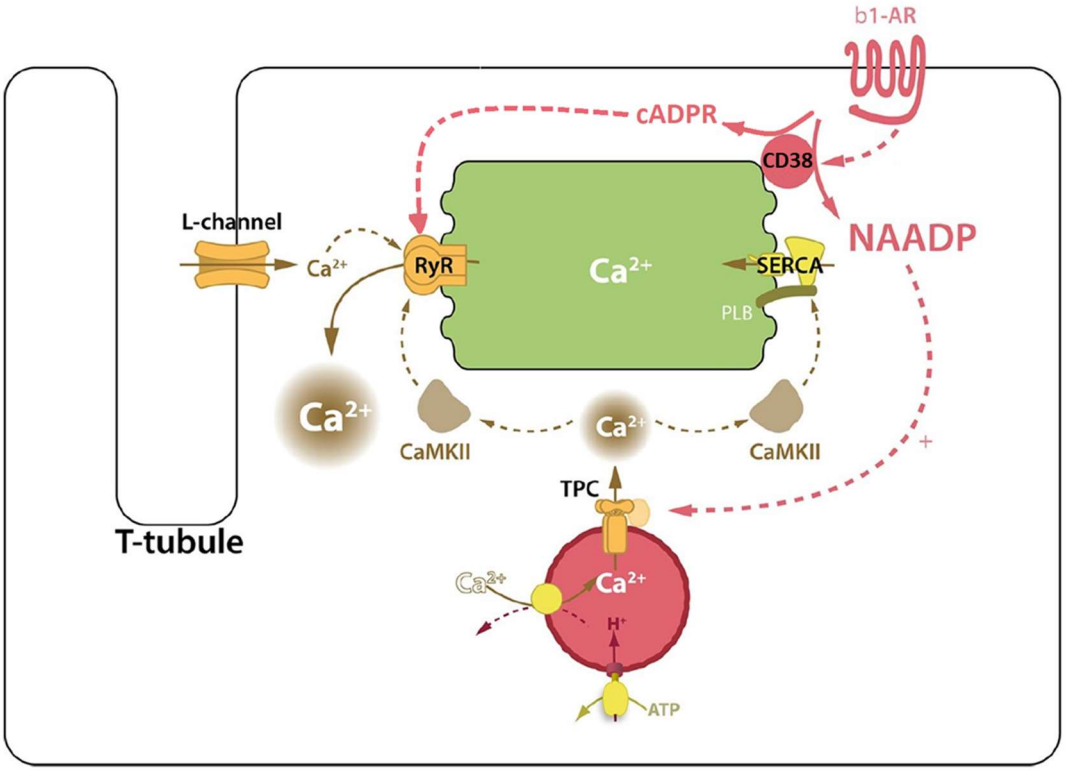


Figure 1.5: Roles of CD38 in the heart.

On β-adrenoceptor stimulation, NAADP and cADPR are believed to be produced by CD38 in the heart. NAADP presumably binds to TPC2 on the lysosome to release Ca^{2+} which is then taken into the SR by SERCA in a CAMKII dependent manner. This, in turn, gives rise to enhanced Ca^{2+} release from the SR (Two-pool hypothesis). cADPR is believed to elicit a response by the RyR by directly or indirectly binding to it. Enhanced Ca^{2+} release from the SR is also an effect of cADPR in the myocyte. Illustration modified from (Capel et al. 2015)

was abolished by cADPR antagonist 8-bromo-cADPR. Also, cardiomyocytes from *CD38*$^{-/-}$ mice showed a decrease in Ca^{2+} increase and cADPR production under the influence of isoprenaline (Gul et al. 2016). Similarly, 8-amino-cADPR and 8-bromo-cADPR was shown to block oscillatory activity such as Ca^{2+} waves, spontaneous action potentials, transient inward currents and after-depolarisations linked to overloading of intracellular Ca^{2+} stores under the influence of high concentrations of isoprenaline (Rakovic et al. 1999).

Although cADPR has been strongly linked to Ca^{2+} release from the SR, the mechanism of this phenomenon is debated. Sitsapesan et al. reported that in single channel experiments, cADPR increased the open probability of RyR channel in a concentration dependent manner in the absence of ATP and increased the open probability of RyR in the absence of ATP. They suggested that cADPR does not directly trigger Ca^{2+} release from the SR since it must compete with β-NAD, ADPR and ATP (Sitsapesan, McGarry, and Williams 1994). Other studies have also claimed from single channel experiments that cADPR fails to activate RyR receptors (Fruen et al. 1994; Copello et al. 2001). Noguchi et al. showed that cADPR bind to FKBP12.6 binding proteins in islet microsomes. They suggested that binding of cADPR to FKBP12.6 frees RyR from FKBP12.6 and hence causing it to release Ca^{2+} (Noguchi et al. 1997).

NAADP is also believed to elicit profound effects in cardiac tissues. This is discussed in detail in (Section 1.6.6). A summary of the effects of CD38 in the heart is given in Figure 1.5.

1.5.7 CD38 in cardiac pathology

Cardiac hypertrophy is the abnormal enlargement of the heart muscle due to underlying cardiac diseases such as congestive heart failure, hypertension, valve disease (McKinsey 2007; MacDonald et al. 2008). An angiotensin II (Ang-II) mediated pathway has been suggested for the development of cardiac hypertrophy. Ang-II induced Ca^{2+} increase affects calcineurin which in turn evokes nuclear translocation of the transcription factor NFAT3, which leads to the upregulation of cardiac-specific gene expressions that promotes hypertrophy (Molkentin et al. 1998). Gul et al., proposed the activation of ADPR cyclase activation by angiotensin and cADPR production. They showed that the ADPR-cyclase inhibitor 2,2'-dihydroxyazobenzene (DHAB) inhibited Ang-II mediated cADPR formation and hypertrophy in rat cardiomyocytes. They also reported that in the rat angiotensin-dependent model of hypertension, 2K1C (two-kidney one clip), Ang-II induced hypertrophy was reversed by DHAB treatment (Gul et al. 2008; Gul et al. 2009). In a recent study, Guan and co-workers implicated a role for CD38 in cardiac hypertrophy. Hypertension was generated in wildtype and *CD38*$^{-/-}$ mice by chronic infusion of Ang-II over 14 days via an osmotic mini-pump. They observed that the incidence of hypertrophy and fibrosis was more severe in the wild-type mice as compared to the *CD38*$^{-/-}$ mice, suggesting an important role of CD38 in the severity of cardiac hypertrophy. Moreover, in vitro studies using CD38 knockdown H9c2 cell lines showed a decrease in atrial natriuretic factor (ANF) and brain natriuretic peptide (BNP) which are considered to be markers of hypertrophy (Guan et al. 2017). Another recent study proposed that β-adrenergic stimulation also induced the development of cardiac hypertrophy. Chronic isoprenaline treatment led to hypertrophy in wild-type mice while the *CD38*$^{-/-}$ mice showed resistance to hypertrophy, interstitial fibrosis, decreased

fractional shortening and ejection fraction (Gul et al. 2016). Contradictory research has also shown that *CD38*$^{-/-}$ mice have an inclination for hypertrophy development (Takahashi et al. 2003; Gan et al. 2011).

When blood flow is restricted to sections of the cardiac muscle, shortage of cellular metabolites to keep the tissue alive leads to ischaemia. Restoring blood flow to these tissues leads to myocardial ischaemia/reperfusion (IR) injury. Reactive oxygen species (ROS) have been established to contribute to IR injury as superoxide anions and hydroxyl radicals are observed during IR (Downey 1990; Bolli et al. 1989; Garlick et al. 1987). Also, during IR, an increase in intracellular Ca^{2+} is observed while the contractility is decreased (Xie et al. 2003). Xie et al. discovered an increase in intracellular cADPR in langendorff perfused hearts subjected to IR injury and the increase in cADPR was associated with the increase in ARC activity. Inclusion of oxygen free radical scavengers prevented this increase in cADPR and ARC activity, suggesting an association between ROS and ARCs in IR injury where ROS led to the overproduction of cADPR which were lethal to the cells. This was confirmed through the addition of the oxidant *t*-butyl hydroperoxide which increased the ARC activity, leading to increased cADPR production, intracellular Ca^{2+} increase and subsequently cell death. This series of events was abolished by 8-bromo-cADPR (Xie et al. 2003). In another study, Reyes et al. observed that isolated rat hearts subjected to IR injury showed a depletion of the CD38 substrate NADPH and an increase in the production of the CD38 product ADPRP due to the activity of CD38 and could be prevented by genetic knockdown or inhibition of CD38 by α-NAD (Reyes et al. 2015). A recent study by Guan and co-workers also linked CD38 with IR injury. In wild-type and *CD38*$^{-/-}$ mice subjected to 30 minutes ischaemia followed by 24 hours of reperfusion, the *CD38*$^{-/-}$ mice were observed to be more resistant to IR

injury as compared to the wild-types. To confirm the protective effect of CD38 deficiency, an H9c2 cell line with CD38 knockdown was used. The CD38 knockdown cell line was shown to have higher levels of survival as compared to control cells and IR induced cell death was also diminished in the knockdown cells. They proposed that CD38 deficiency protected the heart through the activation of silent mating type information regulation 2 homolog 1 (SIRT1)/FOXOs- mediated antioxidative stress pathway (Guan et al. 2016).

CD38 is also implicated to play a role in cardiac arrhythmias. Several studies have established the production of cADPR and NAADP in cardiac tissue upon the application of isoprenaline (Macgregor, Rakovic, et al. 2007; Lewis et al. 2012; Gul et al. 2016) suggesting a link between CD38 and cardiac arrhythmias. Early findings by Rakovic et al. showed that in the presence of cADPR inhibitors, guinea-pig cardiomyocytes were more resistant to β-adrenergic stimulation mediated arrhythmias (Rakovic et al. 1999). Kannt et al. suggested that the cardiac ARC inhibitors SAN2589 and SAN4825 were able to abolish spontaneous action potentials in guinea-pig papillary muscles. Moreover, SAN4825 was able to suspend ventricular fibrillation and cardiac arrest in guinea-pigs treated with ouabain which led to Ca^{2+} overload induced arrhythmias suggesting a role for cardiac ARCs in the generation of arrhythmias (Kannt et al. 2012). SAN4825, at low micromolar concentrations, was also shown to prevent isoprenaline induced arrhythmias in mouse cardiomyocytes (Warszta et al. 2014). Lin et al. reported that whole hearts from *CD38*$^{-/-}$ mice showed reduced arrhythmias in the presence of isoprenaline as compared to wild-type mice and SAN4825 reduced the isoprenaline induced arrhythmias in wild-type mice (Lin et al. 2017). Similar observations were made by Capel et al. on a TPC2 knockout mouse (*Tpcn2*$^{-/-}$) (TPC2 is considered to be a potential receptor to the CD38

product NAADP) wherein the *Tpcn2*$^{-/-}$ mice were more resistant to acute and chronic effects of isoprenaline induced arrhythmias (Capel et al. 2015). Nebel et al. has also showed that isoprenaline-induced arrhythmias could be abolished by bafilomycin-A1 or the NAADP antagonist 3-carboxy-1-octylcarbamoylmethylpyridinium bromide (BZ194) in mouse isolated cardiomyocytes and in vivo (Nebel et al. 2013).

1.5.8 Other ARCs in mammalian tissue

Although a plethora of studies have implicated CD38 as the primary ARC in mammals, several studies have published the possible existence of other ARCs in mammals. ARCs were discovered in several tissues which had differing biochemical properties as that of CD38. A brief summary of the reported non-CD38 ARCs are given below.

Mészáros et al. reported the existence of two different ARCs in dog and rat cardiac muscles which were able to convert NGD to cGDPR. The two ARCs were differentially isolated from sucrose gradient centrifugation fractions. The ARC bound to the plasma-membrane enriched fraction showed characteristics similar to CD38 as it was inhibited by Dithiothreitol (DTT) and was recognised by a CD38 antibody. However, the ARC isolated from the SR fraction was not inhibited by DTT nor was it detected by the CD38 antibody but was inhibited by the endogenous protein kinase C (PKC)- dependent phosphorylation (Meszaros, Wrenn, and Varadi 1997). The ARC inhibitors discovered by Kannt et al., SAN4825 and SAN2589, were able to inhibit the cyclase activity of pig and rat SR membrane fractions but only partially inhibited the activity of human CD38. Though CD38 is activated by Zn^{2+}, the ARCs from pig and rat SR membrane fractions were shown to be inhibited by Zn^{2+} (Kannt et al. 2012). In skeletal tissue from rabbit,

Bacher et al. showed that Zn^{2+} and Cu^{2+} inhibited the ARC activity while they were believed to potentiate CD38/ CD157 activity. They also observed that DTT did not affect ARC activity in HSR obtained from skeletal muscle (Bacher et al. 2004; Kukimoto et al. 1996). Similar results were published by Nam et al. in kidney tissue where they were not able to inhibit the cyclisation activity of the ARC by DTT, while Zn^{2+} was found to be inhibitive to the activity. Moreover, they showed that the ADPR-cyclase DHAB was able to block the cyclase activity of the kidney ARC while not affecting the activity of the ARCs from heart, spleen and brain (Nam et al. 2006). While these studies indicate the presence of non-CD38 ARCs in mammalian tissues, further studies need to be performed using *CD38*$^{-/-}$ models to confirm the proposals for the existence and identification of a non-CD38 ARC.

1.6 Nicotinic acid adenine dinucleotide phosphate (NAADP)

1.6.1 Introduction

During the early 1990s, Lee and co-workers observed that the commercially available NADP or the product of alkali treatment of NADP, in large quantities, was able to invoke intracellular calcium release from sea urchin oocytes. Further analysis revealed that rather than the compound itself, its derivative was responsible for the calcium-release activity. This active derivative had a proton NMR spectrum identical to that of NADP but was one mass unit larger than NADP and was subsequently deduced to be NAADP (Aarhus et al. 1995). Further studies on this compound over the next two decades revealed its function as an important Ca^{2+} second messenger in a wide range of cell types. It is considered to

be the most potent calcium activating molecule since it has the ability to mobilise Ca^{2+} ions at picomolar to nanomolar concentrations (Chini and Dousa 1995; Galione 2015).

As discussed earlier, NAADP is produced by the ARCs CD38 and *Aplysia* cyclase by a base exchange reaction between the substrates NADP and NA, where the nicotinamide group of NADP is replaced with NA. This reaction is favoured at an acidic pH. CD38 can also convert NAADP to ADPRP by functioning as a hydrolase (Aarhus et al. 1995; Graeff et al. 2006).

1.6.2 NAADP dependent calcium release

Aarhus et al. showed that NAADP, at a half maximal concentration of 30 nM, triggered release of calcium from sea urchin egg homogenates. It was observed that a higher concentration of NAADP desensitised the sea urchin egg homogenates and at which point, further addition of NAADP did not provoke a response in the form of more calcium release. However, cADPR and Inositol 1,4,5-triphosphate (IP_3) were able to evoke further calcium release from the sea urchin homogenates which suggest the mechanism of calcium release by NAADP was distinct from the other second messengers (Aarhus et al. 1996; Genazzani, Empson, and Galione 1996). This proposal found further strength in the form of studies which showed that antagonists of IP_3 (heparin) and cADPR (8-amino-cADPR) were able to abolish the release of calcium by IP_3 and cADPR, respectively, but were unable to hinder a response by NAADP (Lee and Aarhus 1995). Moreover, removal of functional ER stores from sea urchin egg homogenates and in intact eggs by inhibiting SERCA (using thapsigargin), calcium release response by IP_3 and

cADPR was abolished while NAADP dependent calcium release was observed, albeit reduced (Churchill and Galione 2001).

In another study, sea urchin egg homogenates were centrifuged upon which organelles localized to opposite poles of the cell based on its density. IP_3 and cADPR were able to mobilise Ca^{2+} from the pole enriched with the ER, while NAADP mobilised Ca^{2+} from the opposite pole (Lee and Aarhus 2000). Further studies by Churchill et al., revealed that the organelles that were able to elicit a response from NAADP were "reserve granules" which were related to lysosomes (Churchill et al. 2002).

Lysosomes, were discovered by Christian de Duve in the early 1950s and he was awarded the Nobel prize for his work (Bainton 1981). They were identified as membrane enclosed organelles containing acid hydrolases which targeted different substrates. This suggested a digestive function for these organelles and were named as lysosomes (De Duve et al. 1955). Lysosomes were subsequently identified in all eukaryotic cells and were abundant in cell types with phagocytic activity such as macrophages (Appelqvist et al. 2013). Lysosomes play an important role in recycling and degrading macromolecules received from, endocytic, autophagic and secretory and phagocytic membrane-trafficking pathways (Luzio, Pryor, and Bright 2007). Lysosomes maintain an acidic pH with a luminal pH between 4.6 and 5.0 (Mellman, Fuchs, and Helenius 1986). Lysosomes contain 400 to 600 μM Ca^{2+} and the Ca^{2+} concentration is related to the luminal pH (Lloyd-Evans et al. 2008; Christensen, Myers, and Swanson 2002). The low pH of the lysosome is maintained by a vacuolar-type hydrogen ATPase. Inhibiting a vacuolar H^+-ATPase proton pump of the lysosome with bafilomycin A1 or a protonophore, nigericin, led to its loss of calcium and hence, alkalinisation. It was hypothesised that Ca^{2+} uptake

by lysosomes were controlled by a proton gradient by Ca^{2+}/H^{+} exchangers (Morgan et al. 2011). Consistent to these studies, NAADP was also found to alkalinise lysosomes in both sea urchin eggs and in mammalian cells (Morgan and Galione 2007; Collins et al. 2011). This suggested that unlike IP_3 and cADPR, NAADP mobilises calcium from acidic organelles in most, if not all cells. (Galione 2015; Yamasaki et al. 2004; Morgan et al. 2011; Patel and Muallem 2011).

However, Garrity et al. disagreed with the Ca^{2+} uptake into the lysosome by measuring the lysosomal Ca^{2+} concentration. Genetically encoded calcium indicators targeted to the lysosomes were used to show that inhibition of the vacuolar-type H^{+}-ATPase by bafilomycin A1 affected the pH, but not the calcium content in the lysosome. They suggested a role for the ER in the refilling of Ca^{2+} in lysosomes. Antagonists of IP_3 receptor blocked the lysosomal Ca^{2+} refilling, suggesting that calcium released from the ER in response to IP_3 could be responsible for Ca^{2+} entry into the lysosomes (Garrity et al. 2016). Further studies need to be undertaken with careful thought before invalidating the vast repository of publications that suggest that Ca^{2+} uptake into the lysosomes is controlled through the vacuolar Ca^{2+}/H^{+} exchangers.

Introducing NAADP into sea urchin egg homogenates and mammalian cells like pancreatic acinar cells resulted in a rapid spike in calcium concentration. Interestingly, it also resulted in long term propagation of calcium waves and oscillations. The initial spike of calcium release can be attributed to the action of NAADP and is independent of the influence of ER. This was shown by the non-effectiveness of ryanodine and IP_3 antagonists, and SERCA inhibitors to curb the initial spike caused by NAADP. However, the prolonged effects in the form of waves and oscillations ceased under the influence of

the ER inhibitors and antagonists (Cancela, Churchill, and Galione 1999). This originated the proposal for a "two-pool" mechanism of calcium release triggered by NAADP. The two-pool mechanism suggested that initially NAADP released calcium from acidic stores (pool 1), in an ER independent manner. The calcium released from the acidic stores evoked further calcium releases, likely from the ER (pool 2). This mechanism was named "trigger hypothesis" since the initial calcium release triggered further calcium releases from the ER. It was also hypothesised that a calcium signalling microdomain existed between the two pools (Churchill and Galione 2001). There are evidences of proximity between the ER and endo-lysosomal membranes (Kinnear et al. 2004; Aston et al. 2017). Localised acidic store calcium releases might increase local ER luminal Ca^{2+} and thereby enhance the IP_3 receptors or the ryanodine receptors (Lam and Galione 2013). Direct interactions between the calcium release channels of the acidic stores and the ER has also been proposed (Penny et al. 2014). Another study has suggested a bi-directional calcium signalling mechanism between the acidic stores and the ER in sea urchin eggs. As the calcium release from the acidic stores is amplified by the ER by calcium induced calcium release, similar calcium release from the ER can induce calcium release from the acidic stores, which is believed to be dependent on a mechanism directed by NAADP (Morgan et al. 2013).

A peculiar characteristic of NAADP is in its concentration-response relationship. IP_3 and cADPR follow a sigmoidal dose-response curve on semi-log plot. However, the NAADP concentration-response curve follows a bell-shape (Morgan and Galione 2008; Cancela, Churchill, and Galione 1999). In a study by Cancela and co-workers, NAADP was introduced into pancreatic acinar cells. While nanomolar concentrations of NAADP was able to evoke calcium oscillations, micromolar concentrations of NAADP did not induce

an effect. They observed that cells perfused with high NAADP concentrations failed to evoke a response to caged NAADP. This suggested a self-desensitisation mechanism of NAADP at higher concentrations and opens the prospect of using desensitising doses of NAADP as a specific blocker of the NAADP pathway (Cancela, Churchill, and Galione 1999) .

1.6.3 Intracellular targets of NAADP

As mentioned in the section above, the target receptor of NAADP is distinct from the other calcium second messengers such as IP_3 and cADPR. There are several possible molecular targets suggested for NAADP. Among them, the transient receptor potential mucolipin-1 channel (TRPML1), the transient receptor potential mucolipin-2 channel (TRPML2) the ryanodine receptor type 1 (RyR1), and Two-pore channels (TPCs) have gained much interest over the past few years (Zhang et al. 2009; Dammermann and Guse 2005; Lange et al. 2008; Brailoiu, Churamani, et al. 2009; Calcraft et al. 2009; Zong et al. 2009).

Zhang et al. reconstituted TRPML1 channel purified from rat liver lysosomes into lipid bilayers. They observed an ionic current to low concentrations of NAADP at higher concentrations of NAADP (100 μM) lead to its desensitisation (Zhang et al. 2009). This bell-shaped concentration response curve is a characteristic of NAADP as described earlier in mammalian cells. An anti-TRPML1 antibody was also able to inhibit this current which further strengthened the case of TRPML1 to be the NAADP receptor (Cancela, Churchill, and Galione 1999). Further studies by Zhang et al. used small interfering RNA (siRNA) to knockdown TRPML1 expression in bovine coronary artery

myocytes. Endothelin-1 evoked release of Ca^{2+} from the lysosome followed by a global Ca^{2+} release was seen to be weakened in the TRPML1 siRNA treated cells. Single channel experiments also showed a 70% reduced opening probability of the lysosomal NAADP-sensitive channels from the siRNA treated cells and immunoprecipitation or exposure to anti-TRMML1 antibodies showed to abolish these currents (Zhang et al. 2009). In another study, deletions of TRPML1 gene could abolish the response of NAADP in fibroblasts and transfection and re-expression of TRPML1 could rescue the NAADP responses (Zhang et al. 2011). However, studies by other groups have found contradicting observations. Pryor et al. found no increase in binding of radiolabelled NAADP in cells overexpressing TRPML1. Also, no significant response to NAADP was observed in these cells as compared to control cells (Pryor et al. 2006). In another study, even though lysosomal current could be increased by NAADP in wildtype cells but not in TRPML1 knock out, NAADP was still able to elicit calcium oscillations in the knockouts (Yamaguchi et al. 2011).

Another suggestion for a target of NAADP was in the form of RyRs. Mojzisova et al. observed a direct activation of dog heart RyR incorporated into lipid bilayers by NAADP at high concentrations (1-10 μM) (Mojzisova et al. 2001). Other studies using a lipid bilayer model have also shown a response to NAADP to RyR. Physiological concentrations of NAADP were shown to open a partially purified RyR from skeletal muscle (Hohenegger et al. 2002). However, a desensitisation response was not observed at higher concentrations of CD38. Guse et al. suggested that this might be due to the loss of the machinery needed for the desensitisation response when the receptors are reconstituted into the lipid bilayer (Guse and Wolf 2016). In pancreatic acinar cells, depletion of calcium from the nuclear membrane by NAADP was observed in a RyR

blocker (ryanodine) sensitive manner. Similar results were observed when a mitochondrial Ca^{2+}- uniporter inhibitor (ruthenium red) or thapsigargin. Interestingly, bafilomycin-A1 was not able to inhibit this NAADP response (Gerasimenko et al. 2003). Other groups were unsuccessful in reproducing these results in HEK293 cells expressing RyR1. These cells were also unable to evoke a response by intracellular release of NAADP (Wagner et al. 2014; Ogunbayo et al. 2011). Studies in Jurkat T-lymphocytes showed that microinjection by NAADP caused a global calcium response that could be inhibited by ruthenium red but not by IP_3 antagonist heparin. Genetic knockdown of RyR in these cells also abolished this response (Langhorst, Schwarzmann, and Guse 2004). Differentiation of a short-lived localised effect followed by a global effect (as proposed by the two-pool hypothesis) was not studied in these cells by Langhorst and co-workers. Later, high speed calcium imaging studies showed the presence of an initial short-lived localised response in Jurkat T- cells lacking RyR expression. Bafilomycin-A1 elicited no response to NAADP mediated calcium release but thapsigargin reduced the NAADP response suggesting that the NAADP evoked response in Jurkat T-cells were independent of lysosomes but might be dependent on the ER (Dammermann and Guse 2005; Wolf et al. 2015).

A few studies also reported an extracellular receptor for NAADP, for example, the purinergic receptors (Heidemann, Schipke, and Kettenmann 2005; Singaravelu and Deitmer 2006). In 1321N1 cells transfected with human P2Y11, extracellular NAADP increased the intracellular Ca^{2+} in a concentration dependent manner. This response was not observed in wild-type cells (Moreschi et al. 2008). A P2Y11 antagonist was able to abolish NAADP induced calcium spikes in rat astrocytes in a study by Singaravelu and co-workers. Neither bafilomycin-A1 nor GPN (Gly-Phe-β-naphthylamide), a compound

that disrupts the lysosomes, could abolish the effect of NAADP on these cells (Singaravelu and Deitmer 2006). However, another study in the presence of GPN, the number of astrocytes that responded to extracellular NAADP was reduced. The extracellular application of other metabolites such as NADP, NAAD and NAD also showed similar responses which raised the question as of whether responses to extracellular NAADP were a result of direct activation of the receptors or due to an indirect effect of its metabolic products (Mutafova-Yambolieva et al. 2007; Moreschi et al. 2008; Heidemann, Schipke, and Kettenmann 2005). Studies mentioned in this section suggests that NAADP may act at TRPML1, RyR, or an extracellular receptor. However, the roles of these receptors in terms of NAADP response remain controversial and further studies need to be performed to shed more light on the contradicting observations seen among these receptors. Two-pore channels are now the more widely accepted receptor of NAADP, and this possibility is discussed in more detail in the next section.

1.6.4 Two- Pore channels (TPCs) as NAADP receptors

In search for novel voltage-gated cation channels, Ishibashi and co-workers cloned the first Two-pore channel, TPC1, from a rat kidney cDNA library (Ishibashi, Suzuki, and Imai 2000). It was discovered to have a high homology with a Ca^{2+} channel of the plant Arabidopsis thaliana. Expressing the plant clone, AtTPC1, into yeast and *Arabidopsis* revealed its function in Ca^{2+} transport and signalling (Furuichi, Cunningham, and Muto 2001). As compared to known voltage-gated Na^{+} and Ca^{2+} channels having four repeats of six transmembrane segments, the 819 amino acids long TPC1 was shown to have only two repeats of the six transmembrane segments. Three isoforms of TPCs have been discovered, namely, TPC1, TPC2 and TPC3. All three isoforms have been found to exist

in sea urchins and most vertebrates. However, TPC3 is absent from humans and rodents like mice and rats but is found in other species such as guinea pigs (Calcraft et al. 2009; Zhu et al. 2010). In plant and animal species, TPCs are found on acidic organelles and in the endolysosomal system but are not present in Golgi, ER or mitochondria (Galione 2011). Presence of functional TPC1 and TPC2 genes were discovered in a variety of human tissues like kidney, liver, brain, heart and pancreas (Calcraft et al. 2009; Zong et al. 2009).

Several studies have implicated TPCs as the receptors for NAADP, evoking NAADP mediated calcium release (Brailoiu et al. 2006; Calcraft et al. 2009; Zong et al. 2009). Immunocytochemistry studies revealed the localisation of TPC2 to lysosomes. In HEK293 cells, an anti-hTPC2 antibody was seen to co-localise with lysosome-membrane associated protein 2 (LAMP-2). Moreover, overexpression of TPC2 in these cells showed increased binding of radiolabelled NAADP. Consistent with the two-pool hypothesis, exposure of NAADP in these cells lead to a biphasic Ca^{2+} response in the form of an initial brief calcium increase, following which a larger secondary calcium rise was observed. Both these calcium releases were abolished in the presence of bafilomycin-A1, but IP_3 inhibitors could only abolish the secondary calcium response. Knockdown of TPC2 expression was shown to eliminate these responses. Also, high concentrations of NAADP desensitised TPC2 responsiveness to NAADP. A TPC2 knockout (KO) mouse model (*Tpcn2*$^{-/-}$) was generated by a gene trap method by Calcraft and co-workers. Studies in these animals showed that NAADP mediated calcium release from the lysosomes was absent in their pancreatic β-cells while the wildtype displayed a response. Interestingly, TPC1 overexpressing cells also showed the localised release of calcium in response to NAADP but the secondary response was absent. It was hypothesised that this was due to

the early endosomal distribution of TPC1 which was perhaps more distant from the ER/SR to evoke the secondary calcium response (Calcraft et al. 2009; Galione 2011).

In mouse embryonic fibroblasts (MEFs), NAADP evoked calcium responses which was abolished in the presence of bafilomycin-A1, nigericin and the NAADP analogue Ned-19 (Ruas et al. 2015). In MEFs lacking TPC1 or TPC2, a reduced response to NAADP was observed while in the TPC1/TPC2 double knockout MEFs, this response was completely abolished. Re-expression of TPCs via lentiviral transduction rescued the NAADP mediated Ca^{2+} response in the double knockout MEFs. TPC2 re-expression evoked a more efficient response as compared to TPC1 re-expression. However, expression of TRPML1 channel or a mutant TPC2 with an impaired Ca^{2+} permeability did not rescue the response. These results suggested that the loss of NAADP mediated Ca^{2+} response in TPC double knockouts was due to the absence of TPCs (Ruas et al. 2015). Studies involving incorporation of TPCs into lipid bilayers also suggest a link between TPCs and NAADP. Pitt et al. showed that TPC2 were selective Ca^{2+} channels opened by NAADP in a concentration and pH dependent manner (Pitt et al. 2010). In another study, they observed that TPC1 was permeable to protons (relative permeability sequence: $H^+ > K^+ > Na^+ \geq Ca^{2+}$) and the presence of NAADP or Ca^{2+} was required for the activation of TPC1. They suggested that due to the difference in ion conducting and gating properties of TPC1 and TPC2, they might play complementary roles as Ca^{2+} release channels (Pitt et al. 2014; Pitt, Reilly-O'Donnell, and Sitsapesan 2016).

Controversial studies which disagreed the role of TPCs in NAADP mediated calcium responses were also published. Studies by Wang et al. on cells pre-treated with vacuolin-1 which selectively increased the size of endosomes and lysosomes showed that TPCs

were Na^+- selective channels and were activated by the lipid Phosphatidylinositol 3,5-bisphosphate (PI(3,5)P2) (Wang et al. 2012). (PI(3,5)P2) is known to activate channels such as TRPML1 and RyR, so they might also be able to activate TPCs (Dong et al. 2010; Touchberry et al. 2010). Wang et al. observed that lysosomal lumen predominantly contained Na^+ ions. They proposed that NAADP does not activate TPCs. They also observed that calcium responses to NAADP occurs in pancreatic islet cells even in TPC1 and TPC2 double knockouts suggesting that NAADP mediated calcium response is not TPC dependent (Wang et al. 2012). The opinion of TPCs being Na^+ channels was supported by other studies (Cang, Aranda, and Ren 2014; Cang et al. 2013). The TPC1 and TPC2 double knockout mice used by Wang et al. were regenerated by Ruas and co-workers (Ruas et al. 2015). Ruas et al. observed that the methods used by Wang et al. to silence the *Tpcn* genes only caused the truncation of the proteins and not complete deletion. The truncated proteins were shown to retain their function and its responsiveness to NAADP. This might explain why the pancreatic islet cells in the double knockouts were able to elicit an NAADP response. Jha et al., used approaches similar to Wang et. al and reported that TPC2 was activated by NAADP and was sensitive to Mg^{2+} (Jha et al. 2014).

Even though a multitude of research has suggested a close association between TPCs and NAADP, the question of whether NAADP binds directly to TPCs is debated. TPC1 and TPC2 have molecular weights of 94 kDa and 85 kDa, respectively. In sea urchin egg homogenates, photoaffinity labelling experiments using 5- azido-[32P]-NAADP revealed the labelling of only low molecular weight proteins of 30, 40 and 45 kDa. Similar experiments in mammalian pancreas labelled cytosolic proteins of 22 kDa (Lin-Moshier et al. 2012; Walseth et al. 2012). These experiments led to the proposal that NAADP

might bind to an accessory protein and not interact with TPCs directly. This idea was further strengthened when [32P]-NAADP binding occurred in liver tissue from TPC1/2 double knockouts (Ruas et al. 2015).

Although there are contradicting studies and gaps in knowledge regarding the NAADP binding target, compelling evidence suggests TPCs as a major player in mediating NAADP dependent calcium release from endo-lysosomes. Further studies are required to understand mechanism of the lipid sensitivity to TPCs and also to uncover, if existing, the accessory protein that NAADP binds to provoke a response through TPCs (Morgan and Galione 2014).

1.6.5 Effects of NAADP in non- cardiac tissues

NAADP mediated signalling has been implicated in several different pathways in plant and animal kingdoms. Different tissue systems take advantage of the NAADP pathway to function efficiently.

NAADP was first studied in sea urchin egg homogenates. Further studies revealed that NAADP mediated signalling was important in the fertilisation process in sea urchins, starfish and ascidian eggs (Albrieux, Lee, and Villaz 1998; Churchill and Galione 2000; Santella et al. 2000; Vasudevan, Galione, and Churchill 2008). NAADP has been shown to create a radial increase in Ca^{2+} in the egg cortex to prevent polyspermy (Churchill and Galione 2000). Analysis of sea urchin sperm has shown to contain a Ca^{2+}-activated NAADP synthase activity (Vasudevan, Galione, and Churchill 2008). Also, in sperm, NAADP has been suggested to release Ca^{2+} from an acidic store like acrosome where it

might trigger the acrosome reaction which is necessary for fertilisation process similar to human fertilisation process (Sanchez-Tusie et al. 2014). *Tpcn1*$^{-/-}$ mice are shown to have an impaired acrosome reaction during fertilisation which might explain the difficulty in maintaining *Tpcn1*$^{-/-}$ mice (Arndt et al. 2014; Galione 2015).

NAADP mediated signalling pathways have been known to elicit contractions in smooth muscles. NAADP evoked contractions in permeabilised bladder muscles and gastric fundus smooth muscle which were abolished in the presence of bafilomycin or in *Tpcn2*$^{-/-}$ mice. Studies have revealed that carbachol- evoked contractions in response to muscarinic agonists were dependent on NAADP signalling in these muscles (Pereira et al. 2014; Tugba Durlu-Kandilci et al. 2010). Guinea- pig tracheal muscle tissues extracts were shown to exhibit NAADP synthesising and metabolising activities and was affected by Ned-19 and reduced in *CD38*$^{-/-}$ mice (Aley et al. 2013; Deshpande et al. 2005).

The NAADP pathway has been implicated in several immune and hematopoietic cells due to the presence of acidic organelles or granules. A number of studies on T-lymphocytes has revealed the close association between NAADP mediated signalling and the immune response action of these cells. NAADP mediated Ca^{2+} release has been suggested to play an important role in the exocytosis of primary T-cells (Galione 2015). IP_3 and ionomycin were unable to induce exocytosis in these cells. TPCs were expressed on lytic granules and were required to evoke a Ca^{2+} release leading to its exocytosis (Davis et al. 2012). Microinjection of NAADP into Jurkat cells evoked a Ca^{2+} response in the unique concentration dependent bell-shaped manner associated with NAADP. Desensitisation of this pathway with high concentration of NAADP rendered the actions of IP_3 also ineffective suggesting a tightly knit association between these calcium second

messenger pathways (Gasser, Bruhn, and Guse 2006). In a study on lymphokine-activated killer cells, CD38 expression was observed to control the interleukin-8 response to elevate NAADP levels. The role of cADPR, ER, cAMP, exchange factor directly activated by cAMP (EPAC) and Rap1 was suggested in the production of NAADP from acidic organelles in these cells (Rah et al. 2010). NAADP has also been suggested to be involved in the functioning of megakaryocytes and in the formation of osteoclasts (Dionisio et al. 2011; Notomi, Ezura, and Noda 2012).

Several studies have suggested the importance of NAADP pathway in the nervous system. Early studies have suggested the existence of an NAADP pathway distinct from IP_3 or cADPR/ RyR- sensitive mechanisms in microsomes from rat brain (Bak et al. 1999). In frog neuromuscular junction, NAADP was shown to increase transmitter release. NAADP pathway involving CD38 has been suggested to be linked with autism as NAADP is believed to be involved in the exocytosis of oxytocin granules in the posterior pituitary gland from a number of studies (Jin et al. 2007; Ceroni et al. 2014; Young 2007; Galione 2015). In medulla oblongata neurons, NAADP invoked depolarisations of the membrane potential which were caused by localised Ca^{2+} from acidic stores. These effects were abolished by bafilomycin but were independent of the IP_3 pathway (Brailoiu, Brailoiu, et al. 2009). In hippocampal neurons and glia, application of glutamate evoked intracellular Ca^{2+} signals which were prevented by disrupting the lysosomes using bafilomycin and GPN. It was proposed that NAADP-evoked Ca^{2+} release affected IP_3 induced calcium release from the ER and this was necessary from metabotropic receptor mediated signalling (Pandey et al. 2009). Adding to the roles of NAADP in nervous system as stated above, NAADP pathway was also revealed to be involved in neurosecretion, neurite outgrowth and neuronal differentiation. They have

also been suggested to play a role in astrocytes, microglial cells and oligodendrocytes (Bezin et al. 2006; Galione 2015). Disrupted NAADP pathway has been connected to certain neurodegenerative diseases. A gain of function mutation of the kinase LRRK2 which has been associated with familial Parkinson's disease has been suggested to be linked to TPC2 in mouse models with Parkinson's disease. The increased autophagosome activity seen in LRRK2 mutants were reproduced by the application of NAAPD and was inhibited by Ned-19 (Gomez-Suaga and Hilfiker 2012). NAADP pathway has also been suggested to be associated in familial Alzheimer's disease. Presenilin 1 (PSEN) proteins, are generally known to be mutated in familial Alzheimer's disease. In mouse embryonic fibroblasts of lacking PSEN proteins, the lysosomal luminal calcium was observed to be reduced. It is suggested that the mutation in PSEN leads to a disrupted Ca^{2+} communication between the ER and the lysosomes resulting in impaired functioning of the lysosomes. Also, reduced TPC1 and TPC2 levels were observed in these models hence strengthening the argument (Coen et al. 2012; Neely Kayala et al. 2012).

1.6.6 Effect of NAADP in cardiac physiology

Early studies by Chini and Dousa found a link between the cardiac system with the NAADP pathway. They observed that cardiac tissue samples from rat were able to synthesise NAADP by the base-exchange reaction (Chini and Dousa 1995). Over the next two decades, compelling evidence has been published by multiple groups for a role for NAADP in the cardiac system.

Bak et al. used a radioactive analogue of NAADP, [^{32}P]-NAADP to identify its binding sites in rabbit heart microsome fractions. Two high affinity binding sites with dissociation

constants of 120 pM and 4 nM were reported in their studies. They also observed release of Ca^{2+} with an EC_{50} of 323 ±14 nM. This release of Ca^{2+} was not affected by inhibitors of IP_3 (heparin), cADPR (8-amino-cADPR) or the mitochondrial Ca^{2+} uniporter (ruthenium red). This suggested that the Ca^{2+} by NAADP in cardiac microsomes were through a mechanism distinct from the other calcium second messengers (Bak et al. 2001). A study by Mojzisová et al. showed that NAADP induced a Ca^{2+} release from the rat heart microsomes. To examine whether NAADP was releasing calcium from the SR, they incorporated RyR2 from dog hearts into lipid bilayers and studied the effect of NAADP (1-10 μM). They observed that NAADP increased the open probability of RyR2 suggesting that NAADP was involved in excitation- contraction coupling by affecting the RyR2 channels (Mojzisova et al. 2001). However, studies by Copello and co-workers showed the absence of an effect by NAADP in SR microsome fractions from dog hearts. Single channel experiments incorporating cardiac RyRs into lipid bilayers were also insensitive to NAADP. They also reported that cADPR did not bind to the SR microsomes nor was it able to release Ca^{2+}. They proposed the absence of NAADP/ cADPR sensitive Ca^{2+} release systems in cardiac muscles (Copello et al. 2001; Venturi et al. 2012). Similar studies by Pitt et al. suggested that NAADP did not affect the opening probabilities of RyR channels in rabbit skeletal or cardiac RyRs (Pitt et al. 2010).

A functional role of NAADP in heart was first observed by Macgregor and co-workers in guinea-pig ventricular cardiomyocytes. Electrically stimulated cardiomyocytes were loaded with a fluorescent cytoplasmic calcium indicator and a ‘caged’ NAADP which could be released by a pulse of ultraviolet (UV) light. On exposing the cell to a UV pulse of 500 ms, a gradual increase in the resting (diastolic) calcium concentrations and the amplitude of the calcium transient was observed over a minute. This effect was inhibited

by bafilomycin, desensitising concentrations of NAADP or by inhibiting SR function by ryanodine and thapsigargin. NAADP also induced an increase in contraction strength and an increase in frequency and amplitude of Ca^{2+} sparks which was abolished in the presence of bafilomycin-A1 (Macgregor, Yamasaki, et al. 2007). Similar results were observed by another study on guinea-pig atrial cardiomyocytes by Collins et al. Photorelease of caged NAADP increased the Ca^{2+} transient amplitude without affecting the L-type Ca^{2+} current suggesting that the increase in Ca^{2+} was not due to its entry through the L-type calcium channels. Increased Ca^{2+} amplitude and frequency were also observed in the presence of a cell permeant form of NAADP, NAADP- AM. These effects were eliminated in the presence of bafilomycin-A1 or GPN which implicated the lysosomes as important responders to NAADP in cardiomyocytes. They also observed an increased caffeine-induced Ca^{2+} release following NAADP photorelease suggesting that exposure to NAADP led to an increase in SR Ca^{2+} load and Ca^{2+} release (Collins et al. 2011). It was hypothesised that NAADP mobilised Ca^{2+} from acidic calcium stores which increased the SR Ca^{2+} load which in turn resulted in increased Ca^{2+} release from the SR leading to larger Ca^{2+} transient amplitudes and contraction.

Nebel et al. reported that in quiescent mouse cardiomyocytes, application of nanomolar concentrations of NAADP through a patch pipette resulted in an increase in intracellular calcium. A calcium transient was observed in 60 seconds which was abolished in the presence of bafilomycin-A1, BZ194 (an NAADP antagonist) and ruthenium red (Nebel et al. 2013). In another study, inhibitors of CaMKII (KN93 and AIP) were also able to abolish the global calcium transient implicating the role of CaMKII in the NAADP pathway (Capel et al. 2015). Nebel et al. also reported that in the presence of BZ194, spontaneous calcium transients induced by high concentrations of the β- adrenergic

agonist isoprenaline was also blocked in electrically paced cardiomyocytes. Moreover, isoprenaline induced arrhythmias were also reduced in live mice in the presence of BZ194. They proposed that NAADP was involved in the β-adrenoceptor pathway and played an active role in the generation of arrhythmias (Nebel et al. 2013). Further studies by Capel et al. also corroborated this hypothesis (Capel et al. 2015). They observed a reduced effect of isoprenaline on the Ca^{2+} transient amplitudes in the presence of bafilomycin-A1 or Ned-19. They also observed that the increase in Ca^{2+} transients and contractions caused by isoprenaline in wildtype mice cardiomyocytes was attenuated in *Tpcn2*$^{-/-}$ mice. Whole hearts from *Tpcn*$^{-/-}$ showed a reduced inotropic effect and a higher resistance to arrhythmias caused by isoprenaline. In a recent study by Lin et al., Ca^{2+} transients and contraction amplitudes in the presence of isoprenaline were reduced in *CD38*$^{-/-}$ mice as compared to wild-type mice. Also, disrupting the lysosomal function with bafilomycin-A1 reduced the isoprenaline-induced increase in Ca^{2+} transients in wildtype mice but not in the CD38 knockouts. Moreover, whole hearts from *CD38*$^{-/-}$ mice showed less arrhythmias as a response to high doses of isoprenaline as compared to wild-types, hence, reinforcing the link between CD38, TPCs and the NAADP pathway. Additionally, Lin and co-workers also showed that membrane fractions of wild-type mice supported the synthesis of NAADP and cADPR while their *CD38*$^{-/-}$ counterparts did not. Also, permeabilised cardiomyocytes improved NAADP synthesis suggesting a role for intracellular CD38 for NAADP production (Lin et al. 2017).

Recent studies in the heart also provided more support to the two-pool hypothesis (Churchill and Galione 2001). Aston et al. presented evidence for a close association of the lysosomes and the SR in ventricular myocytes. Using high magnification techniques such as 2D electron microscopy and 3D electron tomographic reconstructions, they

suggested the presence of a subcellular microdomain between these organelles which might allow Ca^{2+} release from acidic stores to raise the local Ca^{2+} concentrations to affect SERCA, PLB, RyR, and CaMKII to and hence, the functioning of the SR (Lam and Galione 2013; Berridge 2006; Aston et al. 2017). This was further supported by Lin et al. by immunolabelling experiments, where they showed a co-localisation of CD38 and RyR2 in rabbit ventricular myocytes (Lin et al. 2017). Aston et al. also observed a close association of lysosomes with mitochondria which might indicate a role in NAADP pathway in reperfusion-induced cell deaths (Davidson et al. 2015; Aston et al. 2017).

1.6.7 Effect of NAADP in cardiac pathology

Several studies over the last decade have implicated the NAADP pathway in various cardiac diseases. The influence of NAADP has been indicated to play a role in cardiac hypertrophy, arrhythmias, and ischaemia-reperfusion injuries (Nebel et al. 2013; Gul et al. 2016; Davidson et al. 2015; Capel et al. 2015).

Kannt et al. reported that arrhythmias caused by SR Ca^{2+} overload in guinea-pig papillary muscles could be curbed by the cardiac ARC inhibitors SAN2589 and SAN4825. SAN4825 was shown to prevent arrhythmias in single cardiomyocytes as well as in vivo (Kannt et al. 2012; Warszta et al. 2014). Work by Nebel et al. showed that isoprenaline-induced arrhythmias could be abolished by bafilomycin-A1 or the NAADP antagonist BZ194 in mouse isolated cardiomyocytes and in vivo (Nebel et al. 2013). Capel et al. showed that in whole hearts from mice with disrupted NAADP pathway (*Tpcn2*$^{-/-}$), increased current and pacing frequencies were required to induce arrhythmias caused by β-adrenoceptor activation with isoprenaline. In another set of in vivo experiments where

a chronic activation of β-adrenoceptors was achieved by administrating 10 mg/kg/day of isoprenaline for 14 days, *Tpcn2*$^{-/-}$ mice were observed to have higher threshold for arrhythmias (Capel et al. 2015).

The NAADP pathway has also been indicated to be involved in cardiac hypertrophy. *Tpcn2*$^{-/-}$ mice exposed to chronic doses of isoprenaline via an osmotic mini-pump were shown to have less hypertrophied hearts as compared to the wildtypes. The ex-vivo hearts from the hypertrophied wild-types mice had a lower threshold to arrhythmias as compared to the *Tpcn2*$^{-/-}$ mice (Capel et al. 2015). Gul et al., in their studies on *CD38*$^{-/-}$ mice, observed that the knockout mice showed lower incidence to isoprenaline-induced hypertrophy as compared to wildtypes. They reported a significant increase in weight/body weight ratios, cross-sectional area of cardiomyocytes, and cardiac fibrosis in the wild-types as compared to the *CD38*$^{-/-}$ mice. The wildtype mice presented reductions in fractional shortening and ejection fractions, while the knockouts had these characteristics preserved.

Ischaemia-reperfusion injury in the heart has also been reported to be affected by the NAADP pathway. High concentrations of extracellular NAADP has been observed to have cardioprotective effects in terms of ischaemia-reperfusion injury and is believed to act via cell membrane purinergic receptors such P2Y11. Improvement in function recovery, necrosis and arrhythmogenesis during ischaemia-reperfusion injury has been observed through the activation of these receptors by extracellular NAADP (Djerada et al. 2013; Djerada and Millart 2013). However, contradictory studies by Davidson et al. implicated the NAADP pathway in the severity of ischaemia-reperfusion injury. They reported that in the presence of the NAADP antagonist Ned-K, cardiomyocytes had

improved survival and reduced Ca^{2+} oscillations after reoxygenation following ischaemia. Ned-K was also shown to decrease infarct size in in vivo mice. Additionally, TPC1 knockout mice were also protected from the effects of injury suggesting the role of NAADP in ischaemia-reperfusion injury. The knockout mice had a reduced size in area of infarcts as compared to the wild-types. Ned-K and bafilomycin-A1 delayed the opening of mitochondrial permeability transition pores (mPTP) in wildtype mice. Davidson and co-workers hypothesised that the cardio-protection in the knockout mice might be via the prevention of reperfusion-induced Ca^{2+} oscillations that led to mPTP opening, which has been linked to cell death in ischaemia-reperfusion injury (Davidson et al. 2015).

1.7 Other calcium mobilising molecules

1.7.1 Inositol 1,4,5-triphosphate (IP_3)

Unlike the β-adrenergic signalling cascade that is initiated by activating the GCPR $G_{\alpha s}$, stimulation of the GCPR $G_{\alpha q}$ leads to the activation of phospholipase C (PLC) which in turn hydrolyses the membrane phospholipid phosphatidylinositol 4,5-bisphosphate (PIP_2) to form diacylglycerol (DAG) and IP_3. While DAG stays in the plasma membrane due to its hydrophobicity, the hydrophilic IP_3 diffuses into the cytoplasm and can act on its specific receptor. The IP_3 receptor (IP_3R) is an intracellular ligand gated Ca^{2+} release channel and are mainly present on the SR membrane and the nuclear envelope (Zima et al. 2007; Roderick and Bootman 2003). There are three subtypes of IP_3Rs, with IP_3R2 being the major subtype found in hearts (Wojcikiewicz 1995). The number of IP_3Rs on

the SR and nuclear envelope is much lower than RyRs with the ratio being approximately 100:1 (Bootman et al. 2009). IP_3Rs are found to be more abundant in the atria than in the ventricles and are located along the junctional SR but not in the non-junctional SR (Lipp et al. 2000).

Lipp et al. used a membrane permeant ester IP_3 ester, IP_3-BM, which activated the IP3Rs resulting in spontaneous Ca^{2+} release events. Moreover, in electrically stimulated cells, IP3-BM increased the calcium transient amplitudes, thereby suggesting a role for IP_3 in cardiac excitation-contraction coupling (Lipp et al. 2000). In cat atrial myocytes, the hormone endothelin-1 caused increase in cytosolic Ca^{2+} levels, increased Ca^{2+} transients and spontaneous Ca^{2+} releases from the SR in the form of waves and sparks. These effects were abolished in the presence of the IP_3R blocker 2-APB. Moreover, exposure to IP_3 following inhibition of Ca^{2+} release from RyRs using tetracaine, IP_3 mediated calcium 'puffs' were observed which were different from the RyR dependent Ca^{2+} sparks (Zima and Blatter 2004). Further studies by Wang et al. showed that α1-adrengeric pathway activation by phenylephrine increased the LTCC currents and were reduced by IP_3 inhibitors 2-APB, intracellular heparin and xestopongin and suggested that these effects involved NO synthesis (Wang et al. 2005). The Ca^{2+} release properties of IP_3 were further supported by Li et al. where mice lacking IP_3R2 had no effect on application of endothelin-1. The IP_3R2 and wildtype mice showed similar responses to isoprenaline suggesting a mechanism independent of β-adrenergic pathway (Li et al. 2005). In ventricular myocytes, endothelin-1 induced Ca^{2+} transients amplitude increase in paced myocytes was blocked by 2-APB. Also, similar Ca^{2+} transient effects were observed when treating the cells with a membrane permeant IP_3 ester which were also blocked by 2-APB, suggesting a role for IP_3 in ventricular myocyte inotropy (Proven et al. 2006). Domeier

and co-workers also observed an increase in Ca^{2+} transient amplitudes and Ca^{2+} sparks frequency on the application of IP_3 in permeabilised rabbit ventricular myocytes and was inhibited by 2-APB and heparin. In intact cells, endothelin-1 induced Ca^{2+} transient increase was abolished by 2-APB or by an adenoviral expression of an IP_3 buffer trap that buffered cellular IP_3 (Domeier et al. 2008). IP_3 is also known to regulate cardiac pacemaking. In mouse sinoatrial node (SAN) preparations, membrane permeant IP_3 analogue, IP_3-BM and endothelin-1 increased the Ca^{2+} transient amplitude and pacemaker rate in an 2-APB sensitive manner (Ju et al. 2011).

IP_3 mediated Ca^{2+} signalling mechanism has also been implicated in cardiac pathophysiology. Increased expression of IP_3Rs were reported in aortic-banded hypertrophic mice as well as human heart failure after ischaemia dilated cardiomyopathy (Harzheim et al. 2009). Chronic stimulation of α1- adrenergic and endothelin receptors also increase cardiac hypertrophy (Sugden and Clerk 2005; Singal, Dhalla, and Tappia 2004). Interestingly, in a recent publication, IP_3 mediated Ca^{2+} release was associated with anti-arrhythmogenic cardio-protection. Blanch and Egger reported that stimulation of IP_3 mediated Ca^{2+} release in IP_3R2 overexpressing mouse model led to a decrease in spontaneous SR Ca^{2+} release and occurrence of pro-arrhythmic Ca^{2+} waves. They hypothesised that increased IP_3 activity leads to “eventless” Ca^{2+} leak from the SR which leads to reduced SR Ca^{2+} content making it harder to achieve the threshold for the arrhythmogenic Ca^{2+} spark generation (Blanch and Egger 2018).

1.7.2 Cyclic adenosine diphosphate ribose (cADPR)

As discussed earlier (section 1.5.2), cADPR is believed to be formed by the cyclisation of NAD by CD38 (Lee and Aarhus 1991; Lin et al. 2017). Early studies by Clapper et al., revealed the Ca^{2+} mobilising properties of cADPR in sea urchin eggs. They reported that in the presence of the substrate NAD, there was a delayed Ca^{2+} release which was independent of the Ca^{2+} release mechanism of IP_3. Later studies hypothesised that cADPR was acting via the potentiation of the CICR through RyRs (Galione, Lee, and Busa 1991). Additional protein factors such as calmodulin and FK506-binding proteins were required for the Ca^{2+} releasing properties of cADPR (Lee et al. 1994; Tang et al. 2002). cADPR has also been implicated in activation of the cell surface Ca^{2+} influx channel, Transient receptor potential cation channel, subfamily M, member 2 (TRPM2). cADPR might be involved in temperature sensing mechanism and regulation of insulin secretion through this channel (Lange et al. 2008; Togashi et al. 2006).

Several studies have suggested a role for cADPR in cardiac function. Rakovic et al. reported a reduction in calcium transients and contraction strength in isolated guinea-pig cardiomyocytes in the presence of cADPR antagonist 8-amino-cADPR. Moreover, 8-amino-cADPR did not affect L-type Ca^{2+} current suggesting the presence of endogenous cADPR and its role in normal cardiac contraction. 8-amino-cADPR induced no further reduction of contraction was seen in myocytes that were treated with ryanodine suggesting a role of cADPR in Ca^{2+} release from the SR (Rakovic et al. 1996). Further experiments by Macgregor et al. in guinea-pig ventricular myocytes showed that photorelease of caged cADPR increased Ca^{2+} transients and contraction amplitudes without increasing the SR load. In permeabilised rat ventricular myocytes, application of

cADPR increased Ca^{2+} spark frequencies but did not change the SR load for up to 3 minutes. However, prolonged exposure of 10 minutes increased the SR load. The authors suggested dual action of cADPR in the heart wherein there is a rapid effect on the CICR without increased SR load and a slower effect with an increase in SR load. They hypothesised that on long exposure, cADPR might directly alter SERCA or may interact with phospholamban to increase Ca^{2+} uptake into the SR (Macgregor, Rakovic, et al. 2007). Studies in cardiac microsomes also showed Ca^{2+} release by cADPR. cADPR was shown to release Ca^{2+} from canine cardiac SR microsomes in a concentration dependent manner (Lahouratate, Guibert, and Faivre 1997). However, Lukyanenko et al. hypothesised that the primary effect of cADPR in cardiac system is SR Ca^{2+} uptake. They showed that in rat cardiac SR microsomes, the SR Ca^{2+} uptake was increased in the presence of cADPR (Lukyanenko et al. 2001). Although cADPR has a definite effect on the heart, the exact mechanism of its action is still under study.

cADPR might also play a role in cardiac dysfunction. Studying cADPR signalling with respect to β-adrenergic response has provided some interesting clues linking cADPR signalling to arrhythmias. Xie et al. reported that in rat cardiomyocytes, isoprenaline induced increase in intracellular Ca^{2+} was blocked in the presence of the cADPR inhibitor, 8-Bromo-cADPR (Xie et al. 2005). Similarly, in guinea-pig cardiomyocytes, arrhythmogenic oscillations like spontaneous Ca^{2+} waves and afterdepolarisations were abolished in the presence of the cADPR antagonists, 8-amino-cADPR and 8-Br-cADPR (Rakovic et al. 1999). Studies have shown that high concentrations of isoprenaline increased cADPR generation in cardiomyocytes (Lewis et al. 2012; Gul et al. 2016). Gul et al. reported that hearts from *CD38*$^{-/-}$ mice showed higher protection from arrhythmias when exposed to high concentrations of isoprenaline as compared to wildtype mice. The

authors proposed that the CD38 mediated cADPR pathway was responsible for this effect (Gul et al. 2016). However, Lin et al., proposed a combined action of cADPR and NAADP in cardioprotection from acute arrhythmias (Lin et al. 2017). Gul et al., also reported that *CD38*$^{-/-}$ mice showed reduced hypertrophy of the heart following chronic infusion of isoprenaline suggesting a role for cADPR in cardiac hypertrophy (Gul et al. 2016).

1.8 Specific aims of this thesis

We hypothesise that:

1. CD38 is an intracellular enzyme, associated with the SR, and this enzyme catalyses the synthesis of the Ca^{2+} mobilising agents, cADPR and NAADP in heart muscle.
2. NAADP acts on acidic organelles (termed lysosomes) in heart muscle to release Ca^{2+} into a microdomain close to the SR, and this in turn leads to additional Ca^{2+} uptake into the SR by SERCA following activation of CaMKII.
3. An increase in Ca^{2+} loaded into the SR by the above mechanisms increases the amplitude of Ca^{2+} transients accompanying action potentials in heart muscle.

To test the hypotheses above, the specific aims formed for this thesis were:

1. To study calcium handling in murine atrial tissue with respect to the NAADP pathway at both basal state and under the influence of β- adrenoceptor stimulation using wildtype and *CD38*$^{-/-}$ mice (Chapter 3).

2. To study the close association between the NAADP signalling pathway and SR Ca^{2+} load in wildtype and *CD38*$^{-/-}$ mice ventricular myocytes using a low affinity Ca^{2+} indicator to directly visualise SR Ca^{2+} changes (Chapter 4).
3. To study whether CD38 is the primary ARC in sheep cardiac SR membrane enriched preparation (Chapter 5).
4. An additional aim is to validate a cell type-specific optogenetic pacing strategy in Sino-atrial node containing atrial preparations (SAP) and to compare its Ca^{2+} handling properties pre and post optogenetic pacing (Chapter 6).

Chapter 2

Methods and Materials

2.1 Animals

The C57BL/6 mice were obtained from Envigo (UK), Charles river (UK) and Oxford University Biomedical Services (UK). The *CD38*$^{-/-}$ mouse line was developed by Cockayne et al. (1998) and obtained from Jackson laboratory (CD38^{tm1Lnd}/J). This CD38 KO model was created by using neomycin resistance gene to replace the Exons 2 and 3 of the CD38 gene of a C57BL/6 mouse, hence resulting in the loss of CD38 protein expression since Exons 2 and 3 are responsible for encoding the catalytic site for CD38 (Cockayne et al. 1998). This CD38 knockout model was further verified by the lack of CD38-specific mRNA transcripts and immunolabelling by the rat anti-CD38 antibody, and by the dramatically reduced NAD glycohydrolase activity (Cockayne et al. 1998). A breeding pair of the *CD38*$^{-/-}$ mice was obtained from Dr Margarida Ruas from Professor Antony Galione's lab.

Ai27D mice (Jackson Lab stock #012567) express a reporter construct at the ROSA26 locus, in which a floxed STOP cassette is positioned upstream of a hChR2(H134R)-tdTomato fusion gene. Exposure to Cre recombinase results in the removal of the STOP cassette and the expression of hChR2(H134R)-tdTomato protein. Channelrhodopsin 2 (ChR2) gene is derived from *Chlamydomonas reinhardtii*, humanised, and imbued with a gain-of-function H134R mutation to heighten the amplitude of photocurrents, before being fused to the gene for the fluorescent red tdTomato marker. Pnmt-cre mice – previously developed by Stephen Ebert et al. contain the cre open reading frame inserted at the Pnmt locus, just downstream of the 5' untranslated region (Ebert et al. 2004). When PNMT transcription is activated, production of the phenylethanolamine N-methyltransferase (Pnmt) protein is disturbed and Cre recombinase is produced instead.

The Lei lab have crossed the Pnmt-cre and Ai27D strains, to produce a novel mouse line (Wang et al. 2017). In these mice, cells where PNMT expression is at one time upregulated, hChR2(H134R)-tdTomato expression is 'unlocked', and these cells and their daughters are thereafter receptive to optogenetic stimulation with 450-490nm blue light. For the optogenetic studies in this thesis (chapter 6), $Pnmt^{cre/+}$/ChR2 (heterozygous) mice were used (< 6 months old), which express the Cre construct alongside functional Pnmt.

2.2 Mouse atrial preparation

All procedures on C57BL/6 and *CD38*$^{-/-}$ mice (8-12 weeks old, both males and females) were in accordance with the Schedule 1 of the Animals (Scientific Procedures) Act 1986 (HMSO). The mouse was first treated by intraperitoneal injection with heparin (200 units) under non-recovery terminal general anaesthesia by injection of an overdose of 1.2% Avertin solution (0.5-0.8 mL I.P. (2,2,2-tribromoethanol, Sigma-Aldrich, Poole, Dorset, UK). The mouse was killed by cervical dislocation after 15 minutes and the heart was quickly excised and washed in Modified Tyrode's Solution (see Table 2.2) by gently pushing the blood out of the heart to prevent the clotting of blood in the small coronary arteries. The heart was then pinned onto a Polydimethylsiloxane (PDMS) coated dish filled with warm (37 °C), oxygenated (95 % O_2 + 5 % CO_2 gas) Modified Tyrode's solution. The lungs, connective tissue around the heart and the ventricles were carefully removed to expose the atria. The atrial tissue was carefully pinned onto the PDMS coated dish with fine insect pins. For experiments that use only the left atrium, the left atrium was separated from the rest of the whole atria and pinned down on a small rectangular piece of PDMS. The left atrium was also opened to expose the left atrial endocardium. Similarly, for experiments that use only right atrium containing the SAN, the left atrium

was removed and the right atrium containing the SAN was opened from the AV junction to expose the SAN.

For preparation of sino-atrial preparation (SAP) of $Pnmt^{cre/+}$/ChR2 mice for optogenetic experiments, the whole atria was separated from the heart as described above. The right atrium was opened from AV junction to expose the intercaval region containing the SAN, following which left atrium was opened to expose the left atrial endocardium. The SAP was then pinned down on a piece of rectangular PDMS and prepared for dye loading.

2.3 Mouse ventricular myocyte isolation

The protocol for isolation of mouse ventricular cardiomyocytes was adapted from one that was previous described by Ackers-Johnson et al. (Ackers-Johnson et al. 2016). EDTA solution and Perfusion solution (see Table 2.2) were prepared prior to the isolation procedure. Two 10 mL syringes were filled with EDTA solution and one syringe was filled with perfusion solution. All syringes were attached with 27 G x 0.5-inch hypodermic needles (BD Bioscience, Singapore). One 60 mm petri dish was filled with EDTA solution and one 60 mm petri dish was filled with perfusion solution. Collagenase solution (see Table 2.2) was prepared and placed in a 37 °C incubator to warm up. 10 mL of Stop solution was prepared with perfusion buffer containing 5% fetal bovine serum.

The C57BL/6 and *CD38*$^{-/-}$ mice (8-12 weeks old, both males and females) were treated by intraperitoneal injection with heparin (200 units) under non-recovery terminal general anaesthesia by injection of an overdose of 1.2% Avertin solution. After 15 minutes, the mouse was killed by cervical dislocation. The mouse chest was wiped with 70% ethanol and opened using skin forceps and blunt ended scissors to expose the heart. The lungs

were removed for better visibility of the heart. The descending aorta and inferior vena cava were cut, and the heart was held using the forceps. One EDTA solution containing syringe was injected into the base of the right ventricle which was identified due to its darker colour. 7 mL of the EDTA solution was injected into the right ventricle over 1 minute which cleared out most of the blood in the right ventricle. During this process, cessation of contractions of the heart could be observed and the heart tend to look lighter due to the removal of blood. Care was taken as not to penetrate the ventricle by more than a few millimetres. The ascending aorta was then clamped using a Reynold's forceps and the heart was excised by cutting around the Reynold's forceps. The clamped heart was completely submerged in the petri dish containing EDTA solution and quickly placed under a stereomicroscope to continue the cardiomyocyte isolation protocol. The left ventricle was identified as the larger ventricle forming an apex at the base of the heart. The second EDTA solution containing syringe was carefully injected into the apex of the left ventricle. Enough pressure was created by the injection to inflate the heart. The solution was slowly injected into the ventricle at the rate of 1 mL per 2 minutes. Blood can be seen clearing out of the coronary arteries and the heart turns pale during the injection. After 10 mL of the solution was injected, the syringe is removed, and the heart is transferred to the petri dish containing the perfusion solution. Into the same perforation of the left ventricle created during the EDTA solution injection, perfusion buffer syringe needle was inserted. Perfusion buffer was slowly injected into the ventricle at the rate of 1.5 mL per minute. This cleared out the EDTA from the heart chambers and circulation. After 2 or 3 minutes of injection, the needle was removed. A new 60 mm petri dish and a 10 mL syringe was filled with the warmed collagenase solution. The collagenase stock was returned to the incubator to warm up for subsequent injections. The heart was fully submerged into the petri dish containing the collagenase solution and the syringe needle

was inserted into the perforation on the left ventricle. The collagenase solution was then injected into the ventricle at the rate of 2 mL per minute. Following the application of 10 mL collagenase solution, the needle is removed from the heart, and 10 mL of the collagenase solution was removed from the petri dish so as to prevent overflow. A new syringe was filled with fresh warmed collagenase solution (from the incubator) and the injection was repeated. This progression of collagenase solution injection was continued till the heart started losing its shape and rigidity, multiple holes appeared on the heart, and ejection of myocytes into the solution. At this point, the injection was stopped, and the clamp was removed. A sharp pair of scissors was used to separate the ventricles from the atria. The ventricles were then transferred to an unused 60 mm petri dish containing 3 mL warmed collagenase solution. The ventricles were then gently fragmented into 1 mm x 1 mm pieces using two sharp ended forceps. A wide-bore glass pipette with a rubber bulb was used to gently triturate the pieces of tissue for two minutes to further dissociate the cardiomyocytes into the solution. 5 mL of the stop buffer was added into the cell suspension to inhibit further tissue digestion. Gentle trituration was performed for two more minutes. An additional 5 mL of the stop buffer was then added to the cell suspension. A 100 µm cell strainer (Corning, Sigma- Aldrich, UK) was placed on top of a 50 mL falcon tube and the cell suspension was poured into the falcon tube through the cell strainer. This separated the undissociated chunks of tissue and led to the collection of a homogenous solution of ventricular cardiomyocytes. A drop of the cell suspension was inspected under a microscope to determine the quality of the cells. A good isolation was determined by a large number of rod-shaped cells with visible cross-striations while a majority of number of round, hypercontracted cells suggested a poor isolation.

The healthy cells were then enriched by sequential gravity settling. The 50 mL falcon tube containing the cell suspension was rested vertically for gravity settling for 15 minutes. The healthy cardiomyocytes settle faster into a pellet than the non-myocytes, extracellular debris, and the dead cardiomyocytes. After 15 minutes, the solution was removed, leaving the pellet intact. 10 mL of fresh Modified Tyrode's isolation solution (see Table 2.2) supplemented with 0.5-1% bovine serum albumin (BSA) was used to resuspend the cardiomyocyte pellet and the gravity settling was repeated. The pellet was obtained and resuspended in fresh Modified Tyrode's isolation solution containing 50 μM calcium chloride, following which gravity settling was repeated. This process was repeated 2 more times by resuspending the cardiomyocyte pellet in increasing concentrations of calcium chloride (150 μM and 250 μM). After the gravity settling stages, the cells were resuspended in 25 mL of Modified Tyrode's isolation solution containing 250 μM calcium and transferred into a new 50 mL falcon tube and stored horizontally in a 37 °C mini incubation oven (Bio-Rad, UK).

2.4 Sheep sarcoplasmic reticulum-enriched membrane preparation

The components of the solutions required for the Sheep sarcoplasmic reticulum- enriched membrane preparation (SRMP) is given in Table 2.2. The sheep hearts were collected from a local abattoir. The hearts were excised from the carcass and transported to the lab in ice-cold cardioplegic solution. The fat and connective tissue was trimmed out and the heart was cut into large chunks. The cardiac muscles were then stored in liquid nitrogen till needed to prepare the SRMP.

All steps of the SRMP preparation was performed in a cold room maintained at 4 °C. All tools and solutions required for this protocol were stored in the cold room overnight to

avoid heat damage during the SRMP preparation. The frozen tissue was first pulverised using a mortar and pestle. Liquid nitrogen was intermittently poured into the mortar to keep the muscle chunks ice cold while pulverising. 400 mL of SRMP Solution A and 2 mL of PMSF solution was added to the blender pot and then the pulverised tissue added to it. The mixture was then homogenised with a hand blender (Braun GmbH, Kronberg, Germany). The blending was done in short pulses so that the mixture does not heat up. Further homogenisation was done using an Ultra-Turrax homogeniser (IKA Werke GmbH & Co. KG, Staufen, Germany). The muscle solution was then centrifuged for 20 minutes at 6000 x g in a GSA Sorvall rotor (Fisher Scientific UK Limited, Loughborough, UK). The supernatant was decanted and filtered through a sieve to remove fat. The supernatant was then centrifuged for 1 hour at 4°C in a Sorvall A-641 rotor at 100,000 x g. The pellet containing the mixed membranes was resuspended in 10 mL Solution B supplemented with 10% sucrose. The mixture was carefully added to a discontinuous sucrose gradient of 20%, 30% and 40% w/v and centrifuged for 2 hours at 4°C in a Sorvall AH629 swing out rotor at 100,000 x g. This separated the different membrane fractions according to their densities. The 30%-40% interface contained the SR fraction with a high density of RyR channels (HSR) and the 20%-30% interface contained the K^+ and Cl^- channels (LSR). The HSR and LSR were collected and resuspended in Solution D before being centrifuged for 1 hr at 4°C in a Sorvall T865 rotor at 100,000 x g. The pellet was resuspended in Solution C and homogenised with a handheld glass homogeniser. It was then aliquoted and snap frozen in liquid nitrogen before being transferred to -80 °C. This preparation was termed SRMP.

2.5 Mouse mixed membrane preparation

The components of the solutions for the mixed membrane preparation can be found in Table 2.2. The mixed membrane preparation was done in a cold room maintained at 4°C.

10 mice were killed by cervical dislocation and their hearts were quickly excised and stored in liquid nitrogen until required for the mixed membrane preparation. All tools and solutions required for this protocol were stored in the cold room overnight to avoid heat damage during the mixed membrane preparation.

The mouse hearts were first pulverised in a pestle and mortar. The pulverised tissue was then resuspended in 90 mL Solution A to which 0.45 mL of PMSF solution and 90 µL protease inhibitor was added and homogenised in a blender (Braun GmbH, Kronberg, Germany). Further homogenisation was done using an Ultra-Turrax homogeniser (IKA Werke GmbH & Co. KG, Staufen, Germany). The tissue was then centrifuged for 20 minutes at 6000 x g in a GSA Sorvall rotor (Fisher Scientific UK Limited, Loughborough, UK). The supernatant was then centrifuged for 1 hour at 4 °C in a Sorvall A-641 rotor at 120,000 x g. The resulting pellets were resuspended in a minimum volume of solution C, aliquoted and snap frozen in liquid nitrogen before being stored at -80 °C.

2.6 Reverse Transcription Polymerase Chain Reaction (RT-PCR)

RT-PCR was done on RNA isolated from sheep cardiac tissue. The sheep heart was collected from a local abattoir. A small 2 cm x 2 cm chunk of tissue was cut from the ventricles of the heart and snap frozen in liquid nitrogen before being stored in a -80 °C freezer until needed for RNA extraction.

High quality RNA was extracted from the sheep cardiac tissue using RNeasy® Fibrous Tissue Mini Kit (Qiagen, UK). The extracted RNA samples were aliquoted and stored at -20 °C. The quantity and quality of the extracted RNA was checked by measuring the UV absorption of the RNA sample using a nanodrop (NanoDrop 2000c, Thermo Scientific). Absorption at 260 nm (A260) is used for the quantification of the RNA. A A260 reading of 1.0 corresponds to 40 µg/mL of RNA. Adsorption measurements were also taken at 230 nm (A230) and 280nm (A280). A ratio of A260 and A280 was an indication of the level of protein contamination in the RNA sample. A ratio of 1.8 - 2.1 was considered to be an acceptable quality of RNA. A ratio of A260 and A230 indicates the level of chemical contamination in the RNA sample in the form of guanidine salts and phenol from the RNA extraction process. Ratios of 1.5 and above indicates acceptable levels of chemical contamination.

Primers for the RT- PCR were designed using the Primer-Blast tool from the NCBI website. SHEEP CD38 SEQUENCE (XR_001041278.2) and Ovis aries bone marrow stromal cell antigen 1 (CD157/ BST1), transcript variant X1, mRNA (XM_015096300.1) were used as the template sequences for CD38 and CD157, respectively, for which primers were designed. Primer pairs with a melting temperature ($T_{m)}$ of 59 °C and 45 – 60% GC content were selected. A primer pair for Sheep GAPDH (glyceraldehyde-3-phosphate dehydrogenase [Ovis aries]: ADH43296.1) was designed as the positive control. The expected band sizes were 489 bp for CD38, 407 bp for CD157 and 497 bp for GAPDH.

RT-PCR was performed using a commercially available RT-PCR kit (QIAGEN® OneStep RT-PCR kit, Qiagen, UK). A master mix was made using the PCR buffer, dNTP mix, RNase-free water, and RT-PCR enzyme mix. The master mix was aliquoted into

individual PCR tubes and 170 ng RNA and 0.6 µM primer pairs were added such that the total reaction volume was 20 µl. Sheep GAPDH RNA was used as the positive control reaction and a negative control reaction (without template RNA) was also set up. The conditions employed for RT-PCR is given in Table 2.1.

After the RT-PCR process, electrophoresis was performed on the samples on a 1.5% agarose gel containing ethidium bromide (0.2 µg/mL) at 90 mV for 1 hour. The DNA ladder used was Quick-Load® 2-Log DNA Ladder, 0.1–10.0 kb (Thermo Fisher). The gel was then visualised on a UV transilluminator (Labnet International, USA).

2.7 Detection of ADP-ribosyl cyclase activity using NGD assay

The ARC activity of a given cell or tissue homogenates can be detected by a continuous assay, using NGD as the enzyme substrate. NGD is an analogue of NAD where the adenine group has been substituted with guanine. When NGD is converted to cGDPR through cyclisation by the ARC, its production can be detected using a fluorometric method via the fluorescence of cGDPR (Graeff et al. 1994). The cGDPR formation can be monitored through its fluorescence intensity at 410 ± 5 nm with an excitation wavelength of 300 ± 10 nm.

Protein sample was diluted in SRMP solution E (see Table 2.2) and 200 µL was added to one well of a Flat bottom 96-well plate (Greiner bio-one, Germany). The 96-well plate was placed in FLUOstar Omega plate reader (BMG Labtech, UK) for fluorescence measurement. Fluorescence recordings were taken every 10 seconds till a steady state reading was observed. 500 µM NGD was then added to the protein sample to initiate the enzymatic reaction. The production of the fluorescent product, cGDPR, was observed as

an increase in fluorescence values. The rate of cyclase activity of the protein sample was then defined by the change in fluorescence with time, which is the slope of the curve in the fluorescence versus time plot obtained by linear regression.

2.8 Drug docking

Drug docking studies were done to test whether the flavonoid Kuromanin bound to CD38. This was mainly performed by Autodock Vina (The Scripps Research Institute). Crystallographic structure of human CD38 (2HCT) was downloaded from Protein Data Bank (RCSB PDB) in pdb format. 3D structures of kuromanin (Pubchem ID: 441667) and NAD+ (ChemSpider ID: 5682) were downloaded from PubChem and ChemSpider, respectively.

Autodock Vina is a docking tool that uses the bound conformation preference and free energy of binding between a ligand and protein to identify potential ligand-receptor binding conformations. It uses a hybrid combination of knowledge-based and empirical approach for its scoring function. The negative free energy is an indication of the affinity of ligand-protein complex and is calculated as sum of the ligand efficiency (binding energy per atom of ligand to protein), intermolecular energy (energy between non-bounded atoms, that is the energy between atoms separated by 3-4 bonds or between atoms in different molecules), desolvation energy (electrostatic and/or van der Waals energy loss of the interaction between ligand or protein and solvent upon binding), and electrostatic energy (change on the electrostatic non bounded energy of ligand or protein upon binding). All possible conformations are scored by Autodock Vina and are presented in descending order of their negative free energies (Trott and Olson 2010).

To prepare the pdb files for docking, the protein was first processed in PyMOL software (Schrödinger). Ligands, water molecules and cofactors were removed from the protein structure. The protein was then visualised in Autodock Vina, polar hydrogens were added and saved in pdbqt format. Similar processing was done for kuromanin and NAD+ and was saved in pdbqt format. The blind docking simulation was then performed on Autodock Vina and the negative binding energies (kcal/mol) were obtained for the different binding conformations. The lowest binding energy conformations were then opened in PyMOL software to obtain 3D images of the docking. The human CD38 amino acids that interact with Kuromanin and NAD+ were visualised and 3D conformations for the docking were obtained. A 3D conformation containing superimposition of kuromanin and NAD+ to show overlapping binding of kuromanin and NAD+ was created by using Discovery Studio Visualiser software (BIOVIA).

2.9 Western blotting

Western blotting was performed on sheep cardiac SRMP and mouse mixed membrane preparation.

Protein samples (30 μg) were diluted with phosphate-buffered saline (PBS) and 4X Laemelli buffer (Bio-Rad, UK) to achieve a final volume of 30 μL. For reducing conditions, the Laemelli buffer contained 4% β-mercaptoethanol. For non-reducing conditions, no β-mercaptoethanol was used. The samples were heated at 95 ºC in a heat block for 5 minutes before being loading onto a precast SDS-PAGE gel (4–20% Mini-PROTEAN® TGX™ Precast Protein Gels, Bio-Rad, UK). PageRuler™ Plus Prestained Protein Ladder, 10 to 250 kDa (Thermo Fisher) was used as the ladder to indicate molecular weight. Electrophoresis was performed at 150 Volts for 1 hour using a mini-

Protean tetra-cell system with PowerPac™ power supply (Bio-Rad, UK) in running buffer (see Table 2.2)

Wet transfer onto Immun-Blot® Low Fluorescence PVDF Membrane (Bio-Rad, UK) was then performed at 300 milliamps for 1 hour in transfer buffer (see Table 2.2). After the membrane transfer process, blocking of the PVDF membrane was done using 50% Odyssey TBS blocking buffer (Li-Cor, USA) to prevent non-specific binding of antibody. This was done for 1 hour at room temperature.

The PVDF membrane was then incubated overnight at 4 ºC in 5 mL blocking buffer containing the primary antibody at 1:1000 concentration (CD38 Antibody (H-11): sc-374650, Santa Cruz Biotech, Germany), supplemented with 0.1% Tween-20 detergent. The PVDF membrane was then washed four times in PBS containing 0.1% Tween-20 detergent. The membrane was then incubated for 1 hour in 35 mL blocking buffer containing 1:15000 concentration secondary antibody (IRDye® 800CW Donkey anti-Mouse IgG Secondary Antibody, Li-Cor), supplemented with 0.05 % SDS and 0.2 % Tween-20. The membrane was washed in 2 more times in PBS containing 0.1% Tween-20 detergent and then three times in PBS without Tween-20. The membrane was then imaged using a Li-Cor Odyssey infrared scanner (Li-Cor, USA). The images obtained were analysed using ImageLab software (Bio-Rad).

2.10 Immunoprecipitation

Immunoprecipitation was done to purify CD38 from sheep cardiac SRMP. The immunoprecipitation process was done using a Dynabeads™ Protein G Immunoprecipitation Kit (Invitrogen, USA) following manufacturer's instructions. The

principle of immunoprecipitation using Dynabeads™ Protein G is as follows: Antibodies binds to the magnetic Dynabeads™ Protein G via their Fc-region when they are incubated together in an Eppendorf tube for a short duration. The tube was then placed on a DynaMag™ Magnet (Invitrogen, USA), and the magnetic beads containing the antibody adhered to the side of the tube facing the magnet, allowing efficient removal of the supernatant. The bead-bound antibody was then used for immunoprecipitation of the target antigen from the protein mixture. The bound mixture was then collected by placing the tube containing magnetic beads bound antigen-antibody complex on DynaMag™ Magnet. The purified protein was eluted from the beads using the elution buffer in the kit.

Following the kit protocol, 50 µL Dynabeads™ magnetic beads was first incubated with 10 µL of the antibody for 10 minutes at room temperature (CD38 Antibody (H-11): sc-374650, Santa Cruz Biotech, Germany). The mixture was then placed on the DynaMag™ Magnet and supernatant removed. 500 µg SRMP was diluted in 300 µL PBS and was incubated in the Dynabeads-antibody complex for 45 minutes. The beads-antibody-antigen complex was then washed three times with the kit provided 'washing buffer' to remove possible contaminant proteins. The antibody-antigen complex was then eluted from the beads using 20 µL of the kit provided 'elution buffer'.

The success of the immunoprecipitation process was validated using an SDS-PAGE gel electrophoresis and staining with Coomassie brilliant blue dye. 20 µL of the eluted antibody-antigen complex was supplemented with PBS and 4X Laemelli buffer containing 4% β-mercaptoethanol (Bio-Rad, UK) to achieve a final volume of 30 µL and was heated at 95 ºC for 5 minutes. The samples were then loading onto a precast SDS-PAGE gel (4–20% Mini-PROTEAN® TGX™ Precast Protein Gels, Bio-Rad, UK). PageRuler™ Plus Prestained Protein Ladder, 10 to 250 kDa (Thermo Fisher) was used as

the ladder to indicate molecular weight. Electrophoresis was performed at 150 Volts for 1 hour using a mini-Protean tetra-cell system with PowerPac™ power supply (Bio-Rad, UK) in a buffer containing tris base 25 mM, glycine 190 mM and SDS 0.1% (w/v).

The gel was then transferred to the fixing/ destaining solution (methanol 50%, 40% distilled water and 10% acetic acid) and kept on a shaker for 1 hour. The gel was then transferred to a 0.25% Coomassie brilliant blue stain containing solution (0.25% (w/v) Coomassie brilliant blue (Bio-Rad, UK), methanol 50%, 40% distilled water and 10% acetic acid) and was incubated for 1 hour with shaking. The gel was then placed in destaining solution (methanol 50%, 40% distilled water and 10% acetic acid) and gently agitated using the shaker. The destaining solution was removed and replenished every 15 minutes. The destaining process was performed till bands on the gel were clearly visible.

2.11 Mass spectrometry

Protein liquid chromatography-mass spectrometry (LC-MS) was performed on the immunoprecipitated protein sample at the Target Discovery Institute (TDI, University of Oxford) by Dr Roman Fischer's team.

For preparation of the samples for mass spectrometry, the sample was suspended in 100 mM Tris-HCL buffer (pH 7.8). Proteins were digested overnight at 37'C using 1 µg Trypsin (Promega, UK). Trypsin was inactivated by acidification with 100% formic acid to a final concentration of 1%. Peptides were cleaned-up on SOLA C18 cartridges, dried down in a vacuum centrifuge and reconstituted with 10ul 2% ACN / 0.1% formic acid.

Peptides were injected into a LC-MS system comprised of a Dionex Ultimate 3000 nano LC and a Thermo Q-Exactive. Peptides were separated on a 50-cm-long EasySpray column (ES803; Thermo Fisher) with a 75-µm inner diameter and a 60-minute gradient of 2 to 35% acetonitrile in 0.1% formic acid and 5% DMSO at t flow rate of 250 nL/min. MS1 spectra were acquired with a resolution of 70,000 and AGC target of 3e6 ions for a maximum injection time of 100 ms. The Top15 most abundant peaks were fragmented after isolation with a mass window of 1.6 Th at a resolution of 17,500. Normalized collision energy was 28% (HCD).

2.12 Fluorescence imaging

Fluorescence is the emission of one or more photons of light by the fluorophore or fluorescent probe that has been activated by the absorption of a quantum of electromagnetic radiation. In biological studies, fluorescent probes are designed to respond to a specific stimulus such as the binding of an intracellular ion (e.g. Ca^{2+}). In a fixed chemical and physical environment with constant illumination, the intensity of fluorescence is proportional to the concentration of the relevant ion. The absorption of a photon by a fluorescent probe causes it to move from its ground state to its excited state and emits photons. The emitted photon normally has less energy than the excitation photon due to some energy loss of the probe in its excited state (e.g. vibration transferring heat to the surrounding solution). The lower energy level of the emitted photon means that it will have a longer wavelength than the excitation photon.

2.12.1 Mouse atrial preparation Ca^{2+} and transmembrane voltage (V_m) dye loading and optical imaging

The fluorescence indicator used for Ca^{2+} transients in the mouse atrial preparation was Rhod-2, AM (AAT Bioquest Inc, Sunnyvale, USA). Rhod-2, AM is a single wavelength Ca^{2+} indicator based on tetramethylrhodamine with a peak excitation wavelength of 557 nm and a peak emission of 581 nm and binds to Ca^{2+} with a dissociation constant (K_d) of 570 nM (Paredes et al. 2008). Though Rhod-2 salt is cell impermeant due to its hydrophilic nature, the acetoxymethyl ester (AM) form of the indicator is sufficiently hydrophobic and can cross the cell membrane easily after which the intracellular esterases cleave the AM group, thereby trapping the active dye inside the cell. A stock of Rhod-2, AM was prepared by dissolving 10 mg of Rhod-2, AM in 10 mL of dimethyl sulfoxide (DMSO) to give a final stock concentration of 8.9 mM. The dye solution was stored at -20 ºC in 15 µL aliquots.

V_m was measured using the near-red voltage sensitive dye, Di-4-ANBDQPQ (University of Connecticut Health Center, USA). Di-4-ANBDQPQ has the advantages of easy cell loading, higher signal to noise ratio and slower internalisation rate, making it ideal for membrane voltage measurements (Matiukas et al. 2007). Di-4-ANBDQPQ has an excitation peak at 603 nm and an emission peak at 812 nm. Since there is no overlap between the excitation or emission wavelengths of Di-4-ANBDQPQ and Rhod-2, AM, this pair of dyes are an attractive option for dual dye mapping experiments where a near simultaneous measurement of Ca^{2+} transients and V_m is performed (Wang et al. 2014). A stock concentration of 29 mM of Di-4-ANBDQPQ dissolved in ethanol was prepared and stored at -20 ºC in 10 µL aliquots.

The mouse atrial sample was prepared as described above (Section 2.2). The atrial tissue (left atrium or right atrium containing the SAN) was then pinned down onto a small rectangular piece of PDMS gel by using fine insect pins. The dye loading solution was prepared on the day of experiment. The Ca^{2+} dye solution was prepared by dissolving 15 µL Rhod-2, AM in 15 mL Modified Tyrode's solution in a 50 mL falcon tube to give a final concentration of 10 µM. 10 µL Pluronic F-127 (20% solution in DMSO, Invitrogen, Carlsbad, CA, USA) was also added into the dye loading solutions to better disperse Rhod-2, AM into the solution. The PDMS gel (containing the atrial preparation) was then dropped in to the falcon tube containing the dye loading solution. The atrial preparation containing falcon tube was placed in a 36 ºC waterbath. The solution was oxygenated constantly by gentle bubbling with 95% O_2 / 5% CO_2 (heavy bubbling was avoided since it led to formation of foam due to the presence of Pluronic F-127 in the solution resulting in suboptimal dye loading). The atrial sample was incubated in the dye loading solution for 15 minutes. For the V_m dye loading, the dye loading solution was prepared by dissolving 5 µL of the Di-4-ANBDQPQ stock in 15 mL Modified Tyrode's solution in a 50 mL falcon tube to give a final concentration of 10 µM. Dye loading was performed in a similar way as to the Rhod-2, AM loading protocol, except that the incubation time was 10 minutes for Di-4-ANBDQPQ. Once the dye loading process was complete, the PDMS gel containing the atrial preparation was transferred to custom-made chamber for optical imaging. The chamber was filled with 15 mL of Modified Tyrode's solution. To prevent motion artefacts which could potentially disrupt the optical signals, the Modified Tyrode's solution was supplemented with 10 µM blebbistatin, an excitation- contraction uncoupler (Dou, Arlock, and Arner 2007). The solution was bubbled in the imaging chamber with 95 % O_2 / 5 % CO_2 gas to keep the tissue well oxygenated. The chamber was equipped with two carbon fibre electrodes on its longitudinal sides for electrical

stimulation. For experiments that required electrical stimulation, the electrodes were connected to a custom stimulator (Pharmacology Dept., Oxford) and a 1401 Micro3 digitiser (CED, Milton, Cambridgeshire) and pulse trains were devised using Spike2 software.

For optical imaging, a custom-designed system equipped with an electron multiplying charge coupled device (EMCCD) camera (Evolve 128, Photometrics, Tucson, AZ, USA) was used. Two green (to excite Ca^{2+} sensitive dye Rhod-2, AM; peak wavelength of 530 nm) and two red (to excite the voltage sensitive dye Di-4-ANBDQPQ; peak wavelength of 627 nm) LED lights (Cairn Research, Faversham, UK) were placed around the imaging chamber so as to uniformly illuminate the atrial preparation. The green LEDs were fitted with excitation bandpass filters (S555/25X, Chroma Technology GmbH, Germany) and the red LEDs were fitted with excitation bandpass filters (HQ640/50, Chroma Technology GmbH, Germany) to efficiently select the best excitation wavelength range for Rhod-2, AM and Di-4-ANBDQPQ, respectively. A multi-bandpass emission filter (ET595/50+700LP, Chroma Technology GmbH, Germany) was placed in front of the camera lens to avoid bleed-through of the excitation light and to selectively let the fluorescence emission to pass through. CaT (calcium transient) and V_m measurements were taken at high resolution (128 x 128 pixels; pixel size 66 x 66 μm) at a rate of 500 frames/sec.

Imaging was done using the EMCCD camera and controlled by the acquisition software Metamorph (Molecular Devices, California, USA). During recordings, the excitation lights were turned on and bubbling was temporarily stopped (to avoid distortion of the signals due to bubbles and motion of the solution). The data obtained from optical

imaging was analysed by ImageJ software (NIH, USA) and the optical mapping analysis software ElectroMap (O'Shea et al. 2019).

Similar imaging protocol was used for imaging SAP for optogenetic study. For optogenetic stimulation of $Pnmt^{cre/+}$/ChR2 mice SAP, rhythmic trains of blue (470nm) LED light pulses were used to stimulate the ChR2 protein overexpressed in PdCMs in the tissue. Pulse trains were devised using Spike2 software – where the time (S1) interval between pulses could be set – connected to a 1401 Micro3 digitiser (CED, UK). A constant current LED controller (Pharmacology Dept., Oxford) was used to define the pulse duration and LED current. This fed through an LED source, and the trains were administered onto the tissue via a liquid lightguide mounted over the bath containing the SAP.

2.12.2 Mouse ventricular cardiomyocyte sarcoplasmic reticulum Ca^{2+} dye loading and imaging

The fluorescent probe Mag-Fluo-4, an analog of the commonly used Ca^{2+} indicator Fluo-4, was used to image SR Ca^{2+}. The cell-permeant Mag-fluo-4, AM (Thermo Fisher Scientific, UK) with a K_d for Ca^{2+} of 22 μM, makes it useful as a low-affinity Ca^{2+} indicator. Fluo-based dyes, including Mag-Fuo-4, do not have a significant spectral shift (in either their emission or excitation wavelength) when they are bound to Ca^{2+} ions, so they are non-ratiometric. Hence, calculating absolute values of Ca^{2+} in the SR of the cardiomyocytes was not possible. The Ca^{2+} - bound Mag-Fluo-4, AM, can be excited with light at 488 nm and emitted fluorescence upon excitement can be expected at 510 nm. A stock solution of Mag-Fluo-4, AM was prepared by dissolving 50 μg (one vial) of Mag-Fluo-4, AM in 10 μL of pluronic F-127 (20% solution in DMSO, Invitrogen, Carlsbad,

CA, USA) and sonicating for 10 minutes in an ultrasonic cleaner (James Products Limited, UK) to obtain a homogenous solution. 1 mL of Modified Tyrode's isolation solution (supplemented with 250 µM calcium chloride) was added and sonicated for a further 10 minutes to obtain a final stock concentration of 60.5 µM. The dye solution was then aliquoted and stored at -20 ºC and used within one week.

The components of the solutions required for the sarcoplasmic reticulum Ca^{2+} imaging is given in Table 2.2. Isolated cardiomyocytes (section 2.3) were stored in Modified Tyrode's isolation solution (supplemented with 0.5-1% BSA and 250 µM calcium chloride). 10 µL of the dye solution was added to 90 µL cardiomyocyte suspension for a final dye concentration of 6 µM. The Mag-Fluo-4, AM treated cells were incubated in a 37 ºC mini incubation oven (Bio-Rad, UK) for 45 minutes. After the dye loading process, the cardiomyocytes were irreversibly permeabilised by saponin to remove the residual Mag-Fluo-4, AM from the cytoplasm. For this, the myocytes were first centrifuged at 0.4 G for 1 minute and the supernatant discarded. The pellet was resuspended in 100 µL Modified Tyrode's isolation solution (supplemented with 100 µM EGTA) and gently mixed to remove Ca^{2+} to avoid Ca^{2+} overload during the permeabilisation. This myocyte suspension was then centrifuged at 0.4 G for 1 minute and the supernatant discarded. This washing step was repeated twice after which the pellet was resuspended in 100 µL Internal solution and gently mixed for 30 seconds and centrifuged at 0.4 G for 1 minute. The pellet was then resuspended in 100 µL saponin containing Permeabilisation solution and gently mixed for 45 – 60 seconds. The myocytes were then centrifuged at 0.4 G for 1 minute and the pellets were resuspended in 100 µL Final internal solution. The cells were then seeded on a glass slide coated with Corning® Cell-Tak™ cell adhesive

(Corning Inc, New York, USA) and imaging experiments were carried out within 15 minutes.

A Nipkow spinning disk confocal microscope was used for imaging SR Ca^{2+}. Excitation light of 488 nm was provided by an Argon laser (Coherent, USA). The laser light passed through a confocal scanning unit (CSU-10, Yokogawa Electric Corporation, Tokyo, Japan) and entered a Nikon Axiovert 200 microscope (Zeiss, Germany) set up at a magnification of 40x by an oil immersion objective. The fluorescence signals were collected through the objective directed to an Andor iXON897 EMCCD camera (Oxford Instruments, UK). Images were recorded at a rate of 1 frame every 5 seconds for a period of 5 minutes at room temperature. To normalise the Ca^{2+} changes, a bolus of 10 mM caffeine was added to the cells at the end of each experiment to empty the SR so that the measurements could be expressed as F/F_{Caff}, where F_{Caff} is the fluorescence recorded after emptying the SR. The SR Ca^{2+} recordings were analysed using ImageJ software (NIH, USA) and Clampfit software (Axon Instruments, USA).

2.13 Recipes for solution

The recipes used for all solutions in this thesis is given in Table 2.2.

2.14 Suppliers of drugs and chemicals

All chemicals used in this thesis were obtained from Sigma-Aldrich (UK) unless otherwise specified. Solutions were made using double-deionised water with a resistivity of 18 MΩ.cm.

The SAN4825 compound was a kind gift from Sanofi (France).

Collagenase type II and IV were obtained from Worthington Biochemical (USA).

2.15 Statistics

Statistical analysis in this thesis comparing two groups were done by paired or unpaired student's t-tests for normally distributed populations. For populations not distributed normally, a Mann-Whitney test was used for unpaired data and a Wilcoxon's signed-ranked test was used for paired data.

When comparisons for more than two groups were made, an analysis of variance (ANOVA) was performed, with post-hoc tests, where appropriate. Post-hoc tests using Tukey's method was used when the mean of every group was compared to the means of every other group. Bonferroni's method was used when the mean of a particular groups were selected for comparison. Dunnet's test was used when the means of particular groups were compared to the mean of the control group.

The data in this thesis is expressed as mean ± SEM. All statistical analysis was performed on Graphpad Prism 7.

2.16 Experimental design

It is accepted that experimenter bias can be an important factor in interpreting results, and that best practice follows procedures that minimise the possible contribution of this bias. In the experiments performed in this thesis, protocols of data acquisition and automated analysis strategies were designed during the planning stage with considerations to remove experimenter bias. During experiments, measurements were made by computer-based software that returned unbiased values. No attempts were made to modify or reject any

of these measurements. Although blinding/randomisation was not used in selecting animals (between wildtype and KO), there were no systematic assignments of the order of treatments. For example, for a particular procedure it was never the case that all experiments on wildtype mice were done in one sequence followed by all experiments on KO mice. Also, randomisation was achieved by changing the order of pharmacological treatments, i.e., one type of treatment was not performed in a series of experiments, instead, different treatments were performed alternatively. These strategies, to an extent, reduced the overall risk of bias in acquisition and analysis of data in this thesis.

2.17 Group sizes for experiments

For experiments in this thesis, a minimum sample size of six was chosen, since this is the minimum size for which it would be possible to reach a P value less than 0.05 using non-parametric methods (Colquhoun 1971). This minimum sample size also permitted observations with $P < 0.05$ with drug effects in the chapters of this thesis. It is recognised that choice of sample size is the result of a compromise between minimising use of animals and ensuring that observations can detect differences (defined as showing a P value less than 0.05). Using accepted parametric methods, including 't' tests, P values less than 0.01 were frequently observed with the sample sizes used.

In chapters 3 and 6, one experiment using an atrial preparation from one mouse was considered as an "independent experiment" and was represented as n=1. In chapter 4, experiment on one isolated cardiomyocyte constituted one "independent experiment" and was represented as n=1. 8-10 cardiomyocytes from at least 4 mice (due to the limited number of mice available) were used for each experimental condition in chapter 4.

Step	**Time/ cycles**	**Temperature**
Reverse Transcription	30 minutes	50 ºC
Initial PCR activation	15 minutes	95 ºC
3- step cycling:		
1. Denaturation	45 seconds	94 ºC
2. Annealing	45 seconds	59 ºC
3. Extension	1 minute	72 ºC
Number of cycles	30 cycles	
Final Extension	10 minutes	72 ºC

Table 2.1: Conditions for RT-PCR

Solutions	Ingredients (in mM)
Modified Tyrode's solution (atrial tissue)	NaCl 119, $NaHCO_3$ 25, NaH_2PO_4 1.0, KCl 4.7, $MgCl_2$ 1.2, $CaCl_2$ 1.35, and glucose 10; pH = 7.4
Modified Tyrode's Isolation solution (ventricular myocytes)	NaCl 140, $MgCl_2$ 1.1, KCl 5.4, NaH_2PO_4 1, HEPES 5, glucose 10; pH 7.4, adjusted with NaOH
EDTA solution	NaCl 130, KCl 5, NaH_2PO_4 0.5, HEPES 10, glucose 10, BDM 10, Taurine 10, EDTA 5; pH 7.8, adjusted with NaOH
Perfusion solution	NaCl 130, KCl 5, NaH_2PO_4 0.5, HEPES 10, glucose 10, BDM 10, Taurine 10, $MgCl_2$ 1; pH 7.8, adjusted with NaOH
Collagenase solution	Collagenase II 160 units/mL, collagenase IV 160 units/mL, Protease XIV 0.21 units/mL dissolved in Perfusion solution
Cardioplegic solution	NaCl 102, KCl 21.4, $MgCl_2$ 16, Na-lactate 28.7, $CaCl_2$ 2.4, procaine 1; pH 7.4, adjusted with NaOH
SRMP solution A	Sucrose 300, KPIPES 20; pH 7.2, adjusted with KOH
SRMP solution B	KCl 2000, KPIPES 25, $MgCl_2$ 0.5, EGTA 0.5, $CaCl_2$ 0.5; pH 7.2, adjusted with KOH
SRMP solution C	Sucrose 400, HEPES 5; pH 7.2, adjusted with Tris
SRMP solution D	0.4 KCl
SRMP solution E	KCL 150, $MgCl_2$ 0.5, HEPES 10; pH 7.2, adjusted with KOH
sucrose gradients	KCl 400, KPIPES 5, $MgCl_2$ 0.1, EGTA 0.1, CaCl2 0.1; pH 7.2, adjusted with KOH + 10/20/30/40% sucrose
PMSF solution	1; dissolved in methanol
Internal solution	K-Asp 120, K_2 ATP 3, $MgCl_2$ 3, EGTA 0.1, HEPES 10, phosphocreatine 10, creatine phosphokinase 5 units/L; pH 7.2 adjusted with KOH
Permeabilisation solution	K-Asp 120, KCl 20, $MgCl_2$ 3.7, EGTA 1, HEPES 10, saponin 0.005%; pH 7.2 adjusted with KOH
Final internal solution	K-Asp 120, K_2ATP 3, $MgCl_2$ 3, EGTA 0.1, phosphocreatine 10, HEPES 10, creatine phosphokinase 5 units/L, Dextran 4% (w/v); pH 7.2 adjusted with KOH
Running buffer	Tris base 25, glycine 190, SDS 0.1% (w/v)
Transfer buffer	Tris base 25, glycine190, methanol 20% (v/v).

Table 2.2: List of solutions

Chapter 3

Contribution of NAADP signalling pathway on calcium handling at rest and during β-adrenoceptor activation in murine atria

3.1 Background

Early studies on sea urchin egg homogenates reported the discovery and the Ca^{2+} releasing capabilities of NAADP (Aarhus et al. 1995). Since then, numerous studies have established NAADP as the most potent Ca^{2+} activating second messenger due to its ability to release Ca^{2+} from intracellular stores at picomolar to nanomolar concentrations (Chini and Dousa 1995). NAADP has been reported to regulate Ca^{2+} release in a variety of mammalian cell types, which includes T-lymphocytes, pulmonary artery smooth muscle cells, pancreatic acinar and β-cells and cardiomyocytes (Boittin, Galione, and Evans 2002; Cancela, Churchill, and Galione 1999; Galione 2015; Macgregor et al. 2007; Collins et al. 2011; Capel et al. 2015).

NAADP is believed to contribute to the action of β-adrenoreceptor activation in the cardiac system. Several studies have reported an increase in the production of NAADP in cardiomyocytes when exposed to the β-adrenoceptor agonist isoprenaline (Gul et al. 2016; Macgregor et al. 2007; Lin et al. 2017; Lewis et al. 2012). Functional studies by Macgregor et al. provided insights into the role of NAADP in cardiac function. In Ca^{2+} indicator loaded isolated guinea-pig ventricular myocytes, photorelease of NAADP from a 'caged' NAADP compound resulted in the increase of Ca^{2+} transients. An increase in contraction strength and Ca^{2+} amplitude were observed by the introduction of NAADP. These effects were abolished by bafilomycin A1 or by desensitising concentrations of NAADP (Macgregor et al. 2007). Experiments on guinea-pig atrial myocytes showed similar results wherein photorelease of caged NAADP resulted in increased Ca^{2+} transients and Ca^{2+} sparks. There was no change in the L-type Ca^{2+} currents, thereby excluding the role of Ca^{2+} entry through the LTCC. This increase in Ca^{2+} transients were

sensitive to the disrupted functioning of the lysosomes through GPN or bafilomycin A1 (Collins et al. 2011). Capel et al. observed a reduced effect of isoprenaline on Ca^{2+} amplitudes and contraction in the presence of bafilomycin A1 and the NAADP antagonist Ned-19. Moreover, attenuated Ca^{2+} transients and contractions were observed in *TPC2*$^{-/-}$ mice as compared to wildtype mice. It was thus hypothesised that NAADP mobilised Ca^{2+} from acidic stores which in turn increased SR Ca^{2+} levels, resulting in enhanced Ca^{2+} transients (Capel et al. 2015).

Since the NAADP pathway is an integral part of β-adrenergic stimulation, it might also be responsible in part for the arrhythmogenic effects of β-adrenergic stimulation. Promising observations have already been published that link NAADP pathway to β-adrenergic stimulation mediated cardiac arrhythmias. Work by Nebel et al. on isolated ventricular cardiomyocytes showed that isoprenaline-induced arrhythmias were reduced in the presence of an NAADP antagonist, BZ194 (Nebel et al. 2013). Capel et al showed that hearts from *TPC2*$^{-/-}$ mice showed higher resistance to arrhythmias induced by chronic isoprenaline treatment when exposed to burst pacing than the wildtype mice (Capel et al. 2015). More recently, Lin et al. also reported a higher resistance of *CD38*$^{-/-}$ mice to arrhythmias as compared to wildtypes when treated with high doses of isoprenaline (Lin et al. 2017).

Disruption of the lysosomes with bafilomycin A1 is achieved by discharging Ca^{2+} from these acidic Ca^{2+} stores. Though NAADP also releases Ca^{2+} from lysosomes, the effect of bafilomycin A1 and NAADP on Ca^{2+} handling in a myocyte are dissimilar. This paradox might be due to the different sites of action by NAADP and bafilomycin A1 on the lysosome. NAADP is believed to elicit a sufficiently large release of Ca^{2+} from the lysosomes near the SR uptake sites by binding to a receptor (TPC2 being the most likely

candidate) and can provoke SERCA to take up the extra Ca^{2+} into the SR, while bafilomycin A1, a vacuolar H^{+}-ATPase proton pump inhibitor, might cause a slower leak of Ca^{2+} from the lysosomes which might not rise sufficiently near the SERCA sites to enhance Ca^{2+} uptake into the SR.

An intrinsic activity of NAADP pathway has been suggested in cardiac muscle. In the absence of β-adrenergic stimulation in guinea-pig cardiomyocytes, Ca^{2+} transient amplitudes were observed to be blunted in the presence of bafilomycin A1 and Ned-19. This effect was more pronounced in atrial cardiomyocytes than in ventricular myocytes since the atrial myocytes showed a decrease in Ca^{2+} transient amplitudes by 50% while the ventricular myocytes showed a decrease in amplitude by 20-25%. Since bafilomycin A1 and the NAADP antagonist supressed Ca^{2+} activity of the SR at resting conditions, a role for NAADP pathway in intrinsic Ca^{2+} handling was hypothesised (Macgregor et al. 2007; Collins et al. 2011). However, studies in *TPC2*$^{-/-}$ mice did not show a difference in basal Ca^{2+} transient amplitude from wildtype mice. Moreover, contraction strength as well as Ca^{2+} spark frequency were not significantly different between the mice models (Elson 2011). In addition, treating the myocytes with bafilomycin A1 or Ned-19 failed to evoke a response on the *TPC2*$^{-/-}$ mice at resting conditions.

In mammalian tissues, CD38 is thought to be responsible for the production of NAADP by the base exchange reaction of the substrates NADP and NA (Chini and Dousa 1995). Therefore, using a CD38 genetic knockout mouse model to study the calcium handling properties of NAADP will help understand better the mechanisms of NAADP signalling pathway. This chapter addresses the NAADP signalling pathway in intact murine atrial tissues using the CD38 genetic knockout mouse model, *CD38*$^{-/-}$. Optical mapping using Ca^{2+} and membrane voltage indicators were used to study the Ca^{2+} handling and action

potential characteristics of the NAADP pathway. There are certain advantages to using intact cardiac tissues to address pharmacological research questions. Compared to single cells or monolayer cell cultures, intact tissues have locally preserved cell-cell electrical and mechanical connections and reflect a better *in vivo* profile (Kohl and Gourdie 2014; Camelliti, Borg, and Kohl 2005).

The aim of this chapter was to study calcium handling in murine atrial tissue with respect to the NAADP pathway at both basal state and under the influence of β-adrenoceptor stimulation using wildtype and *CD38*$^{-/-}$ mice. Calcium handling and membrane voltage properties of wildtype and a genetically modified mouse model (*CD38*$^{-/-}$) were compared at their basal state in the form of a comparison of their Ca^{2+} transient and action potential profiles to evaluate the presence or absence of an intrinsic activity of NAADP pathway in murine cardiac atria. The contribution of the NAADP pathway to β-adrenergic responses in the atria were also studied using *CD38*$^{-/-}$ mice atria and by using pharmacological inhibitors (bafilomycin A1).

3.2 Methods

The methods used in this chapter have been detailed in chapter 2. Wildtype and *CD38*$^{-/-}$ mice (aged 10-14 weeks, both males and females) were sacrificed by concussion and cervical dislocation before the heart was quickly excised. The cardiac atria were isolated as described in Section 2.2.

For experiments performed on the left atria, the left atrium was isolated from the whole atrial preparations. To obtain Ca^{2+} transient signals, the left atrial tissue was incubated in 10 μM of the Ca^{2+} indicator, Rhod-2, AM in Modified Tyrode's solution for 15 minutes before being pinned onto a custom-made imaging chamber filled with Modified Tyrode's solution and placed under the optical mapping setup as described in Section 2.12.1. The optical mapping set-up is shown is Figure 3.1. The temperature was maintained at 36º C using a heating pad. 10 μM blebbistatin was added to the chamber and a 5-minute incubation was sufficient to stop the beating of the atria. The chamber, equipped with two carbon fibre electrodes on its longitudinal sides facilitated the electrical stimulation of the atrial tissue at 5 Hz. While signal recordings were not taken, the chamber was vigorously oxygenated by bubbling with 95% O_2 / 5% CO_2. LED lights were placed around the chamber to ensure uniform lighting to the tissue. To take a fluorescent recording, the bubbling was stopped, followed by a wait of a few seconds to allow the solution to become clear. Calcium transients were recorded using the image acquisition software Metamorph. A 20 x 20-pixel region was selected from the tissue samples and analysed by the softwares ImageJ and Electromap to keep the analysis region constant across samples. The fluorescent values were normalised to the baseline values (F_0) and represented as $((F- F_0)/F_0)$ (represented as $\Delta F/F_0$ in the Figures of this chapter) and the

highest average Ca^{2+} transient amplitude was calculated as the peak Ca^{2+} transient amplitude.

Due to the limited availability of *CD38*$^{-/-}$ mice, the left atria were used for Ca^{2+} transient studies while action potential signals were recorded on the spontaneously beating right atria (which includes the sino-atrial node). The action potentials recordings were obtained by incubating the spontaneously beating right atria in 10 μM of the membrane voltage indicator, Di-4-ANBDQPQ for 10 minutes before being pinned onto the imaging chamber and optically imaged as mentioned above. These membrane voltage indicator loaded right atria were also used to study the heart rate experiments. The recordings were analysed with ImageJ and Electromap.

3.3 Results

3.3.1 Intrinsic activity of the NAADP pathway in murine cardiac atria

To test whether the NAADP pathway has an ongoing activity in the atria under resting conditions, various calcium handling and membrane potential parameters, and heart rates were tested and compared in wildtype and *CD38*$^{-/-}$ mice. Any differences in these characteristics can unlock potential clues in the functioning of the NAADP pathway in cardiac physiology.

3.3.1.1 No differences were observed in the Ca^{2+} transient amplitudes of electrically stimulated atria at resting conditions between wildtype and *CD38*$^{-/-}$ mice.

The peak Ca^{2+} transient amplitudes from wildtype and *CD38*$^{-/-}$ mice were recorded and analysed at resting conditions (without the influence of drugs) at a pacing frequency of 5 Hz. No significant differences were observed between the resting Ca^{2+} transient amplitudes of wildtype and *CD38*$^{-/-}$ mice atrial tissues (Figure 3.2). The mean Ca^{2+} transient amplitude of the wildtype atria was observed to be 0.51 ± 0.08, while the mean Ca^{2+} transient amplitude of the *CD38*$^{-/-}$ atria was 0.41 ± 0.06 (P=0.59, n=7).

3.3.1.2 Wildtype and *CD38*$^{-/-}$ mice had comparable resting heart rates

Resting heart rates of wildtype and *CD38*$^{-/-}$ mice were compared and no significant differences were observed between the two groups (P=0.114) (Figure 3.3). The mean heart rate of wildtype mice were 245 ± 8 beats per minute while *CD38*$^{-/-}$ mice had a mean heart rate of 269 ± 11 beats (n=7 for both groups).

3.3.1.3 No significant differences observed between the Ca^{2+} transient durations and action potential durations in isolated atria at resting conditions between wildtype and *CD38*$^{-/-}$ mice.

The Ca^{2+} transient durations (CaDs) were calculated from the recorded Ca^{2+} transients of electrically paced left atria from wildtype and *CD38*$^{-/-}$ mice at resting conditions. Ca^{2+} transients were analysed using Electromap software to measure their duration at 10%, 50% and 80% repolarisation (CaD10, CaD50 and CaD80, respectively). The pacing frequency was constant was 5 Hz.

No significant difference was observed for the CaDs of wildtype and *CD38*$^{-/-}$ mice at resting conditions (P=0.84, n=6). The mean data of the CaDs of the two groups are shown in Figure 3.4.

The action potential durations (APD) were calculated from the recorded action potentials of spontaneously beating right atria from wildtype and *CD38*$^{-/-}$ mice at resting conditions measured using the transmembrane voltage indicator Di-4-ANBDQPQ. Di-4-ANBDQPQ was loaded on the atrial tissue and optical mapping was used to record action potential signals. The action potentials were analysed using Electromap software to measure their duration at 10%, 50% and 90% repolarisation (APD10, APD50 and APD90, respectively).

No significant difference was observed for the APDs of wildtype and *CD38*$^{-/-}$ mice at resting conditions (P=0.36, n=6). The mean data of the APDs of the two groups are shown in Figure 3.6.

3.3.1.4 The conduction velocity at resting conditions were not significantly different in electrically stimulated atria of wildtype and *CD38*$^{-/-}$ mice.

Conduction velocity was analysed from the Ca^{2+} transient signals obtained from isolated left atria of wildtype and *CD38*$^{-/-}$ mice stimulated at 5 Hz using electromap. At resting conditions, the conduction velocity was not significantly different in wildtype and *CD38*$^{-/-}$ mice (P=0.79, n=6) (Figure 3.5). The mean conduction velocity of wildtype mice was 33.5 ± 7.3 cm/sec while the mean conduction velocity of *CD38*$^{-/-}$ mice was 31.4 ± 3.5 cm/sec.

3.3.1.5 Bafilomycin A1 had no effect on the Ca^{2+} transient amplitudes and resting heart rates of isolated atria from wildtype and *CD38*$^{-/-}$ mice at resting conditions.

To assess whether the NAADP pathway had an active intrinsic effect on Ca^{2+} transient amplitudes in murine atria, bafilomycin A1 was used to disrupt the lysosomes. Isolated left atria from wildtype and *CD38*$^{-/-}$ mice were preincubated in 5 μM bafilomycin A1 containing Modified Tyrode's solution for 1 hour before the dye loading process and optical imaging. The pacing frequency was held constant at 5 Hz. Ca^{2+} transients were then recorded and analysed using Electromap to calculate the Ca^{2+} transient amplitudes. Spontaneously beating right atria from wildtype and *CD38*$^{-/-}$ mice were preincubated in 5 μM bafilomycin A1 containing Modified Tyrode's solution for 1 hour before analysing the heart rates.

There were no significant differences observed between Ca^{2+} transient amplitudes in the isolated left atria of wildtype mice in the presence and absence of bafilomycin A1 (P=0.9871, n=6). Similarly, no significant differences could be observed in the Ca^{2+}

transient amplitudes in *CD38*$^{-/-}$ mice in the presence and absence of bafilomycin A1 (P=0.9970, n=6). These results are summarised in Figure 3.7.

Wildtype mice showed no difference in heart rate in the presence or absence of bafilomycin A1 (P=0.997, n=7). No significant differences could be observed in the resting heart rates of *CD38*$^{-/-}$ mice in the presence or absence of bafilomycin A1 (P=0.250, n=7). These results are summarised in Figure 3.8.

3.3.2 Effect of NAADP pathway in murine cardiac atria during β-adrenoreceptor activation

To study the role of NAADP pathway when murine atria is exposed to β-adrenergic stress, a series of experiments were performed using wildtype and *CD38*$^{-/-}$ mice by exposing them to the β-adrenoreceptor agonist isoprenaline under different conditions.

3.3.2.1 The effect of isoprenaline on calcium transient amplitudes and heart beating rate were blunted in *CD38*$^{-/-}$ mice as compared to wildtype mice.

Ca^{2+} indicator Rhod-2, AM loaded isolated left atria of wildtype and *CD38*$^{-/-}$ was electrically stimulated at 5 Hz. 10 nM isoprenaline was added to the imaging chamber and the Ca^{2+} transients were recorded after 3 minutes. The Ca^{2+} transients were analysed using Electromap and the peak Ca^{2+} amplitudes were calculated. The increase in Ca^{2+} transient amplitudes due to the effect of isoprenaline was calculated as the percentage change of Ca^{2+} transient amplitude before and after isoprenaline treatment. The increase in Ca^{2+} transient amplitude in *CD38*$^{-/-}$ mice was reduced as compared to the wildtype mice. While the mean increase of the Ca^{2+} transient amplitude was 59.3 ± 4.9% after the isoprenaline treatment in wildtype mice, it was 35.9 ± 2.6% in *CD38*$^{-/-}$ mice after

isoprenaline treatment. The mean difference between the two groups were 23.4 ± 5.4% (P=0.0016, n=6 in both groups). The results are summarised in Figure 3.9.

To test the effect of isoprenaline in the heart beating rate of wildtype and *CD38*$^{-/-}$ mice, 10 nM isoprenaline was added to spontaneously beating right atria and recordings were taken after 3 minutes. The increase in heart beating rate was calculated as a percentage change of the heart rate before and after isoprenaline. *CD38*$^{-/-}$ mice showed a reduced increase in the heart beating rate as compared to the wildtype mice when exposed to isoprenaline. The mean increase of heart rate in *CD38*$^{-/-}$ mice was 26.5 ± 2.1% and the mean increase in wildtype mice was 46.3 ± 3.3% when treated with isoprenaline. The increase in heart rate in *CD38*$^{-/-}$ was reduced by 19.9 ± 4% as compared to the wildtype when treated with isoprenaline (P=0.0006, n=6). These results are summarised in Figure 3.13.

3.3.2.2 The effect of isoprenaline on calcium transient amplitudes and heart beating rate were reduced in wildtype mice in the presence of bafilomycin A1.

Isolated left atria from wildtype mice were preincubated in 5 µM bafilomycin A1 (or DMSO in control samples) for 1 hour before Rhod-2, AM loading and optical imaging at a pacing frequency of 5 Hz. 10 nM isoprenaline was added to the imaging chamber and the Ca^{2+} transients were recorded after 3 minutes. The increase in Ca^{2+} transient amplitudes due to the effect of isoprenaline was calculated as the percentage change of Ca^{2+} transient amplitude before and after isoprenaline treatment. The control tissues showed a Ca^{2+} transient amplitude increase of 59.3 ± 4.8% after isoprenaline treatment. The bafilomycin A1 treated atrial tissue showed an increase of 35.3 ± 2.7% after isoprenaline treatment. The bafilomycin A1 treated tissues had a 24 ± 5.6% reduced effect

on Ca^{2+} transient amplitudes as compared to control tissues (P=0.0015, n=6 for each group) (Figure 3.10).

Spontaneously beating right atria of wildtype mice were preincubated in 5 μM bafilomycin A1 (or DMSO in control samples) for one hour. 10 nM isoprenaline was then added to the imaging chamber and heart beating rates were observed after 3 minutes. The increase in heart beating rate was calculated as a percentage change of the heart rate before and after isoprenaline. While the control tissue samples showed a heart rate increase of 46.3 ± 3.7%, the bafilomycin A1 treated atrial tissues showed an increase of heart rate by 25.7 ± 2.3%. The bafilomycin A1 treated tissue had a blunted increase in heart rate as compared to the control atrial tissues (20.7 ± 4.1%) (P=0.0005, n=6 for each group) (Figure 3.14).

3.3.2.3 Bafilomycin A1 had no effect on the Ca^{2+} transient amplitudes and heart beating rate in *CD38*$^{-/-}$ mice treated with isoprenaline

Isolated left atria from *CD38*$^{-/-}$ mice were preincubated in 5 μM bafilomycin A1 (or DMSO in control samples) for 1 hour before Rhod-2, AM loading and optical imaging at a pacing frequency of 5 Hz. 10 nM isoprenaline was added to the imaging chamber and the Ca^{2+} transients were recorded after 3 minutes. There were no significant differences in the increase in Ca^{2+} transient amplitudes in the DMSO treated or bafilomycin A1 treated atrial tissues on the application of isoprenaline (Figure 3.11). The mean Ca^{2+} transient amplitude increases of the DMSO treated and bafilomycin A1 treated atrial tissues were 35.9 ± 2.6% and 33.6 ± 4%, respectively (P=0.647, n=6).

Spontaneously beating right atria of *CD38*$^{-/-}$ mice were preincubated in 5 μM bafilomycin A1 (or DMSO in control samples) for one hour. 10 nM isoprenaline was then added to the imaging chamber and heart beating rates were observed after 3 minutes. There were no significant differences in the increase in heart beating rate in the DMSO treated or bafilomycin A1 treated atrial tissues on the application of isoprenaline (Figure 3.15). The mean heart rate increase in DMSO treated atrial tissue was 26.5 ± 2.1% while the bafilomycin A1 treated tissue samples showed a mean increase of 27 ± 2% (P=0.659, n=6).

A summary of the effect of β-adrenoreceptor activation on Ca^{2+} transient amplitudes and heart rate on bafilomycin A1 treated wildtype and *CD38*$^{-/-}$ mice is shown on Figure 3.12. and Figure 3.16, respectively.

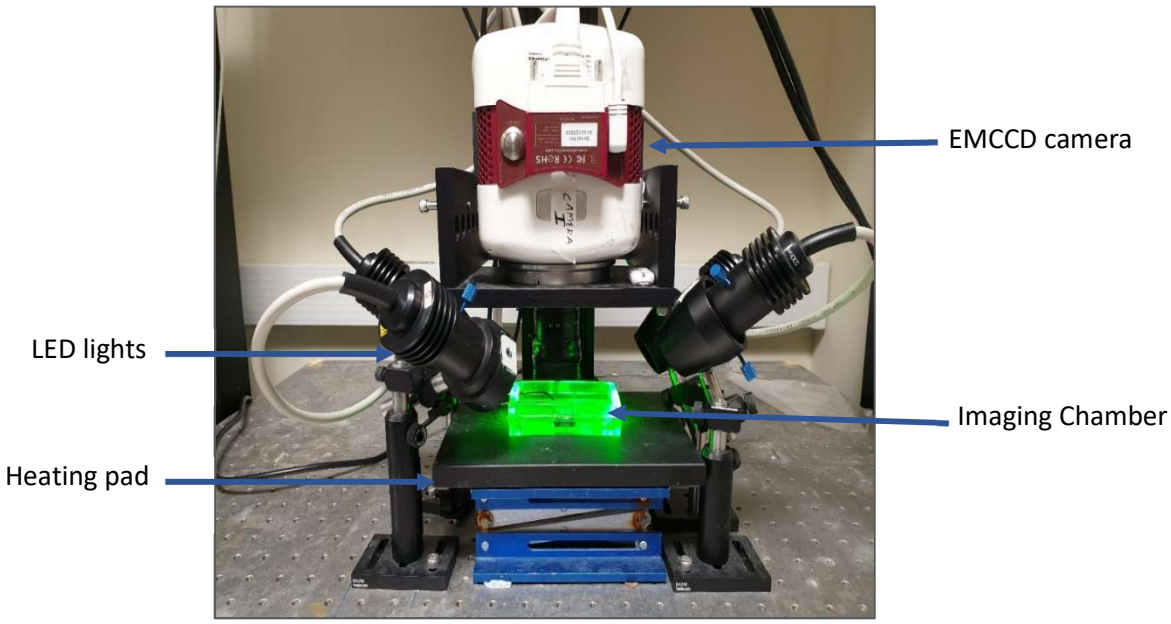


Figure 3.1: Imaging set-up for the optical mapping of Rhod-2 and Di-4-ANBDQPQ in murine isolated atrial tissues.

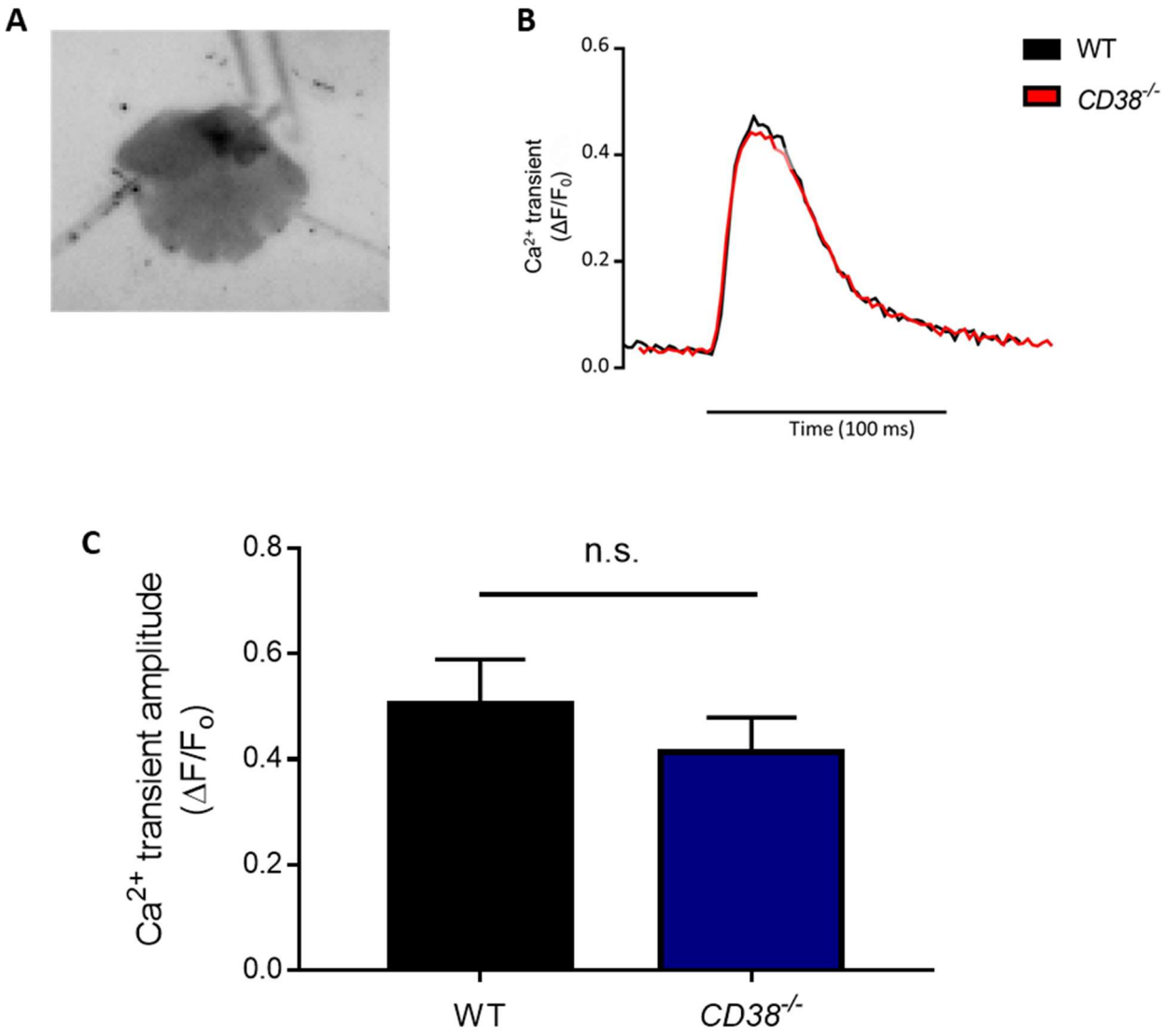


Figure 3.2: Baseline calcium transient amplitudes of electrically stimulated isolated left atria of wildtype and *CD38*$^{-/-}$ mice.

A show a sample image of an isolated left atrium.

B shows representative raw traces of Ca^{2+} transients from isolated left atria of wildtype and *CD38*$^{-/-}$ mice

C No significant differences were seen in the baseline calcium transients of wildtype and *CD38*$^{-/-}$ mice.

Note: Rhod-2, AM loaded mouse left atrial tissue was electrically paced at 5 Hz in a chamber filled with Modified Tyrode's solution supplemented with 10 µM blebbistatin at 36 ˚C (n=7 for each group). Fluorescence signal was analysed using ImageJ and Electromap. Numerical data is reported as the mean ± SEM. P>0.05, Mann-Whitney test was used to compare the means of the two groups.

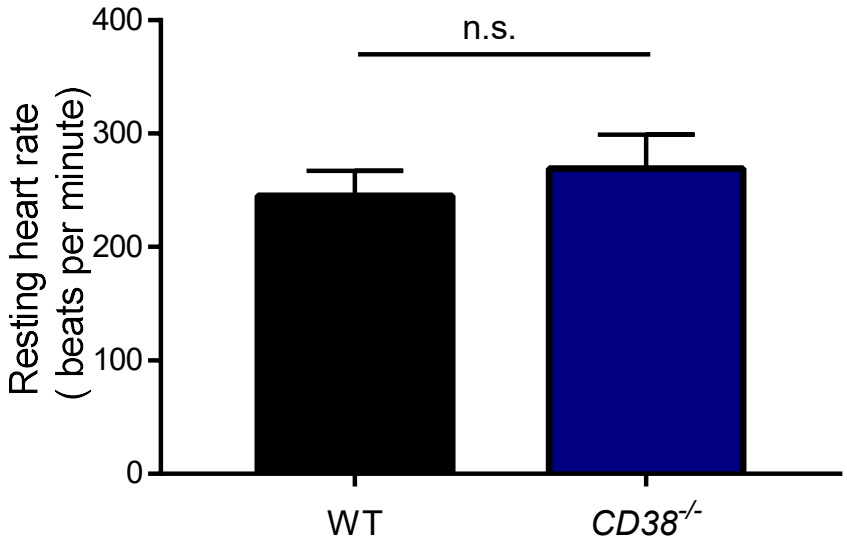


Figure 3.3: Resting heart rate of spontaneously beating isolated right atria of wildtype and *CD38*$^{-/-}$ mice.

No significant differences were seen in the baseline heart rates of wildtype and *CD38*$^{-/-}$ mice.

Note: Mouse right atrial tissue was placed in a chamber filled with Modified Tyrode's at 36 ˚C (n=7 for each group). Numerical data is reported as the mean ± SEM. P>0.05, Unpaired Student's t-test was used to compare the means of the two groups.

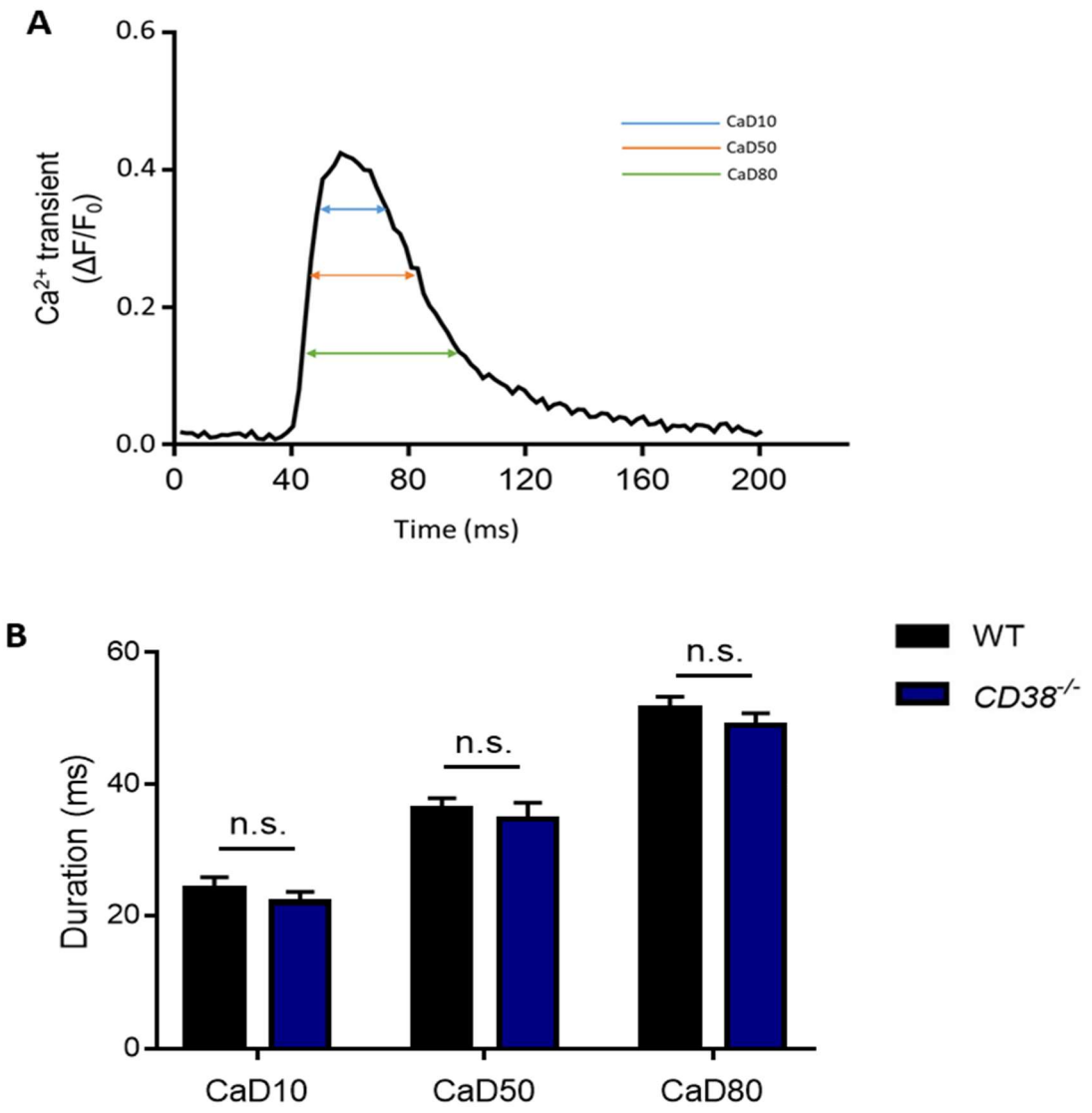


Figure 3.4: Calcium transient durations (CaD10, CaD50, CaD80) of electrically stimulated isolated left atria of wildtype and *CD38*$^{-/-}$ mice at resting conditions.

A shows a representative calcium transient illustrating CaD10 (calcium transient duration at 10% of the decay); and CaD50 (calcium transient duration at 50% of the decay) and CaD80 (calcium transient duration at 80% of the decay).

B There are no significant differences in the calcium transient durations (CaD10, CaD50 and CaD80) between wildtype and *CD38*$^{-/-}$ mice at resting conditions.

Note: Rhod-2, AM loaded mouse left atrial tissue was electrically paced at 5 Hz in a chamber filled with Modified Tyrode's solution supplemented with 10 μM blebbistatin at 36 ˚C (n=6 for each group). Fluorescence signal was analysed using ImageJ and Electromap. Numerical data is reported as the mean ± SEM. P>0.05, two-way ANOVA with Bonferroni's multiple comparisons test was used to compare the means of the two groups.

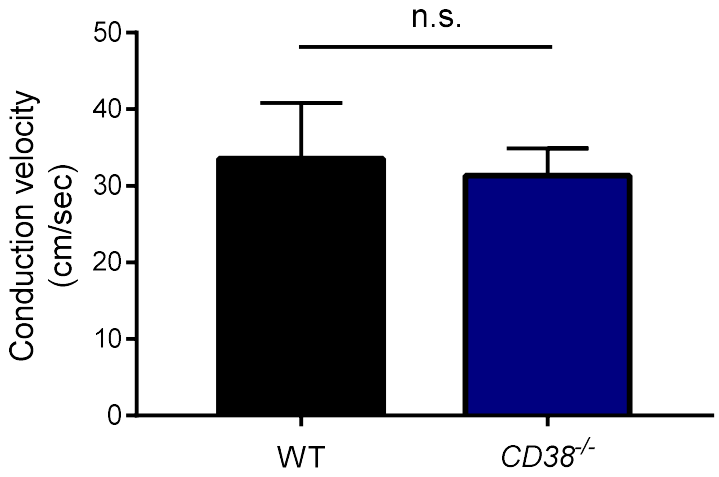


Figure 3.5: Baseline conduction velocity of electrically stimulated isolated left atria of wildtype and *CD38*$^{-/-}$ mice.

No significant differences were seen in the baseline conduction velocities of wildtype and *CD38*$^{-/-}$ mice.

Note: Rhod-2, AM loaded mouse left atrial tissue was electrically paced at 5 Hz in a chamber filled with Modified Tyrode's solution supplemented with 10 μM blebbistatin at 36 ˚C (n=6 for each group). Fluorescence signal was analysed using ImageJ and Electromap. Numerical data is reported as the mean ± SEM. P>0.05, Student's t-test was used to compare the means of the two groups.

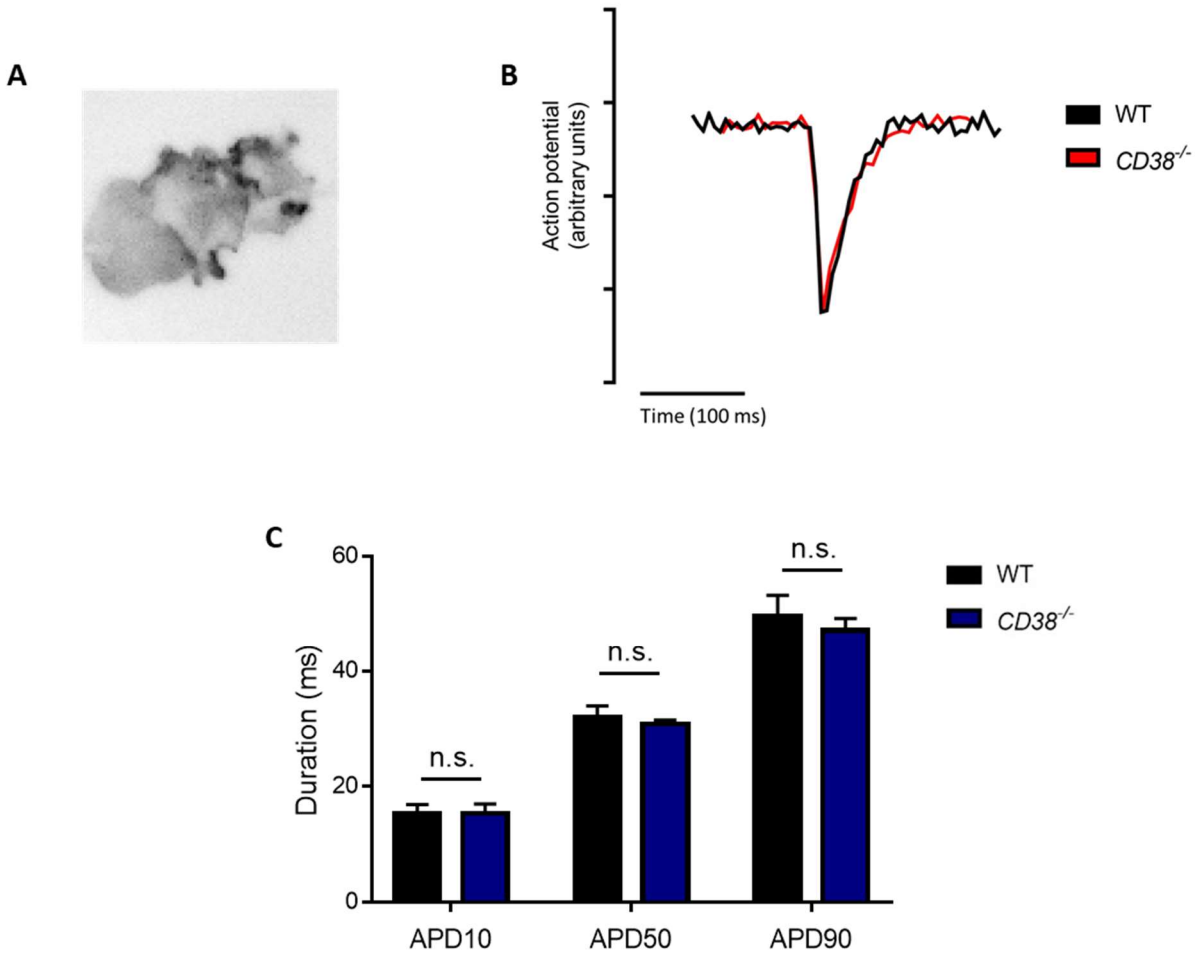


Figure 3.6: Action potential durations (APD10, APD50, APD90) of spontaneously beating isolated right atria of wildtype and *CD38*$^{-/-}$ mice at resting conditions.

A show a sample image of a spontaneously beating right atrium containing the SA node.

B shows representative raw traces of action potentials from spontaneously beating right atria of wildtype and *CD38*$^{-/-}$ mice

C shows the APD10, APD50 and APD90 in wildtype and *CD38*$^{-/-}$ mice at resting conditions. There are no significant differences in the action potential durations between the two groups.

Note: Di-4-ANBDQPQ loaded spontaneously beating mouse right atrial tissue was placed in a chamber filled with Modified Tyrode's solution supplemented with 10 µM blebbistatin at 36 ˚C (n=6 for each group). Fluorescence signal was analysed using ImageJ and Electromap. Numerical data is reported as the mean ± SEM. P>0.05, two-way ANOVA with Bonferroni's multiple comparisons test was used to compare the means of the two groups.

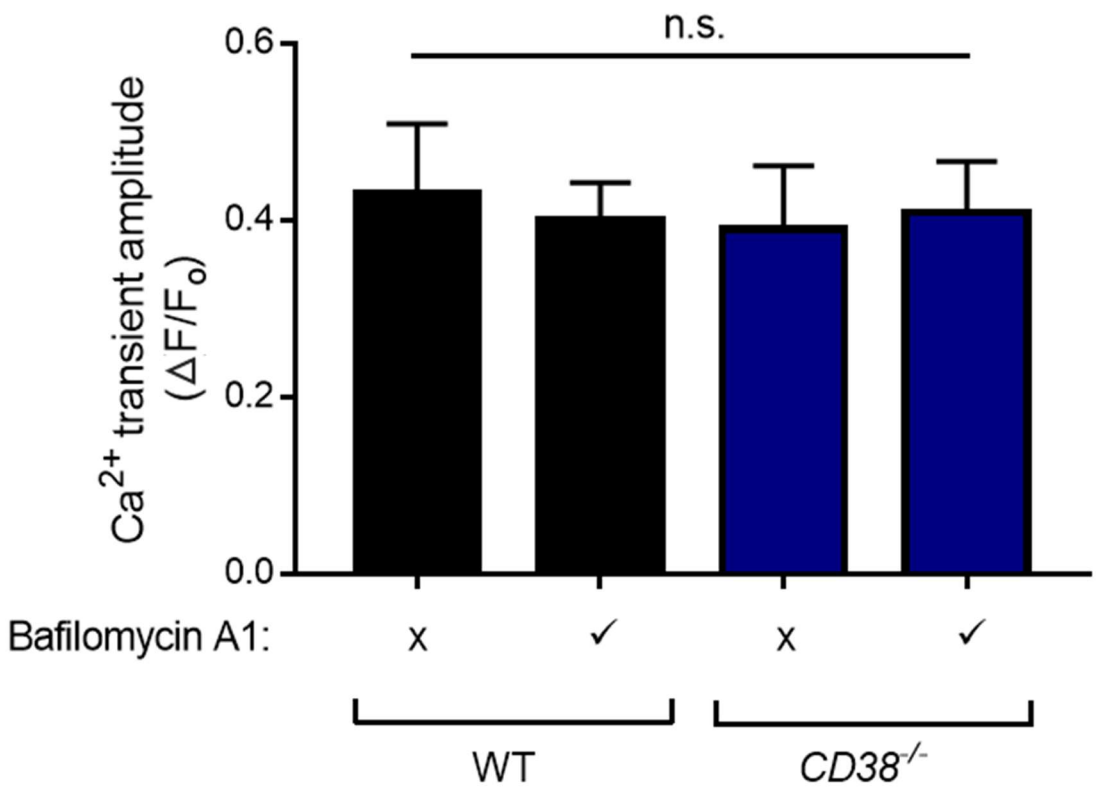


Figure 3.7: Baseline calcium transient amplitudes of electrically stimulated isolated left atria of wildtype and *CD38*$^{-/-}$ mice in the presence of Bafilomycin A1.

No significant differences were seen in the baseline calcium transients of wildtype and *CD38*$^{-/-}$ mice in the presence of Bafilomycin A1 (5 μM).

Note: Rhod-2, AM loaded mouse left atrial tissue was electrically paced at 5 Hz in a chamber filled with Modified Tyrode's solution supplemented with 10 μM blebbistatin at 36 ˚C (n=6 for each group). Fluorescence signal was analysed using ImageJ and Electromap. Numerical data is reported as the mean ± SEM. P>0.05, One-way ANOVA with Tukey's multiple comparisons test was used to compare the means of the groups.

.

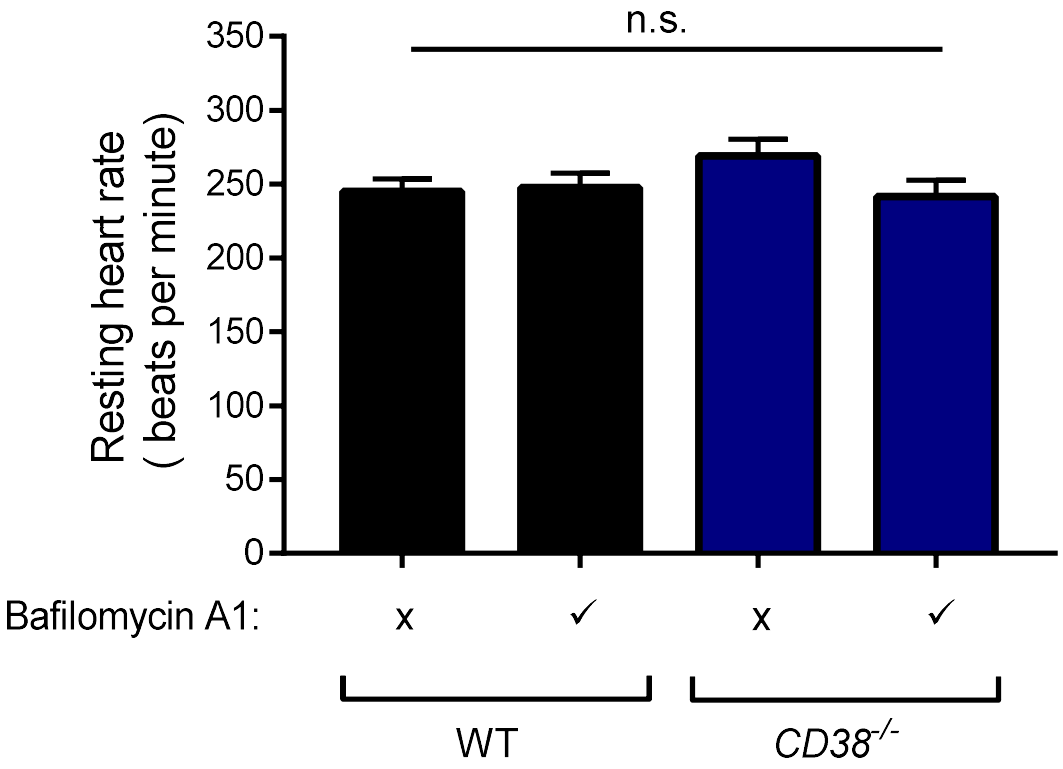


Figure 3.8: Resting heart rate of spontaneously beating isolated right atria of wildtype and *CD38*$^{-/-}$ mice in the presence of bafilomycin A1.

No significant differences were seen in the baseline heart rates of wildtype and *CD38*$^{-/-}$ mice in the presence of Bafilomycin A1 (5 μM).

Note: Mouse right atrial tissue was placed in a chamber filled with Modified Tyrode's at 36 ˚C (n=7 for each group). Numerical data is reported as the mean ± SEM. P>0.05, One-way ANOVA with Tukey's multiple comparisons test was used to compare the means of the groups.

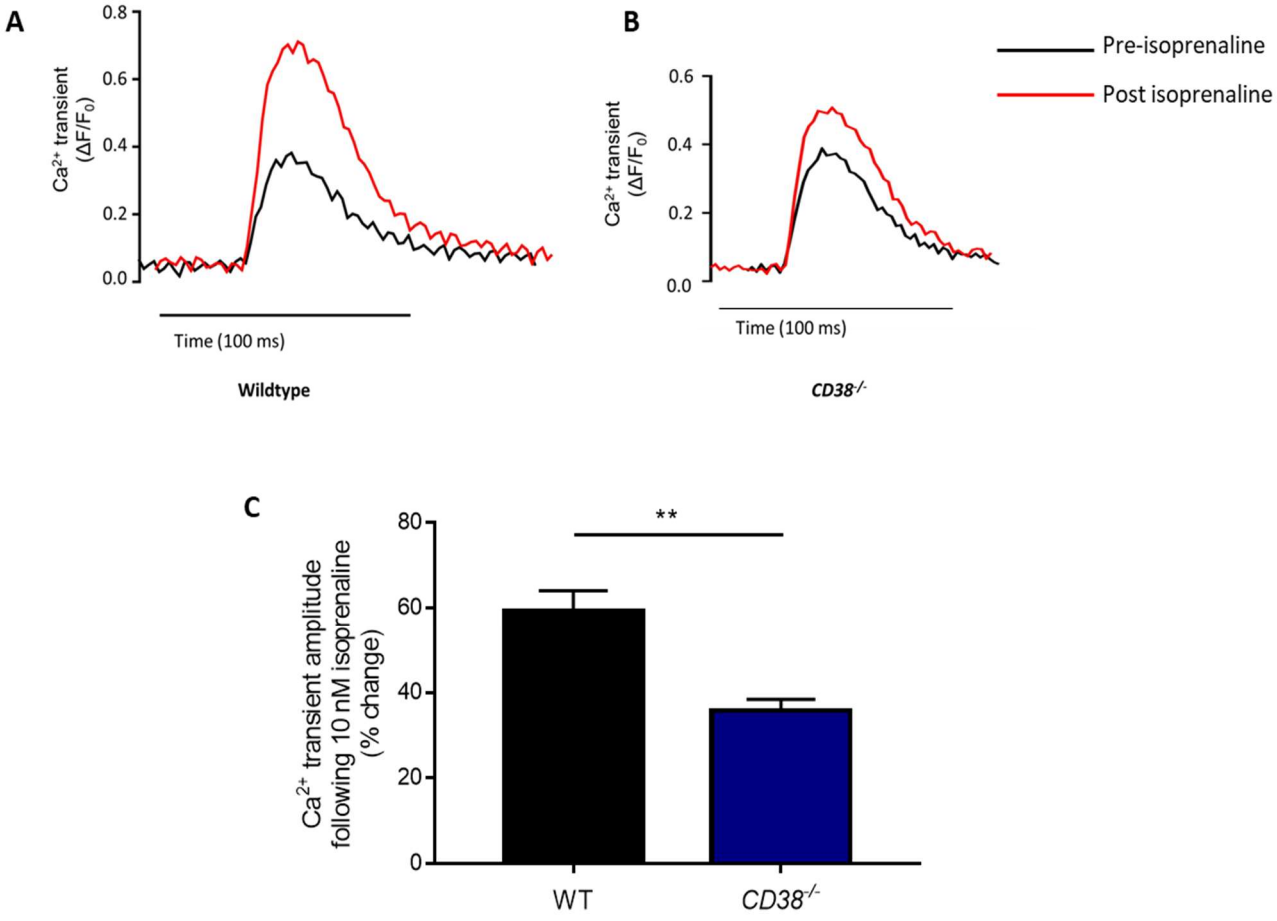


Figure 3.9: Percentage change in calcium transient amplitudes of electrically stimulated isolated left atria of wildtype and *CD38*$^{-/-}$ mice during activation of β–adrenoreceptors.

A shows a representative Ca^{2+} transient trace in isolated left atria of wildtype mouse before and after exposure to 10 nM isoprenaline.

B shows a representative Ca^{2+} transient trace in isolated left atria of *CD38*$^{-/-}$ mouse before and after exposure to 10 nM isoprenaline

C In the presence of 10 nM isoprenaline, the increase in Ca^{2+} transient amplitude in wildtype mice was significantly more than that of *CD38*$^{-/-}$ mice.

Note: Rhod-2, AM loaded mouse left atrial tissue was electrically paced at 5 Hz in a chamber filled with Modified Tyrode's solution supplemented with 10 µM blebbistatin at 36 ˚C (n=6 for each group). 10 nM isoprenaline was added to the chamber and recordings were taken after 3 minutes. Fluorescence signal was analysed using ImageJ and Electromap. Numerical data is reported as the mean ± SEM. ** denotes P<0.01, Unpaired Student's t-test was used to compare the means of the two groups.

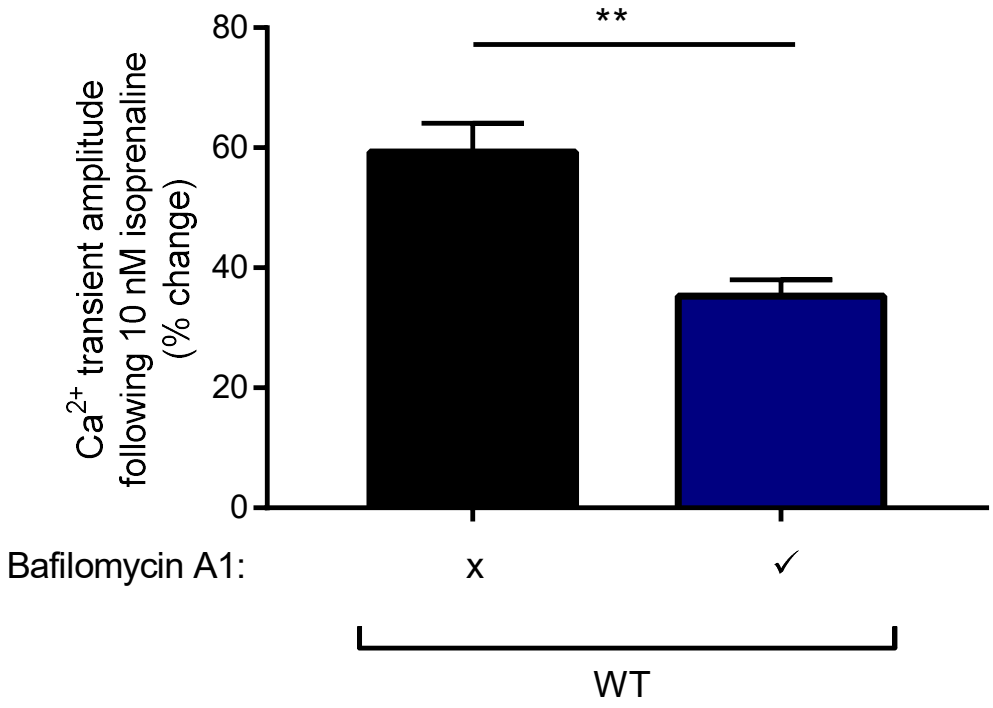


Figure 3.10: Percentage change in calcium transient amplitudes of electrically stimulated isolated left atria of wildtype mice during activation of β–adrenoreceptors in the presence of bafilomycin A1 (5 µM).

On the application of 10 nM isoprenaline, the increase in Ca^{2+} transient amplitude was significantly blunted when the atrial tissue of wildtype mice was preincubated with bafilomycin A1 (5 µM) as compared to non-treated atrial tissue.

Note: Rhod-2, AM loaded mouse left atrial tissue was electrically paced at 5 Hz in a chamber filled with Modified Tyrode's solution supplemented with 10 µM blebbistatin at 36 ˚C (n=6 for each group). 10 nM isoprenaline was added to the chamber and recordings were taken after 3 minutes. Fluorescence signal was analysed using ImageJ and Electromap. Numerical data is reported as the mean ± SEM. ** denotes $P<0.01$, Unpaired Student's t-test was used to compare the means of the two groups.

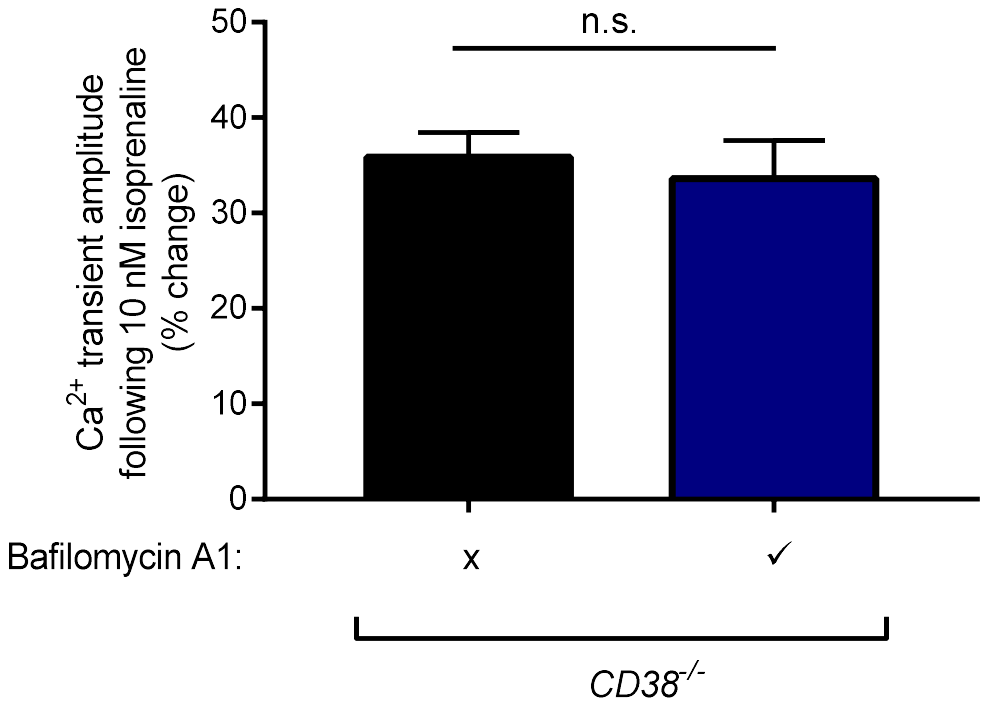


Figure 3.11: Percentage change in calcium transient amplitudes of electrically stimulated isolated left atria of *CD38*$^{-/-}$ mice during activation of β–adrenoreceptors in the presence of Bafilomycin A1 (5 µM).

On the application of 10 nM isoprenaline, there was no significant difference in the increase of Ca^{2+} transient amplitude when the atrial tissue of *CD38*$^{-/-}$ mice was preincubated with bafilomycin A1 (5 µM) and the untreated atrial tissue.

Note: Rhod-2, AM loaded mouse left atrial tissue was electrically paced at 5 Hz in a chamber filled with Modified Tyrode's solution supplemented with 10 µM blebbistatin at 36 ˚C (n=6 for each group). 10 nM isoprenaline was added to the chamber and recordings were taken after 3 minutes. Fluorescence signal was analysed using ImageJ and Electromap. Numerical data is reported as the mean ± SEM. P>0.05, Unpaired Student's t-test was used to compare the means of the two groups.

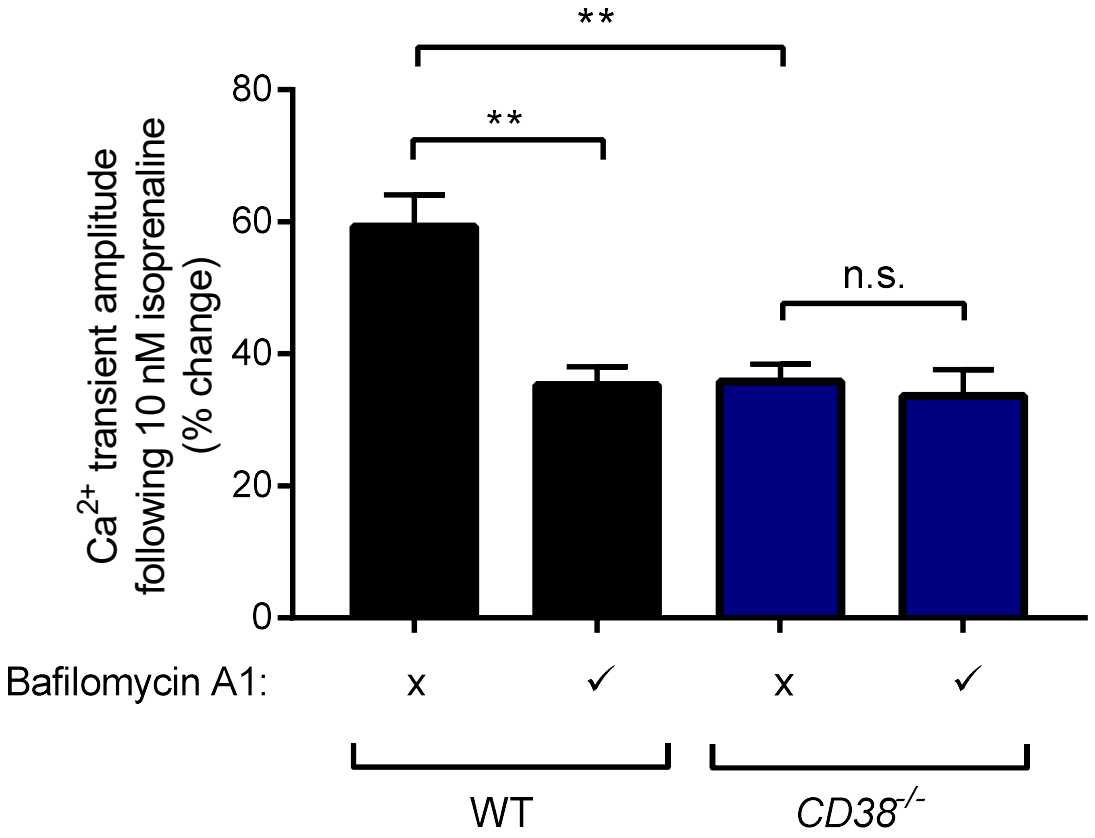


Figure 3.12: Summary of percentage change in calcium transient amplitudes of electrically stimulated isolated left atria of wildtype and *CD38*$^{-/-}$ mice during activation of β–adrenoreceptors in the presence of Bafilomycin A1 (5 μM).

On the application of 10 nM isoprenaline, there was significant differences in the increase of Ca^{2+} transient amplitude when the atrial tissue of wildtype mice was preincubated with bafilomycin A1 (5 μM) as compared to preincubation with DMSO. Significant differences were seen in the increase of Ca^{2+} transient amplitude between atrial tissue of wildtype mice and *CD38*$^{-/-}$ mice when exposed to 10 nM isoprenaline in the absence of bafilomycin A1. No significant change was seen in Ca^{2+} transient amplitude when the atrial tissue of *CD38*$^{-/-}$ mice was preincubated with bafilomycin A1 (5 μM) as compared to preincubation with DMSO.

Note: Rhod-2, AM loaded mouse left atrial tissue was electrically paced at 5 Hz in a chamber filled with Modified Tyrode's solution supplemented with 10 μM blebbistatin at 36 ˚C (n=6 for each group). 10 nM isoprenaline was added to the chamber and recordings were taken after 3 minutes. Fluorescence signal was analysed using ImageJ and Electromap. Numerical data is reported as the mean ± SEM. ** denotes $p<0.01$, One-way ANOVA with Tukey's multiple comparisons test was used to compare the means of the groups.

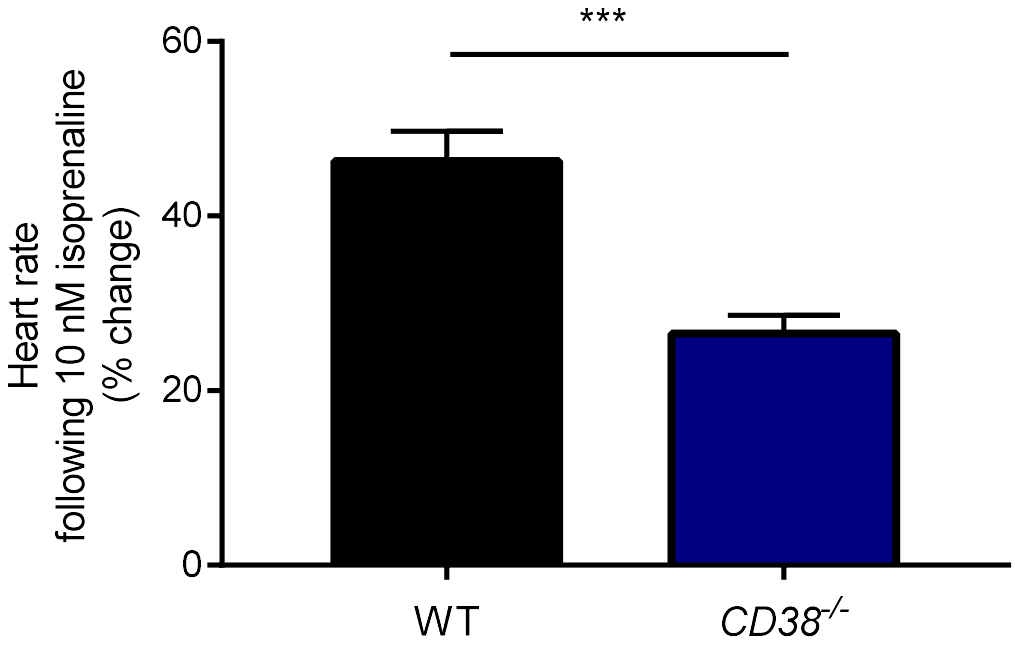


Figure 3.13: Percentage change in heart rate of spontaneously beating isolated right atria of wildtype and *CD38*$^{-/-}$ mice during activation of β–adrenoreceptors.

In the presence of 10 nM isoprenaline, the increase in heart rate in wildtype mice was significantly more than that of *CD38*$^{-/-}$ mice.

Note: Mouse right atrial tissue was placed in a chamber filled with Modified Tyrode's at 36 ˚C (n=6 for each group). 10 nM isoprenaline was added to the chamber and recordings were taken after 3 minutes. Numerical data is reported as the mean ± SEM. *** denotes $P<0.001$, unpaired Student's t-test was used to compare the means of the two groups.

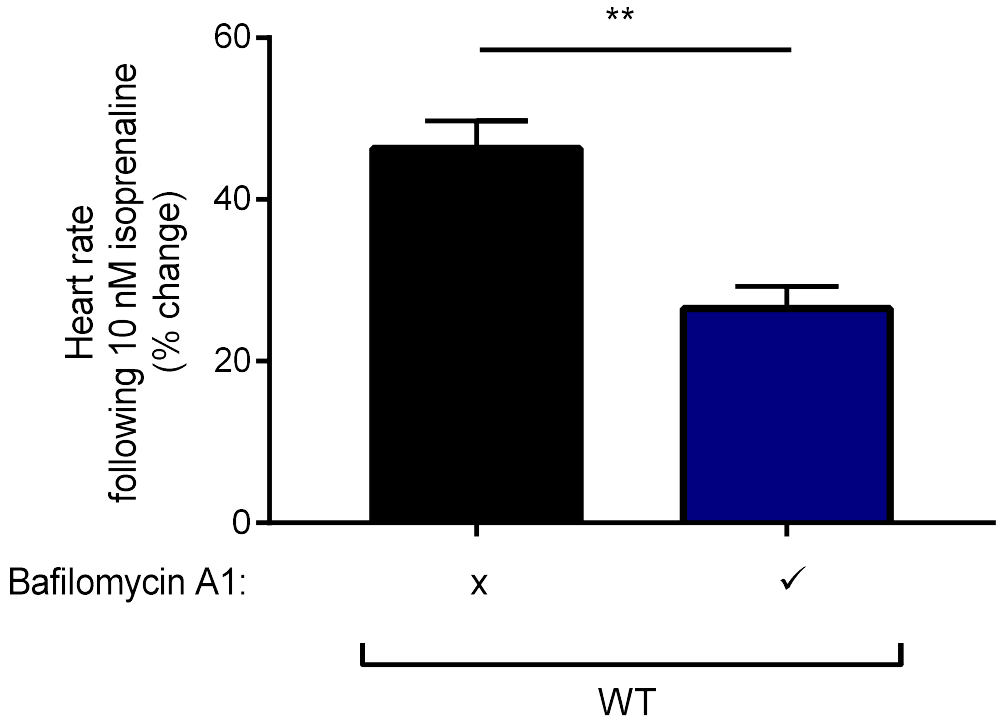


Figure 3.14: Percentage change in heart rate of spontaneously beating isolated right atria of wildtype mice during activation of β–adrenoreceptors in the presence of Bafilomycin A1 (5 µM).

On the application of 10 nM isoprenaline, the increase heart rate was significantly blunted when the atrial tissue of wildtype mice was preincubated with bafilomycin A1 (5 µM) as compared to non-treated treated atrial tissue.

Note: Mouse right atrial tissue was placed in a chamber filled with Modified Tyrode's at 36 ˚C (n=6 for each group). 10 nM isoprenaline was added to the chamber and recordings were taken after 3 minutes. Numerical data is reported as the mean ± SEM. ** denotes $P<0.01$, unpaired Student's t-test was used to compare the means of the two groups.

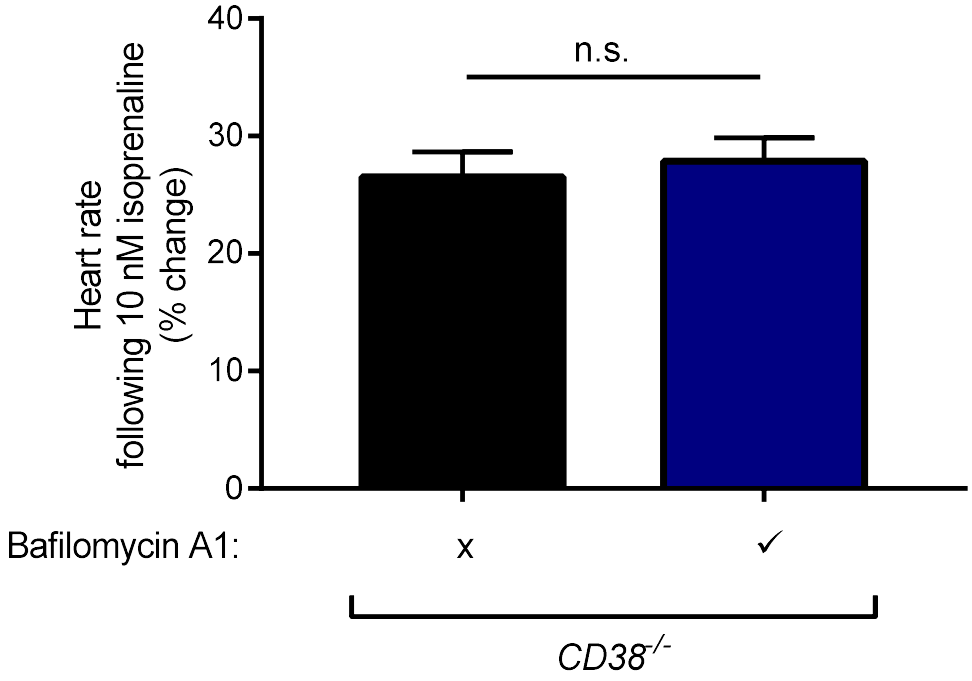


Figure 3.15: Percentage change in heart rate of spontaneously beating isolated right atria of *CD38*$^{-/-}$ mice during activation of β–adrenoreceptors in the presence of Bafilomycin A1 (5 µM).

On the application of 10 nM isoprenaline, there was no significant difference in the increase of Ca^{2+} transient amplitude when the atrial tissue of *CD38*$^{-/-}$ mice was preincubated with bafilomycin A1 (5 µM) and the untreated atrial tissue.

Note: Mouse right atrial tissue was placed in a chamber filled with Modified Tyrode's at 36 ˚C (n=6 for each group). 10 nM isoprenaline was added to the chamber and recordings were taken after 3 minutes. Numerical data is reported as the mean ± SEM. P>005, unpaired Student's t-test was used to compare the means of the two groups.

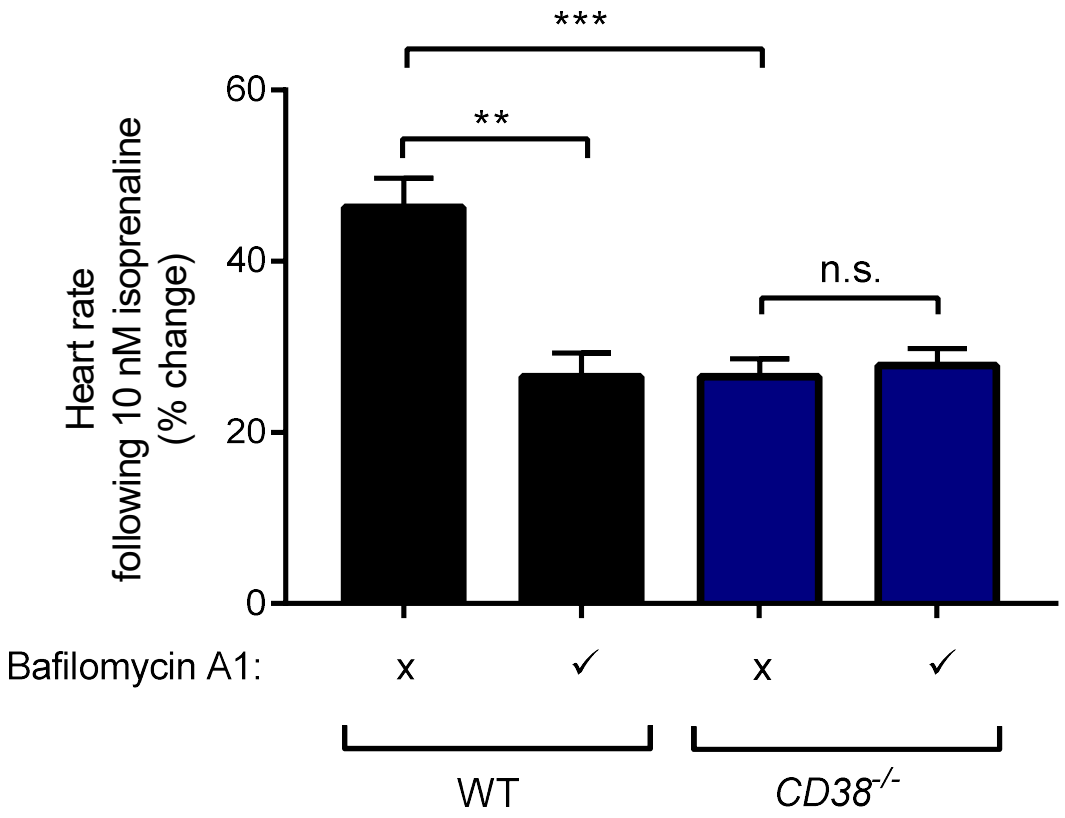


Figure 3.16: Summary of percentage change in heart rate of spontaneously beating isolated right atria of wildtype and *CD38*$^{-/-}$ mice during activation of β–adrenoreceptors in the presence of Bafilomycin A1 (5 µM).

On the application of 10 nM isoprenaline, there was significant differences in the increase of heart rate when the atrial tissue of wildtype mice was preincubated with bafilomycin A1 (5 µM) as compared to the non-treated atrial tissue. Significant differences were seen in the increase of heart rate between atrial tissue of wildtype mice and *CD38*$^{-/-}$ mice when exposed to 10 nM isoprenaline in the absence of bafilomycin A1. No significant change was seen in heart rate when the atrial tissue of *CD38*$^{-/-}$ mice was preincubated with bafilomycin A1 (5 µM) as compared to untreated atrial tissue.

Note: Mouse right atrial tissue was placed in a chamber filled with Modified Tyrode's at 36 ˚C (n=6 for each group). 10 nM isoprenaline was added to the chamber and recordings were taken after 3 minutes. Numerical data is reported as the mean ± SEM. ** denotes P<0.01, *** denotes P<0.001, One-way ANOVA with Tukey's multiple comparisons test was used to compare the means of the groups.

3.4 Discussion

The first half of this chapter addressed the possibility of an ongoing intrinsic activity of the NAADP pathway in murine cardiac atria. Analysis of Ca^{2+} transient properties and action potential durations of wildtype and *CD38*$^{-/-}$ mice revealed no evidence of a constitutive functioning of the NAADP signalling pathway.

3.4.1 Does NAADP pathway have an intrinsic activity in murine atria when β-adreneroceptors are not stimulated?

Work by Macgregor et al. on guinea-pig ventricular cardiomyocytes suggested a role for the NAADP pathway in the underlying Ca^{2+} handling properties of a cardiomyocyte. Application of bafilomycin A1 on stimulated ventricular myocytes in the absence of β-adrenergic stimulation showed a reduction in its Ca^{2+} transient amplitude. This reduction was in the order of 20-25% (Macgregor et al. 2007). Similar work on guinea-pig atrial cardiomyocytes by Collins et al. showed nearly a 50% reduction of the Ca^{2+} transient amplitudes when the atrial myocytes were incubated with bafilomycin A1 (Collins et al. 2011). Also, the higher reduction of Ca^{2+} amplitudes observed in the atrial myocytes than in ventricular myocytes was achieved by a much lesser concentration of bafilomycin A1; 100 nM as compared to 1 μM bafilomycin A1 used in the ventricular myocyte experiments. This opened the possibility of a higher influence of the NAADP pathway in atrial cardiomyocytes than in ventricular cardiomyocytes. It was hypothesised that in the absence of NAADP pathway stimulation, bafilomycin A1 might cause the leakage of Ca^{2+} from the acidic stores which might trigger Ca^{2+} sparks from the SR, resulting of expulsion of Ca^{2+} from the SR. This idea was supported by the selective inhibition of SR functions by ryanodine and thapsigargin, which stopped further reduction of Ca^{2+} transient

amplitude by bafilomycin A1 (Collins et al. 2011). Combining both the studies as described above, there appears to be evidence for the presence of an intrinsic NAADP pathway in cardiac muscles in guinea-pigs.

Interestingly, resting atrial myocytes also have an intrinsic activity of adenylyl cyclases, AC1 and AC8 being considered the primary adenylyl cyclases contributing to this activity. This intrinsic activity is not present in ventricular myocytes (Mattick et al. 2007; Collins and Terrar 2012). The ongoing activity of these adenylyl cyclases might increase the activity of cAMP and thereby, NAADP production by CD38. This might be responsible for the ongoing activity of NAADP in atrial cardiomyocytes. More studies are required to address the possible interplay between the adenylyl cyclases and the NAADP signalling pathway.

Even though work on guinea-pig cardiomyocytes show evidence for a constitutive NAADP signalling pathway, recent studies on murine ventricular cardiomyocytes have contradicted these studies. In *TPC2*$^{-/-}$ mice, the Ca^{2+} transient amplitudes were comparable to their wildtype counterparts in the absence of β-adrenergic stimulation (Capel et al. 2015). There were no observable differences in the Ca^{2+} spark frequency or contraction strengths between the wildtypes and the knockouts. Moreover, the NAADP antagonist Ned-19 did not change the Ca^{2+} transient amplitudes at basal level in wildtype mice (Elson 2011).

All these studies on murine cardiomyocytes mentioned above were performed on isolated ventricular cardiomyocytes. Since guinea-pig atrial myocytes showed a higher response to NAADP antagonism than ventricular myocytes, it was worth studying the ongoing effects of the NAADP pathway in murine atrial cardiomyocytes/ tissues with genetic

knockouts and pharmacological inhibition. Atrial tissue experiments were chosen for the studies in this chapter for the ease of tissue isolation and due to the advantages of tissue level studies and optical mapping as mentioned in the background section of this chapter. Moreover, isolation of atrial cardiomyocytes was deemed a difficult protocol and the quality of cells obtained were not good or consistent enough for experiments.

There were no significant differences observed in the Ca^{2+} transient properties of wildtype and *CD38*$^{-/-}$ mice at their basal conditions. Ca^{2+} transient amplitudes between the *CD38*$^{-/-}$ mice and their wildtype counterparts were comparable. This suggests the lack of an enhanced Ca^{2+} loading of the SR in the wildtype mice as compared to the genetic knockouts. The Ca^{2+} transient durations provide important clues of Ca^{2+} reuptake into the SR and Ca^{2+} extrusion from the cardiomyocyte into the extracellular space at later stages of the Ca^{2+} transient triggered by an action potential. The absence of a significant difference in the Ca^{2+} transient durations between wildtype and *CD38*$^{-/-}$ mice reaffirms the lack of an enhanced reuptake of Ca^{2+} into the SR by SERCA or increased Ca^{2+} extrusion from the cell through the Na^{+}/ Ca^{2+} exchanger. Comparable conduction velocities between the two groups also suggest that NAADP signalling pathway do not elicit any tissue level responses with respect to the Ca^{2+} handling. Adding to the comparable Ca^{2+} handling properties of wildtype and *CD38*$^{-/-}$ mice, lack of differences in action potential durations and comparable heart beating rate between the two genotypes further strengthens the argument for the non-functional NAADP signalling pathway in the murine atrial cardiac system in the absence of β-adrenoceptor stimulation. To assess whether the lack of differences in the basal level activity of Ca^{2+} handling in wildtype and *CD38*$^{-/-}$ is due to compensatory mechanisms arising due to the knockout of CD38 gene, pharmacological inhibition of the lysosomes using bafilomycin A1 was tested on

wildtype and *CD38*$^{-/-}$ knockout mice and their Ca^{2+} transient amplitudes were compared. Preincubation of the atrial tissues with bafilomycin A1 for up to 1 hour did not cause any differences in the Ca^{2+} transient amplitudes in either the wildtype or in the knockout mice. It is reasonable to assume that the lack of effect of bafilomycin A1 on basal levels of the Ca^{2+} transient amplitudes in atrial tissues might be due to difficulty in penetration of bafilomycin A1 into the cardiac tissue. However, bafilomycin A1 was successful in reducing the Ca^{2+} transient amplitude in wildtype mice when exposed to the β-adrenoceptor stimulant, isoprenaline. Therefore, the experiments in this chapter support the earlier studies on murine ventricular cardiomyocytes which show a lack of ongoing NAADP signalling activity in murine cardiac system. One possible explanation as to why an ongoing activity of NAADP was seen in guinea-pigs and not in mice might be the difference in species. Guinea-pigs might have a stronger ongoing activity of the NAADP pathway while smaller rodents such as mice might not have the NAADP pathway functioning at the basal level.

Although results from this chapter and previous studies have suggested the lack of a basal activity for the NAADP pathway, its presence in the murine cardiac system cannot be completely dispelled. Gul et al. have shown the presence of NAADP in cardiomyocytes without β-adrenergic stimulation (Gul et al. 2016). Perhaps the level of NAADP basal levels are too low to activate the NAADP pathway or the effect might be too low to be detected by the current experimental techniques available. The resolution of the experimental techniques used to address these research questions might not be high enough to observe a significant effect of the NAADP pathway in its constitutive function in the Ca^{2+} handling in mice cardiomyocytes, particularly, if the changes in Ca^{2+} handling properties due to this pathway is small at the basal level. One limitation of using

fluorescent indicators to assess Ca^{2+} transients is the buffering capacity of these indicators. The K_d of the Ca^{2+} indicator influences the fluorescence response kinetics to Ca^{2+} changes. If the Ca^{2+} indicator's affinity for Ca^{2+} is too high (K_d < 570 nM), then the Ca^{2+} transient can be misrepresented in the form of longer Ca^{2+} transient durations and untrue Ca^{2+} transient amplitudes (Paredes et al. 2008; Jaimes et al. 2016). Rhod-2 has a K_d in the range of 570-710 nM, and is considered to be in the acceptable range for measuring Ca^{2+} transients in animals used to study cardiac physiology (Kong and Fast 2014). Although Rhod-2 has a K_d in the acceptable range for Ca^{2+} transient studies, it is still a reasonably high affinity dye and might potentially mask small changes in Ca^{2+} handling physiology in cardiac tissues. Moreover, since Rhod-2 is a non-ratiometric dye, occurrences of non-uniform dye loading, heterogenous tissue structure, non-uniform excitation light, dye washout and photobleaching, among others can cause variations in Ca^{2+} signal recorded. Most, if not all, of these problems can be alleviated by using a low affinity ratiometric Ca^{2+} indicator. Further testing of a range of Ca^{2+} indicators will help in the process of identifying the ideal Ca^{2+} indicator to study small changes in Ca^{2+} handling properties in cardiac tissues and single myocytes.

An important consideration to be taken into account is whether CD38 is responsible for the production of NAADP and also whether CD38 is the only enzyme that can produce NAADP in the heart. Malavasi et at. reported that the homologue of *Aplysia* cyclase, CD38, was the primary ARC in mammalian tissues capable of producing NAADP and cADPR (Malavasi et al. 2008). Other studies have also suggested CD38 as the primary NAADP producing ARC in mammalian tissues such as spleen, liver and pancreas (Chini et al. 2002). Although CD157 is another recognised ARC in mammalian tissues, it is not known to synthesise NAADP by the base exchange reaction. A recent study by Higashida

and co-workers have reported that though CD157 presented cADPR synthesis capabilities, it lacked the ability to synthesise NAADP (Higashida et al. 2017). A few studies have also reported the existence of other non-CD38 ARCs in mammalian tissues. The main difference between these ARCs and CD38 is in its potentiation and inhibition responses to Zn^{2+} and Cu^{2+}. The lack of study of these ARCs on a CD38 knockout mouse model is a focal limitation. Strong evidence of CD38 being the only ARC capable of synthesising NAADP was published by Lin et al. recently. They studied the NAADP synthesising capabilities of cardiac ARCs in a *CD38*$^{-/-}$ mouse model. The authors reported that cardiac membrane preparations from *CD38*$^{-/-}$ mice were incapable of synthesising NAADP or cADPR. If there existed a non-CD38 ARC capable of synthesising NAADP, some level of NAADP synthesis must have been detected in the *CD38*$^{-/-}$ mice (Lin et al. 2017).

3.4.2 Does NAADP pathway play a role in Ca^{2+} handling during β-adrenergic stimulation murine atria?

During the β-adrenergic stimulation, adenylyl cyclases are activated leading to a cascade of events resulting in enhanced functioning of RyRs, LTCC and SERCA. At low levels of β-adrenergic stimulation, positive lusitropic and inotropic effects prove beneficial to an organism's flight or fight response. However, impaired β-adrenergic pathway can result in arrhythmogenic responses and cardiac dysfunction (Section 1.4). Several studies in the past decade have emphasised the role of CD38/ NAADP pathway in the downstream effects of β-adrenoceptor stimulation. Multiple studies have shown the increase of NAADP levels in the presence of the β-adrenoceptor agonist isoprenaline (Macgregor et al. 2007; Lewis et al. 2012; Gul et al. 2016; Lin et al. 2017). Macgregor et

al. showed that photorelease of caged NAADP increased Ca^{2+} transient amplitudes, Ca^{2+} spark amplitude and frequency in guinea-pig ventricular cardiomyocytes (Macgregor et al. 2007). Nebel et al. studied the arrhythmogenic effects of isoprenaline in mouse ventricular cardiomyocytes using the NAADP antagonist, BZ194. A high dose of isoprenaline resulted in the occurrence of after-depolarisations and spontaneous Ca^{2+} transients which were abolished by BZ194. Similarly, bafilomycin A1 was also able to suppress these effects, suggesting a role for NAADP in isoprenaline mediated arrhythmogenic effects (Nebel et al. 2013). Capel and co-workers showed that in the presence of isoprenaline, ventricular cardiomyocytes from *TPC2*$^{-/-}$ mice had blunted responses in Ca^{2+} transient amplitudes and contraction. Wildtype cardiomyocytes treated with bafilomycin A1 also showed similar blunted effects in the presence of isoprenaline. Bafilomycin A1 and Ned-19 also reduced the increase in Ca^{2+} transient amplitudes in guinea-pig cardiomyocytes in the presence of isoprenaline. However, in the experiments using *TPC2*$^{-/-}$ mice, no difference was seen in the L-type Ca^{2+} currents in the wildtypes and the knockouts in when exposed to isoprenaline. This suggests that the difference in Ca^{2+} transient properties is likely to be due to NAADP signalling pathway (Capel et al. 2015).

The experiments in this chapter are the first attempt of studying the effect of NAADP signalling pathway in β-adrenergic responses in murine atrial tissue using the CD38 genetic knockout mice. Additionally, pharmacological intervention using bafilomycin A1 is also used to better understand the mechanism of the NAADP pathway. Providing support to the earlier publications, results in this chapter also support a role for the NAADP pathway in β-adrenergic responses in murine atria. In the presence of 10 nM isoprenaline, *CD38*$^{-/-}$ atrial tissue showed a blunted response in the Ca^{2+} transient increase

as compared to wildtype mice. Moreover, preincubation of the wildtype mice atrial tissue in 5 μM bafilomycin A1 blunted the increase in Ca^{2+} transients in response to isoprenaline. This provides strength to the argument that NAADP produced by CD38 on β-adrenergic stimulation acts on receptors present on the acidic stores, leading to Ca^{2+} mobilisation from the acidic stores resulting in increased Ca^{2+} release from the SR. This is further supported by experiments where preincubation of bafilomycin A1 in *CD38*$^{-/-}$ mice atrial tissue did not cause any significant difference in the increase in Ca^{2+} transients as compared to the DMSO treated *CD38*$^{-/-}$ atrial tissue under the influence of isoprenaline.

The SR mediated Ca^{2+} handling has also been implicated in the pacemaking mechanism of the SAN. Disruption of the functioning of SR by the inhibition of SERCA and RyRs have been shown to have a negative impact on the beating rate of the sino-atrial node (Rigg et al. 2000). Therefore, it was interesting to study whether the CD38/ NAADP pathway played a role in the pacemaking properties of the SAN. As described earlier, at resting level without β-adrenergic stimulation, there were no changes in the beating rate of the SAN. However, under the influence of isoprenaline, there appeared to be a clear effect of the NAADP pathway in the pacemaking mechanisms of the SAN. The positive chronotropic effect of isoprenaline was evidently blunted in isolated atria from *CD38*$^{-/-}$ mice as compared to the wildtype mice. Moreover, preincubation of bafilomycin A1 in wildtype mice blunted the chronotropic effect of isoprenaline, suggesting a role for lysosomal/NAADP pathway in pacemaker function in response to β-adrenergic response. No further reduction in heart rate was observed in *CD38*$^{-/-}$ treated with bafilomycin A1 as compared to the DMSO treated controls. Although the results of these experiments open doors for an active role for the NAADP pathway in pacemaker activity in murine

atria under β-adrenergic stress, further experiments need to be performed to understand the mechanism of these effects in detail.

Although the exact mechanisms for the effects of the NAADP pathway in the β-adrenergic stimulation and Ca^{2+} handling in cardiomyocytes are not known for certain, publications over the past few years have been revealing more players involved in this pathway. Interestingly, the effects of the photorelease of caged NAADP in both atrial and ventricular myocytes were abolished in the presence of the inhibitors of CAMKII, KN93 and AIP (Capel et al. 2015). The possible roles of CAMKII in the CD38 pathway will be discussed in the next chapter.

Along with NAADP, CD38 is also known to synthesise cADPR when exposed to β-adrenergic stimulation. As described in Section 1.7.2, cADPR is also reported to influence the Ca^{2+} handling properties in cardiomyocytes. Interestingly, under the influence of isoprenaline, bafilomycin A1 preincubation and absence of CD38 had an almost identical effect on the Ca^{2+} transient amplitude (Figure 3.12). If the NAADP response and the cADPR response to isoprenaline were non-overlapping, then the reduction in the increase of Ca^{2+} transient amplitude in the *CD38*$^{-/-}$ would have been larger than in the bafilomycin A1 treated atrial tissues that inhibited the NAADP pathway alone. As this effect is not seen in the experiments in this chapter, a complimentary effect of the cADPR and NAADP pathway on the Ca^{2+} handling properties in the cardiomyocyte might be possible. One possible mechanism for this is cADPR playing a more prominent role in Ca^{2+} release from the SR while NAADP acts in Ca^{2+} uptake into the SR (more evidence for Ca^{2+} uptake in the SR due to NAADP is presented in the next chapter) (Meszaros, Bak, and Chu 1993; Lahouratate, Guibert, and Faivre 1997; Bak et al. 2001).

Chapter 4

The effect of NAADP signalling pathway on sarcoplasmic reticulum calcium content in isolated mouse ventricular myocytes

4.1 Background

A number of studies have strongly linked the effect of the NAADP pathway in excitation-contraction coupling with particular emphasis on the β-adrenergic pathway in the heart (Capel et al. 2015; Gul et al. 2016; Lin et al. 2017; Nebel et al. 2013). Exposing cardiomyocytes to NAADP led to enhanced Ca^{2+} transients and contraction. Inhibition of the pathway blunted the effects of β-adrenergic responses in the heart (Lin et al. 2017; Capel et al. 2015; Lewis et al. 2012). More clues of the exact mechanism of this activity are being revealed by different groups as the potential of taking advantage of this pathway to design anti-arrhythmic drugs is increasing.

An established notion regarding NAADP is its ability to act on lysosomes and release Ca^{2+} (Churchill et al. 2002; Calcraft et al. 2009; Galione 2006). However, the mechanism of Ca^{2+} release from the lysosome leading to enhanced Ca^{2+} transients in myocytes is less understood. One can assume that the Ca^{2+} released from the lysosomes adds on to the Ca^{2+} released from the SR leading to enhanced Ca^{2+} transients. However, this seems unlikely to be the full explanation since the volume of lysosomes in a cell is far smaller than that of the SR. For example, in hepatocytes, the volume of its endoplasmic reticulum is approximately 15% while the lysosomal volume is around than 1% (Alberts 2015). Therefore, it is unlikely that Ca^{2+} from the lysosome is simply additive in Ca^{2+} release from the SR to create a larger Ca^{2+} transient. A more accepted hypothesis is an amplification mechanism wherein Ca^{2+} release from the lysosomes results in a much larger Ca^{2+} release from the SR.

One hypothesis for the mechanism of Ca^{2+} amplification on Ca^{2+} release from the lysosomes is called the ‘trigger hypothesis’. According to this hypothesis, the small Ca^{2+}

release from the lysosomes in response to NAADP leads to a global release of Ca^{2+} from the SR. A number of theories have been suggested as of how this phenomenon might take place. One possibility is that Ca^{2+} released from the lysosomes can directly activate the RyRs on the SR and lead to enhanced calcium-induced calcium release. Another possibility suggested by Gul et al. is that increased levels of NAADP leads to the production of its associated molecule cADPR which triggers Ca^{2+} release from the SR via the RyRs (Gul et al. 2016). Yet another possibility is that the small amount of Ca^{2+} released from the lysosomes is sequestered into the SR via SERCA and though this Ca^{2+} does not change the SR luminal Ca^{2+} content significantly, it is adequate to enhance the function of RyRs to increase Ca^{2+} release from the SR (Morgan et al. 2011). A number of reports have been published with evidence for trigger hypothesis in non-cardiac cells. In pulmonary artery smooth muscle cells, NAADP lead to a global increase in Ca^{2+} which was abolished by thapsigargin and ryanodine (inhibitors of SERCA and RyRs, respectively). Though global Ca^{2+} events were abolished by these compounds, localised bursts of Ca^{2+} was visible when exposed to NAADP which supports the trigger hypothesis (Kinnear et al. 2004; Boittin, Galione, and Evans 2002).

For the trigger hypothesis, a favourable setup would be a close relationship between the lysosomes and the SR (Morgan et al. 2011). Kinnear et al. showed that in pulmonary arterial smooth muscle cells, a close association was seen between the lysosomes which were stained by lysotracker Red and RyRs which were stained with BODIPY-ryanodine green. They also showed that co-localisation of type-1 lysosome-associated protein (LAMP-1) and ryanodine receptor type-3 (RyR3) and bursts of Ca^{2+} was seen at these localised regions when the cells were exposed to NAADP (Kinnear et al. 2004; Kinnear et al. 2008).

Recent work by Aston et al provided strong evidence for the existence of microdomains between the SR and lysosomes in cardiac ventricular myocytes. Using 2D electron microscopy and 3D electron tomography techniques, they showed that SR and lysosomes are separated by mere nanometres. A median separation of 3.3 nm between SR and lysosomes was reported in isolated rabbit ventricular myocytes. Moreover, staining of the lysosomal membrane protein LAMP-2 showed periodicity in the cell comparable to the sarcomeric periodicity. Interestingly, LAMP-2 staining was very closely aligned with RyR2 and phospholamban, but not overlapping, strengthening the argument for a microdomain. They also reported co-staining between the NAADP antagonist Ned-19 and lysotracker Red, providing further evidence that lysosomes are the targets of NAADP (Aston et al. 2017).

The advantage of the existence of microdomains between the SR and the lysosomes is directly translated into the profound effects of the NAADP pathway in Ca^{2+} uptake and release from the SR. The first evidence for increased Ca^{2+} uptake into the SR in cardiomyocytes were observed by the Terrar group. Macgregor et al. showed that in electrically stimulated guinea-pig ventricular myocytes, photorelease of NAADP resulted in larger Ca^{2+} transient amplitudes which was sensitive to bafilomycin. The lack of an effect on the L-type calcium channels suggested a role for the interplay between the lysosomes and the SR for this phenomenon. In the presence of ryanodine and thapsigargin, NAADP failed to increase the Ca^{2+} transient amplitude. Evidence for enhanced Ca^{2+} uptake into the SR was observed in the form of observations made on caffeine-induced Ca^{2+} release from the SR. When exposed to high concentrations of caffeine, a RyR agonist, a large unsynchronised release of Ca^{2+} occurs from the SR into the cytoplasm. SR Ca^{2+} content can be measured by recording the change in cytoplasmic

Ca^{2+} using cytoplasmic Ca^{2+} indicator when the cells are exposed to 10 mM caffeine. The authors observed the SR Ca^{2+} levels in the absence of NAADP and after the photorelease of NAADP to study whether NAADP increased the SR Ca^{2+} levels. They observed a 20 % increase in SR Ca^{2+} content after NAADP photorelease, suggesting that NAADP increased the Ca^{2+} load of the SR. They also observed an increase in Ca^{2+} sparks frequency and amplitude in the presence of NAADP, providing more value to the proposal that NAADP enhanced SR Ca^{2+} load (Macgregor et al. 2007). Similar results were observed by Collins et al. in guinea-pig atrial myocytes. In the presence of 60 nM NAADP, caffeine induced Ca^{2+} release from the SR showed that NAADP increased the SR Ca^{2+} levels by 30% (Collins et al. 2011).

The aim of this chapter was to study the close association between the NAADP signalling pathway and SR Ca^{2+} load in wildtype and *CD38*$^{-/-}$ mice ventricular myocytes using a low affinity Ca^{2+} indicator to directly visualise SR Ca^{2+} changes. The commonly used indirect method of studying the SR Ca^{2+} levels suffer from considerable disadvantages. These recordings are static measurements and do not give spatial and temporal information of SR Ca^{2+} levels. Moreover, these measurements can also be skewed by Ca^{2+} release events occurring right before the caffeine application. This chapter attempts to study the effects of the NAADP pathway on the SR Ca^{2+} levels by directly measuring the SR Ca^{2+} levels of isolated ventricular cardiomyocytes using the low affinity Ca^{2+} indicator, Mag-Fluo-4, AM, thereby, circumventing the disadvantages of the indirect method of studying SR Ca^{2+} levels. The effect of NAADP pathway on SR was studied by introducing NAADP into permeabilised ventricular cardiomyocytes from wildtype and *CD38*$^{-/-}$ mice. Further, pharmacological inhibitors (bafilomycin A1 and the CD38 inhibitor SAN4825) were also used to the study the NAADP pathway and its association

with the SR. The effect of β-adrenergic stimulation on the SR/NAADP pathway was studied by observing SR Ca^{2+} levels in the presence of the cAMP, an activator of PKA.

4.2 Methods

The methods used in this chapter has been described in Chapter 2. Wildtype and *CD38*$^{-/-}$ mice (aged 10-16 weeks, both males and females) were sacrificed by concussion and cervical dislocation before the heart was quickly excised. Healthy cardiomyocytes were isolated from the isolated heart as described in Section 2.3. The protocol for ventricular cardiomyocyte isolation was modified from a protocol described before by Ackers-Johnson et al. (Ackers-Johnson et al. 2016). Isolated cells were stored in Modified Tyrode's solution supplemented with 0.5-1% bovine serum albumin and 250 µM $CaCl_2$ at 37 ºC.

For imaging the myocyte SR Ca^{2+}, the fluorescent Ca^{2+} indicator Mag-Fluo-4, AM was used. Cells were incubated in a 6 µM concentration of Mag-Fluo-4, AM for 45 minutes at 37 ºC. Since the myocytes showed contaminating Ca^{2+} indicator loading in the cytoplasm, the cells were permeabilised in 0.005% saponin solution to diffuse Mag-Fluo-4 from the cytoplasm into the extracellular solution. Final internal solution was added into permeabilised cells and was readied for experimentation. Final internal solution was supplemented with 100 nM Ca^{2+}. The Ca^{2+} content of the Final internal solution stock was carefully calibrated to 100 nM using a Calcium Calibration kit (Calcium Calibration buffer kit #1, zero and 10 mM CaEGTA, Thermo Scientific). The permeabilised cells were seeded on a glass slide coated with Corning® Cell-Tak™ cell adhesive. Healthy cells were identified as cells showing clear perpendicular striation (SR Ca^{2+} fluorescence along the junctional SR) across the cell and showing no spontaneous activity. Healthy cells were stable for approximately 15 minutes during which the experiments were performed. For experiments using bafilomycin A1, preincubation of bafilomycin A1 (5

μM) was achieved by adding bafilomycin A1 to the dye-loading solution and all subsequent solutions for cells preparation for experimentation. Experiments that did not use bafilomycin A1 contained an equivalent amount of the solvent, DMSO. NAADP, cAMP and SAN4825 were directed added onto the cells on the glass slide and gently mixed using a blunt ended pipette tip.

The cells were imaged using a Nipkow spinning disk confocal microscope. 488 nm laser light set at 100 μWatts was used for the indicator excitation. Fluorescence acquisition was performed by Andor software at the rate of 1 frame every 5 seconds for 5 minutes at room temperature. To normalise the Ca^{2+} changes, a bolus of 10 mM caffeine was added to the cells at the end of each experiment to empty the SR so that the measurements could be expressed as F/F_{Caff}, where F_{Caff} is the fluorescence recorded after emptying the SR (corresponding to 100 nM Ca^{2+} in the internal solution). The data represented as percentage change is the percentage change of F/F_{Caff} at each time point from the F/F_{Caff} at time 0. Data analysis was performed using Clampfit, ImageJ and Graphpad prism softwares.

4.3 Results

4.3.1 Successful SR Ca^{2+} indicator loading and the effect of permeabilisation on the lysosomes

The first step in studying the SR Ca^{2+} changes in murine ventricular cardiomyocytes was to successfully load the SR Ca^{2+} indicator Mag-Fluo-4, AM into the myocytes. For this to be successful, the Ca^{2+} indicator has to enter the cell from the extracellular solution, and then completely diffuse into the SR. One of the biggest challenges in achieving this is indicator contamination in the cytosol. Once the dye enters the cell, it can be de-esterified and trapped in the cytosol. This results in poor loading of the SR and the SR Ca^{2+} fluorescence recordings measured will be compounded by Ca^{2+} fluorescence from the cytosol resulting in erroneous data. An example of a poorly loaded ventricular cardiomyocyte containing contaminant dye in the cytosol is given in Figure 4.1B. Images of 6 cells each (from 2 mice) of good and poorly loaded cells were recorded. To avoid poor loading, the myocytes were permeabilised with 0.005% saponin. This allowed for the dye trapped in the cytosol to diffuse into the extracellular solution leaving SR loaded dye to be clearly visible. An example of a well loaded cardiomyocyte is shown in Figure 4.1A. A cardiomyocyte with well loaded Mag-Fluo-4, AM can be identified by bright transversal lines separated by approximately 1.8 μm (Figure 4.2). Since the SR is contiguous with the nuclear envelope, bright staining around the nucleus is also characteristic of a well loaded cell (Fernandez-Tenorio and Niggli 2016).

Another aim was to check whether permeabilisation damaged the cardiomyocyte lysosomes. Damaged lysosomes hinder the study of the NAADP pathway in cardiomyocytes. Permeabilisation showed no effect on the lysosomes as comparable

levels of lysotracker green loading was observed in permeabilised and non-permeabilised cells (Figure 4.3). 10 cells were imaged for each condition (from 4 mice).

4.3.2 Wildtype and *CD38*$^{-/-}$ mice had comparable SR Ca^{2+} levels at baseline conditions

Mouse ventricular cardiomyocytes were permeabilised and loaded on a glass slide coated with Corning® Cell-Tak™ cell adhesive. The cells were imaged using a confocal microscope.

The SR Ca^{2+} levels of wildtype and *CD38*$^{-/-}$ mice were obtained as F/F_{Caff} at basal level. There were no significant differences in the basal SR Ca^{2+} levels between the wildtype and the knockout mice ($p=0.74$, $n=8$ from 4 mice for both groups). The mean Ca^{2+} fluorescence levels for wildtype and *CD38*$^{-/-}$ mice were 1.59 ± 0.01 and 1.58 ± 0.02, respectively (Figure 4.4).

4.3.3 Bafilomycin A1 had no effect on the SR Ca^{2+} in wildtype and *CD38*$^{-/-}$ mice ventricular myocytes at baseline conditions

More evidence for the lack of a basal activity of NAADP pathway in murine cardiac system was observed wherein bafilomycin A1 failed to change the SR Ca^{2+} levels in wildtype and *CD38*$^{-/-}$ mice at resting conditions. 5 µM bafilomycin was pre-incubated with the cardiomyocytes and the SR Ca^{2+} fluorescence levels were observed as F/F_{Caff}. There were no significant differences in the SR Ca^{2+} fluorescence levels in wildtype mice preincubated with 5 µM bafilomycin A1 and the DMSO treated controls ($P=0.808$, $n=10$ from 4 mice for both groups). Similarly, *CD38*$^{-/-}$ mice cardiomyocytes showed

comparable levels of SR Ca^{2+} fluorescence between bafilomycin A1 treated and DMSO treated controls (P=0.997, n=10 from 4 mice for both groups). These results are summarised in Figure 4.5.

4.3.4 NAADP increased the SR Ca^{2+} levels in wildtype and *CD38*$^{-/-}$ mice ventricular myocytes

100 nM NAADP was added onto permeabilised ventricular cardiomyocytes and the SR Ca^{2+} levels were observed over 5 minutes. NAADP increased the SR Ca^{2+} content of the myocytes significantly in both wildtype and *CD38*$^{-/-}$ mice.

The mean % changes in F/F_{Caff} from time 0 were calculated for each time point. In wildtype mice, 100 nM NAADP increased the mean SR Ca^{2+} fluorescence levels by 13.4 ± 2.5% at 5 minutes as compared to the H_2O treated controls (P=0.026, n=7 from 4 mice for each group). The data are shown in Figure 4.6.

Similarly, 100 nM NAADP was also able to increase the SR Ca^{2+} fluorescence levels in *CD38*$^{-/-}$ mice. For the % changes in F/F_{Caff} from time 0 calculated for each time point, a mean increase of 14.3 ± 2.5% was observed in SR Ca^{2+} fluorescence the NAADP treated myocytes as compared to the H_2O treated controls (P=0.025, n=7 for each group). Figure 4.7 summarises these data.

4.3.5 Bafilomycin A1 blunted the effect of NAADP on the SR Ca^{2+} levels in wildtype and *CD38*$^{-/-}$ mice ventricular myocytes

5 μM Bafilomycin A1 was added to the cardiomyocytes during the 45 minutes dye incubation and maintained at 5 μM in the permeabilised cardiomyocyte preparation

solutions (saponin containing solutions and final internal solution). 100 nM NAADP was added to the glass slide and the fluorescence intensity was measured for 5 minutes.

In wildtype myocytes, the increase in SR Ca^{2+} levels due to NAADP was significantly blunted by the preincubation of 5 μM bafilomycin A1 as compared to the DMSO treated controls (P=0.021, n=8 from 4 mice for both groups). The mean % changes in F/F_{Caff} from time 0 was calculated for each time points. The DMSO treated controls showed a 12.4 ± 1.7% increase in response to NAADP at 5 minutes while the bafilomycin A1 preincubated cardiomyocytes showed an increase of 5.2 ± 2.3% in the presence of NAADP at 5 minutes. These results are summarised in Figure 4.8.

Similar observations were seen in cardiomyocytes from *CD38*$^{-/-}$ mice. The presence of 5 μM bafilomycin A1 significantly reduced the increase in SR Ca^{2+} levels due to the effect of NAADP as compared to the DMSO treated controls (P=0.045, n=8 from 4 mice for both groups). The mean % changes in F/F_{Caff} from time 0 were calculated for each time points. The DMSO treated controls showed a 11.3 ± 2.3% increase in response to NAADP at 5 minutes while the bafilomycin A1 preincubated cardiomyocytes showed an increase of 2.8 ± 2.1% in the presence of NAADP at 5 minutes. Figure 4.9 summarises these results.

Interestingly, in neither the wildtype nor the *CD38*$^{-/-}$ cardiomyocytes, bafilomycin was able to completely abolish the effect of NAADP. This will be considered in detail in the discussion section of this chapter.

4.3.6 The effect of cAMP on SR Ca^{2+} was reduced in *CD38*$^{-/-}$ mice ventricular myocytes as compared to wildtype mice myocytes.

10 μM cAMP was added onto permeabilised ventricular cardiomyocytes and the SR Ca^{2+} levels were observed over 5 minutes. cAMP increased the SR Ca^{2+} content of the myocytes from both wildtype and *CD38*$^{-/-}$ mice . However, *CD38*$^{-/-}$ showed a significantly smaller increase in SR Ca^{2+} as compared to wildtype mice (P=0.028, n=10 from 4 mice for both groups). The mean % changes in F/F_{Caff} from time 0 was calculated for each time points. While the wildtype cardiomyocytes showed a 34.9 ± 4.3% increase in SR Ca^{2+} levels the presence of cAMP, the *CD38*$^{-/-}$ cardiomyocytes had a blunted increase in SR Ca^{2+} levels at 20.4 ± 4.5% at 5 minutes. Figure 4.10 summarises these results.

4.3.7 The effect of cAMP on SR Ca^{2+} was reduced by bafilomycin A1 in wildtype mice ventricular myocytes.

10 μM cAMP was added onto permeabilised ventricular cardiomyocytes from wildtype mice preincubated with 5 μM bafilomycin and the SR Ca^{2+} levels were observed over 5 minutes. There was a significant reduction in the effect of cAMP on the SR Ca^{2+} levels in bafilomycin A1 treated cardiomyocytes as compared to the DMSO treated controls (P=0.0414, n=9 from 4 mice for both groups) . For the % changes in F/F_{Caff} from time 0 calculated for each time point, the DMSO treated control cardiomyocytes showed a 31.1 ± 5.4% increase in SR Ca^{2+} levels as compared to the bafilomycin A1 treated cardiomyocytes that showed a 15.0 ± 4.6% increase in SR Ca^{2+} levels (Figure 4.11).

4.3.8 Bafilomycin A1 had no effect on SR Ca^{2+} levels in *CD38*$^{-/-}$ mice ventricular cardiomyocytes in the presence of cAMP.

10 μM cAMP was added onto permeabilised ventricular cardiomyocytes from *CD38*$^{-/-}$ mice preincubated with 5 μM bafilomycin and the SR Ca^{2+} levels were observed over 5 minutes. There was no significant difference in the increase in SR Ca^{2+} levels in DMSO treated controls and bafilomycin A1 treated cardiomyocytes (P=0.97, n=10 from 4 mice for both groups). The mean % changes in F/F_{Caff} from time 0 was calculated for each time points. The DMSO treated control cardiomyocytes showed a 21.0 ± 3.8% increase in SR Ca^{2+} levels as compared to the bafilomycin A1 treated cardiomyocytes that showed a 17.0 ± 3.1% increase in SR Ca^{2+} levels. Figure 4.12 summarises these results.

4.3.9 SAN4825 had no effect on SR Ca^{2+} levels in wildtype mice ventricular cardiomyocytes in the presence of cAMP.

3 μM SAN4825 was added to the cardiomyocytes during the 45 minutes dye incubation and maintained at 3 μM in the permeabilised cardiomyocyte preparation solutions (saponin containing solutions and final internal solution).

In wildtype myocytes, the increase in SR Ca^{2+} levels due to 10 μM cAMP was comparable between the 3 μM SAN4825 preincubated cells and the DMSO treated controls cells (P=0.998, n=9 from 4 mice for both groups). The mean % changes in F/F_{Caff} from time 0 was calculated for each time points. The DMSO treated controls showed a 31.1 ± 5.2% increase in response to cAMP at 5 minutes while the SAN4825 preincubated cardiomyocytes showed an increase of 27.0 ± 3.0 % in the presence of cAMP at 5 minutes. These results are summarised in Figure 4.13.

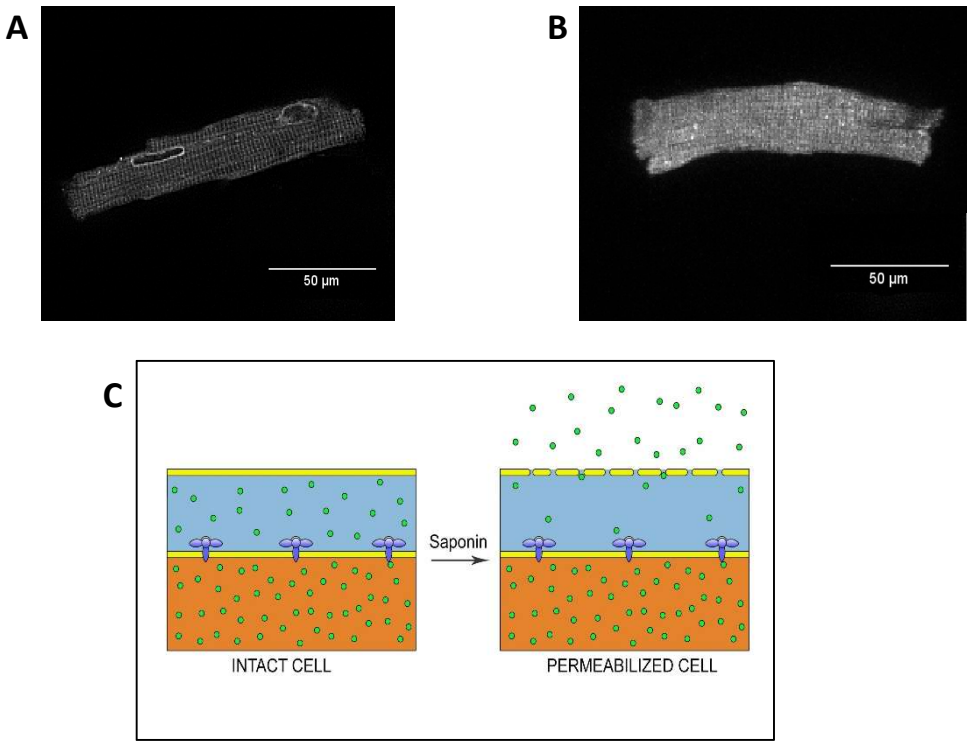


Figure 4.1: Examples of Mag-fluo-4, AM loading in permeabilised and non-permeabilised murine ventricular cardiomyocytes

A shows Mag-Fluo-4, AM loading in ventricular myocyte permeabilised with 0.005% saponin. Periodic transverse lines and brightly stained nuclear envelope is indication of good SR Ca^{2+} staining.
B shows Mag-Fluo-4, AM loading in a non-permeabilised ventricular myocyte.
C is a schematic figure of Ca^{2+} indicator diffusing out of the cytosol of a permeabilised myocyte leaving the indicator in the SR intact.

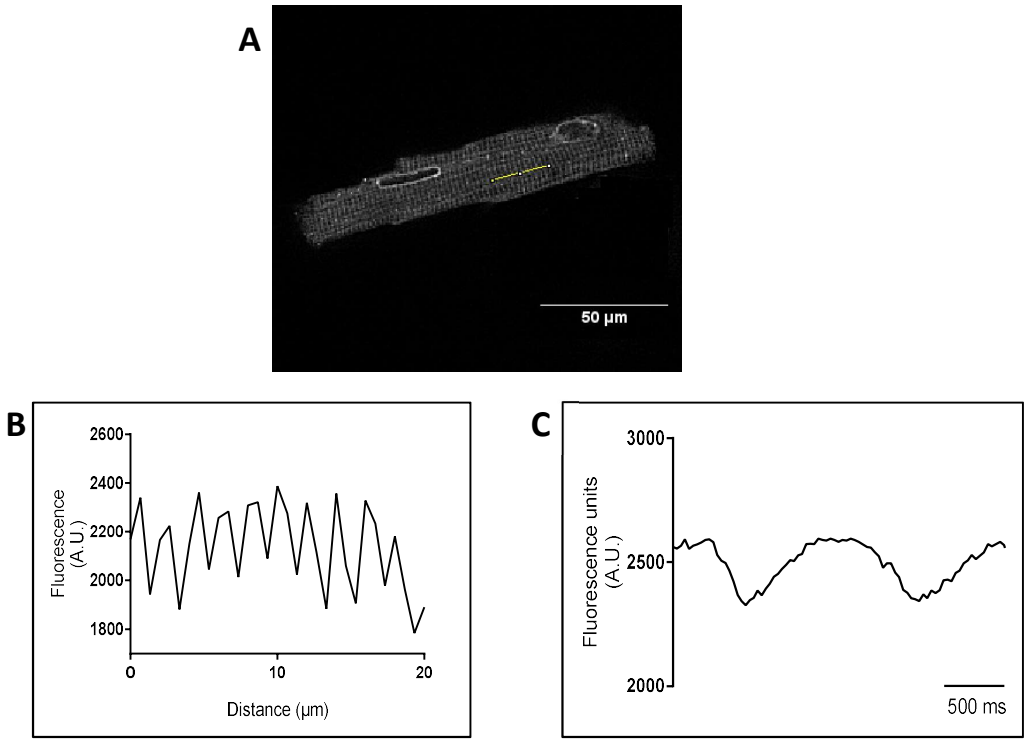


Figure 4.2: Mag-fluo-4, AM loading characteristics in murine ventricular cardiomyocytes

A shows a Mag-Fluo-4, AM loaded ventricular myocyte.
B shows the pattern of Mag-Fluo-4, AM fluorescence intensity along the longitudinal axis of a myocyte (yellow line in **A**). This corresponds to the sarcomeric structure along the junctional SR. The x- axis is distance (in µm) and y-axis is arbitrary fluorescence units.
C is a raw trace of a spontaneous depolarisation of a Mag-Fluo-4, AM loaded myocyte. The inverted signal signifies a fall in fluorescence intensity as Ca^{2+} is released from the SR. The x- axis is time (in ms) and y-axis is arbitrary fluorescence units.

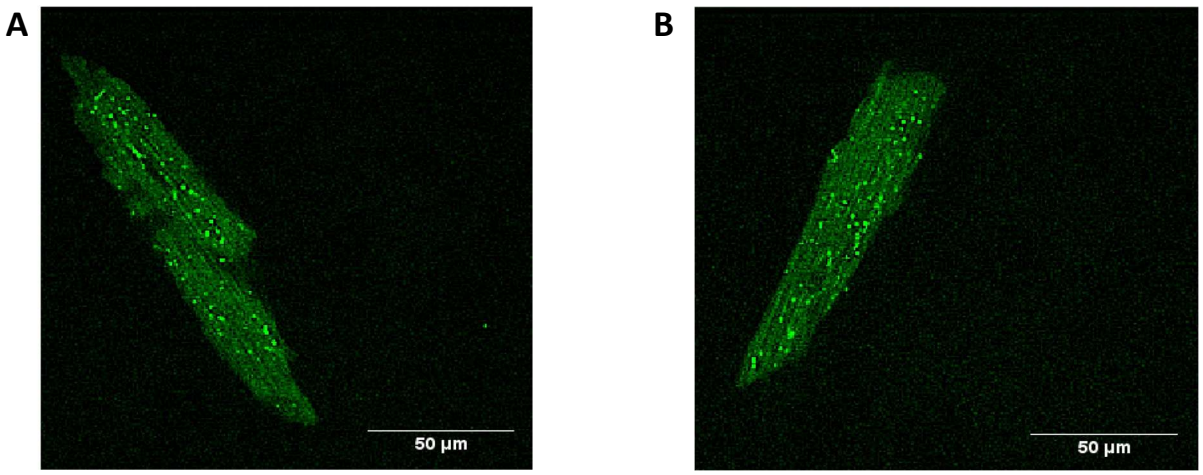


Figure 4.3: Permeabilisation by 0.005% saponin does not affect the lysosomes of murine ventricular myocytes

A shows lysosomal staining by Lysotracker Green in a non-permeabilised cardiomyocyte
B shows lysosomal staining by Lysotracker Green in a cardiomyocyte permeabilised by 0.005% saponin.
Comparable staining was visible by Lysotracker Green in permeabilised and non-permeabilised cardiomyocytes.

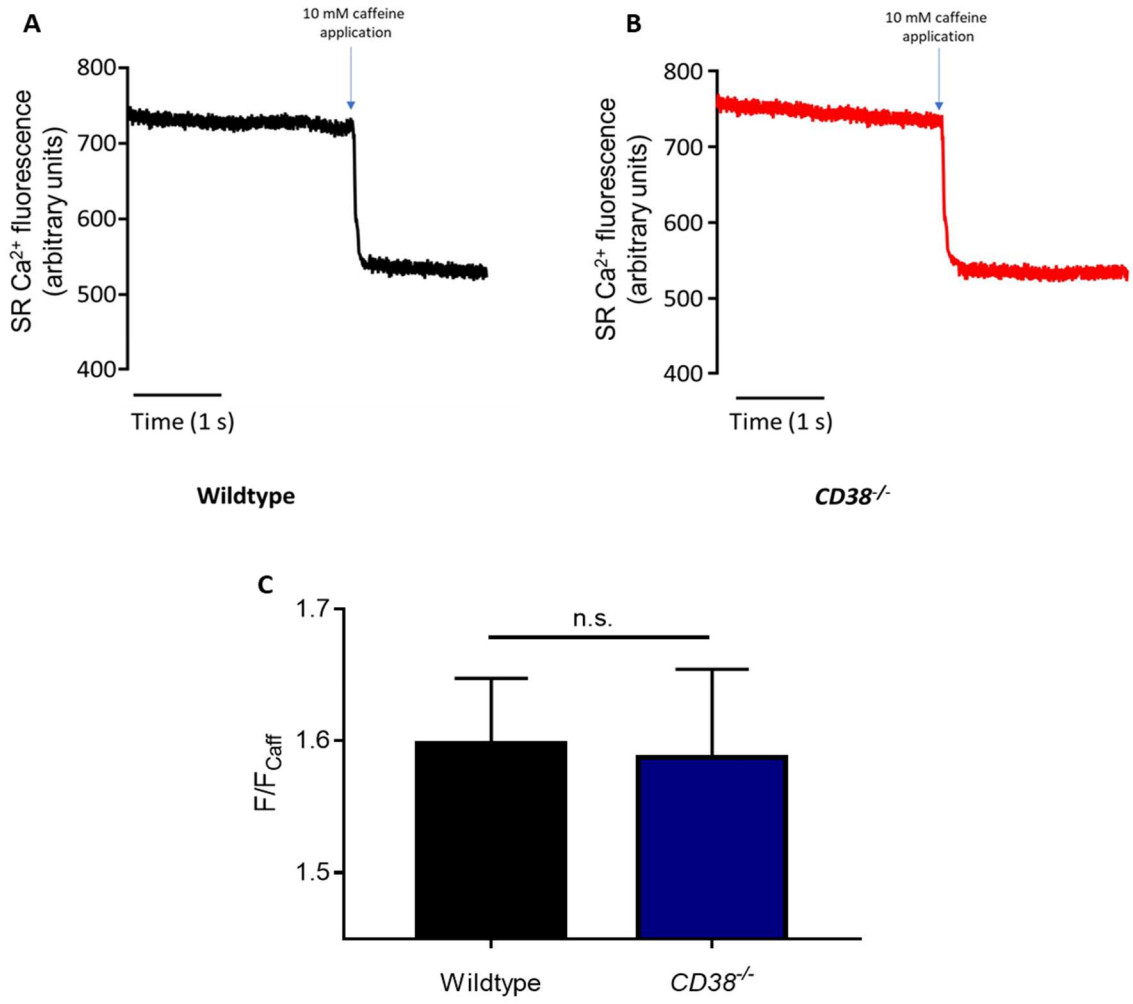


Figure 4.4: SR calcium content of ventricular cardiomyocytes of wildtype and *CD38*$^{-/-}$ mice at resting conditions.

A shows a representative raw trace of SR Ca^{2+} load before and after adding 10 mM caffeine in wildtype mouse ventricular cardiomyocyte.

B shows a representative raw trace of SR Ca^{2+} load before and after adding 10 mM caffeine in *CD38*$^{-/-}$ mouse ventricular cardiomyocyte

C No significant differences were seen in SR calcium concentration of wildtype and *CD38*$^{-/-}$ mice at resting conditions.

Note: Mag-Fluo-4, AM loaded mouse ventricular cardiomyocytes were permeabilised and seeded on a glass slide. Fluorescence was measured using a confocal microscope and the data are represented as F/F_{Caff}, where F_{Caff} is the fluorescence recorded after emptying the SR with 10 mM caffeine. Fluorescence signal was analysed using Clampfit and ImageJ. Numerical data are reported as the mean ± SEM. $P>0.05$, n=8 from 4 mice for both groups, unpaired Student's t-test was used to compare the means of the two groups.

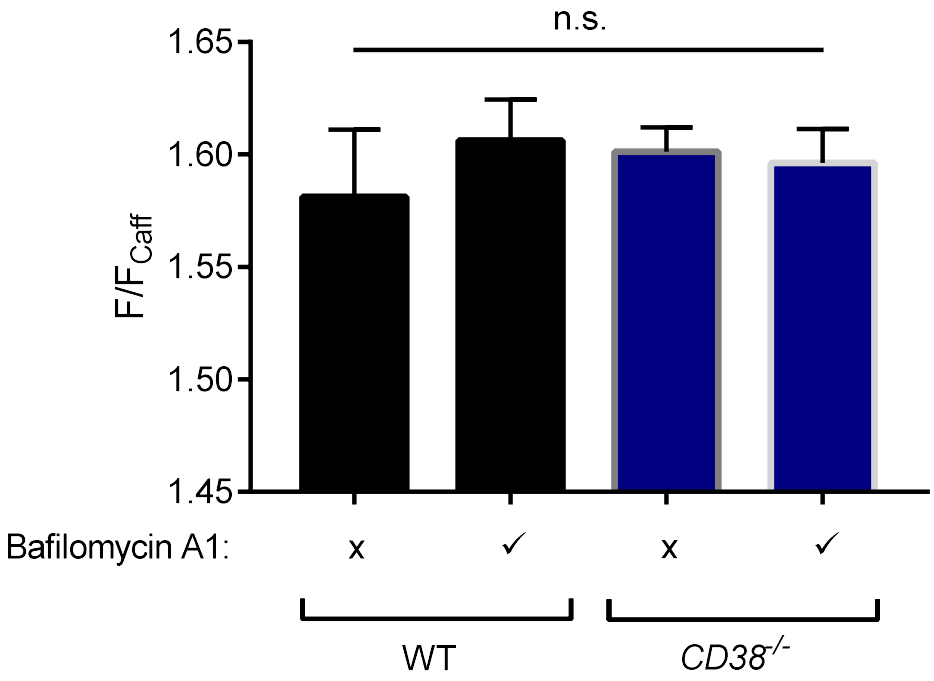


Figure 4.5: SR calcium content of ventricular cardiomyocytes of wildtype and *CD38*$^{-/-}$ mice preincubated with bafilomycin A1.

No significant differences were seen in SR calcium concentration of wildtype and *CD38*$^{-/-}$ mice preincubated with bafilomycin A1.

Note: Mouse ventricular cardiomyocytes were preincubated in 5 µM bafilomycin A1 for 45 minutes. Mag-Fluo-4, AM loaded cardiomyocytes were permeabilised and seeded on a glass slide. Fluorescence was measured using a confocal microscope and the data are represented as F/F_{Caff}, where F_{Caff} is the fluorescence recorded after emptying the SR with 10 mM caffeine. Fluorescence signal was analysed using Clampfit and ImageJ. Numerical data are reported as the mean ± SEM. $P>0.05$, n=10 from 4 mice for both groups. One-way ANOVA with Tukey's multiple comparisons test was used to compare the means of the groups.

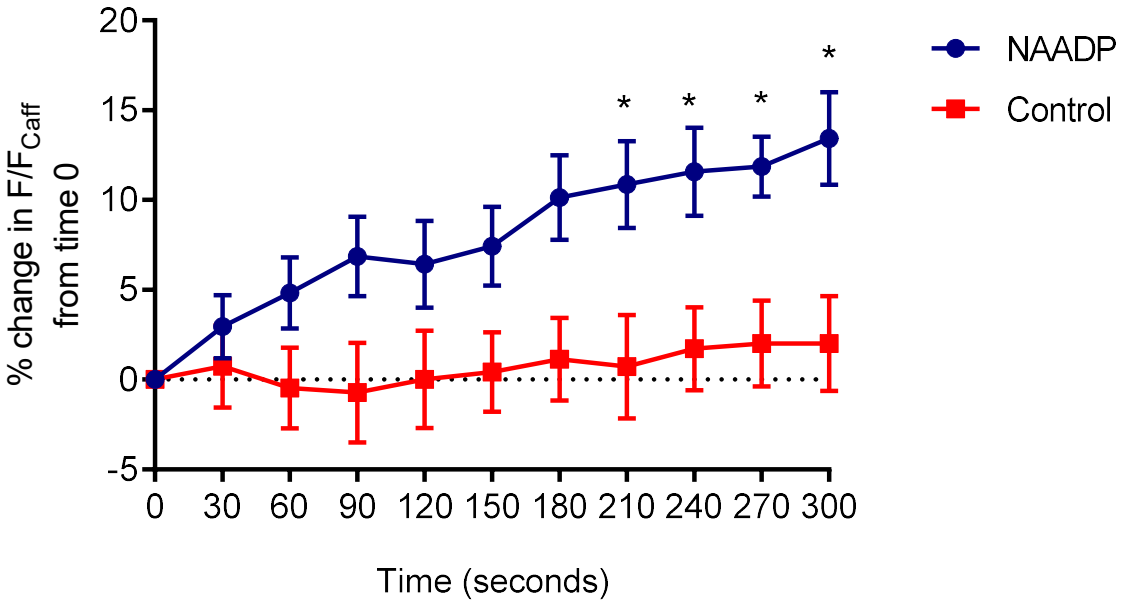


Figure 4.6: Percentage change in SR calcium levels of ventricular cardiomyocytes from wildtype mice in the presence of NAADP.

In wildtype ventricular cardiomyocytes, 100 nM NAADP significantly increased the SR calcium levels as compared to the H_2O treated control cardiomyocytes.

Note: Mag-Fluo-4, AM loaded cardiomyocytes were permeabilised and seeded on a glass slide. 100 nM NAADP was added to the slide and fluorescence was measured over time using a confocal microscope. Data are represented as mean % changes in F/F_{Caff} from time 0, where F_{Caff} is the fluorescence recorded after emptying the SR with 10 mM caffeine. Fluorescence signal was analysed using Clampfit and ImageJ. Numerical data are reported as the mean ± SEM. $P<0.05$, n=7 from 4 mice for both groups. * denotes $P<0.05$. Two-way ANOVA with Bonferroni's multiple comparisons test was used to compare the means at different time points (every 30 seconds) between the groups.

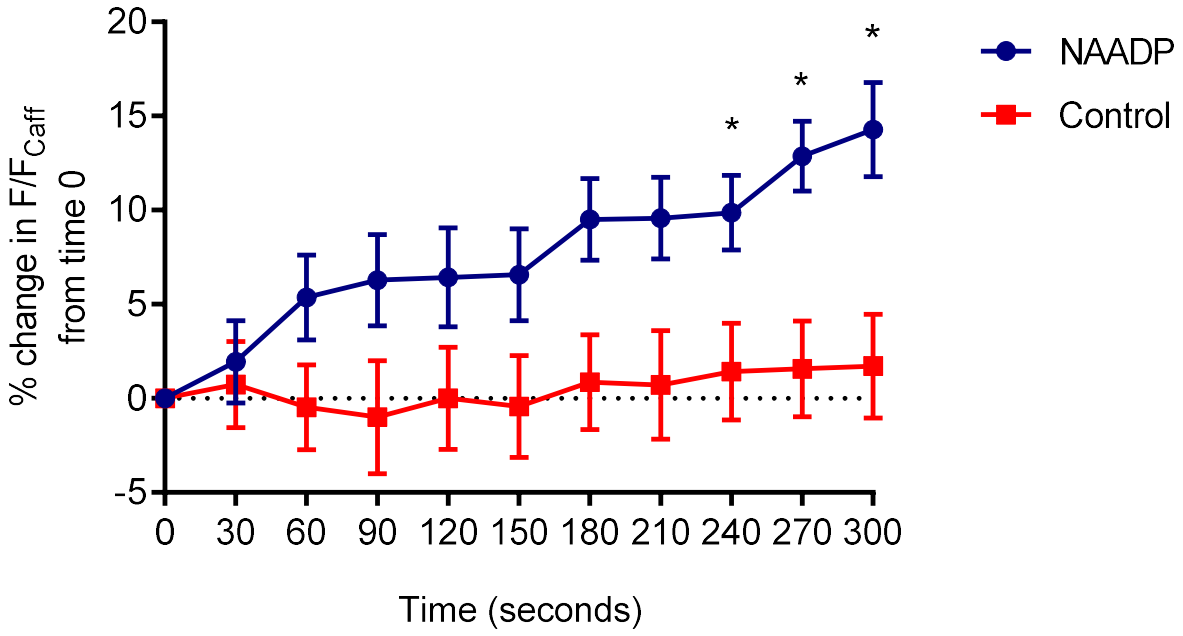


Figure 4.7: Percentage change in SR calcium levels of ventricular cardiomyocytes from *CD38*$^{-/-}$ mice in the presence of NAADP.

In *CD38*$^{-/-}$ ventricular cardiomyocytes, 100 nM NAADP significantly increased the SR calcium levels as compared to the H_2O treated control cardiomyocytes.

Note: Mag-Fluo-4, AM loaded cardiomyocytes were permeabilised and seeded on a glass slide. 100 nM NAADP was added to the slide and fluorescence was measured over time using a confocal microscope. Data are represented as mean % changes in F/F_{Caff} from time 0, where F_{Caff} is the fluorescence recorded after emptying the SR with 10 mM caffeine. Fluorescence signal was analysed using Clampfit and ImageJ. Numerical data are reported as the mean ± SEM. $P<0.05$, n=7 from 4 mice for both groups. * denotes $P<0.05$. Two-way ANOVA with Bonferroni's multiple comparisons test was used to compare the means at different time points (every 30 seconds) between the groups.

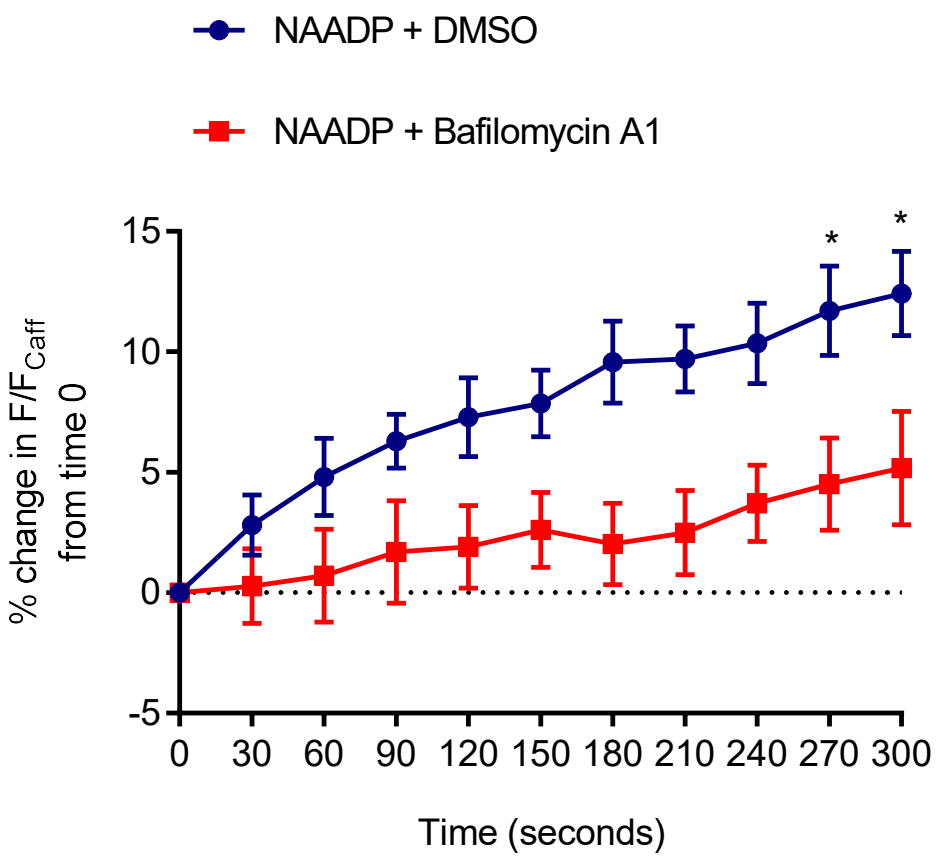


Figure 4.8: Percentage change in SR calcium levels of bafilomycin A1 preincubated ventricular cardiomyocytes from wildtype mice in the presence of NAADP.

In wildtype ventricular cardiomyocytes, preincubation with 5 µM bafilomycin blunted the effects of 100 nM NAADP. The increase in SR calcium levels were significantly blunted in bafilomycin preincubated cardiomyocytes as compared to the DMSO treated cardiomyocytes. However, the bafilomycin was unable to completely abolish the effect of NAADP.

Note: Mouse ventricular cardiomyocytes were preincubated in 5 µM bafilomycin A1 for 45 minutes. Mag-Fluo-4, AM loaded cardiomyocytes were permeabilised and seeded on a glass slide. 100 nM NAADP was added to the slide and fluorescence was measured over time using a confocal microscope. Data are represented as mean % changes in F/F_{Caff} from time 0, where F_{Caff} is the fluorescence recorded after emptying the SR with 10 mM caffeine. Fluorescence signal was analysed using Clampfit and ImageJ. Numerical data are reported as the mean ± SEM. $P<0.05$, n=8 from 4 mice for both groups. * denotes $P<0.05$. Two-way ANOVA with Bonferroni's multiple comparisons test was used to compare the means at different time points (every 30 seconds) between the groups.

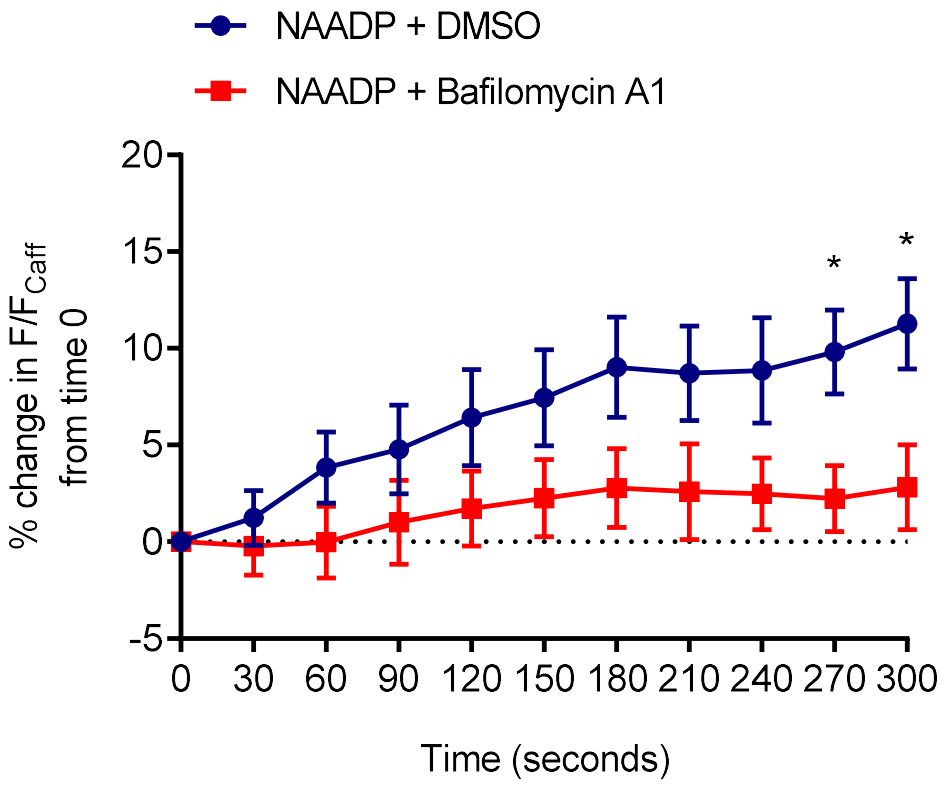


Figure 4.9: Percentage change in SR calcium levels of bafilomycin A1 preincubated ventricular cardiomyocytes from *CD38*$^{-/-}$ mice in the presence of NAADP.

In *CD38*$^{-/-}$ ventricular cardiomyocytes, preincubation with 5 µM bafilomycin blunted the effects of 100 nM NAADP. The increase in SR calcium levels were significantly blunted in bafilomycin preincubated cardiomyocytes
as compared to the DMSO treated cardiomyocytes. However, the bafilomycin was unable to completely abolish the effect of NAADP.

Note: Mouse ventricular cardiomyocytes were preincubated in 5 µM bafilomycin A1 for 45 minutes. Mag-Fluo-4, AM loaded cardiomyocytes were permeabilised and seeded on a glass slide. 100 nM NAADP was added to the slide and fluorescence was measured over time using a confocal microscope. Data are represented as mean % changes in F/F_{Caff} from time 0, where F_{Caff} is the fluorescence recorded after emptying the SR with 10 mM caffeine. Fluorescence signal was analysed using Clampfit and ImageJ. Numerical data are reported as the mean ± SEM. $P<0.05$, n=8 from 4 mice for both groups. * denotes $P<0.05$. Two-way ANOVA with Bonferroni's multiple comparisons test was used to compare the means at different time points (every 30 seconds) between the groups.

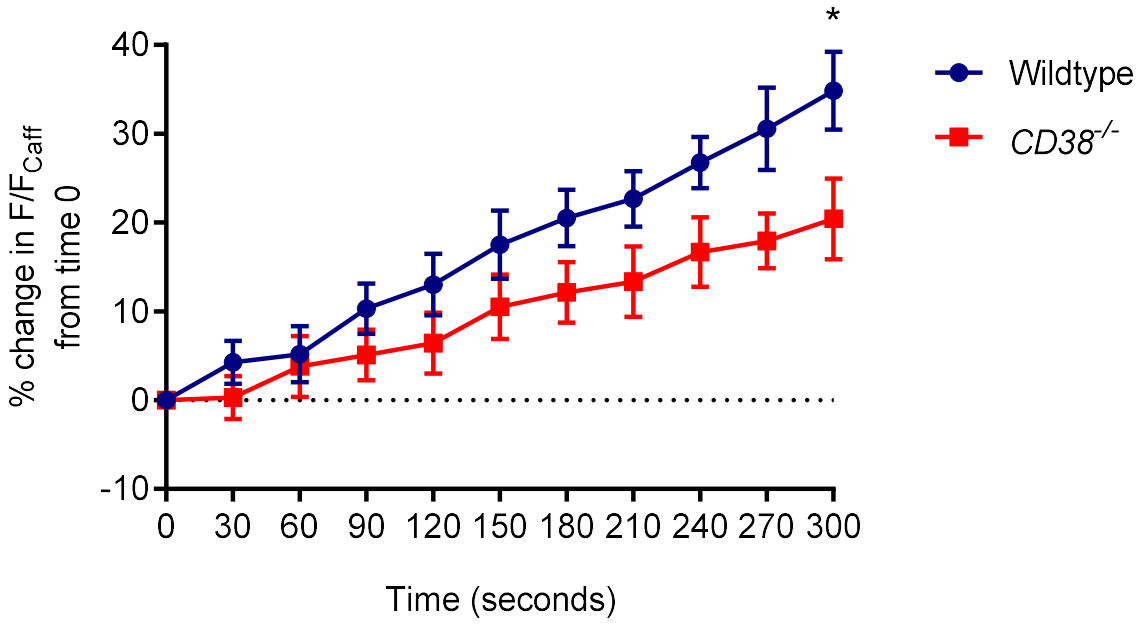


Figure 4.10: Percentage change in SR calcium levels of ventricular cardiomyocytes from wildtype and *CD38*$^{-/-}$ mice in the presence of cAMP.

Cardiomyocytes from *CD38*$^{-/-}$ mice showed a blunted effect in response to 10 µM cAMP as compared to wildtype mice. The increase in SR calcium levels was significantly higher in wildtype mice as compared to *CD38*$^{-/-}$ mice.

Note: Mag-Fluo-4, AM loaded cardiomyocytes were permeabilised and seeded on a glass slide. 10 µM cAMP was added to the slide and fluorescence was measured over time using a confocal microscope. Data are represented as mean % changes in F/F_{Caff} from time 0, where F_{Caff} is the fluorescence recorded after emptying the SR with 10 mM caffeine. Fluorescence signal was analysed using Clampfit and ImageJ. Numerical data are reported as the mean ± SEM. $P<0.05$, n=10 from 4 mice for both groups. * denotes $P<0.05$. Two-way ANOVA with Bonferroni's multiple comparisons test was used to compare the means at different time points (every 30 seconds) between the groups.

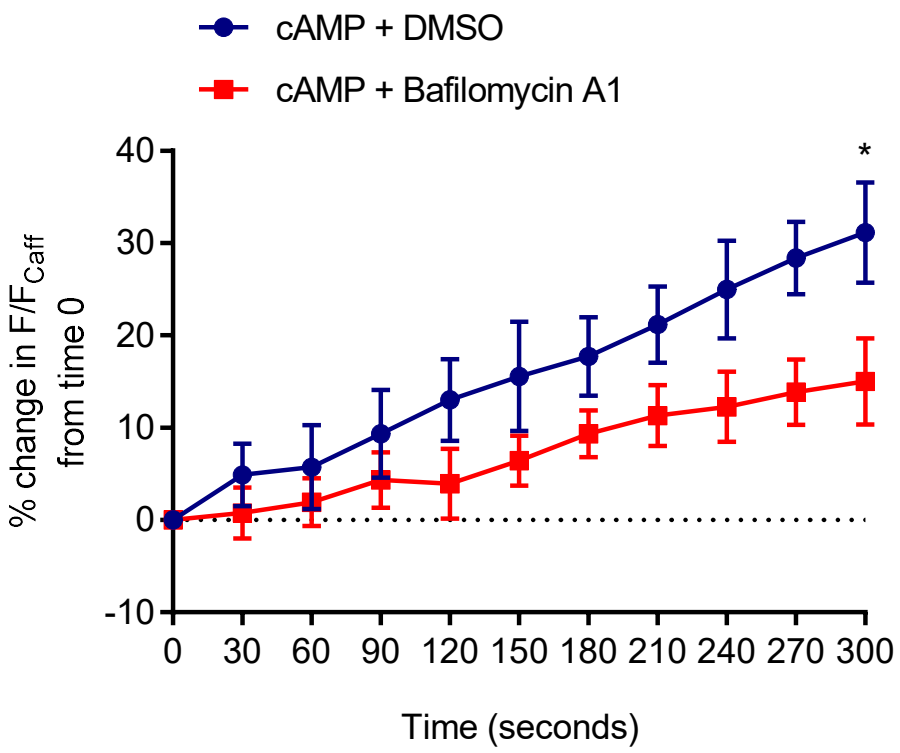


Figure 4.11: Percentage change in SR calcium levels of bafilomycin A1 preincubated ventricular cardiomyocytes from wildtype mice in the presence of cAMP.

In wildtype ventricular cardiomyocytes, preincubation with 5 µM bafilomycin blunted the effects of 10 µM cAMP. The increase in SR calcium levels were significantly blunted in bafilomycin preincubated cardiomyocytes as compared to the DMSO treated cardiomyocytes.

Note: Mouse ventricular cardiomyocytes were preincubated in 5 µM bafilomycin A1 for 45 minutes. Mag-Fluo-4, AM loaded cardiomyocytes were permeabilised and seeded on a glass slide. 10 µM cAMP was added to the slide and fluorescence was measured over time using a confocal microscope. Data are represented as mean % changes in F/F_{Caff} from time 0, where F_{Caff} is the fluorescence recorded after emptying the SR with 10 mM caffeine. Fluorescence signal was analysed using Clampfit and ImageJ. Numerical data are reported as the mean ± SEM. $P<0.05$, n=9 from 4 mice for both groups. * denotes $P<0.05$ Two-way ANOVA with Bonferroni's multiple comparisons test was used to compare the means at different time points (every 30 seconds) between the groups.

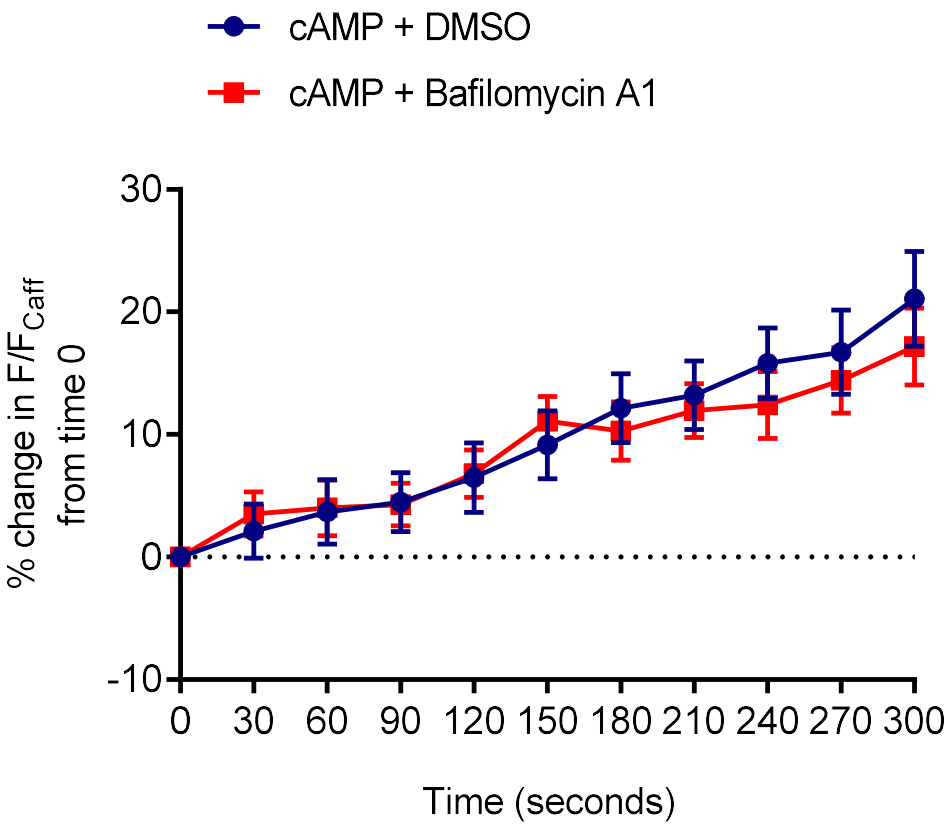


Figure 4.12: Percentage change in SR calcium levels of bafilomycin A1 preincubated ventricular cardiomyocytes from *CD38*$^{-/-}$ mice in the presence of cAMP.

In *CD38*$^{-/-}$ ventricular cardiomyocytes, preincubation with 5 µM bafilomycin did not change the effects of 10 µM cAMP. There was no significant difference in the SR calcium levels between bafilomycin preincubated cardiomyocytes as compared to the DMSO treated cardiomyocytes.

Note: Mouse ventricular cardiomyocytes were preincubated in 5 µM bafilomycin A1 for 45 minutes. Mag-Fluo-4, AM loaded cardiomyocytes were permeabilised and seeded on a glass slide. 10 µM cAMP was added to the slide and fluorescence was measured over time using a confocal microscope. Data are represented as mean % changes in F/F_{Caff} from time 0, where F_{Caff} is the fluorescence recorded after emptying the SR with 10 mM caffeine. Fluorescence signal was analysed using Clampfit and ImageJ. Numerical data are reported as the mean ± SEM. $P>0.05$, $n=10$ from 4 mice for both groups. Two-way ANOVA with Bonferroni's multiple comparisons test was used to compare the means at different time points (every 30 seconds) between the groups.

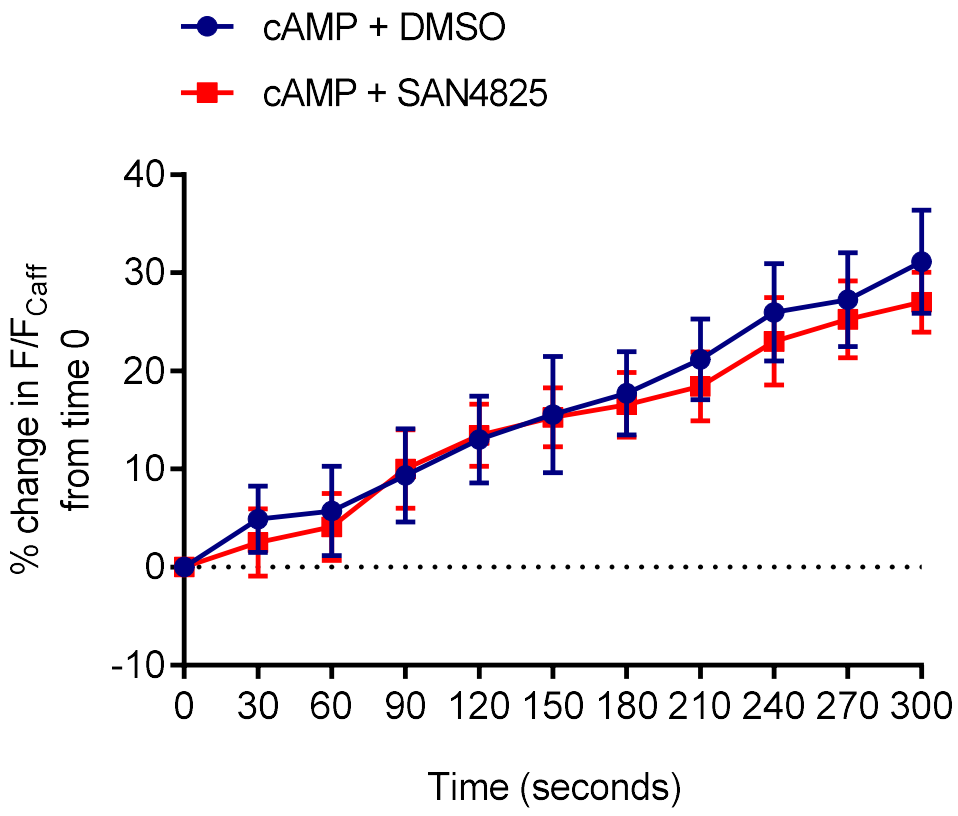


Figure 4.13: Percentage change in SR calcium levels of SAN4825 preincubated ventricular cardiomyocytes from wildtype mice in the presence of cAMP.

In wildtype ventricular cardiomyocytes, preincubation with 3 µM SAN4825 did not change the effects of 10 µM cAMP. There was no significant difference in the SR calcium levels between the SAN4825 preincubated cardiomyocytes as compared to the DMSO treated cardiomyocytes.

Note: Mouse ventricular cardiomyocytes were preincubated in 3 µM SAN4825 for 45 minutes. Mag-Fluo-4, AM loaded cardiomyocytes were permeabilised and seeded on a glass slide. 10 µM cAMP was added to the slide and fluorescence was measured over time using a confocal microscope. Data are represented as mean % changes in F/F_{Caff} from time 0, where F_{Caff} is the fluorescence recorded after emptying the SR with 10 mM caffeine. Fluorescence signal was analysed using Clampfit and ImageJ. Numerical data are reported as the mean ± SEM. $P>0.05$, n=10 from 4 mice for both groups. Two-way ANOVA with Bonferroni's multiple comparisons test was used to compare the means at different time points (every 30 seconds) between the groups.

4.4 Discussion

In this chapter, the NAADP pathway was studied with particular emphasis on SR Ca^{2+} loading. This is the first attempt to directly observe the SR Ca^{2+} content with respect to the NAADP pathway in β-adrenergic response conditions. The role of NAADP pathway in β-adrenergic response is further strengthened by the observations in the genetic knockout of the enzyme responsible for the production of NAADP (CD38). The results presented here are in general agreement with previous publications from the Terrar lab, even though a few unexpected results were observed.

4.4.1 Loading Ca^{2+} indicator into the SR of mouse ventricular myocytes: General considerations

Saponin permeabilises the cell membrane as saponin forms pores on the membrane by forming micelles of cholesterol. Contradicting accounts of the effect on saponin on the lysosomes have been published since lysosomal membrane might contain cholesterol making them prone to permeabilisation by saponin (Gilabert-Oriol et al. 2013; Bottger and Melzig 2013). Lysotracker Green staining showed similar patterns of staining in permeabilised and non-permeabilised cells (Figure 4.3). Since lysotracker green showed variable staining across the z-axis of the cardiomyocytes, a method to accurately determine exact amount of staining across cells and thereby analysis for significance was difficult. However, visually comparable levels of staining between cells suggested that permeabilisation had no effect on the integrity of lysosomes in cardiomyocytes. Moreover, the concentration of saponin used in this study (0.005%) has been shown to keep the SR intact, thereby keeping the variables arising due to permeabilisation of cardiomyocytes to a minimum (Lukyanenko and Gyorke 1999).

Isoprenaline is generally used to simulate β-adrenergic stress in cardiomyocytes. Isoprenaline activates the β-adrenergic pathway by binding to β-adrenergic receptors on the cell membrane. However, since permeabilisation disrupts the cell membrane, isoprenaline mediated activation of β-receptors is hindered (Fernandez-Tenorio and Niggli 2016). Therefore, in the current experiments, the β-adrenergic pathway was stimulated using the downstream effector of β-adrenergic stress, cyclic adenosine monophosphate (cAMP). cAMP activates cAMP dependent protein kinase A (PKA), which in turn phosphorylates troponin I, phospholamban, L-type Ca+ channels, among others resulting in chronotropic, lusitropic, dromotropic and inotropic effects in the heart (Freedman and Lefkowitz 2004). Previous studies have shown an increase in SR Ca^{2+} content in cardiomyocytes in the presence of cAMP in a thapsigargin sensitive manner (Bovo et al. 2017; Fernandez-Tenorio and Niggli 2018).

The techniques used in the experiments reported in this chapter were insufficient to accurately measure the Ca^{2+} concentration in the SR. For absolute values of SR Ca^{2+}, a Ca^{2+} calibration at maximal (using ionomycin or high concentration of Ca^{2+} in the solution) and minimal (using high dose of caffeine) fluorescence values needs to be measured for every cardiomyocyte used in the study. Even though caffeine induced Ca^{2+} release gave a good approximation of the minimal fluorescence value of SR Ca^{2+}, the maximal fluorescence values were difficult to ascertain since the cells behaved abnormally and inconsistently in higher concentrations of Ca^{2+} in the solution. However, dividing the fluorescence signal by the fluorescence value at minimal SR Ca^{2+} (caffeine induced Ca^{2+} release), a relative concentration of SR Ca^{2+} could be determined. Additional evidences to support the results from Chapter 3 regarding the role of the NAADP pathway in Ca^{2+} handling of the heart at resting conditions is provided in this

chapter. In the absence of β-adrenergic or NAADP pathway stimulation, the SR Ca^{2+} content of wildtype and *CD38*$^{-/-}$ mice were comparable, suggesting that at resting levels, the NAADP pathway might not play a role in SR Ca^{2+} handling in mice ventricular myocytes under these conditions. The absence of an effect of preincubation of bafilomycin A1 on the SR Ca^{2+} levels strengthens this hypothesis.

4.4.2 Does the activation of the NAADP pathway increase the SR Ca^{2+} load in murine ventricular myocytes?

Earlier studies in guinea-pig atrial and ventricular cardiomyocytes have reported an increase in SR Ca^{2+} in the presence of photoreleased caged NAADP and AM-ester form of NAADP (Collins et al. 2011; Macgregor et al. 2007). The use of caged and AM-ester form of NAADP was used due to the membrane impermeability of NAADP. In this study, however, NAADP was directly applied to the bath solution and permeabilisation of the cardiomyocytes permitted its entry into the cells. Consistent with the studies in guinea-pig cardiomyocytes, the presence of NAADP increased the SR Ca^{2+} content. This increase in SR Ca^{2+} was sensitive to bafilomycin A1 since the effect of NAADP was significantly blunted in the presence of bafilomycin A1. Interestingly, bafilomycin A1 did not completely abolish the effect of NAADP mediated increase of SR Ca^{2+}. This residual NAADP effect might perhaps be due to incomplete effect of bafilomycin A1 on lysosomal Ca^{2+} content at the concentration of bafilomycin used in this study (5 μM). NAADP might have promoted the release of small concentrations of Ca^{2+} from the lysosomes resulting in reduced Ca^{2+} uptake into the SR. Future studies using a higher concentration of bafilomycin A1 need to be performed to understand this better.

The experiments that used cAMP to simulate β-adrenergic effect in cardiomyocytes also gave results that were expected. cAMP mediated increase in SR Ca^{2+} content was significantly blunted in *CD38*$^{-/-}$ mice suggesting a role of the NAADP/ CD38 pathway in SR Ca^{2+} uptake in response to β-adrenergic stress. Further evidence for lysosomes being the target of NAADP pathway was provided by the experiments using cardiomyocytes which were preincubated by bafilomycin A1. In the presence of bafilomycin A1, the effects of cAMP on SR Ca^{2+} increase were significantly blunted. Moreover, the lack of an effect of bafilomycin A1 on cAMP induced SR Ca^{2+} increase in *CD38*$^{-/-}$ mice adds to a large repertoire of information implicating NAADP to target lysosomes.

4.4.3 Does SAN4825 inhibit the increases in SR Ca^{2+} load in murine ventricular myocytes under β-adrenoceptor stimulation?

Kannt et al. provided evidence for a potential intracellular membrane-bound cardiac ARC which was distinct from the known mammalian ARCS CD38 and CD157/Bst1. This ARC was inhibited by Zn^{2+} while CD38 and CD157 were known to be potentiated by the presence of Zn^{2+}. They used a nicotinamide hypoxanthine dinucleotide (NHD)- based assay to determine the rate of cyclisation by the ARC to convert the non-fluorescent NHD into the fluorescent cyclic inosine diphosphate-ribose (cIDPR). The NHD assay was performed on isolated SR vesicles from pig and rat hearts and the presence of the ARC was reported as the SR vesicles was able to convert NHD to cIDPR. They then performed an elaborate study to find potential inhibitors for this ARC. A high throughput screening of over 17000 molecules revealed two candidates (SAN4825 and SAN2589) that could inhibit the conversion NHD to cIDPR by the ARC. SAN4825 was able to inhibit the activity of the ARC with an IC_{50} of 1.3 μM (Kannt et al. 2012). However, the Terrar group

showed evidences that SAN4825 was targeting the ARC CD38. In sheep cardiac SR membrane preparations, SAN4825 was able to inhibit the production of both NAADP and cADPR, providing evidence for SAN4825 to be an inhibitor for CD38. Additionally, in the presence of SAN4825, Langendorff perfused wildtype mouse hearts were more resistant to isoprenaline induced arrhythmias, and also blunted isoprenaline induced chronotropic effects, which were consistent with the effects seen in CD38 and TPC2 knockout mice. Moreover, through *in silico* studies, they reported that SAN4825 bound to the active site of CD38 and might function as a competitive inhibitor of NAADP and cADPR synthesis (Capel et al. 2015; Warszta et al. 2014; Lin et al. 2017).

Since mounting evidence suggested SAN4825 as an inhibitor for CD38, it was used to study the effect of the CD38 pathway on SR Ca^{2+} loading in murine ventricular cardiomyocytes. Interestingly, in the presence of 3 μM SAN4825, there was no significant reduction in the SR Ca^{2+} levels in the presence of cAMP. This was an unexpected result since previous studies had shown 3 μM SAN4825 to strongly inhibit the production of NAADP in sheep SR membrane preparations and also reduce the effect of isoprenaline induced arrhythmias in mouse Langendorff perfused hearts. This ruled out the possible issues of drug permeability into the cardiomyocytes since it was able to elicit a response in whole hearts and also, the cardiomyocytes used in this study were permeabilised making it easier for the drug to enter the cells. One possibility is that though SAN4825 inhibits the production of NAADP, it may not completely abolish it. Since NAADP is highly potent and can activate the pathway at nanomolar concentrations, minute amounts of NAADP produced might be activating the NAADP pathway and hence, showing an increased loading of SR Ca^{2+} in the presence of cAMP. It is reasonable to ponder as to why would 3 μM SAN4825 be able to abolish arrythmias due to enhanced

β-adrenergic stimulation when it is unable to stop the effect of enhanced SR loading due to β-adrenergic stimulation. This might be because β-adrenergic stimulation heightens the NAADP and cADPR to levels that can provoke arrhythmias while SAN4825 is able to inhibit production of these molecules just enough to prevent the onset of arrhythmias. Although these considerations sound valid in hypothesising the absence of an effect of SAN4825 in cAMP induced SR Ca^{2+} loading, one cannot discard the possibility of loss of viability of the drug since the last experiments performed using this batch of the drug in our laboratory was over two years ago and the quality of the drug might have depreciated over time leading to lack of activity. Perhaps a higher concentration of SAN4825 or a new batch of the drug can be used to repeat these experiments to understand its role in the CD38 pathway.

4.4.4 Probable mechanism of the NAADP pathway in Ca^{2+} handling of the heart under β-adreneroceptor stimulation

The exact mechanisms that tie the NAADP pathway to the Ca^{2+} handling of the heart are still under study. Multiple studies including results from this chapter suggest that activation of the NAADP pathway increases the Ca^{2+} load of the SR, resulting in larger Ca^{2+} releases and hence, enhanced contraction. The Ca^{2+} released from the lysosomes due to NAADP activity can be directly sequestered into the SR which might be facilitated by the favourable locations of the lysosomes and the SR as they have been reported to form microdomains (Aston et al. 2017). However, a Ca^{2+} amplification process that occurs due to Ca^{2+} release from the lysosomes is a more likely hypothesis of enhanced SR Ca^{2+} loading. Recent studies have placed CaMKII as an important part of the NAADP mediated effects in cardiac system. Capel et al. reported that a functional CaMKII was

necessary for the effects of the NAADP pathway in the cardiac system. They suggested that CaMKII may amplify the Ca^{2+} released from the lysosomes resulting in enhanced phosphorylation of phospholamban, thereby increasing Ca^{2+} uptake into the SR (Capel et al. 2015).

CaMKII is a serine/threonine-specific protein kinase that requires the binding of Ca^{2+} and calmodulin for this activation. Capel et al. tested the role of CaMKII in the NAADP signalling pathway by photoreleasing caged NAADP in the presence of the CaMKII inhibitors KN-93 and Autocamtide-2-Related Inhibitory Peptide (AIP). In the presence of KN-93, the increase in Ca^{2+} transient amplitudes was abolished in guinea-pig atrial and ventricular myocytes. In mouse ventricular myocytes, KN-93 and AIP abolished the positive effects of photoreleased NAADP on Ca^{2+} transient amplitude. Moreover, in the presence of KN-92, the structural analog of CaMKII that does not inhibit CaMKII, the NAADP effects on Ca^{2+} transient amplitudes were not affected, suggesting a role for CaMKII in the NAADP pathway in cardiomyocytes (Capel et al. 2015).

CaMKII has the ability to phosphorylate L-type Ca^{2+} channels resulting in enhanced Ca^{2+} currents and also has possible arrhythmogenic effects (Bers and Morotti 2014; Yuan and Bers 1994). However, multiple studies have suggested that the NAADP pathway does not affect the L-type Ca^{2+} currents in guinea-pig and mouse cardiomyocytes (Capel et al. 2015; Collins et al. 2011; Macgregor et al. 2007). Therefore, CaMKII might have another mode of action in cardiomyocytes with respect to the NAADP pathway. Since earlier studies and results from this chapter suggest an increase in SR Ca^{2+} load due to the NAADP pathway, a likely mechanism for action of CaMKII is through its effect on SERCA to enhance Ca^{2+} reuptake into the SR. Phospholamban is a 52 amino acids long phosphoprotein present on the SR in cardiomyocytes. At its dephosphorylated state,

phospholamban inhibits the affinity of SERCA2a for Ca^{2+} and the inhibition is removed on its phosphorylation at Ser16 or Thr17. CaMKII, which is activated by high concentrations of localised Ca^{2+} concentrations. is believed to phosphorylate phospholamban at Thr17 and thereby increase the activity of SERCA (Mattiazzi and Kranias 2011; Maier and Bers 2007). Taking these observations together, a possible mechanism of action of the NAADP pathway in enhancing SR Ca^{2+} load is through the activation of CD38 during β-adrenergic stimulation leading to increased production of NAADP. NAADP leads to release of Ca^{2+} from lysosomes which leads to increases local concentration of Ca^{2+} that can in turn activate CaMKII. The activated CaMKII phosphorylates phospholamban at Thr17 and remove its inhibition from SERCA, ultimately leading to enhanced SR Ca^{2+} loading. Adding strength to this hypothesis is electron microscopy data that suggests the existence of microdomains between SR and lysosomes which might make this process more favourable (Aston et al. 2017).

Another important consideration is the effect of the β-adrenergic/ NAADP pathway on RyR. PKA and CaMKII both have phosphorylation sites on RyRs. PKA phosphorylates RyR at Ser-2809 and CaMKII is known to phosphorylate RyRs at Ser-2814, thereby modifying its sensitivity (Camors and Valdivia 2014). Therefore, in conditions with increased PKA and CaMKII activity (β-adrenergic responses), one can expect an increased RyR open probability. This would mean as the SR Ca^{2+} load increases, increased release of Ca^{2+} via RyRs might also happen due to store-overload, resulting in underestimation of SR Ca^{2+} content changes due to the β-adrenergic or NAADP pathway. A recent study by Fernandez-Tenorio and Niggli reported that SERCA activation increases the threshold for spontaneous Ca^{2+} waves in mouse cardiomyocytes. In the presence of 20 μM cAMP, the threshold for spontaneous Ca^{2+} was increased by

approximately 40% (Fernandez-Tenorio and Niggli 2018). In the current study, the concentration of cAMP used for the experiments was half of that used by the Niggli group (10 μM) and the maximal increase in SR Ca^{2+} observed was 31%. This might perhaps be a reason why spontaneous releases of Ca^{2+} were not observed in the experiments of this chapter. Indeed, on the application of 20 μM cAMP, the SR Ca^{2+} levels were too erratic to study the NAADP pathway reliably. Further experiments need to be performed to investigate the effects of the NAADP mediated CaMKII activation and its effects on specific targets such as SERCA and RyR. Another possibility might be that the SERCA activity is more enhanced by PKA/ CaMKII pathway compared to the RyR and therefore a net increase in Ca^{2+} is observed over time. Using a cytoplasmic Ca^{2+} indicator simultaneously with an SR Ca^{2+} indicator will enable to study the Ca^{2+} uptake and release by the SR more reliably.

More evidence for the role of CD38 in SR Ca^{2+} handling lies in the location of CD38 in cardiomyocytes. Lin et al. reported that providing the NAADP substrates NADP and NA into the extracellular solution did not result in observable increases in the production of NAADP. However, permeabilising the cell membranes with saponin resulted in an increase in the production of NAADP, suggesting an intracellular location for functional CD38. Further experiments in mouse ventricular myocytes using a rabbit polyclonal antibody to CD38 revealed similar results. Very little staining was observed when the cardiomyocytes were intact but cardiomyocyte permeabilisation showed extensive staining for CD38. Interestingly, the CD38 staining showed a striated pattern with spacing less than 2 μm suggesting CD38 localisation near the SR. Similar staining on atrial myocytes confirmed that the localisation was more specific due to its association with the SR rather than with t-tubules, since atrial cells do not have a developed t tubule network.

This staining was absent in *CD38*$^{-/-}$ cardiomyocytes, ruling out non-specific staining (Lin et al. 2017). The localisation of CD38 with the SR and evidences for intracellular production of NAADP and cADPR is consistent with the results of this chapter and Chapter 3 regarding the role of CD38 pathway in Ca^{2+} handling in the heart. The close association of CD38, lysosomes and the SR might have positive collaboration in effecting the roles of NAADP/cADPR on excitation-contraction coupling in the heart.

4.4.5 Limitations of the SR Ca^{2+} dye loading technique

Although the SR Ca^{2+} dye loading technique described in this chapter addresses certain disadvantages of the commonly used technique of recording SR Ca^{2+} (caffeine induced total SR Ca^{2+} release observed by cytoplasmic Ca^{2+} indicator), this technique does suffer from its own limitations. Cytoplasmic contamination of the dye is a major hindrance to successfully map SR Ca^{2+}. Contamination of cytoplasmic dye can mask true effects of changes in SR Ca^{2+} and careful consideration needs to be made to avoid this. Fernandez-Tenorio and Niggli describe three different ways of removing contaminant Ca^{2+} indicator from the cytosol in mouse ventricular cardiomyocytes (Fernandez-Tenorio and Niggli 2016). One method of removing contaminant dye from the cytosol was using a patch pipette to dialyse the internal solution so as to minimise the dye concentration in the cytosol. High skill in patch clamp techniques and long duration of dialysis was required to satisfactorily remove the dye from the cytosol. In the second technique, the cell membrane was permeabilised using a low concentration of saponin. Saponin binds to cholesterol molecules in the cell membrane and forms small pores in the membrane. This enables the dye to diffuse from the cytoplasm to the extracellular solution, leaving the dye to be localised in intracellular organelles. This is the technique used for the

experiments designed in this chapter. The major disadvantage of this technique is that experiments requiring a functional cell membrane and/or electrical activation cannot be performed on this model. Also, valuable intracellular content required for cardiomyocyte functioning may diffuse out of the cell. However, the use of dextran in the solution might increase solution density and prevent critical proteins from diffusing out of the cell. The third approach for removing contaminant Ca^{2+} indicator from the cytosol involves a reversible permeabilisation technique using streptolysin O (SLO), a hemolytic toxin capable of forming pores on the cell membrane in a transient and reversible manner. In a reducing environment, SLO forms pores on the cell membrane which enables diffusion of the cytoplasmic dye into the extracellular solution after which normal redox condition is established leading to closure of the pores (Fernandez-Tenorio and Niggli 2016). Personal communication with the Niggli lab (University of Bern, Switzerland) was a crucial factor is determining the technique used in this chapter. The patch clamp and reversible permeabilisation techniques were difficult to achieve and produced low level of reproducibility. Therefore, permeabilisation of the cell membrane using saponin was used for the experiments designed in this chapter. Although other labs have published reports wherein Ca^{2+} indicators were preferentially loaded into the SR without permeabilisation, these techniques could not be reproduced successfully in our lab (Kabbara and Allen 2001; Wang, De Jesus, and Ripplinger 2015; Belevych et al. 2007).

An ideal model to study SR Ca^{2+} handling in single cells would involve a high signal to noise ratio low affinity Ca^{2+} indicator that preferentially loads into the SR without having contaminant loading in the cytoplasm or other intracellular organelles and also cardiomyocyte preparation involving minimal damage in its resting condition. However, the currently used available SR Ca^{2+} dyes (mainly Mag-fluo-4 and Fluo-5N) have

relatively low signal to noise ratios and suffer greatly from dye bleaching, making it difficult for continuous monitoring of the SR Ca^{2+}. Moreover, Ca^{2+} calibration to determine the absolute Ca^{2+} in the SR has not been fruitful. Refinement of the technique to selectively load the Ca^{2+} indicator into the SR without damaging the cell and using a low affinity ratiometric Ca^{2+} indicator (such as mag-fura-2) to correct for uneven dye loading and dye bleaching might enable the study of SR Ca^{2+} handling in cardiomyocytes with more efficiency. Also, combining the SR Ca^{2+} indicator with a cytoplasmic dye with non-overlapping emission wavelengths could provide a greater resolution for the investigation of the dynamic interactions of the SR and cytoplasmic Ca^{2+}.

Chapter 5

Presence of CD38 in sarcoplasmic reticulum-enriched membrane preparation from sheep hearts

5.1 Background

The first ARC known to catalyse the production of NAADP and cADPR was purified from *Aplysia californica* (Lee and Aarhus 1991). Using sequence comparison, two mammalian homologues of this ARC were discovered, namely, CD38 and CD157/Bst-1 (Itoh et al. 1994; States, Walseth, and Lee 1992).

CD38, since its discovery, has been believed to be a type-II transmembrane protein, with its catalytic C-domain facing the extracellular space (Jackson and Bell 1990). While this orientation is ideal for its immune system specific signalling functionalities, it is difficult to comprehend the catalytic activities of this enzyme in production of NAADP and cADPR from their intracellular substrates NADP, NA and NAD. Additionally, since NAADP and cADPR have been shown to have intracellular targets, if these messengers were to be produced by the extracellular active domain of CD38, they would have to be transported across the cell membrane to target their receptor and elicit a response.

One hypothesis to understand this complex interaction is a vesicular/transporter mechanism wherein functionally active ARCs are sequestered into the intracellular acidic organelles and transporters potentiate the movement of substrates and products to and from organelles, respectively (Davis et al. 2008). Another theory suggests a connexin (Cx43) -mediated release of NAD occurs to the outside of the cell. CD38 mediated production of cADPR occurs and the cADPR is transported back into the cell, hence completing an autocrine loop (Bruzzone et al. 2001; Franco et al. 1998).

An alternative hypothesis has been recently gained traction which suggests the existence of a type-III transmembrane orientation for CD38 having its active C-domain facing the

cytosol. Several groups reported the existence of a type-III CD38 in cells such as HL60 cells differentiated with retinoic acid, U937 monocytic cells activated by interferon γ and in peripheral blood mononuclear cells (Zhao, Lam, and Lee 2012). Concerns whether the disulphide bridges, which are critical in the enzymatic activity of CD38, were stable under the reducing conditions of cytosol were addressed by Zhao et al. The authors demonstrated that the type-III CD38 was functionally active inside the cytosol (Zhao et al. 2011). Also, by mutating the serine residues to aspartate, which is functionally equivalent to physiological phosphorylation, they showed that the type-III orientation of CD38 was more prominent than type-II orientation. This suggested a possible mechanism of CD38 orientation regulation through endogenous phosphorylation of serine (Lee 2014). It was suggested that both type-II and type-III orientations of CD38 exists with each type catering to specific functions in the cell. Perhaps the type-II orientation of CD38 is responsible for slow and long term agonist responses such as cell differentiation, while the type-III orientation might be responsible for fast cellular responses such as stimulation by hormonal agonists (Zhao et al. 2015).

Although CD38 and CD157 are considered to be the primary ARCs in mammalian tissues, the existence of other ARCs has also been suggested in various tissues such as skeletal tissue, kidney, brain and heart. In the heart, a minimum of three studies have suggested the existence of a non-CD38 ARC. Mészáros et al. suggested the existence of two separate ARCs in cardiac muscles, separated by their locations on the plasma membrane and the SR. They separated cardiac muscles from dog and rat into different fractions using differential centrifugation. The plasma membrane associated ARC showed CD38-like properties as it was sensitive to DTT and was labelled by anti-CD38 antibodies. However, the SR membrane associated ARC showed characteristics distinct

from the plasma membrane bound ARC. They showed that the SR bound ARC was inhibited by DTT and was not bound by anti-CD38 antibodies (Meszaros, Wrenn, and Varadi 1997). Another study by Xie et al. showed that in SR membrane preparations from rat hearts, there exists an ARC that did not bind to anti-CD38 antibodies and was not inhibited by DTT but was inhibited by Cu^{2+}. Mass spectrometry analysis of this 42 kDa protein showed no similarity to the protein sequences of CD38 (Xie et al. 2005). Kannt et al. discovered the two ARC inhibiting drugs SAN4825 and SAN2589 capable of inhibiting the ARC activity seen in rat and pig SR membrane preparations. However, these compounds were only able to partially inhibit the activity of human CD38 and or *Aplysia* cyclase transfected into the *Spodoptera frugiperda* cell line SF9. This 35 kDa protein was inhibited by Zn^{2+}, unlike the human CD38 which was potentiated by Zn^{2+} (Kannt et al. 2012).

All the studies described above show the existence of an ARC in cardiac SR membranes even though they show characteristics distinct from CD38. The aim of this chapter is to further evaluate whether or not CD38 is the primary ARC in large mammal model species and its potential localisation to SR membrane. Functional properties of CD38 are assessed in SR membrane preparations in the presence of a CD38 inhibitor (kuromanin). Molecular biology techniques are used to ascertain whether the ARC found in sheep SR is CD38 or a hitherto unknown ARC.

5.2 Methods

All methods used in this chapter are described in detail in Chapter 2.

For the RT-PCR reaction, RNA was isolated from sheep ventricular tissue using an RNA isolation kit. Primers were designed for sheep CD38, CD157/BST1 and GAPDH (positive control) by using the Primer-BLAST tool. RT- PCR was done using a commercially available RT-PCR kit (described in Section 2.6). The RT-PCR products were visualised on a 1.5% agarose gel. The expected band sizes were 489 bp for CD38, 407 bp for CD157 and 497 bp for GAPDH.

For docking studies, Autodock Vina (The Scripps Research Institute) was used. PyRx tool (SourceForge) was used to prepare the human CD38, NAD+ and Kuromanin structures for docking by Autodock Vina. Docking was carried out by Autodock Vina and the docking conformations with the lowest binding energy were identified. At least three docking runs were performed for each condition (NAD+ against human CD38 and Kuromanin against human CD38) to confirm whether consistent results for the lowest binding energy conformations were obtained from the docking software. The 3D visualisations of successful docking were done by PyMOL (Schrödinger) and Discovery Studio Visualiser (BIOVIA). The docking protocol is described in detail in Section 2.8.

Sheep sarcoplasmic reticulum- enriched membrane preparation (SRMP) and mouse mixed membrane preparation were prepared as described in Sections 2.4 and 2.5, respectively. NGD assay was done for detecting ADP ribosyl cyclase activity of sheep cardiac SRMP. To initiate cGDPR production, 500 μM NGD was added to the SRMP sample. Formation of cGDPR was measured using fluorimetry. The rate of cyclase

activity of the protein sample was then defined by the change in fluorescence with time, which is the slope of the curve in the fluorescence versus time plot obtained by linear regression (described in section 2.7). SRMP was either preincubated with DMSO or different concentrations of Kuromanin (10 and 30 μM) for 30 min before being supplemented with 500 μM NGD to produce cGDPR.

For Western blotting experiments, sheep cardiac SRMP and mouse mixed membrane preparation (positive control) was run on an SDS-PAGE gel, after which the was transferred onto a PVDF membrane. Immunoblotting was done on membrane using a 1:1000 concentration of an anti-CD38 antibody raised in mouse against human CD38. The PVDF was visualised on an infra-red detector to detect bands (described in Section 2.8). The results were analysed using ImageLab software (Bio-Rad).

For protein purification, immunoprecipitation was done using a commercially available kit. The purification process was validated by running the sample on an SDS-PAGE gel and then stained by Coomassie brilliant blue dye (described in Section 2.9).

The mass spectrometry (described in Section 2.11) on the protein purified from immunoprecipitation was performed at the Target Discovery Institute (University of Oxford) by Dr Roman Fisher and his team.

5.3 Results

5.3.1 Sheep heart showed an expressed CD38 gene but no functional CD157 gene

To identify whether CD38 was present in sheep heart tissue, RT-PCR was performed and visualised on an agarose gel. Expected bands were seen for CD38 around 500 bp confirming the presence of CD38 mRNA in sheep heart. The absence of a band for CD157 suggests that CD157 is not expressed in the heart. A bright band for the positive control (GAPDH) suggests that the mRNA purification process and RT-PCR was successful. The data is shown in Figure 5.1.

5.3.2 *In silico* evidence suggested Kuromanin binding to the active sites of human CD38

To identify whether the Kuromanin bound to CD38, docking studies were performed using Autodock Vina. Crystal structure of human CD38 (PDB ID: 2HCT) was docked against Kuromanin (Pubchem ID: 441667). Predicted docking conformations showed low negative binding energies (approximately -8.5 kcal/mol). Identifying amino acid residues of CD38 interacting with Kuromanin included the CD38 active site residues Trp125, Arg127, Glu146, Trp189 and Ser193. Figure 5.2 (B) shows a 3D conformation of Kuromanin and the amino acids it interacts with in human CD38.

Docking was also performed with NAD+ (substrate of CD38 which results in the production of cADPR). As expected, predicted docking conformations showed low negative binding energies (approximately -9.5 kcal/mol). NAD+ interacting amino acid residues on human CD38 included the human CD38 active site residues Trp125, Arg127,

Glu146, Trp189 and Ser193 (Liu et al. 2008). Figure 5.2 (A) shows a 3D conformation of NAD+ and the amino acids it interacts with in human CD38. Kuromanin and NAD+ appeared to overlap on the active sites of human CD38 suggesting that Kuromanin had the same binding sites as NAD+ in human CD38 (Figure 5.2 (C)).

5.3.3 Sheep cardiac SRMP showed ARC cyclase activity and was inhibited by the CD38 inhibitor Kuromanin

To validate whether the isolated sheep cardiac SRMP showed ARC properties, NGD assay was performed. NGD is an analogue of the cADPR substrate NAD which on cyclisation forms the fluorescent product cGDPR. Unlike cADPR, cGDPR is resistant to hydrolysis and combined with its fluorescent properties, it is an attractive method to study cyclase properties of ARCs.

Sheep cardiac SRMP showed ARC properties as it was able to convert NGD into cGDPR. The flavonoid CD38 inhibitor kuromanin was able to reduce the production of cGDPR. The rate of cGDPR formation was reduced by 20 ± 5% from the control in the presence of 10 μM kuromanin (P= 0.043) and the reduction was 48 ± 8 % from control in the presence of 30 μM kuromanin (P= 0.001). The significance levels between the groups were calculated by a one-way ANOVA with Dunnett's multiple comparisons test (4 total experiments were performed for each condition on SRMP obtained from 2 separate sheep hearts). Figure 5.3 summarises these data.

5.3.4 Western Blotting suggested the presence of CD38 in sheep cardiac SRMP

To determine whether sheep cardiac SRMP contained CD38, Western blotting was performed on the SRMP using an anti-CD38 antibody raised in mouse against human CD38 (sc-374650, Santa-Cruz Biotechnology). A mouse heart mixed-membrane preparation was used as the positive control.

Under reducing conditions (4% β-mercaptoethanol) positive staining for CD38 was observed in the SRMP in the form of a band at size approximately 45 kDa. Under non-reducing conditions (no β-mercaptoethanol), two bands were observed at sizes approximately 45 kDa and 90 kDa suggesting the existence of sheep CD38 in dimer form. A 45 kDa band was observed on the mouse heart mixed-membrane preparation (Figure 5.4).

5.3.5 Purification of CD38 from SRMP by immunoprecipitation

To further characterize the ARC in SRMP, immunoprecipitation was performed to purify the protein for further analysis. SRMP was incubated with CD38 antibody bound to Dynabeads protein G. Following the manufacturer's protocol, the protein of interest binding to the antibody was extracted and was validated by running the sample on an SDS-PAGE gel and stained with Coomassie brilliant blue.

One sharp band was observed at approximately 45 kDa, suggesting the possibility of successful purification of CD38 protein (Figure 5.5). However, multiple faint bands were observed between 25 and 35 kDa, suggesting non-specific protein pull-down (discussed more in Section 5.4). One band each at 50 kDa and 25 kDa were also observed. These bands correspond to the heavy and light chains of the antibody, respectively. Pre-

treatment of the sample for SDS-PAGE electrophoresis denatures the antibody fragments to heavy and light chain and these are separated on the gel. This is confirmed by performing the immunoprecipitation process with a negative control containing identical conditions to the sample minus the SRMP. As seen in Figure 5.5, the negative control showed only two bands corresponding to 50 kDa and 25 kDa.

5.3.6 Mass spectrometry analysis of the purified protein from immunoprecipitation

To provide more definitive evidence whether the ARC present in SRMP is CD38, the immunoprecipitated protein was analysed by mass spectrometry by Dr Roman Fisher's team at the Target Discovery Institute (University of Oxford). The protein sample was digested by trypsin and injected into an LC-MS. The spectra of peptide fragments obtained were compared to UniProt protein database to determine the presence of CD38.

The sample showed over 1000 hits when compared to UniProt sheep protein database. Since sheep CD38 protein sequence was not available in the database, it was not possible to confirm the presence of the protein against the sheep database. However, the mass spectrometry results revealed the presence of multiple uncharacterised sheep proteins present on the database. Uncharacterised protein sequences of molecular weights similar to CD38 were compared against the known sequences of human and bovine CD38 using 'Align sequences Protein-BLAST' (NCBI). However, no high level of sequence similarity was observed between the uncharacterised proteins and human and bovine CD38. The comparisons are summarised in Table 5.1.

The mass spectrometry results were also compared to human and bovine databases to find similarity to their characterised CD38 protein. No match for CD38 was found with either

databases. Tables 5.2 and 5.3 summarises the top 15 matches of proteins from human and bovine protein databases between 35 and 45 kDa (expected size of CD38).

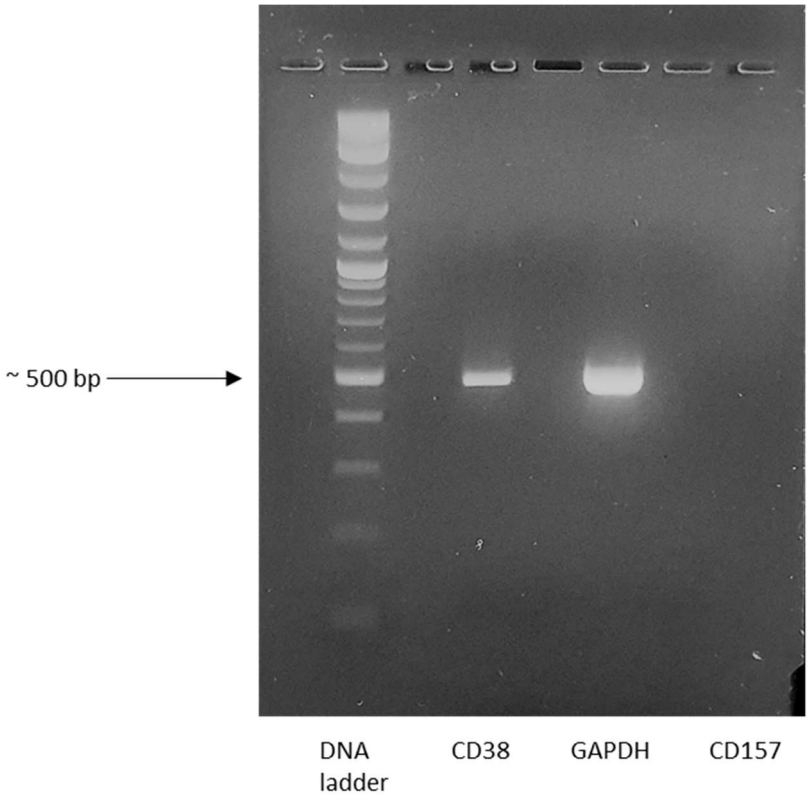


Figure 5.1: Presence of functional CD38 gene in sheep hearts (detected by RT-PCR)

The presence of a band for CD38 confirms the presence of an expressed CD38 gene in sheep hearts. No bands were seen for the primer pairs used to detect an expressed CD157 gene. GAPDH was used as the positive control for the RT-PCR experiments.

Note: The DNA ladder used was Quick-Load® 2-Log DNA Ladder, 0.1–10.0 kb

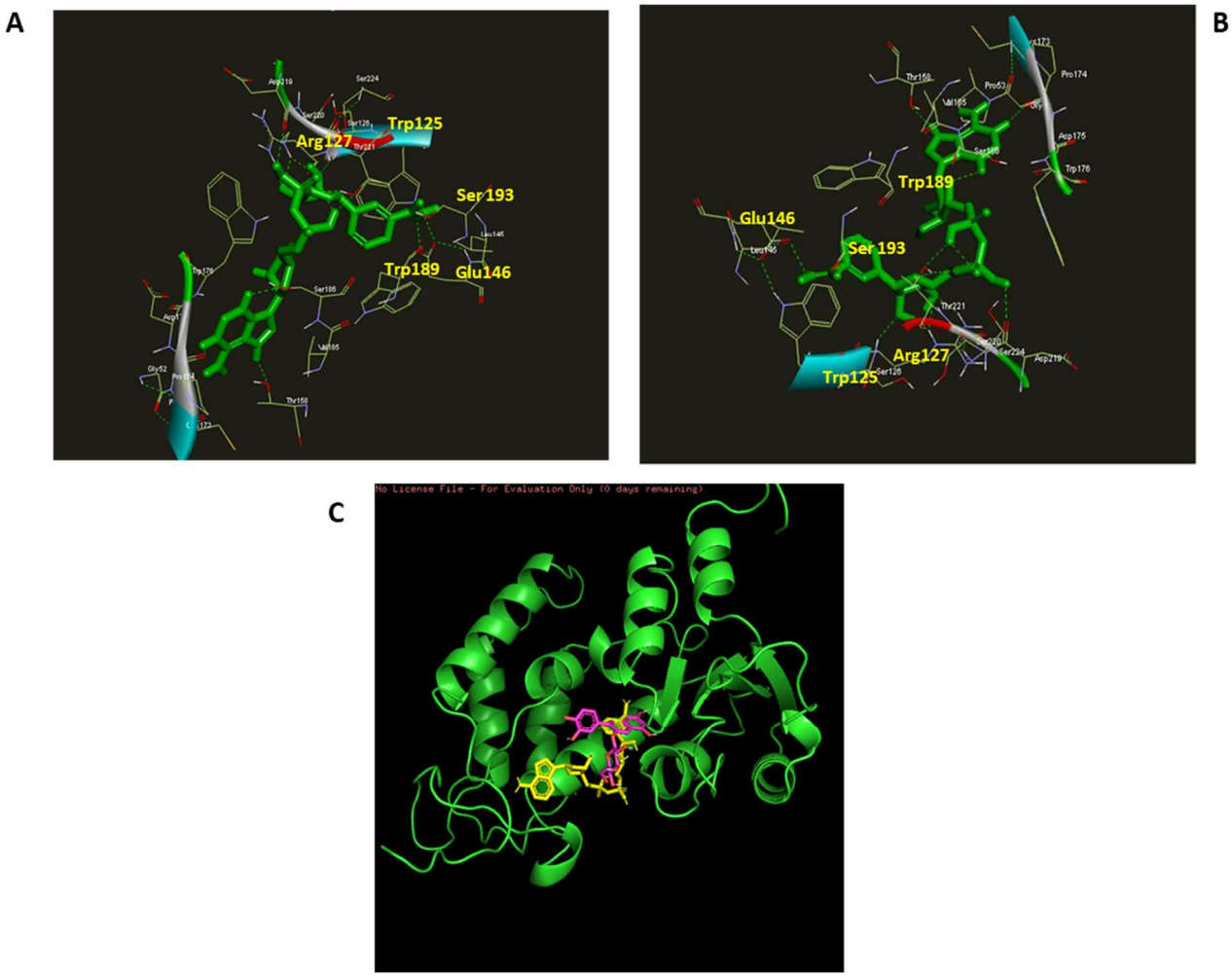


Figure 5.2: *In silico* evidence of Kuromanin binding to the active sites of human CD38

A shows NAD+ (bold green) with its interacting amino acids on CD38. The known active sites amino acids of human CD38 are highlighted in yellow.
B shows kuromanin (bold green) with its interacting amino acid residues on CD38. The active site residues of human CD38 are highlighted in yellow.
C shows the superimposition of NAD+ (yellow) to the most favourable binding conformation of kuromanin (pink) at the active site of human CD38.

Note: **A** and **B** were generated by the molecular visualisation software PyMOL. **C** was generated using the docking simulation software Discovery Studio Visualiser.
The known active site residues of human CD38 to which both NAD+ and kuromanin (highlighted in yellow in **A** and **B**) showed to interact were Trp125, Arg127, Glu146, Trp189, Ser193

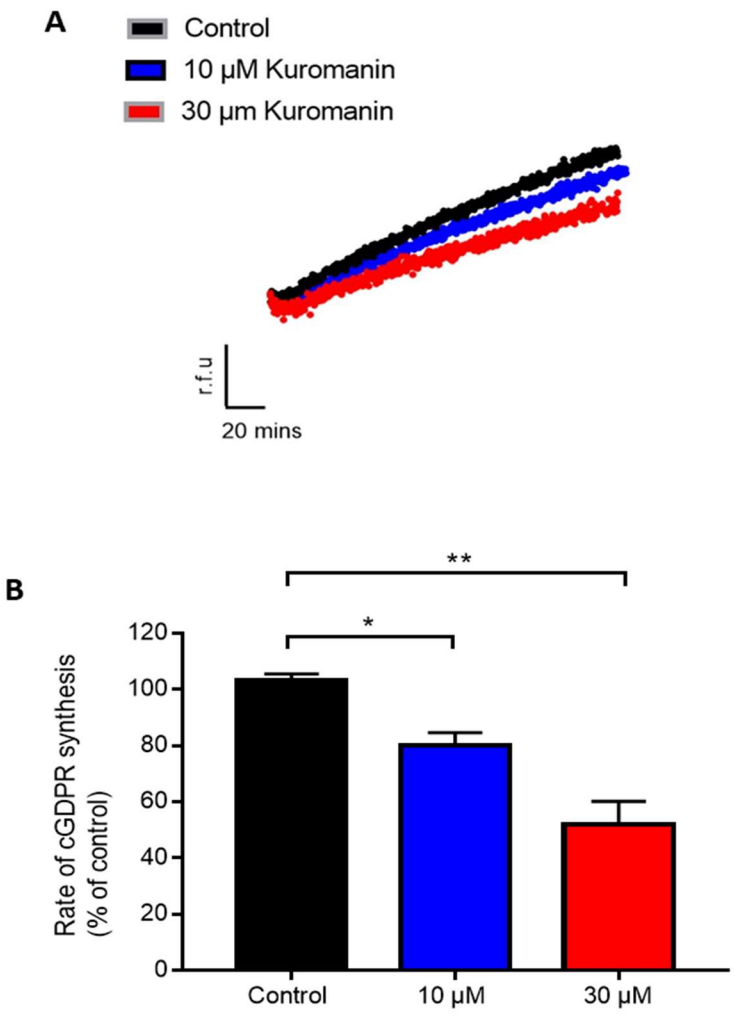


Figure 5.3: cGDPR production by sheep cardiac SRMP is inhibited by Kuromanin

Kuromanin significantly inhibited the production of cGDPR by sheep cardiac SRMP supplemented with 500 µM of the substrate NGD.

A shows a representative trace of cGDPR synthesis indicated by an increase in fluorescence by sheep cardiac SRMP when supplemented with NGD (500 µM). Kuromanin inhibited the synthesis of cGDPR in a dose-dependent manner.
B shows the inhibitory effect of Kuromanin on the rate of production of cGDPR in sheep cardiac SRMP.

Note: SRMP was either preincubated with DMSO or different concentrations of Kuromanin for 30 min before being supplemented with 500 µM NGD to produce cGDPR. The numerical data in **B** is represented as mean ± SEM. ** denotes $p<0.01$, * denotes $p<0.005$. One-way ANOVA with Dunnett's multiple comparisons test was used to compare the means of the groups (4 total experiments were performed for each condition on SRMP obtained from 2 separate sheep hearts).

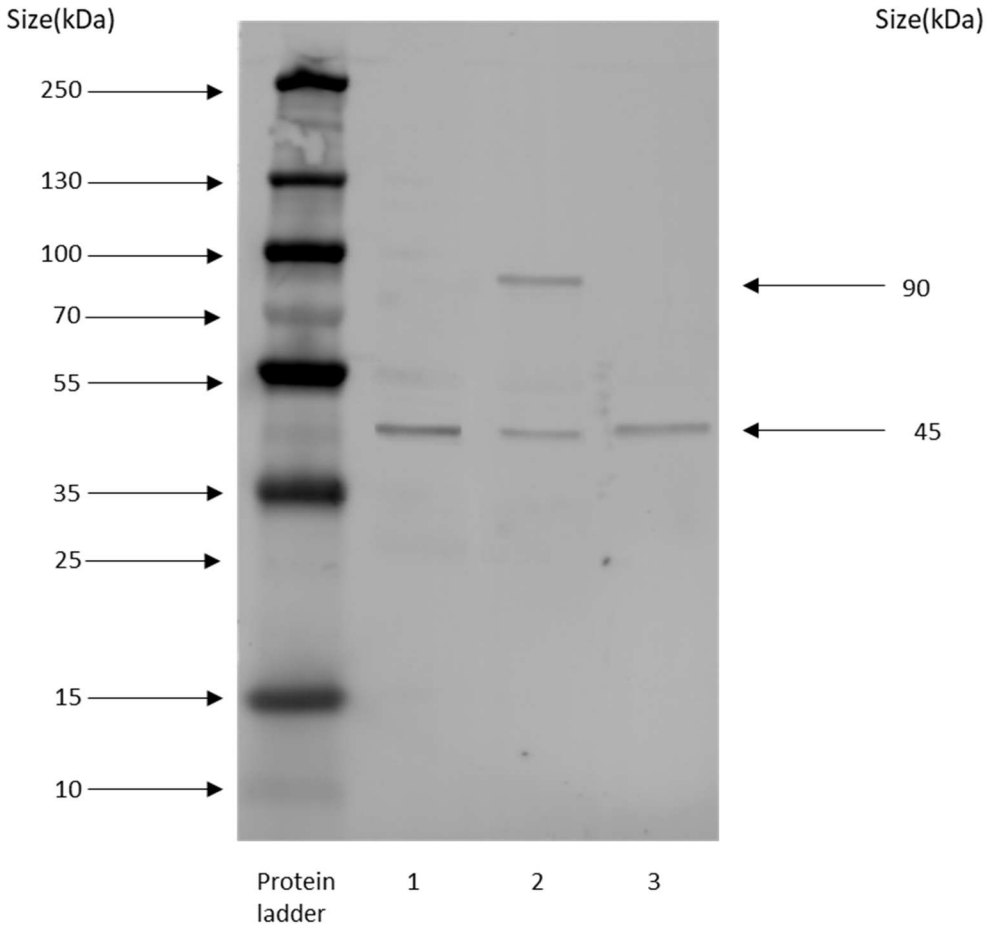


Figure 5.4: Western blot showing the presence of CD38 in sheep cardiac SRMP

1 shows the presence of a band at the size of 45 kDa in sheep cardiac SRMP immunoblotted against mouse CD38 antibody under reducing conditions.
2 shows the presence of a bands at the sizes 45 kDa and approximately 90 kDa in sheep cardiac SRMP immunoblotted against mouse CD38 antibody under non-reducing conditions.
3 shows the presence of a 45 kDa band in mouse mixed membrane preparation immunoblotted against mouse CD38 antibody in reducing conditions (positive control)

Note: The protein ladder used was PageRuler™ Plus Prestained Protein Ladder, 10 to 250 kDa

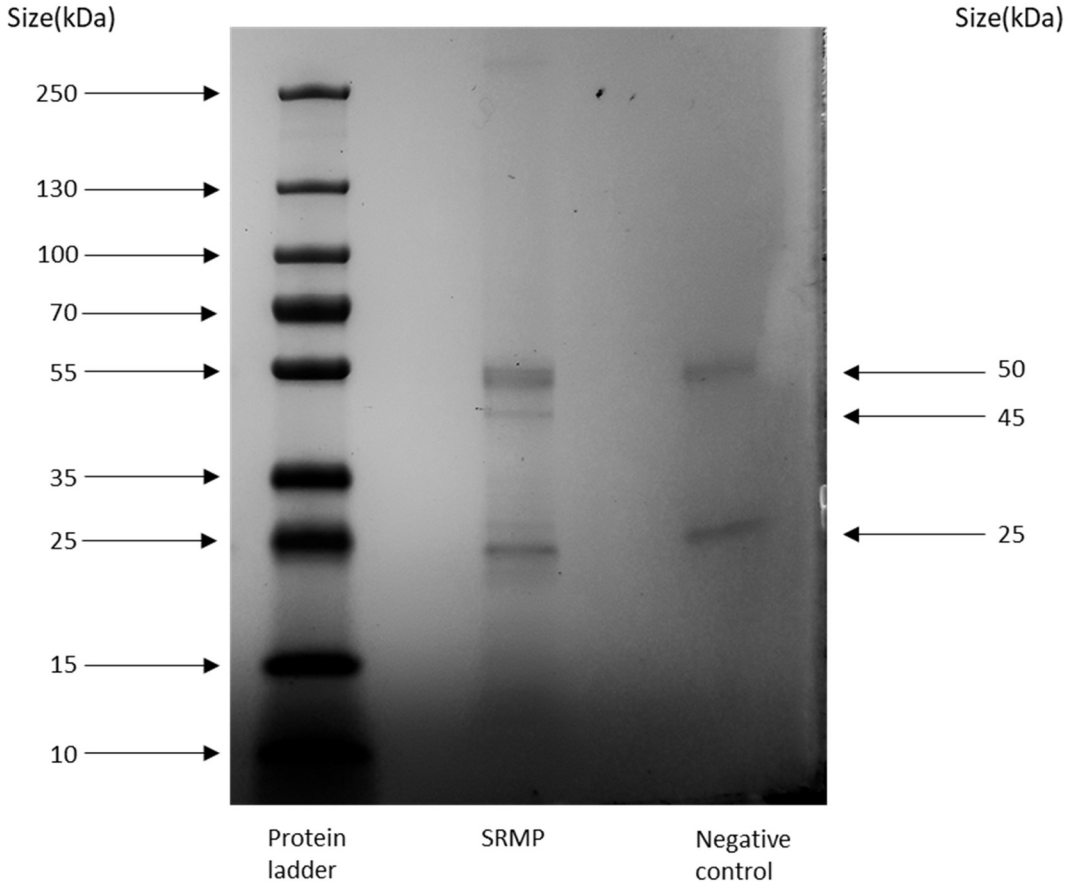


Figure 5.5: Coomassie Brilliant blue staining of SDS-PAGE gel run with products obtained after Immunoprecipitation of CD38 from sheep cardiac SRMP.

Coomassie staining of immunoprecipitation products (using mouse CD38 antibody) from sheep cardiac SRMP shows a band at 45 kDa suggesting successful protein pull-down. Multiple bands were observed between 35 and 20 kDa suggesting non-specific bindings. A band at 50 kDa and 25 kDa is the light and heavy chains of the antibody. This can be observed in the negative control which contains only the antibody and no SRMP.

Note: The protein ladder used was PageRuler™ Plus Prestained Protein Ladder, 10 to 250 kDa

Protein/ Accession	Molecular Weight (Da)	% similarity to Human CD38	% similarity to Bovine CD38
tr|W5QH43|W5QH43_SHEEP	46674	22	34
tr|W5QAS6|W5QAS6_SHEEP	46327	22	35
tr|W5QA76|W5QA76_SHEEP	36775	No similarity	34
tr|W5Q082|W5Q082_SHEEP	41122	No similarity	27
tr|W5PD11|W5PD11_SHEEP	42778	No similarity	35
tr|W5PI58|W5PI58_SHEEP	42961	24	35
tr|W5PRM8|W5PRM8_SHEEP	39200	No similarity	35
tr|W5Q694|W5Q694_SHEEP	32960	24.5	25
tr|W5P530|W5P530_SHEEP	46396	31	27
tr|W5P529|W5P529_SHEEP	46171	31	27
tr|W5P1M4|W5P1M4_SHEEP	41675	31	30
tr|W5PQS6|W5PQS6_SHEEP	42774	36	26
tr|W5P4H9|W5P4H9_SHEEP	41805	22	38
tr|W5PI58|W5PI58_SHEEP	42961	24	39
tr|W5PMJ1|W5PMJ1_SHEEP	41224	20	37

Table 5.1: List of top 15 matched uncharacterised sheep proteins obtained from mass spectrometry and their % similarity to human and bovine CD38 protein sequences.

No high level of similarities were observed between the uncharacterised sheep proteins with human or bovine CD38 protein sequence.

Protein/ Accession	Description	Molecular Weight (Da)	% Coverage
P63258|ACTG_BOVIN	Actin, cytoplasmic 2 OS=Bos taurus OX=9913 GN=ACTG1 PE=1 SV=1	41793	51
P60712|ACTB_BOVIN	Actin, cytoplasmic 1 OS=Bos taurus OX=9913 GN=ACTB PE=1 SV=1	41737	51
P00515|KAP2_BOVIN	cAMP-dependent protein kinase type II-alpha regulatory subunit OS=Bos taurus OX=9913 GN=PRKAR2A PE=1 SV=2	45094	42
Q3ZC07|ACTC_BOVIN	Actin, alpha cardiac muscle 1 OS=Bos taurus OX=9913 GN=ACTC1 PE=2 SV=1	42019	47
Q3ZC09|ENOB_BOVIN	Beta-enolase OS=Bos taurus OX=9913 GN=ENO3 PE=2 SV=1	47096	40
P04272|ANXA2_BOVIN	Annexin A2 OS=Bos taurus OX=9913 GN=ANXA2 PE=1 SV=2	38612	46
P68138|ACTS_BOVIN	Actin, alpha skeletal muscle OS=Bos taurus OX=9913 GN=ACTA1 PE=1 SV=1	42051	47
Q08DN8|FLOT1_BOVIN	Flotillin-1 OS=Bos taurus OX=9913 GN=FLOT1 PE=2 SV=1	47353	44
A6QLR4|FLOT2_BOVIN	Flotillin-2 OS=Bos taurus OX=9913 GN=FLOT2 PE=2 SV=1	46995	40
Q9XSC6|KCRM_BOVIN	Creatine kinase M-type OS=Bos taurus OX=9913 GN=CKM PE=1 SV=2	42989	44
P05131|KAPCB_BOVIN	cAMP-dependent protein kinase catalytic subunit beta OS=Bos taurus OX=9913 GN=PRKACB PE=1 SV=2	40594	40
P81287|ANXA5_BOVIN	Annexin A5 OS=Bos taurus OX=9913 GN=ANXA5 PE=1 SV=3	36089	50
P00125|CY1_BOVIN	Cytochrome c1, heme protein, mitochondrial OS=Bos taurus OX=9913 GN=CYC1 PE=1 SV=2	35297	44
O77784|IDH3B_BOVIN	Isocitrate dehydrogenase [NAD] subunit beta, mitochondrial OS=Bos taurus OX=9913 GN=IDH3B PE=2 SV=2	42497	40
Q32LG3|MDHM_BOVIN	Malate dehydrogenase, mitochondrial OS=Bos taurus OX=9913 GN=MDH2 PE=1 SV=1	35669	39

Table 5.2: List of top 15 matches of bovine proteins of similar molecular weight as CD38 against sheep cardiac SRMP purified by immunoprecipitation and analysed by mass spectrometry.

Mass spectrometry analysis did not reveal the presence of a protein in sheep cardiac SRMP purified by immunoprecipitation that showed similarity to bovine CD38.

Protein/ Accession	Description	Molecular Weight (Da)	% Coverage
P68032|ACTC_HUMAN	Actin, alpha cardiac muscle 1 OS=Homo sapiens	42019	67
P60709|ACTB_HUMAN	Actin, cytoplasmic 1 OS=Homo sapiens OX=9606 GN=ACTB PE=1 SV=1	41737	56
P63261|ACTG_HUMAN	Actin, cytoplasmic 2 OS=Homo sapiens OX=9606 GN=ACTG1 PE=1 SV=1	41793	56
P68133|ACTS_HUMAN	Actin, alpha skeletal muscle OS=Homo sapiens OX=9606 GN=ACTA1 PE=1 SV=1	42051	66
P08559|ODPA_HUMAN	Pyruvate dehydrogenase E1 component subunit alpha, somatic form, mitochondrial OS=Homo sapiens OX=9606 GN=PDHA1 PE=1 SV=3	43296	44
P06732|KCRM_HUMAN	Creatine kinase M-type OS=Homo sapiens OX=9606 GN=CKM PE=1 SV=2	43101	36
P13929|ENOB_HUMAN	Beta-enolase OS=Homo sapiens OX=9606 GN=ENO3 PE=1 SV=5	46987	34
P04075|ALDOA_HUMAN	Fructose-bisphosphate aldolase A OS=Homo sapiens OX=9606 GN=ALDOA PE=1 SV=2	39420	42
P07355|ANXA2_HUMAN	Annexin A2 OS=Homo sapiens OX=9606 GN=ANXA2 PE=1 SV=2	38604	35
P28289|TMOD1_HUMAN	Tropomodulin-1 OS=Homo sapiens OX=9606 GN=TMOD1 PE=1 SV=1	40569	34
P00558|PGK1_HUMAN	Phosphoglycerate kinase 1 OS=Homo sapiens OX=9606 GN=PGK1 PE=1 SV=3	44615	26
Q9BT78|CSN4_HUMAN	COP9 signalosome complex subunit 4 OS=Homo sapiens OX=9606 GN=COPS4 PE=1 SV=1	46269	27
P63092|GNAS2_HUMAN	Guanine nucleotide-binding protein G(s) subunit alpha isoforms short OS=Homo sapiens OX=9606 GN=GNAS PE=1 SV=1	45665	30
Q15365|PCBP1_HUMAN	Poly(rC)-binding protein 1 OS=Homo sapiens OX=9606 GN=PCBP1 PE=1 SV=2	37498	30
P50148|GNAQ_HUMAN	Guanine nucleotide-binding protein G(q) subunit alpha OS=Homo sapiens OX=9606 GN=GNAQ PE=1 SV=4	42142	27

Table 5.3: List of top 15 matches of human proteins of similar molecular weight as CD38 against sheep cardiac SRMP purified by immunoprecipitation and analysed by mass spectrometry.

Mass spectrometry analysis did not reveal the presence of a protein in sheep cardiac SRMP purified by immunoprecipitation that showed similarity to human CD38.

5.4 Discussion

This chapter attempted to characterize the ARC present in sheep cardiac SRMP, and experiments were designed and performed to assess whether the ARC characteristics seen in the SRMP is that of CD38. Strong pieces of evidence point to this possibility even though the mass spectrometry data failed to detect the presence of CD38.

5.4.1 Does a functional CD38 gene exist in sheep heart?

The first aim of the chapter was to check the presence of a functional CD38 gene in sheep heart. Sheep cardiac SRMP is shown to have ARC properties, therefore, presence of a functional CD38 gene would strengthen the case for CD38 being the primary ARC in sheep hearts. For this purpose, reverse-transcription polymerase chain reaction (RT-PCR) was performed on RNA extracted from sheep ventricular tissue. The advantage of using RT-PCR is that selective amplification of mRNA would suggest the presence of an expressed gene. Moreover, this technique is highly sensitive and can amplify even low copy numbers of the desired mRNA (picogram level) making it an attractive tool to check the presence of CD38 in cardiac tissue. RT-PCR showed the presence of an expressed CD38 gene in sheep cardiac tissue. Additionally, since no amplification of CD157 gene was observed in the RT-PCR experiments, a lack of functional CD157 is suggested. However, only one primer pair for CD157 was tested in the experiments designed for this chapter. The lack of amplification of CD157, though unlikely, can be due to unfavourable sensitive PCR conditions such as %GC content or melting temperature for the chosen pair of primers. Repeating RT-PCR with more primer pairs and optimisation of RT-PCR conditions might be necessary to confirm the absence of CD157 in sheep hearts. CD157 is suggested to catalyse the cyclisation of NAD to cADPR but lacks the ability to produce

NAADP from NADP and NA (Malavasi et al. 2008). Previous study by Terrar group has shown that sheep cardiac SRMP is capable of producing both cADPR and NAADP, suggesting CD38 to be a more likely candidate as the cardiac ARC (Lin 2017). Further validation for the presence (or absence) of CD157 was not pursued in this chapter since the main focus of study of this chapter was the ARC CD38 in sheep cardiac SRMP.

5.4.2 Would SR be a suitable place for CD38?

The use of cardiac SRMP in this chapter was to study the presence of CD38 with special consideration to its localisation with the SR. The existence of a type-III orientation of CD38 has been briefly discussed in the background section of this chapter. The association of ARCs with the SR has been published by multiple groups before (Kannt et al. 2012; Meszaros, Wrenn, and Varadi 1997; Xie et al. 2005; Lin 2017; Lin et al. 2017) (discussed in Section 5.1). Research has also shown evidence for CD38 to be expressed in the lysosomes (Cosker et al. 2010; Davis et al. 2008; Fang et al. 2018). One major support for lysosomal localisation of CD38 is the enhanced production of NAADP at acidic pH. Studies in Terrar lab on sheep cardiac SRMP has shown that even though NAADP production is maximal at acidic pH, it is not abolished at pH 7.2. At pH 7.2, NAADP production is approximately 25% of that at pH 4.5 (Lin 2017). This is of particular interest considering that the threshold of NAADP to release Ca^{2+} from lysosomes is very low at the nanomolar range (Macgregor, Yamasaki, et al. 2007; Nebel et al. 2013). Perhaps the low production of NAADP at pH 7.2 is sufficient to elicit the NAADP signalling pathway in the heart. Experiments performed in the Terrar lab have shown that in intact mouse ventricular myocytes, CD38 staining using a rabbit polyclonal antibody showed localised staining in patches on the cell membrane, consistent with the presence of type-II orientation of CD38. However, permeabilisation of the cells with

Triton X-100 or saponin resulted in enhanced intracellular staining of CD38. The staining followed a striated pattern that resembled the sarcomeric spacing. This staining was absent on *CD38*$^{-/-}$ mice myocytes. Moreover, in rabbit atrial cardiomyocytes treated with Triton X-100, similar striated pattern was observed that colocalised with RyR immunostaining, suggesting a close special association between them. The positive staining on atrial cells suggests that staining obtained is due to the SR association of CD38 rather than with the t-tubules since atrial cells have poorly developed t-tubule network and do not show regular sarcomere spacing as like ventricular cells. Aston et al. has reported lysosomes also have close proximity with the SR, however, the striated pattern for lysosomal markers were less distinct than for the CD38 staining (Aston et al. 2017; Lin et al. 2017). The observations reported above give reasonable evidence for a close association of CD38 to the SR. The expression of CD38 on the SR has some strategic advantages considering the functions of NAADP and cADPR with respect to Ca^{2+} handling in the heart. The SR has been reported to have close proximity to the lysosomes and NAADP releases Ca^{2+} from the lysosomes to affect SR Ca^{2+} handling. Also, cADPR is believed to act on RyR to elicit Ca^{2+} releases from the SR (Aston et al. 2017; Macgregor, Rakovic, et al. 2007). The localisation of intracellular CD38 on to the SR might promote the products of CD38 (NAADP and cADPR) to be in close proximity to their targets and the local rises in concentration of these products might improve the probability to bind to their targets (potentially TPC2 for NAADP and RyR for cADPR).

The best method to study the association between the SR and CD38 would be to obtain a pure SR preparation but this is limited by the lack of techniques to reliably isolate proteins exclusively from the SR. The technique devised in this chapter to isolate the SRMP, however, is an acceptable technique used widely to study SR proteins including RyR

(O'Brien et al. 2019; Sitsapesan, McGarry, and Williams 1994; Sitsapesan et al. 1991; Li et al. 2015). Nevertheless, the relative purity of SR preparations has been supported by previous studies using biochemical and electron microscopy approaches (Holmberg and Williams 1990; Meszaros, Wrenn, and Varadi 1997; Saito et al. 1984). An added advantage of using SR membrane preparations from sheep is that much larger quantities of SRMP can be produced from sheep hearts than from hearts of smaller animals such as mouse or rats. For example, to obtain an equivalent amount of SRMP obtained from one ventricle of a sheep heart, approximately 10 mouse hearts are required. However, a lack of gene and protein databases as extensive as mouse databases and the inability to create genetically modified animals present as disadvantages to use sheep cardiac SRMPs.

5.4.3 Is there evidence for the existence of CD38 in the SRMP from sheep hearts?

Flavonoids are a class of plant secondary metabolites found in fruits, vegetables, roots, stems and grains. They are known to possess biochemical and antioxidant effects which are protective against diseases like cancer, atherosclerosis, Alzheimer's disease, among others (Lee et al. 2009; Panche, Diwan, and Chandra 2016). Kellenberger et al. used invitro enzymatic assays to find flavonoid inhibitors of human CD38 purified after being expressed on *Pichia pastoris*. Using a high-throughput screening, they discovered 20 flavonoids that were capable of inhibiting the cyclase activity of CD38. Among them, kuromanin was a potent inhibitor (IC_{50}= ~ 6 μM) of the cyclase activity of CD38 (Kellenberger et al. 2011). Kuromanin has been shown to effectively inhibit the activity of CD38 in multiple studies over the past few years (Vaisitti et al. 2015; Horenstein et al. 2016; Schiavoni et al. 2018; Morandi et al. 2015; Al-Abady et al. 2013). Docking studies

performed in this chapter suggests that Kuromanin binds to CD38 and occupies the active site of CD38 (Liu et al. 2008). Similar docking sites and interactions with amino acid residues of the active site of CD38 for Kuromanin and the known substrate of CD38, NAD, suggests that Kuromanin binds to the active site of CD38. This was confirmed by NGD assay wherein Kuromanin was able to inhibit the cyclase activity of sheep cardiac SRMP in a dose dependent manner. NGD assay is a commonly used technique to assess ribosyl cyclase activity. This assay used NGD (an analogue of NAD) that forms cGDPR in the presence of an ARC. cGDPR being a fluorescent product and resistant to hydrolysis unlike cADPR, makes it an attractive substrate to study the cyclase activity of ARCs. These results provide more strength for the presence of a functionally active CD38 in sheep SRMP. Although docking studies in this chapter provide clues as to where kuromanin might bind on CD38, this cannot be considered as definitive evidence as to its binding location. Binding locations were considered by lowest binding energy conformations based on the Autodock software's scoring algorithm. These results can vary depending on the docking softwares used. However, the results obtained from the docking studies can be used to formulate a hypothesis for the exact binding locations of kuromanin on CD38 which could then be tested through mutagenesis experiments.

Immunoblotting experiments using western blotting technique was employed to provide further evidence for the presence of CD38 in sheep cardiac SRMP. A well validated mouse CD38 antibody was used against sheep cardiac SRMP and was immunoblotted on a PVDF membrane (Mottahedeh et al. 2018; Ovacik et al. 2019). A 45 kDa protein was detected which corresponds to the size of CD38. Similar band of 45 kDa seen on mouse mixed membrane preparations (used as positive control) suggests that the band seen on sheep cardiac SRMP is likely CD38. Interestingly, under non-reducing conditions (in the

absence of β-mercaptoethanol), an additional band could be observed with size approximately 90 kDa. This observation is of particular interest considering the property of CD38 to form oligomers. Chidambaram et al. showed that in porcine heart microsomes, a single 45 kDa band was seen under reducing conditions. However, under non-reducing conditions, a series of bands ranging from 45 – 285 kDa was observed, suggesting the existence of oligomers of CD38. These oligomers were stable under high concentrations of SDS and also showed higher cyclase activity than the monomeric form (Chidambaram, Wong, and Chang 1998). More studies of human CD38 transfected in HeLa cells and mouse CD38 on lymphocytes also were observed to be expressed as dimers and tetramers (Bruzzone et al. 1998; Hara-Yokoyama et al. 2012). Moreover, crystallised bovine CD38 were reported to form homodimers (Egea et al. 2012). Considering these studies, it is reasonable to expect the dimer form of CD38 to exist in sheep hearts as observed in the western blot experiments in this study.

Although previous studies from the Terrar lab and the results discussed above provide strong indication for CD38 to exist in sheep cardiac SRMP and act as the primary ARC, the absence of one crucial piece of evidence in the form of mass spectrometry data renders this narrative incomplete. Positive evidence for CD38 in SRMP by Western blotting and NGD assays pushed us to validate the protein using mass spectrometry technique. For this purpose, reasonably purified protein would be required. Immunoprecipitation was the technique employed in this chapter to isolate the protein binding to the anti-CD38 antibody. Mass spectrometry analysis was done to compare the sample to a sheep protein database (UniProt) to identify the protein. A total of 1876 hits were observed against the protein sample suggesting possible contamination on the sample with other proteins. Although multiple hits are expected from mass spectrometry analysis due to its high level

of sensitivity, such large number of hits is considered unfavourable. The success of the immunoprecipitation process was tested on an SDS-PAGE gel to look for the protein at the desired size of 45 kDa. A series of bands of sizes 45 kDa and below were observed. Unlike the western blotting experiment where only 1:1000 antibody concentration (5 µL in 5 mL) was required for a positive result, the immunoprecipitation protocol required a much larger concentration of antibody (10 µL in 1 mL). This might have led to non-specific bindings that were observed on the Coomassie stained SDS-PAGE gel. However, a prominent band at the size of interest suggested that the protein pull-down technique was moderately successful. This band was extracted, and the mass spectrometry analysis was repeated. Though the sample showed considerably lesser number of hits (approximately 1000), the possibility of contamination of the sample with other proteins was still high. No direct hits for CD38 were observed from the results. This was expected since no validated protein sequence of sheep CD38 is currently available. The logic of running the sample against the sheep database was to identify uncharacterised proteins of size of approximately 45 kDa and compare these with validated CD38 protein sequences of other organisms. However, none of the uncharacterised proteins showed high level of similarities to CD38 from human or bovine origin. The analysis spectrum was widened by comparing the protein sample to human and bovine protein databases to look for possible hits for CD38. No hits for CD38 were observed in this analysis either. Absence of positive result from mass spectrometry analysis does not confirm the absence of CD38 in sheep cardiac SRMP. Perhaps the purification step used in this chapter was not sensitive or accurate enough for mass spectrometry analysis. A better protein purification process needs to be designed to identify the protein responsible for the producing cADPR and NAADP in sheep cardiac SRMP and reliably extract them.

Previous studies have suggested the presence of non-CD38 ARCs in various tissues including the heart. The main differences between CD38 and these suggested ARCs lie in the effect of divalent ions such as Zn^{2+} and Cu^{2+} on their catalytic activities as observed from cyclisation assays and in the absence of a protein in the expected range of 42-45 kDa (size of CD38 protein) from immunoblotting experiments. Moreover, studies using inhibitors showed differences in their effect on the ARCs as compared to CD38. For example, ganglioside GT1b was shown to inhibit an ARC from rat vascular smooth muscle cells but not did not have an effect on CD38 (de Toledo et al. 2000). There are limitations to the techniques used by these studies to characterise the ARCs observed in tissues. Although CD38 and the other ARCs show differing responses to divalent ions, little is known regarding the exact mechanism of the relationship between these divalent ions to the ARCs. The ions might be directly binding to the ARCs thereby eliciting a change in its catalytic properties or might be evoking a change in ARC properties by binding to an accessory protein. The differences in the ARCs responses to the divalent ions might be due to unintended removal of these accessory proteins during purification steps or its difference in expression in various tissues of study. Contradictory pharmacological studies have also hindered confirmation of the presence of a non-CD38 ARC in the heart. Nam et al. reported that 2,2'-dihydroxyazobenzene (DHAB) inhibited ARCs in the kidney but not the heart while Gul et al. showed that cardiac ARC was inhibited by DHAB (Gul et al. 2009; Nam et al. 2006; Gul et al. 2008). The use of *CD38*$^{-/-}$ models to study the biochemical and pharmacological properties would be the ideal method of validating the presence or absence of non-CD38 ARCs. Functional experiments in Chapters 3 and 4 strongly suggest the existence of CD38 as the ARC that contributes to the calcium handling properties of NAADP. Moreover, Lin et al. have shown that mixed mouse membrane homogenates from *CD38*$^{-/-}$ lacked the ability to

produce NAADP and cADPR providing more evidence for CD38 to be the primary ARC in cardiomyocytes (Lin et al. 2017). Combining these observations and the results of this chapter, a strong case for CD38 being the primary ARC responsible for Ca^{2+} handling properties in the heart and its close association to the SR is presented.

Chapter 6

A protocol for optical mapping of murine sinoatrial preparation with optogenetic pacing.

6.1 Background

The heartbeat begins in the SAN arising in a subset of nodal cells that display a spontaneous diastolic depolarization (Bleeker et al. 1980). Establishing stable pacemaker rhythm in the developing murine heart seems to require endogenous secretion of catecholamines, and catecholaminergic signalling via β-receptors (Ebert and Taylor 2006). Phenylethanolamine-N-methyltransferase (Pnmt) is the enzyme which catalyses the conversion of noradrenaline to adrenaline, the final stage in this synthetic pathway. Cells expressing Pnmt (Pnmt+ cells) are found in developing murine hearts as early as embryonic day (E) 8.5 (Ebert et al. 2004). This means that cardiac Pnmt+ cells are present before the sympathetic innervation of the heart develops—and before the development of the entire canonical adrenergic system. At this vital early period in development, around the time the primitive heart makes its very first attempts to beat, "intrinsic cardiac adrenergic" (ICA) cells are numerous across the developing myocardium, and in the pacemaker and conduction systems (Ebert and Thompson 2001). After this, more Pnmt+ cells immigrate to the heart with the neural crest (Owji, Varudkar, and Ebert 2013). While some catecholamine-secreting cells from this mixed lineage seem to persist into adulthood, most Pnmt+ cells differentiate into working cardiomyocytes and down-regulate their expression of Pnmt accordingly (Wang et al. 2017; Ebert and Taylor 2006; Huang et al. 1996; Owji, Varudkar, and Ebert 2013). Cells derived from this adrenergic lineage were fate-mapped, using a Pnmt-cre LacZ cross, and found to localise primarily to the left side of the adult heart (Ebert et al. 2004; Osuala et al. 2011). Perhaps unsurprisingly, given the extent to which ICA cells are involved with the foetal pacemaker and conduction systems, a number of Pnmt+-derived cardiomyocytes (PdCMs) have been found in the SAN and AVN (Ebert and Taylor 2006; Ebert and

Thompson 2001; Wang et al. 2017). PdCMs may help support the SAN in the adult mouse heart, but this remains to be thoroughly investigated.

Sinus node dysfunction (SND) associated with abnormal impulse formation or propagation in the SAN affects approximately 1 in 600 cardiac patients aged >65 years and is responsible for nearly 50% of the 1 million permanent pacemaker implants per year worldwide. Although SND occurs most commonly in elderly patients in the absence of clinically apparent accompanying cardiac disease, its pathogenesis is unclear. The development of novel pharmacological therapies to cure these patients relies on the thorough understanding of both normal physiology and pathophysiology of the SAN and atria (de Marneffe et al. 1993).

Among the animal models used for studying the basic molecular mechanisms of the SAN and atrial biology and disease, mice are being widely used due to their feasibility for modifications in the expression of different genes that encode ion channels or calcium handling proteins. It is therefore highly valuable to develop robust methodologies and techniques for studying SAN and atrial electrophysiological properties.

Recent advance in the technique of optogenetics provide an unprecedented opportunity for defining specific cell-type function in a highly complex multicellular system. This technique has enabled us to control the activity of one cell type while leaving others unaltered, with high temporal resolution and cellular precision. Since the first demonstrations of utility in mammalian neurons in 2005, optogenetics has spurred immense research activity in neuroscience and has extended to the cardiac field over the past few years (Boyden et al. 2005; Boyle et al. 2013; Nussinovitch and Gepstein 2015). The Lei lab had recently deployed a cell-type specific optogenetic approach to study the

properties of Pnmt+ cell-derived cardiomyocytes in the murine heart (Wang et al. 2017). Additionally, optical mapping using fluorescent dyes provides exciting opportunities for high spatio-temporal study of cellular electrophysiological events, including Ca^{2+} dynamics of the heart. The combination of these two technologies therefore allows development of unprecedented platforms for studying physiological events (e.g. voltage and Ca^{2+} signals) in a cell type selective manner at high spatio-temporal resolution.

The aim was to validate a cell type-specific optogenetic pacing strategy in Sino-atrial node containing atrial preparations (SAP) and to compare its Ca^{2+} handling properties pre and post optogenetic pacing. A protocol for the use of a combination of optogenetic and optical mapping techniques for investigating intracellular Ca^{2+} transients and pacemaker activity with high temporal and spatial resolution in specific cardiac tissues has been described. The protocol can be a powerful tool for studying sino-atrial preparation (SAP) physiology and pathophysiology using the mouse as a model system. Potential application of this technique towards development of novel strategies to treat SND is deliberated in the discussion section of this chapter.

6.2 Methods

The methods used in this chapter is described in detail in Chapter 2.

Pnmt-cre/ChR2 mice (aged less than 6 months, 4 males and 3 females) were sacrificed by concussion and cervical dislocation before the heart was quickly excised. The whole atrium was dissected out of the heart as described in Section 2.2. The SAP was prepared by opening the AV junction to expose the intercaval region containing the SAN, following which left atrium was opened to expose the left atrial endocardium. As the pacemaker cells are widely distributed throughout the entire region located between the superior (SVC) and inferior vena cava (IVC) and between the crista terminalis and intra-atrial septum (Glukhov et al., 2010), the SAP contains the SAN and the two atria intact (A sample SAP is shown in Figure 6.1 (A)). The SAP was then incubated in the Ca^{2+} indicator (Rhod-2, AM), the protocol of which is described in 2.12.1. Following the dye loading, the SAP was pinned onto a custom-made imaging chamber filled with 10 μM blebbistatin containing Modified Tyrode's solution and placed under the optical mapping setup at 36 ºC. The EMCCD recorded changes in fluorescence at a frequency of 0.52 kHz with a pixel size of 66 x 66 μm for periods of 10-20 seconds at a time using the acquisition software Metamorph.

Since PdCMs express channelrhodopsin-2 (ChR2), they could be excited by exposure to 470 nm blue light. For the production of optogenetic pacing spikes, rhythmic trains of blue (450 - 490nm) LED light pulses were used. Pulse trains were devised using Spike2 software. For most experiments, 150-160 ms cycle length (6.25 - 6.67 Hz) was used. A constant current LED controller was used to define pulse duration (13-14 ms) and LED

current. This fed through an LED source, and the pacing trains were administered onto the tissue via liquid light guide (as illustrated in Figure 6.1 (B)).

The image analysis software Electromap was used for analysis the images obtained in these experiments. 'Frame removal' setting on the software was used to subtract optogenetic pacing peaks, in order to analyse underlying transients and average the signals together for the three conditions: before the pacing train; during; and after. Statistics for this chapter was performed on GraphPad Prism 7.

6.3 Results

6.3.1 Optogenetic pacing of sino-atrial preparations from Pnmt-cre/ChR2 mice

SAPs were incubated with Rhod-2 and calcium transients were recorded via EMCCD—before, during, and after applying optogenetic pacing. Decreased cycle lengths were observed during optogenetic pacing in all regions of the tissue, and at lower pacing frequencies close to 100% 1:1 coupling was achieved. This indicates that optogenetic pacing of PdCMs can control the heart rate of our SAPs. Optogenetic pacing frequency of 6.25 Hz reduced the mean cycle length (averaged across 7 SAPs) from 264.3 ± 42.7 ms before pacing and changed to 159.2 ± 1.4 ms during pacing ($p<0.02$). This decrease in mean cycle length was reversible; after cessation of pacing, mean cycle length rose to 281.9 ± 48.9 ms, not significantly different from the mean cycle length before pacing ($p=0.62$). In summary, optogenetic pacing at a frequency of 6.25 Hz was both controlled and reversible (Figure 6.2 (B)). As pacing frequency increases, especially above 6.67 Hz, the tissue is increasingly likely to be refractory when the next pacing spike hits. At higher frequencies, the SAPs began to lose coupling at 1:1, and the tissue began to move towards 2:1 coupling instead (Figure 6.2 (B)).

Whilst, in theory, a low frequency (5Hz for example) could have yielded 100% 1:1 coupling, this rate of optogenetic pacing would have been slower than the sinus rhythm in some tissues, therefore, cannot be achieved with an intact functioning SAN containing SAP.

6.3.2 Optogenetic pacing of PdCMs can create a novel leading pacemaker site in a murine SAP

Optogenetic pacing of a sino-atrial preparation could shift the activation nadir to the left, creating a new leading pacemaker site or 'Neonode'. Activation patterns in the SAP were plotted using ElectroMap, with the midpoint of the upstroke of the calcium transient used as a pixel-by-pixel readout of tissue activation. The earliest-activating pixel was designated the activation nadir for that tissue. The activation nadir before pacing was always in the nodal region. Optogenetic pacing of PdCMs could move this activation nadir to the left (Figure 6.3 (A)), establishing a new leading pacemaker site towards the left atrium. This change in the location of the leading pacemaker was reversible upon cessation of pacing. Left-shift of the leading pacemaker occurred in 4 out of 7 SAPs; note that one leftward deviation appears more upward relative to the SVC-IVC axis—this is due to contortion of the tissue (Figure 6.3). Although no leading pacemaker shift occurred in 3 SAPs, there was augmented conduction: optogenetic pacing leads to a left-shift of the activation curve (Figure 6.4 (A)). This was most noticeable in the first few milliseconds of tissue activation (Figure 6.4 (A), inset). Optogenetic pacing reduced the time to 5% tissue activation from 1.6 ± 0.2 ms to 0.9 ± 0.2 ms ($p=0.03$), the time to 10% tissue activation from 2.4 ± 0.3 ms to 1.5 ± 0.3 ms ($p=0.02$), and the time to 20% tissue activation from 3.9 ± 0.5 ms to 2.3 ± 0.3 ms ($p=0.02$), but at all points ≥ 30% tissue activation, there was no significant difference in activation time (Figure 6.4 (A and B)). Also, the conduction velocity did not change significantly with optogenetic pacing: from 26.9 ± 3.3 cm/s before to 28.6 ± 2.5 cm/s during pacing ($p=0.34$) (Figure 6.4 (C)).

6.3.3 Optogenetic pacing of PdCMs has only minor impact on calcium dynamics.

Although small alterations to calcium cycling in the SAPs were observed, for the most part there was no change in calcium dynamics with optogenetic pacing. Calcium transient rise time, calcium transient duration to 50% of the decay (CaD50), and calcium transient duration to 75% of the decay (CaD75) were calculated using ElectroMap as illustrated in Figure 6.5 (A). Rise time is a measure of upstroke duration, calculated between 10% and 90% of the upstroke in order to exclude analytical uncertainty in terms of noise. There was no significant effect of pacing on rise time in the right atrium or in the neonodal regions but in the left atrium, rise time fell from 17.2 ± 0.9 ms before pacing to 15.2 ± 1.1 ms during pacing ($p<0.002$), and rose again after pacing to 18.6 ± 1.0 ms ($p<0.05$, during vs. after); and, in the nodal region, rise time fell from 17.5 ± 1.0 ms to 15.2 ± 1.1 ms ($p<0.03$), and rose again after pacing to 18.4 ± 1.0 ms ($p=0.02$, during vs. after). In neither region was there a significant difference between the before and after conditions (left atrium: $p=0.39$; nodal region: $p=0.61$). The reduction in rise time with optogenetic pacing was reversible upon cessation of pacing (Figure 6.5 (B)). There was no overall significant effect of optogenetic pacing on either CaD50 ($p=0.15$) or CaD75 ($p=0.34$) (Figure 6.5 (C) and (D). In summary, rise time is shorter in the left atrium and in the SAN region during optogenetic pacing, and this is a reversible change. Beyond this, calcium handling in the murine SAP appears to be only marginally affected.

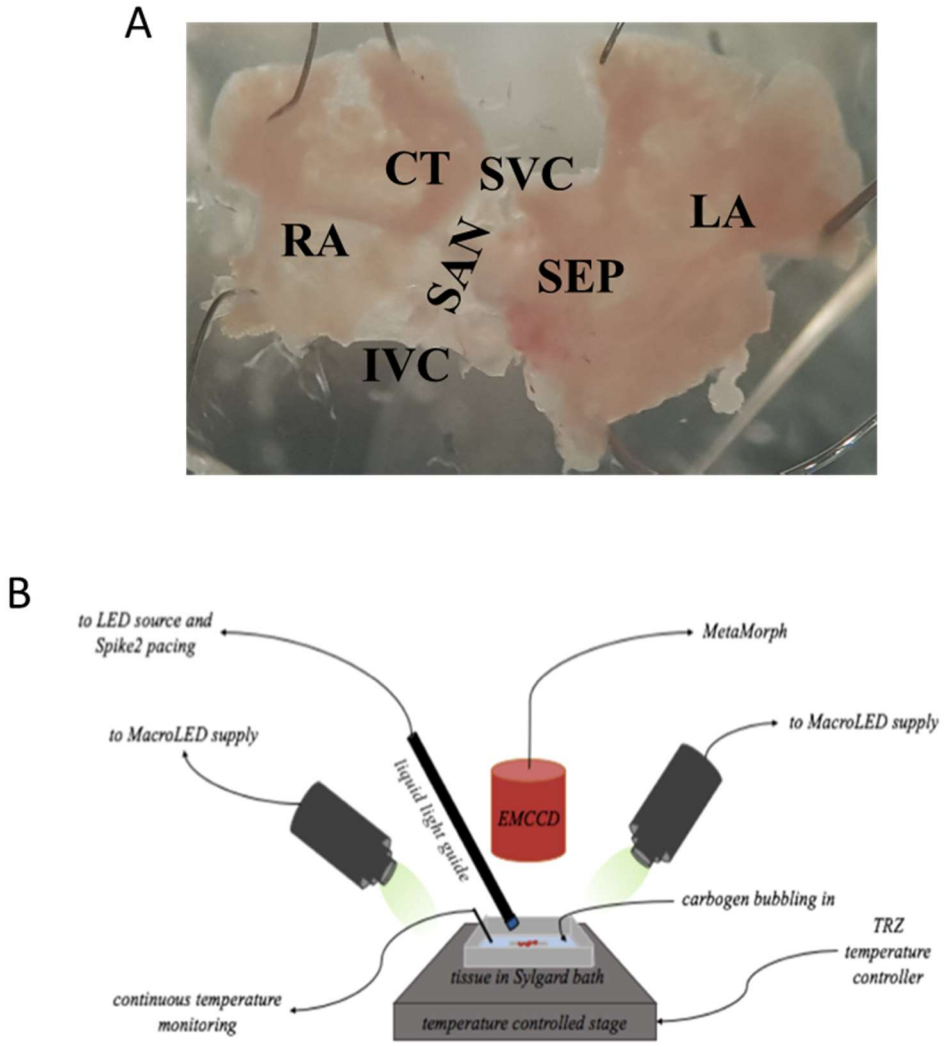


Figure 6.1: Representative murine cardiac Sino-Atrial Preparation (SAP) and the schematic of the optical imaging apparatus

A shows a sample SAP. RA- Right Atrium, LA- Left Atrium, CT- Crista Terminalis, SVC- Superior vena cava, IVC- Inferior vena cava, SAN- Sino-atrial node, SEP- septum.
B Schematic of the optoimaging apparatus used in this chapter. 530 nm (green) light is used to excite Rhod-2 fluorescence for imaging calcium transients, while 488 nm (blue) light from the liquid light guide is used for photostimulation via ChR2.

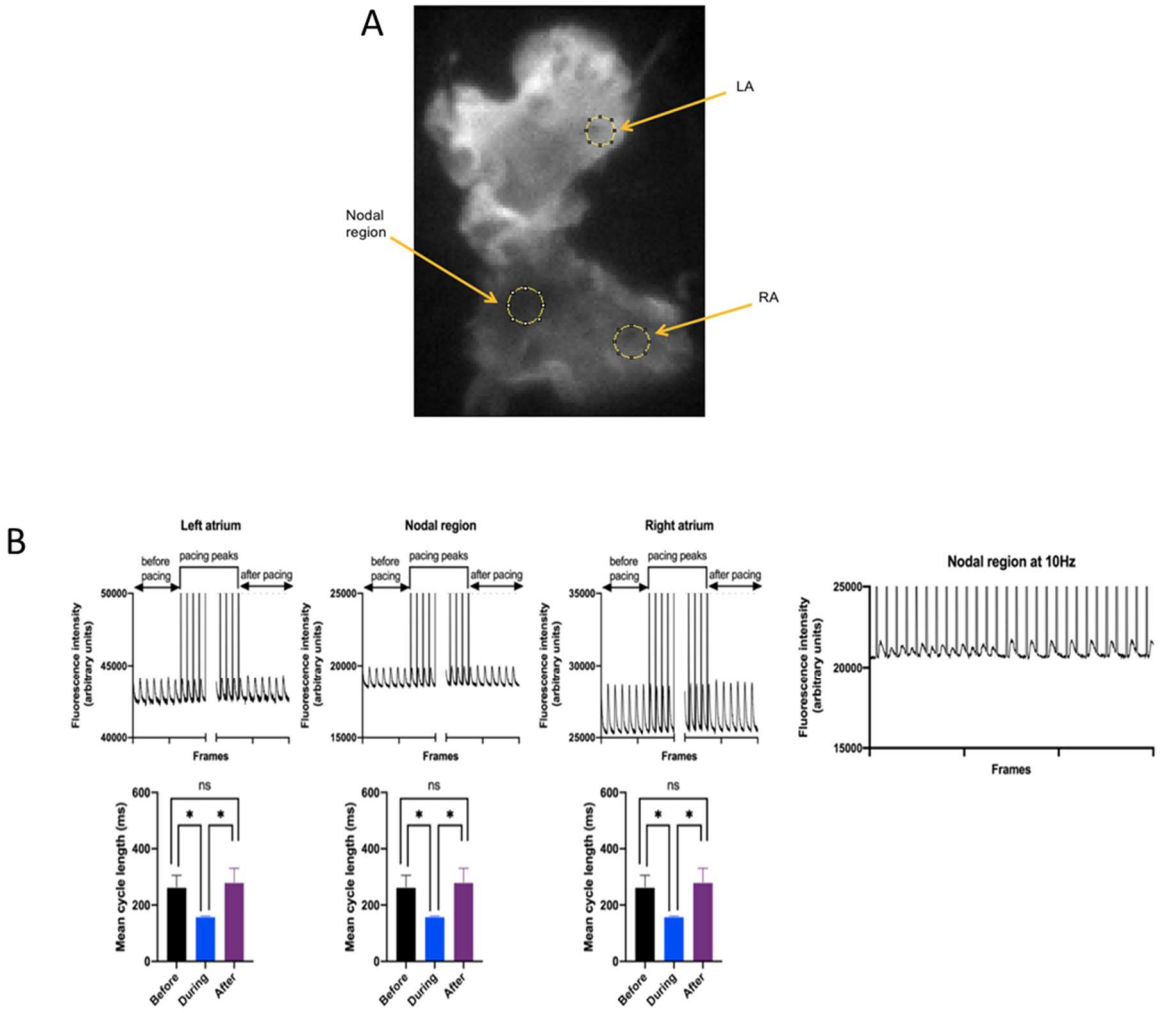


Figure 6.2: Effect of optical pacing on Ca^{2+} transients in murine cardiac SAP.

A shows a representative SAP where Ca^{2+} transients are observed from regions of interests (ROI) in left atrium, SAN and right atrium.
B shows representative traces from the three ROIs selected in **A**. 1:1 coupling of optical pacing to Ca^{2+} transient can be observed in all ROIs. The bar graphs show the mean cycle lengths before, during and after light pacing at left atrium, SAN and right atrium at 6.25 Hz (n=7). The mean cycle lengths were significantly reduced at the faster light pacing and returned to baseline values after light pacing.
Response of SAN Ca^{2+} transients to 10 Hz light pacing is shown on the right. At high optical pacing frequencies, 1:1 coupling is lost.

Note: Numerical data are reported as the mean ± SEM. * denotes $P<0.05$. Wilcoxon's signed-rank tests was used to compare the means of the groups (n=7).

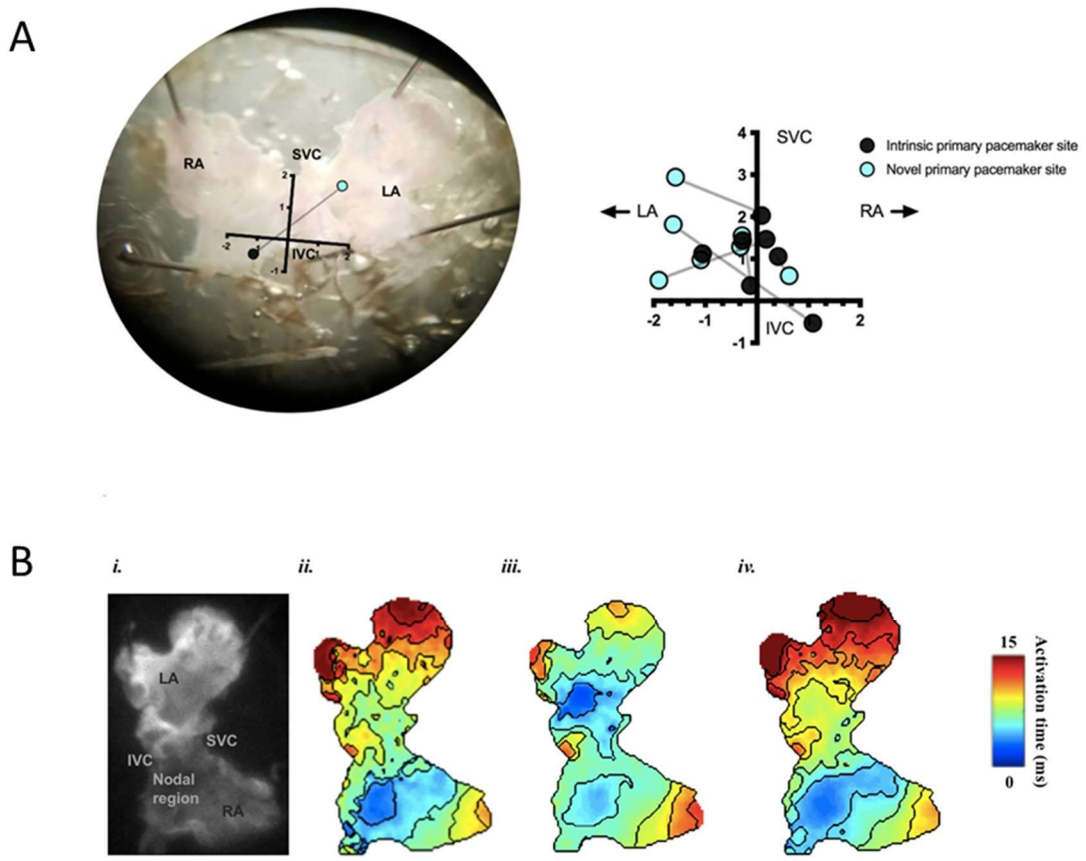


Figure 6.3: Shift of leading pacemaker site during optogenetic pacing

A left image shows a representative SAP with shift of the leading pacemaker plotted relative to the SVC-IVC axis (black: site of the leading pacemaker before pacing; cyan: site of the leading pacemaker during pacing). On the right, leading pacemaker shifts for all 7 SAPs plotted relative to the SVC-IVC axis. Recordings from the same specimen are joined by grey lines. SVC: superior vena cava; IVC: inferior vena cava; RA: right atrium; LA: left atrium. Distance is in mm.
B (i) shows freeze-frame during recording of representative SAP (as in **A**) to demonstrate anatomy; Rest of **B** shows activation maps- **(ii)** before, **(iii)** during, and **(iv)** after an optogenetic pacing train of 50 spikes delivered at 6.25 Hz; scale bar given. Formation of a left atrial 'neonode' is evident in **(iii)**.

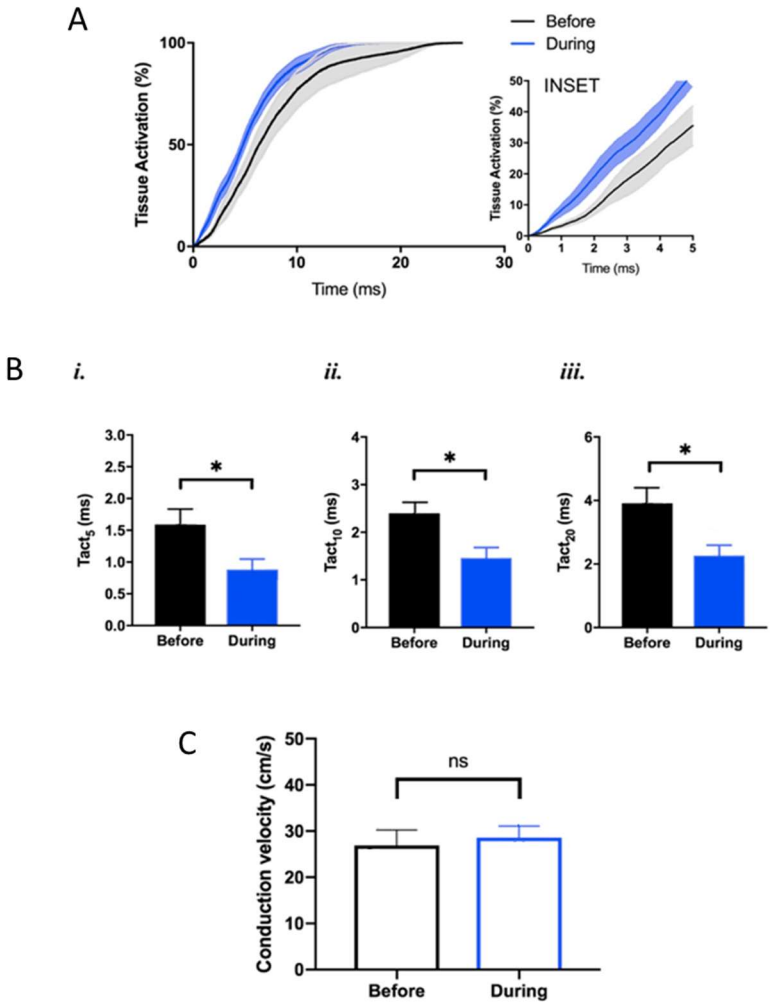


Figure 6.4: Effect of optogenetic pacing on tissue activation and conduction velocity in SAP.

A shows the grouped activation curve from 7 SAPs illustrating change in % tissue activation with time in the averaged atrial beat (black: before pacing; blue: during pacing). Lines trace the mean % activation at each time point, ± SEM which is denoted by shading. Inset shows a zoomed section of the first 5 ms of activation. Although the rate of tissue activation is rapid in the initial stages, in later stages (after 30% tissue activation), there is no difference.
B bar graphs showing **(i)** Tact5 (time taken for 5% of the tissue to activate), **(ii)** Tact10 (time to 10% tissue activation), and **(iii)** Tact20 (time to 20%) illustrate early snapshots of the grouped activation curve in **A**. Black: before pacing, blue: during pacing. During pacing, the SAP had significantly faster tissue activation as compared to before pacing, up to time to 30 % activation.
C shows the mean conduction velocity before and during optical pacing. There was no significant difference in conduction velocity before and during light pacing.
Note: Numerical data in **B** and **C** are reported as mean ± SEM. * denotes $P<0.05$. Paired student's t- test was used to compare the means of the groups.

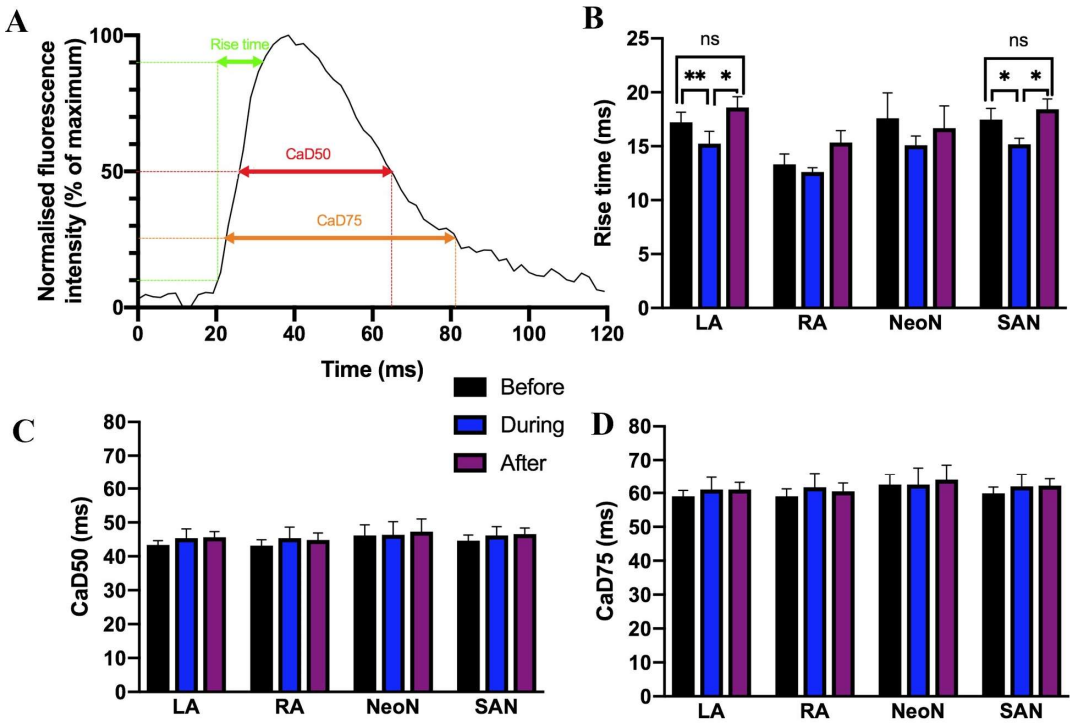


Figure 6.5: Effect of optogenetic pacing on rise time and Ca^{2+} transient durations in SAP.

A shows a representative calcium transient illustrating rise time; CaD50 (calcium transient duration at 50% of the decay); and CaD75 (calcium transient duration at 75% of the decay).
B shows changes in mean rise time with optogenetic pacing, grouped by region. LA = left atrium; RA = right atrium; NeoN = neonodal region (n=4); and SAN = nodal region. Black: before pacing; blue: during pacing; purple: after pacing. The rise times were significantly reduced in left atrium and SAN but reverted to baseline values after pacing.
C shows mean CaD50 values, before, during, and after optogenetic pacing, grouped by region. Abbreviations and colours same as in **(B)**. There is no overall significant effect of optogenetic pacing on CaD50.
D shows mean CaD75 values, before, during, and after optogenetic pacing, grouped by region. Abbreviations and colours same as in **(B)**. There is no overall significant effect of optogenetic pacing on CaD75.
Note: Numerical data in **B, C** and **D** are reported as mean ± SEM. ** denotes P<0.01, * denotes P<0.005. One-way ANOVA with Tukey's multiple comparisons test was used to compare the means of the groups (n=7).

6.4 Discussion

6.4.1 Does optogenetic pacing disturb the normal conduction and Ca^{2+} handling properties of murine SAP?

In this chapter, a detailed protocol for optical mapping of murine sinoatrial preparations with optogenetic pacing has been described. Combination of high-resolution optical imaging of mouse with cell-specific optogenetic stimulation allows unique spatial control and study of activation within the SAP, not possible with traditional direct or field electrode techniques. In summary, optogenetic pacing of PdCMs unlocks the possibility of establishing a novel left-shifted leading pacemaker site, with only minimal, controlled disturbance to normal tissue activation rate, and little or no disturbance to the pathways along which conduction normally propagates, and minimal disruption to Ca^{2+} transient properties. The present protocol has demonstrated this principle with Pnmt+ cardiomyocytes, however the protocol can be valuable for any mouse models that cell specifically express opsins such as ChR2 within the sinoatrial region of the heart. Therefore, such an approach represents a powerful tool for enhanced electrophysiological understanding of supraventricular physiology and pathophysiology.

6.4.2 Can the technique of optogenetic pacing of PdCMs be applied to study sinoatrial dysfunctions?

In vivo experiments in anaesthetised mice have used gene delivery of ChR2 via viral vector for their biopacemaker approach (Nussinovitch and Gepstein 2015). Cell-type specificity in that case was achieved via injection of the cardiotropic adeno-associated virus subtype 9 (AAV9) which targets cardiomyocytes with satisfactory selectivity. There may also be untapped advantages to refining viral vectors to target cardiomyocyte subpopulations currently only accessible via cre-loxP. Cx40-cre/ChR2 mice express

hChR2-tdTomato ubiquitously throughout the atria and also in the Purkinje fibres, and these hearts can be optogenetically paced *in vivo* (Zaglia et al. 2015). Here, the possibility of using another cre-loxP model, Pnmt-cre/ChR2 mice, in a biopacemaker approach has been explored, the advantage here being that it may be possible to establish novel leading pacemaker sites to partially overdrive a dysfunctional sinus node. Adeno-associated viruses have previously been engineered to target genetically-defined subpopulations of neurons—for example, selectively delivering EGFP to OXT-expressing neurons in the supraoptic nucleus, while avoiding neuronal populations expressing AVP; a technology which was also later utilised to deliver ChR2 selectively to an OXT-expressing subpopulation of neurons in the paraventricular hypothalamus (Fields et al. 2012; Atasoy et al. 2012). A recent study has applied this technology in the heart successfully and used optogenetic techniques to manipulate cardiac function. Yu et al. used adeno-associated virus as vector to deliver ArchT, an inhibitory light sensitive opsin to dog left stellate ganglion (LSG), which has been associated with ventricular arrythmias (Yu et al. 2017; Puddu et al. 1988; Garcia-Calvo et al. 1992). After 4 weeks, an LED was fitted into the heart to target the LSG. They observed that optogenetic modulation significantly inhibited LSG function and neuronal activity. Moreover, they observed that the left ventricular effective refractory period and APD90 was prolonged. All these characteristics had returned to baseline level once illumination was turned off. They also observed that ischaemia induced ventricular arrhythmias were significantly reduced in the animals (Yu et al. 2017).

Although selective ChR2 transfer to Pnmt+ cardiomyocytes would not lead to successful transfection of all PdCMs (owing to widespread downregulation of Pnmt in PdCMs during embryonic development), a search for alternative promoters is ongoing. While

simple stimulation of atrial muscle can generate some leading pacemaker shift there appear to be special distributional and functional aspects of PdCMs which make them a promising candidate for future applications in biopacemaking: their unique left-lateralisation; their relative abundance; and the putative role of Pnmt+ cells in synchronising pacemaker activity in the developing myocardium (Yamamoto et al. 1998; Ebert and Taylor 2006; Osuala et al. 2011; Wang et al. 2017). In the work described in this chapter, the characteristic distribution of PdCMs was utilised to establish novel sites of pacemaker activity, though it remains unclear to what extent they can be taken advantage of as a functionally important cardiomyocyte subpopulation. The Lei lab hypothesises that PdCM cells overexpressing ChR2 may be a viable site for spatially targeted optical pacing when sinus node pacemaker cells are dysfunctional. Groundwork for the future has been laid in this chapter. However, substantial future studies are required to improve this technique which includes focus on exploring dual dye imaging to characterise Ca^{2+} handling and membrane voltage characteristics, and improved image processing software. Higher resolution and novel optical imaging modalities for 3D optical mapping are also important future directions of optical mapping that combines optogenetic modulation.

Chapter 7

Conclusion and future work

7.1 Conclusion

The observations from this thesis adds to the accumulating evidence for the role of CD38 and its Ca^{2+} mobilising products, NAADP and cADPR in cardiac Ca^{2+} handling, particularly under the influence of β-adrenergic stimulation.

Chapter 3 focussed on the influence of the NAADP pathway in mouse cardiac atria. The first part of Chapter 3 evaluated the existence of intrinsic NAADP pathway activity at resting levels in mouse atria (without β-adrenergic stimulation). Previous studies by Macgregor et al. and Collins et al. suggested a role for an the NAADP pathway in the underlying Ca^{2+} handling properties of a cardiomyocyte. In the presence of bafilomycin A1, guinea-pig ventricular myocytes showed a 25% reduction in the Ca^{2+} transients and a 50% reduction in Ca^{2+} transients were observed in atrial myocytes (Collins et al. 2011; Macgregor et al. 2007). However, recent studies in *TPC2*$^{-/-}$ mice showed no difference in the Ca^{2+} transient amplitudes as compared to wildtype mice in the absence of β-adrenergic stimulation suggesting a lack of intrinsic NAADP pathway at basal levels. Moreover, the NAADP antagonist Ned-19 did not affect Ca^{2+} transient amplitudes, strengthening the hypothesis that activation of the NAADP signalling pathway required β-adrenergic stimulation (Capel et al. 2015; Elson 2011). The results in the first half of Chapter 3 provide further evidence for the possibility of a lack of active NAADP pathway at basal levels in murine cardiac atria. *CD38*$^{-/-}$ mice showed no difference in the Ca^{2+} transient amplitudes or basal heart rate in the absence of β-adrenergic stimulation as compared to wildtype mice. Moreover, Ca^{2+} transient characteristics including CaD10, CaD50 and CaD80 showed comparable characteristics between the wildtype and KO. Additionally, presence of bafilomycin A1 also did not affect the Ca^{2+} transient amplitude or resting

heart rate in murine atria, suggesting a lack of a constitutive NAADP signalling pathway in mice. The discussion section of Chapter 3 (Section 3.4) discussed the potential limitations of the techniques used in the experiments to observe these results and possible improvements to the experimental setup are suggested.

Although NAADP signalling pathway seemed to elicit no effect on mouse atria on basal levels, it was observed to have profound effects under the influence of β-adrenergic pathway, as shown in the second half of Chapter 3. The genetic knockout of the enzyme responsible for the production of NAADP affected the Ca^{2+} handling properties in mouse atria under the effect of the β-adrenergic receptor agonist isoprenaline. In the presence of 10 nM isoprenaline, the increase in Ca^{2+} transients in *CD38*$^{-/-}$ mice was significantly blunted as compared to the wildtype mice. This is consistent with all the studies previously done in the Terrar lab on guinea-pig atrial and ventricular myocytes, as well as mice ventricular myocytes (Capel et al. 2015; Lin et al. 2017; Macgregor et al. 2007). Additionally, *CD38*$^{-/-}$ mice showed a blunted increase in heart rate in the presence of isoprenaline as compared to wildtype mice. The specificity of these observations to NAADP pathway was given more strength when pharmacological interventions to disrupt the NAADP pathway (bafilomycin A1) was able to mirror these effects in wildtype mice.

In Chapter 4, a closer look into the mechanism of NAADP signalling pathway with respect to the sarcoplasmic reticulum Ca^{2+} handling was studied. For this purpose, an experimental system was designed to directly observe Ca^{2+} in the SR of mouse ventricular myocytes. The low affinity Ca^{2+} indicator Mag-Fluo-4, AM was used to visualise the SR Ca^{2+} content and track its changes over time.

In the initial parts of the chapter, a suitable method to reliably load the SR Ca^{2+} dye without dye contamination in the cytoplasm was studied. Though this could only be achieved by cardiomyocyte permeabilisation, this model did provide observable results pertaining the effect of NAADP signalling pathway on SR Ca^{2+} handling in mouse ventricular myocytes. At basal levels, the SR Ca^{2+} content of wildtype mice and *CD38*$^{-/-}$ were comparable and also, bafilomycin A1 was not able to affect the SR Ca^{2+} load in either mouse models, providing more evidence for the lack of a constitutive NAADP signalling pathway in mouse cardiac system. However, in the presence of the cAMP (to simulate β-adrenergic response), the increase in SR Ca^{2+} in *CD38*$^{-/-}$ mice was significantly blunted as compared to the wildtype ventricular myocytes. This increase in Ca^{2+} was sensitive to bafilomycin A1 in wildtype myocytes but not in *CD38*$^{-/-}$ mice providing more evidence for a role for lysosomal/NAADP signalling pathway in SR Ca^{2+} loading under the effect of β-adrenergic stress. A more direct observation of the effect of NAADP signalling pathway in SR Ca^{2+} load was seen on exposing the myocytes to NAADP. In the presence of NAADP, a significant increase in SR Ca^{2+} load was observed in both wildtype and *CD38*$^{-/-}$ mice in a bafilomycin A1 sensitive manner. Interestingly, the CD38 inhibitor SAN4825 was unable to affect the increase in SR Ca^{2+} load in response to cAMP. Possible reasons as of why this might have occurred have been discussed in the discussion section of Chapter 4 (Section 4.4). Overall, the data obtained in Chapter 4 are consistent with earlier studies from Terrar lab suggesting that activation of the NAADP pathway increased the SR Ca^{2+} load in guinea-pig atrial and ventricular myocytes (Collins et al. 2011; Macgregor et al. 2007). The experiments in Chapter 4 are the first attempt at studying this effect on mouse ventricular myocytes and also directly observing this effect using an SR Ca^{2+} specific dye. However, this SR Ca^{2+} dye loading technique and the experimental design used in Chapter 4 had its limitations. Permeabilisation of

cardiomyocytes for efficient dye loading and performing the experiments at room temperature might have significantly altered the physiological conditions of cardiomyocyte function. This might have had a profound effect on the basal SR Ca^{2+} levels in wildtype and *CD38*$^{-/-}$ myocytes and therefore could have limited the technique to observe a constitutive effect of NAADP pathway in the myocytes. These conditions, to an extent, might also have masked the true effects of NAADP and cAMP on SR Ca^{2+} load. Nevertheless, a new door has been opened to directly visualise SR Ca^{2+} load in cardiomyocytes and through optimisation of the technique and simultaneously observing cytoplasmic (using a cytoplasmic calcium dye) and SR Ca^{2+}, much can be learnt about the Ca^{2+} handling in cardiomyocytes with respect to mechanism of CD38 signalling pathway (including the effects of NAADP and cADPR).

The observations in Chapter 3 and 4 underline the importance of the NAADP pathway in the cardiac system under the effect of β-adrenergic stimulation. Combining these results with previous studies that link the NAADP pathway to cardiac arrythmias, the NAADP pathway can potentially be targeted to design novel drugs to treat arrhythmias. Future studies are needed to reveal the exact mechanism of NAADP signalling pathway in the cardiac system to take full advantage of its clinical implications. A hypothesis for the association of NAADP pathway and cardiomyocyte Ca^{2+} handling is that β-adrenergic stimulation activates CD38 enzyme resulting in enhanced NAADP production, which in turn releases Ca^{2+} from lysosomes (potentially via TPC2). The local increase in Ca^{2+} might activate CaMKII which might enhance SERCA function, thereby, increasing the Ca^{2+} load of the SR. A schematic diagram summarising this hypothesis is shown in Figure 7.1.

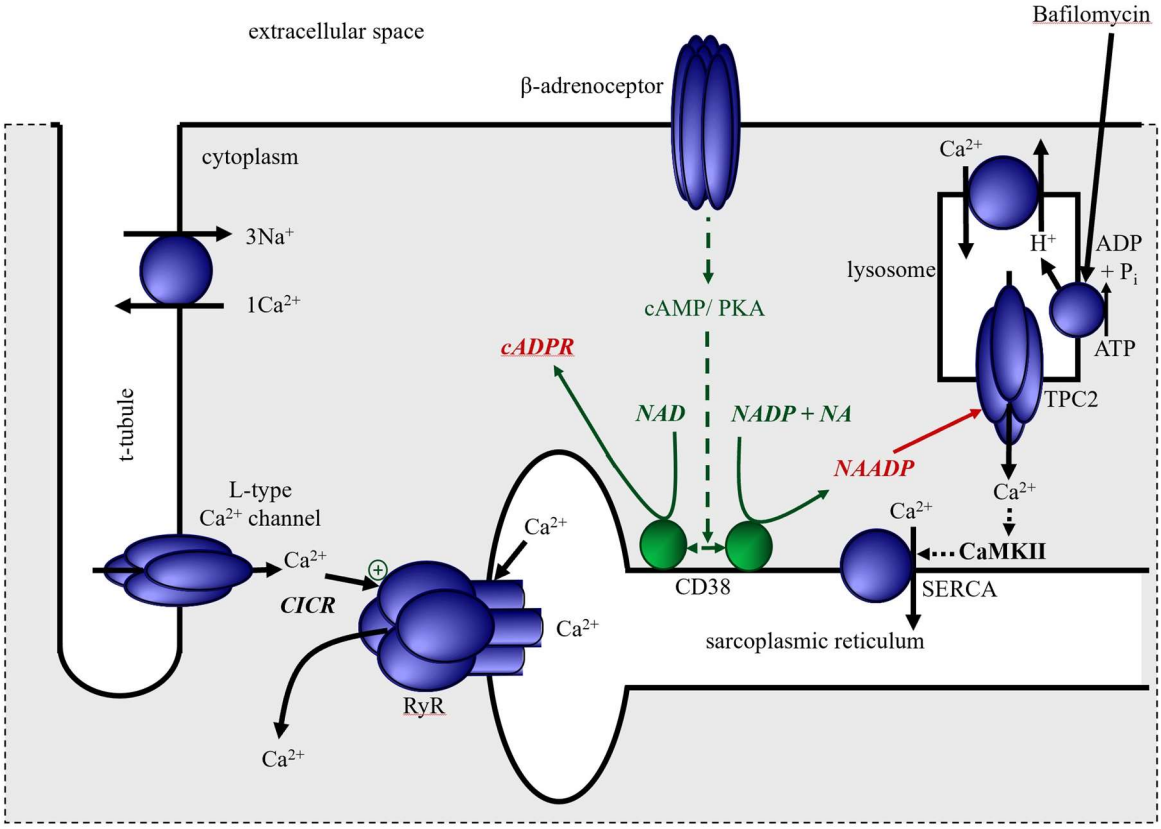


Figure 7.1: Schematic for the proposed mechanism for the NAADP pathway in response to β-adrenergic stimulation in cardiomyocytes.

Stimulation of β-adrenoceptor leads to production of cAMP by adenylyl cyclases. PKA mediated CD38 activation produces cADPR and NAADP (the exact mechanism of CD38 activation is not known, although PKA mediated activation is hypothesised). NAADP releases Ca^{2+} from lysosomes (via TPC2) leading to activation of CaMKII due to local increase in Ca^{2+}. CaMKII phosphorylates phospholamban at Thr17 and SERCA inhibition is lifted leading to enhanced loading of Ca^{2+} into the SR. This, in turn, leads to more Ca^{2+} being released during each CICR event, thus giving rise to a positive inotropic effect.

Chapter 5 attempted to characterise the ARC present in sheep cardiac SRMP. Although CD38 has been suggested as an enzyme that can produce both NAADP and cADPR, several studies have attributed a non-CD38 ARC to catalyse the conversion of NAD to cADPR in the heart (Aarhus et al. 1996; Kannt et al. 2012; Meszaros, Wrenn, and Varadi

1997; Xie et al. 2005). Recent studies in Terrar Lab showed that sheep SRMP had the capability of producing both NAADP and cADPR (Lin 2017). Studies in Chapter 5 was designed to elucidate whether the ARC present in sheep SRMP was CD38. Reverse-transcription PCR experiments not only showed the presence of a functional CD38 gene in sheep hearts, but also showed the absence of an expressed CD157 gene, the only other known mammalian ARC, providing more evidence that CD38 is the primary ARC in the heart. The CD38 inhibitor Kuromanin was able to inhibit the production of cGDPR from NGD, suggesting that presence of CD38 of sheep cardiac SRMP. *In silico* studies showed potential binding sites of kuromanin on human CD38 and showed similar binding to CD38 as its known cADPR substrate NAD. It was shown to interact with the amino acids responsible for the active sites of human CD38. Positive immunoblotting studies with a validated CD38 antibody showed the presence of CD38 in sheep cardiac SRMP. Moreover, the presence of a dimeric form of CD38 is suggested as two bands were observed in the western blot experiments using non-reducing conditions for sample preparation. To find the homogeneity of the sheep cardiac ARC with known mammalian CD38, attempts were made using immunoprecipitation technique to isolate the protein and perform a mass spectrometry analysis. Even though the immunoprecipitation process showed moderately successful protein isolation, mass spectrometry analysis could not detect the presence of CD38 like protein in the sheep SRMP sample. Future experiments can be designed to isolate the ARC from sheep cardiac SRMP more reliably and can be analysed using mass spectrometry to study its homogeneity with human CD38. Moreover, since sheep CD38 protein has not been characterised yet, attempts can also be made to sequence the sheep ARC. The major conclusions derived from Chapter 5 are that sheep cardiac SRMP shows ARC properties, suggesting the presence of a functional ARC associated with the SR. With previous studies from the Terrar lab suggesting an

association of CD38 with the SR and the presence of microdomains between the SR and lysosomes in myocytes provide strong arguments for the presence of CD38 in cardiac SRMP.

Finally, in Chapter 6 a protocol for combining optical mapping with optogenetic pacing is discussed to study intracellular Ca^{2+} transients in murine atrial tissues. The Ca^{2+} handling properties of genetically modified mice that specifically express ChR2 on Pnmt-derived cardiomyocytes were analysed. At high pacing rates, a shift in primary pacemaker sites could be seen towards the left atrium where the PdCMs were localised. This shift in pacemaker site had minimum disturbance on the Ca^{2+} handling properties of the atrial tissue. Potential application of targeting PdCMs as candidates for biopacemaking was also suggested in the discussion section of Chapter 6 (Section 6.4). Although targeting PdCMs to treat sinus node dysfunctions such as Sick sinus syndrome is still at its infancy, future work can be done to better understand the function of PdCMs in the heart and strategies can be developed to take advantage of its cardiac distribution to develop therapeutic techniques.

7.2 Future work

The observations reported in this thesis can be used for several exciting studies in the future pertaining to the roles of CD38 and its enzymatic products NAADP and cADPR in cardiac function in with special emphasis on its role in β-adrenergic responses of the heart leading to arrhythmias. A few exciting future studies in this regard are discussed in this section.

Chapters 3 and 4 of this thesis showed the effect of the NAADP signalling pathway in atrial and ventricular Ca^{2+} handling when the β-adrenergic pathway is stimulated. However, the exact mechanism of the action of the NAADP signalling pathway has not been completely uncovered. Previous studies in the Terrar lab has implicated CaMKII to play an important role in this pathway (Capel et al. 2015). This can be further evaluated to reveal more evidence for CaMKII as a downstream mediator of the NAADP pathway. Experiments can be designed to observe the production of NAADP and cADPR in the presence of CaMKII inhibitors such as KN93 and AIP. Moreover, evaluation of Ca^{2+} uptake and release from the SR in response to NAADP and cADPR antagonists in the presence of CaMKII inhibitors can shed more light on the mechanism of its action on SERCA and RyR on CD38 activation.

Although most experiments in this thesis were designed to observe the NAADP pathway in the heart, the other product of CD38, cADPR, also has an important role in heart especially under the effect of β-adrenergic stimulation. In Chapters 3 and 4, bafilomycin A1 preincubation in wildtype mice and the genetic knockout of CD38 was shown to reduce the effect of isoprenaline to a similar level. As previously shown by Rakovic et al., the cADPR inhibitor 8-Br-cADPR could also reduce the Ca^{2+} transients in cardiomyocytes (Rakovic et al. 1996). As CD38 produces both NAADP and cADPR upon β-adrenoceptor activation, if NAADP and cADPR had non-overlapping effects in cardiac Ca^{2+} handling, the reduction of Ca^{2+} transients in *CD38*$^{-/-}$ mice must have had been much larger than the treatment of bafilomycin A1 in wildtype mice. However, since this is not seen, a complementary action of NAADP and cADPR is suggested in response to isoprenaline in the heart. Since cADPR is known to have an effect on SR Ca^{2+} release and NAADP on SR Ca^{2+} loading, cADPR and NAADP might be working in tandem to

increase the intracellular Ca^{2+} upon β-adrenergic stimulation. Experiments designed to potentiate the activity of one of the CD38 products and inhibit the other might reveal more about the interplay between these two products and its overall effect on the Ca^{2+} handling properties of the heart.

Development of techniques to allow direct differentiation of iPSCs towards atrial or ventricular cardiomyocytes holds promise in studying the CD38 pathway within the context of human cardiac biology. The Terrar and Lei laboratories have recently fine-tuned techniques to induce direct differentiation of iPSCs into functional atrial cardiomyocytes. This enables the scope of studying the specifics of NAADP and cADPR pathway in human cardiomyocytes and generating potential therapeutic targets to treat CD38-mediated arrhythmias in humans. This has the advantage of overcoming possible species-specific differences in NAADP pathway as discussed earlier in Chapter 3 (Section 3.4). Moreover, this model would be ideal to study the differences in expression of type-II and type-III CD38 in the heart. This is of particular relevance to realise whether the expression of the two types of CD38 varies in disease models. Also, the mechanism of the production of NAADP and cADPR can be studied as to whether CD38 is sequestered into intracellular acidic organelles and transporters potentiate the movement of substrates and products to and from organelles or whether the products are formed by the type-III CD38 associated with the SR.

Bibliography

Aarhus, R., D. M. Dickey, R. M. Graeff, K. R. Gee, T. F. Walseth, and H. C. Lee. 1996. 'Activation and inactivation of Ca2+ release by NAADP+', *J Biol Chem*, 271: 8513-6.

Aarhus, R., R. M. Graeff, D. M. Dickey, T. F. Walseth, and H. C. Lee. 1995. 'ADP-ribosyl cyclase and CD38 catalyze the synthesis of a calcium-mobilizing metabolite from NADP', *J Biol Chem*, 270: 30327-33.

Ackers-Johnson, M., P. Y. Li, A. P. Holmes, S. M. O'Brien, D. Pavlovic, and R. S. Foo. 2016. 'A Simplified, Langendorff-Free Method for Concomitant Isolation of Viable Cardiac Myocytes and Nonmyocytes From the Adult Mouse Heart', *Circ Res*, 119: 909-20.

Adebanjo, O. A., H. K. Anandatheerthavarada, A. P. Koval, B. S. Moonga, G. Biswas, L. Sun, B. R. Sodam, P. J. Bevis, C. L. Huang, S. Epstein, F. A. Lai, N. G. Avadhani, and M. Zaidi. 1999. 'A new function for CD38/ADP-ribosyl cyclase in nuclear Ca2+ homeostasis', *Nat Cell Biol*, 1: 409-14.

Al-Abady, Z. N., B. Durante, A. J. Moody, and R. A. Billington. 2013. 'Large changes in NAD levels associated with CD38 expression during HL-60 cell differentiation', *Biochem Biophys Res Commun*, 442: 51-5.

Alberts, B. 2015. *Molecular Biology of the cell* (Garland Science: New York).

Albrieux, M., H. C. Lee, and M. Villaz. 1998. 'Calcium signaling by cyclic ADP-ribose, NAADP, and inositol trisphosphate are involved in distinct functions in ascidian oocytes', *J Biol Chem*, 273: 14566-74.

Aley, P. K., N. Singh, G. C. Brailoiu, E. Brailoiu, and G. C. Churchill. 2013. 'Nicotinic acid adenine dinucleotide phosphate (NAADP) is a second messenger in muscarinic receptor-induced contraction of guinea pig trachea', *J Biol Chem*, 288: 10986-93.

Appelqvist, H., P. Waster, K. Kagedal, and K. Ollinger. 2013. 'The lysosome: from waste bag to potential therapeutic target', *J Mol Cell Biol*, 5: 214-26.

Arndt, L., J. Castonguay, E. Arlt, D. Meyer, S. Hassan, H. Borth, S. Zierler, G. Wennemuth, A. Breit, M. Biel, C. Wahl-Schott, T. Gudermann, N. Klugbauer, and I. Boekhoff. 2014. 'NAADP and the two-pore channel protein 1 participate in the acrosome reaction in mammalian spermatozoa', *Mol Biol Cell*, 25: 948-64.

Aston, D., R. A. Capel, K. L. Ford, H. C. Christian, G. R. Mirams, E. A. Rog-Zielinska, P. Kohl, A. Galione, R. A. Burton, and D. A. Terrar. 2017. 'High resolution structural evidence suggests the Sarcoplasmic Reticulum forms microdomains with Acidic Stores (lysosomes) in the heart', *Sci Rep*, 7: 40620.

Atasoy, D., J. N. Betley, H. H. Su, and S. M. Sternson. 2012. 'Deconstruction of a neural circuit for hunger', *Nature*, 488: 172-7.

Bacher, I., A. Zidar, M. Kratzel, and M. Hohenegger. 2004. 'Channelling of substrate promiscuity of the skeletal-muscle ADP-ribosyl cyclase isoform', *Biochem J*, 381: 147-54.

Bainton, D. F. 1981. 'The discovery of lysosomes', *J Cell Biol*, 91: 66s-76s.

Bak, J., R. A. Billington, G. Timar, A. C. Dutton, and A. A. Genazzani. 2001. 'NAADP receptors are present and functional in the heart', *Curr Biol*, 11: 987-90.

Bak, J., P. White, G. Timar, L. Missiaen, A. A. Genazzani, and A. Galione. 1999. 'Nicotinic acid adenine dinucleotide phosphate triggers Ca2+ release from brain microsomes', *Curr Biol*, 9: 751-4.

Belevych, A., Z. Kubalova, D. Terentyev, R. L. Hamlin, C. A. Carnes, and S. Gyorke. 2007. 'Enhanced ryanodine receptor-mediated calcium leak determines reduced sarcoplasmic reticulum calcium content in chronic canine heart failure', *Biophys J*, 93: 4083-92.

Berridge, M. J. 2006. 'Calcium microdomains: organization and function', *Cell Calcium*, 40: 405-12.

Bers, D. M. 2002. 'Cardiac excitation-contraction coupling', *Nature*, 415: 198-205.

Bers, D. M., W. H. Barry, and S. Despa. 2003. 'Intracellular Na+ regulation in cardiac myocytes', *Cardiovasc Res*, 57: 897-912.
Bers, D. M., and S. Morotti. 2014. 'Ca(2+) current facilitation is CaMKII-dependent and has arrhythmogenic consequences', *Front Pharmacol*, 5: 144.
Bezin, S., G. Charpentier, P. Fossier, and J. M. Cancela. 2006. 'The Ca2+-releasing messenger NAADP, a new player in the nervous system', *J Physiol Paris*, 99: 111-8.
Blanch, I. Salvador J., and M. Egger. 2018. 'Obstruction of ventricular Ca(2+) -dependent arrhythmogenicity by inositol 1,4,5-trisphosphate-triggered sarcoplasmic reticulum Ca(2+) release', *J Physiol*, 596: 4323-40.
Bleeker, W. K., A. J. Mackaay, M. Masson-Pevet, L. N. Bouman, and A. E. Becker. 1980. 'Functional and morphological organization of the rabbit sinus node', *Circ Res*, 46: 11-22.
Boittin, F. X., A. Galione, and A. M. Evans. 2002. 'Nicotinic acid adenine dinucleotide phosphate mediates Ca2+ signals and contraction in arterial smooth muscle via a two-pool mechanism', *Circ Res*, 91: 1168-75.
Bolli, R., M. O. Jeroudi, B. S. Patel, C. M. DuBose, E. K. Lai, R. Roberts, and P. B. McCay. 1989. 'Direct evidence that oxygen-derived free radicals contribute to postischemic myocardial dysfunction in the intact dog', *Proc Natl Acad Sci U S A*, 86: 4695-9.
Bootman, M. D., C. Fearnley, I. Smyrnias, F. MacDonald, and H. L. Roderick. 2009. 'An update on nuclear calcium signalling', *J Cell Sci*, 122: 2337-50.
Bottger, S., and M. F. Melzig. 2013. 'The influence of saponins on cell membrane cholesterol', *Bioorg Med Chem*, 21: 7118-24.
Bovo, E., S. Huke, L. A. Blatter, and A. V. Zima. 2017. 'The effect of PKA-mediated phosphorylation of ryanodine receptor on SR Ca(2+) leak in ventricular myocytes', *J Mol Cell Cardiol*, 104: 9-16.
Boyden, E. S., F. Zhang, E. Bamberg, G. Nagel, and K. Deisseroth. 2005. 'Millisecond-timescale, genetically targeted optical control of neural activity', *Nat Neurosci*, 8: 1263-8.
Boyle, P. M., J. C. Williams, C. M. Ambrosi, E. Entcheva, and N. A. Trayanova. 2013. 'A comprehensive multiscale framework for simulating optogenetics in the heart', *Nat Commun*, 4: 2370.
Brailoiu, E., D. Churamani, X. Cai, M. G. Schrlau, G. C. Brailoiu, X. Gao, R. Hooper, M. J. Boulware, N. J. Dun, J. S. Marchant, and S. Patel. 2009. 'Essential requirement for two-pore channel 1 in NAADP-mediated calcium signaling', *J Cell Biol*, 186: 201-9.
Brailoiu, E., D. Churamani, V. Pandey, G. C. Brailoiu, F. Tuluc, S. Patel, and N. J. Dun. 2006. 'Messenger-specific role for nicotinic acid adenine dinucleotide phosphate in neuronal differentiation', *J Biol Chem*, 281: 15923-8.
Brailoiu, G. C., E. Brailoiu, R. Parkesh, A. Galione, G. C. Churchill, S. Patel, and N. J. Dun. 2009. 'NAADP-mediated channel 'chatter' in neurons of the rat medulla oblongata', *Biochem J*, 419: 91-7, 2 p following 97.
Brodde, O. E., H. Bruck, and K. Leineweber. 2006. 'Cardiac adrenoceptors: physiological and pathophysiological relevance', *J Pharmacol Sci*, 100: 323-37.
Bruzzone, S., L. Guida, L. Franco, E. Zocchi, G. Corte, and A. De Flora. 1998. 'Dimeric and tetrameric forms of catalytically active transmembrane CD38 in transfected HeLa cells', *FEBS Lett*, 433: 275-8.
Bruzzone, S., L. Guida, E. Zocchi, L. Franco, and A. De Flora. 2001. 'Connexin 43 hemi channels mediate Ca2+-regulated transmembrane NAD+ fluxes in intact cells', *FASEB J*, 15: 10-12.
Calcraft, P. J., M. Ruas, Z. Pan, X. Cheng, A. Arredouani, X. Hao, J. Tang, K. Rietdorf, L. Teboul, K. T. Chuang, P. Lin, R. Xiao, C. Wang, Y. Zhu, Y. Lin, C. N. Wyatt, J. Parrington, J. Ma, A. M. Evans, A. Galione, and M. X. Zhu. 2009. 'NAADP

mobilizes calcium from acidic organelles through two-pore channels', *Nature*, 459: 596-600.
Camelliti, P., T. K. Borg, and P. Kohl. 2005. 'Structural and functional characterisation of cardiac fibroblasts', *Cardiovasc Res*, 65: 40-51.
Camors, E., and H. H. Valdivia. 2014. 'CaMKII regulation of cardiac ryanodine receptors and inositol triphosphate receptors', *Front Pharmacol*, 5: 101.
Cancela, J. M., G. C. Churchill, and A. Galione. 1999. 'Coordination of agonist-induced Ca2+-signalling patterns by NAADP in pancreatic acinar cells', *Nature*, 398: 74-6.
Cang, C., K. Aranda, and D. Ren. 2014. 'A non-inactivating high-voltage-activated two-pore Na(+) channel that supports ultra-long action potentials and membrane bistability', *Nat Commun*, 5: 5015.
Cang, C., Y. Zhou, B. Navarro, Y. J. Seo, K. Aranda, L. Shi, S. Battaglia-Hsu, I. Nissim, D. E. Clapham, and D. Ren. 2013. 'mTOR regulates lysosomal ATP-sensitive two-pore Na(+) channels to adapt to metabolic state', *Cell*, 152: 778-90.
Capel, R. A., E. L. Bolton, W. K. Lin, D. Aston, Y. Wang, W. Liu, X. Wang, R. A. Burton, D. Bloor-Young, K. T. Shade, M. Ruas, J. Parrington, G. C. Churchill, M. Lei, A. Galione, and D. A. Terrar. 2015. 'Two-pore Channels (TPC2s) and Nicotinic Acid Adenine Dinucleotide Phosphate (NAADP) at Lysosomal-Sarcoplasmic Reticular Junctions Contribute to Acute and Chronic beta-Adrenoceptor Signaling in the Heart', *J Biol Chem*, 290: 30087-98.
Capel, R. A., and D. A. Terrar. 2015. 'The importance of Ca(2+)-dependent mechanisms for the initiation of the heartbeat', *Front Physiol*, 6: 80.
Ceroni, F., A. Sagar, N. H. Simpson, A. J. Gawthrope, D. F. Newbury, D. Pinto, S. M. Francis, D. C. Tessman, E. H. Cook, A. P. Monaco, E. Maestrini, A. T. Pagnamenta, and S. Jacob. 2014. 'A deletion involving CD38 and BST1 results in a fusion transcript in a patient with autism and asthma', *Autism Res*, 7: 254-63.
Chidambaram, N., and C. F. Chang. 1998. 'Functional role of glycosylation on the recombinant CD38/ADP-ribosyl cyclase in CHO cells', *Int J Biochem Cell Biol*, 30: 1011-8.
Chidambaram, N., E. T. Wong, and C. F. Chang. 1998. 'Differential oligomerization of membrane-bound CD38/ADP-ribosyl cyclase in porcine heart microsomes', *Biochem Mol Biol Int*, 44: 1225-33.
Ching, L. L., A. J. Williams, and R. Sitsapesan. 2000. 'Evidence for Ca(2+) activation and inactivation sites on the luminal side of the cardiac ryanodine receptor complex', *Circ Res*, 87: 201-6.
Chini, E. N., C. C. Chini, I. Kato, S. Takasawa, and H. Okamoto. 2002. 'CD38 is the major enzyme responsible for synthesis of nicotinic acid-adenine dinucleotide phosphate in mammalian tissues', *Biochem J*, 362: 125-30.
Chini, E. N., and T. P. Dousa. 1995. 'Enzymatic synthesis and degradation of nicotinate adenine dinucleotide phosphate (NAADP), a Ca(2+)-releasing agonist, in rat tissues', *Biochem Biophys Res Commun*, 209: 167-74.
Christensen, K. A., J. T. Myers, and J. A. Swanson. 2002. 'pH-dependent regulation of lysosomal calcium in macrophages', *J Cell Sci*, 115: 599-607.
Churchill, G. C., and A. Galione. 2000. 'Spatial control of Ca2+ signaling by nicotinic acid adenine dinucleotide phosphate diffusion and gradients', *J Biol Chem*, 275: 38687-92.
———. 2001. 'NAADP induces Ca2+ oscillations via a two-pool mechanism by priming IP3- and cADPR-sensitive Ca2+ stores', *EMBO J*, 20: 2666-71.
Churchill, G. C., J. S. O'Neill, R. Masgrau, S. Patel, J. M. Thomas, A. A. Genazzani, and A. Galione. 2003. 'Sperm deliver a new second messenger: NAADP', *Curr Biol*, 13: 125-8.

Churchill, G. C., Y. Okada, J. M. Thomas, A. A. Genazzani, S. Patel, and A. Galione. 2002. 'NAADP mobilizes Ca(2+) from reserve granules, lysosome-related organelles, in sea urchin eggs', *Cell*, 111: 703-8.

Cockayne, D. A., T. Muchamuel, J. C. Grimaldi, H. Muller-Steffner, T. D. Randall, F. E. Lund, R. Murray, F. Schuber, and M. C. Howard. 1998. 'Mice deficient for the ecto-nicotinamide adenine dinucleotide glycohydrolase CD38 exhibit altered humoral immune responses', *Blood*, 92: 1324-33.

Coen, K., R. S. Flannagan, S. Baron, L. R. Carraro-Lacroix, D. Wang, W. Vermeire, C. Michiels, S. Munck, V. Baert, S. Sugita, F. Wuytack, P. R. Hiesinger, S. Grinstein, and W. Annaert. 2012. 'Lysosomal calcium homeostasis defects, not proton pump defects, cause endo-lysosomal dysfunction in PSEN-deficient cells', *J Cell Biol*, 198: 23-35.

Collins, T. P., R. Bayliss, G. C. Churchill, A. Galione, and D. A. Terrar. 2011. 'NAADP influences excitation-contraction coupling by releasing calcium from lysosomes in atrial myocytes', *Cell Calcium*, 50: 449-58.

Collins, T. P., and D. A. Terrar. 2012. 'Ca(2+)-stimulated adenylyl cyclases regulate the L-type Ca(2+) current in guinea-pig atrial myocytes', *J Physiol*, 590: 1881-93.

Copello, J. A., Y. Qi, L. H. Jeyakumar, E. Ogunbunmi, and S. Fleischer. 2001. 'Lack of effect of cADP-ribose and NAADP on the activity of skeletal muscle and heart ryanodine receptors', *Cell Calcium*, 30: 269-84.

Cosker, F., N. Cheviron, M. Yamasaki, A. Menteyne, F. E. Lund, M. J. Moutin, A. Galione, and J. M. Cancela. 2010. 'The ecto-enzyme CD38 is a nicotinic acid adenine dinucleotide phosphate (NAADP) synthase that couples receptor activation to Ca2+ mobilization from lysosomes in pancreatic acinar cells', *J Biol Chem*, 285: 38251-9.

Cui, Y., A. Galione, and D. A. Terrar. 1999. 'Effects of photoreleased cADP-ribose on calcium transients and calcium sparks in myocytes isolated from guinea-pig and rat ventricle', *Biochem J*, 342 (Pt 2): 269-73.

Dammermann, W., and A. H. Guse. 2005. 'Functional ryanodine receptor expression is required for NAADP-mediated local Ca2+ signaling in T-lymphocytes', *J Biol Chem*, 280: 21394-9.

Davidson, S. M., K. Foote, S. Kunuthur, R. Gosain, N. Tan, R. Tyser, Y. J. Zhao, R. Graeff, A. Ganesan, M. R. Duchen, S. Patel, and D. M. Yellon. 2015. 'Inhibition of NAADP signalling on reperfusion protects the heart by preventing lethal calcium oscillations via two-pore channel 1 and opening of the mitochondrial permeability transition pore', *Cardiovasc Res*, 108: 357-66.

Davis, L. C., A. J. Morgan, M. Ruas, J. L. Wong, R. M. Graeff, A. J. Poustka, H. C. Lee, G. M. Wessel, J. Parrington, and A. Galione. 2008. 'Ca(2+) signaling occurs via second messenger release from intraorganelle synthesis sites', *Curr Biol*, 18: 1612-8.

De Duve, C., B. C. Pressman, R. Gianetto, R. Wattiaux, and F. Appelmans. 1955. 'Tissue fractionation studies. 6. Intracellular distribution patterns of enzymes in rat-liver tissue', *Biochem J*, 60: 604-17.

de Lucia, C., A. Eguchi, and W. J. Koch. 2018. 'New Insights in Cardiac beta-Adrenergic Signaling During Heart Failure and Aging', *Front Pharmacol*, 9: 904.

de Marneffe, M., J. M. Gregoire, P. Waterschoot, and M. P. Kestemont. 1993. 'The sinus node function: normal and pathological', *Eur Heart J*, 14: 649-54.

de Toledo, F. G., J. Cheng, M. Liang, E. N. Chini, and T. P. Dousa. 2000. 'ADP-Ribosyl cyclase in rat vascular smooth muscle cells: properties and regulation', *Circ Res*, 86: 1153-9.

Deshpande, D. A., T. A. White, S. Dogan, T. F. Walseth, R. A. Panettieri, and M. S. Kannan. 2005. 'CD38/cyclic ADP-ribose signaling: role in the regulation of calcium homeostasis in airway smooth muscle', *Am J Physiol Lung Cell Mol Physiol*, 288: L773-88.

Dibb, K. M., J. D. Clarke, D. A. Eisner, M. A. Richards, and A. W. Trafford. 2013. 'A functional role for transverse (t-) tubules in the atria', *J Mol Cell Cardiol*, 58: 84-91.

DiFrancesco, D., and J. S. Borer. 2007. 'The funny current: cellular basis for the control of heart rate', *Drugs*, 67 Suppl 2: 15-24.

Dionisio, N., L. Albarran, J. J. Lopez, A. Berna-Erro, G. M. Salido, R. Bobe, and J. A. Rosado. 2011. 'Acidic NAADP-releasable Ca(2+) compartments in the megakaryoblastic cell line MEG01', *Biochim Biophys Acta*, 1813: 1483-94.

Djerada, Z., and H. Millart. 2013. 'Intracellular NAADP increase induced by extracellular NAADP via the P2Y11-like receptor', *Biochem Biophys Res Commun*, 436: 199-203.

Djerada, Z., H. Peyret, S. Dukic, and H. Millart. 2013. 'Extracellular NAADP affords cardioprotection against ischemia and reperfusion injury and involves the P2Y11-like receptor', *Biochem Biophys Res Commun*, 434: 428-33.

Domeier, T. L., A. V. Zima, J. T. Maxwell, S. Huke, G. A. Mignery, and L. A. Blatter. 2008. 'IP3 receptor-dependent Ca2+ release modulates excitation-contraction coupling in rabbit ventricular myocytes', *Am J Physiol Heart Circ Physiol*, 294: H596-604.

Dong, X. P., D. Shen, X. Wang, T. Dawson, X. Li, Q. Zhang, X. Cheng, Y. Zhang, L. S. Weisman, M. Delling, and H. Xu. 2010. 'PI(3,5)P(2) controls membrane trafficking by direct activation of mucolipin Ca(2+) release channels in the endolysosome', *Nat Commun*, 1: 38.

Dou, Y., P. Arlock, and A. Arner. 2007. 'Blebbistatin specifically inhibits actin-myosin interaction in mouse cardiac muscle', *Am J Physiol Cell Physiol*, 293: C1148-53.

Downey, J. M. 1990. 'Free radicals and their involvement during long-term myocardial ischemia and reperfusion', *Annu Rev Physiol*, 52: 487-504.

Ebert, S. N., Q. Rong, S. Boe, R. P. Thompson, A. Grinberg, and K. Pfeifer. 2004. 'Targeted insertion of the Cre-recombinase gene at the phenylethanolamine n-methyltransferase locus: a new model for studying the developmental distribution of adrenergic cells', *Dev Dyn*, 231: 849-58.

Ebert, S. N., and D. G. Taylor. 2006. 'Catecholamines and development of cardiac pacemaking: an intrinsically intimate relationship', *Cardiovasc Res*, 72: 364-74.

Ebert, S. N., and R. P. Thompson. 2001. 'Embryonic epinephrine synthesis in the rat heart before innervation: association with pacemaking and conduction tissue development', *Circ Res*, 88: 117-24.

Egea, P. F., H. Muller-Steffner, I. Kuhn, C. Cakir-Kiefer, N. J. Oppenheimer, R. M. Stroud, E. Kellenberger, and F. Schuber. 2012. 'Insights into the mechanism of bovine CD38/NAD+glycohydrolase from the X-ray structures of its Michaelis complex and covalently-trapped intermediates', *PLoS One*, 7: e34918.

Eisner, D. A., J. L. Caldwell, K. Kistamas, and A. W. Trafford. 2017. 'Calcium and Excitation-Contraction Coupling in the Heart', *Circ Res*, 121: 181-95.

Eisner, D. A., and W. J. Lederer. 1985. 'Na-Ca exchange: stoichiometry and electrogenicity', *Am J Physiol*, 248: C189-202.

El-Armouche, A., and T. Eschenhagen. 2009. 'Beta-adrenergic stimulation and myocardial function in the failing heart', *Heart Fail Rev*, 14: 225-41.

Elson, L. 2011. 'Regulation of cardiac Ca2+ signalling mechanisms and contractile function by nicotinic acid adenine dinucleotide phosphate', University of Oxford

Fabiato, A. 1983. 'Calcium-induced release of calcium from the cardiac sarcoplasmic reticulum', *Am J Physiol*, 245: C1-14.

———. 1985. 'Time and calcium dependence of activation and inactivation of calcium-induced release of calcium from the sarcoplasmic reticulum of a skinned canine cardiac Purkinje cell', *J Gen Physiol*, 85: 247-89.

Fang, C., T. Li, Y. Li, G. J. Xu, Q. W. Deng, Y. J. Chen, Y. N. Hou, H. C. Lee, and Y. J. Zhao. 2018. 'CD38 produces nicotinic acid adenosine dinucleotide phosphate in the lysosome', *J Biol Chem*, 293: 8151-60.

Fawcett, D. W., and N. S. McNutt. 1969. 'The ultrastructure of the cat myocardium. I. Ventricular papillary muscle', *J Cell Biol*, 42: 1-45.

Fernandez-Tenorio, M., and E. Niggli. 2016. 'Real-time intra-store confocal Ca(2+) imaging in isolated mouse cardiomyocytes', *Cell Calcium*, 60: 331-40.

———. 2018. 'Stabilization of Ca(2+) signaling in cardiac muscle by stimulation of SERCA', *J Mol Cell Cardiol*, 119: 87-95.

Fernandez-Velasco, M., A. Rueda, N. Rizzi, J. P. Benitah, B. Colombi, C. Napolitano, S. G. Priori, S. Richard, and A. M. Gomez. 2009. 'Increased Ca2+ sensitivity of the ryanodine receptor mutant RyR2R4496C underlies catecholaminergic polymorphic ventricular tachycardia', *Circ Res*, 104: 201-9, 12p following 09.

Fernandez, J. E., S. Deaglio, D. Donati, I. S. Beusan, F. Corno, A. Aranega, M. Forni, B. Falini, and F. Malavasi. 1998. 'Analysis of the distribution of human CD38 and of its ligand CD31 in normal tissues', *J Biol Regul Homeost Agents*, 12: 81-91.

Fields, R. L., T. A. Ponzio, M. Kawasaki, and H. Gainer. 2012. 'Cell-type specific oxytocin gene expression from AAV delivered promoter deletion constructs into the rat supraoptic nucleus in vivo', *PLoS One*, 7: e32085.

Franco, L., L. Guida, S. Bruzzone, E. Zocchi, C. Usai, and A. De Flora. 1998. 'The transmembrane glycoprotein CD38 is a catalytically active transporter responsible for generation and influx of the second messenger cyclic ADP-ribose across membranes', *FASEB J*, 12: 1507-20.

Franco, L., E. Zocchi, C. Usai, L. Guida, S. Bruzzone, A. Costa, and A. De Flora. 2001. 'Paracrine roles of NAD+ and cyclic ADP-ribose in increasing intracellular calcium and enhancing cell proliferation of 3T3 fibroblasts', *J Biol Chem*, 276: 21642-8.

Frank, J. S., G. Mottino, D. Reid, R. S. Molday, and K. D. Philipson. 1992. 'Distribution of the Na(+)-Ca2+ exchange protein in mammalian cardiac myocytes: an immunofluorescence and immunocolloidal gold-labeling study', *J Cell Biol*, 117: 337-45.

Freedman, N. J., and R. J. Lefkowitz. 2004. 'Anti-beta(1)-adrenergic receptor antibodies and heart failure: causation, not just correlation', *J Clin Invest*, 113: 1379-82.

Fruen, B. R., J. R. Mickelson, N. H. Shomer, P. Velez, and C. F. Louis. 1994. 'Cyclic ADP-ribose does not affect cardiac or skeletal muscle ryanodine receptors', *FEBS Lett*, 352: 123-6.

Fukushi, Y., I. Kato, S. Takasawa, T. Sasaki, B. H. Ong, M. Sato, A. Ohsaga, K. Sato, K. Shirato, H. Okamoto, and Y. Maruyama. 2001. 'Identification of cyclic ADP-ribose-dependent mechanisms in pancreatic muscarinic Ca(2+) signaling using CD38 knockout mice', *J Biol Chem*, 276: 649-55.

Furuichi, T., K. W. Cunningham, and S. Muto. 2001. 'A putative two pore channel AtTPC1 mediates Ca(2+) flux in Arabidopsis leaf cells', *Plant Cell Physiol*, 42: 900-5.

Galione, A. 2006. 'NAADP, a new intracellular messenger that mobilizes Ca2+ from acidic stores', *Biochem Soc Trans*, 34: 922-6.

———. 2011. 'NAADP receptors', *Cold Spring Harb Perspect Biol*, 3: a004036.

———. 2015. 'A primer of NAADP-mediated Ca(2+) signalling: From sea urchin eggs to mammalian cells', *Cell Calcium*, 58: 27-47.

Galione, A., H. C. Lee, and W. B. Busa. 1991. 'Ca(2+)-induced Ca2+ release in sea urchin egg homogenates: modulation by cyclic ADP-ribose', *Science*, 253: 1143-6.

Gao, Y., and K. Mehta. 2007. 'N-linked glycosylation of CD38 is required for its structure stabilization but not for membrane localization', *Mol Cell Biochem*, 295: 1-7.

Garcia-Calvo, R., F. J. Chorro, M. Sendra, A. Alberola, J. Sanchis, J. Navarro, V. Valentin, V. Lopez-Merino, and L. Such. 1992. 'The effects of selective stellate

ganglion manipulation on ventricular refractoriness and excitability', *Pacing Clin Electrophysiol*, 15: 1492-503.
Garlick, P. B., M. J. Davies, D. J. Hearse, and T. F. Slater. 1987. 'Direct detection of free radicals in the reperfused rat heart using electron spin resonance spectroscopy', *Circ Res*, 61: 757-60.
Garrity, A. G., W. Wang, C. M. Collier, S. A. Levey, Q. Gao, and H. Xu. 2016. 'The endoplasmic reticulum, not the pH gradient, drives calcium refilling of lysosomes', *Elife*, 5.
Gasser, A., S. Bruhn, and A. H. Guse. 2006. 'Second messenger function of nicotinic acid adenine dinucleotide phosphate revealed by an improved enzymatic cycling assay', *J Biol Chem*, 281: 16906-13.
Genazzani, A. A., R. M. Empson, and A. Galione. 1996. 'Unique inactivation properties of NAADP-sensitive Ca2+ release', *J Biol Chem*, 271: 11599-602.
Gerasimenko, J. V., Y. Maruyama, K. Yano, N. J. Dolman, A. V. Tepikin, O. H. Petersen, and O. V. Gerasimenko. 2003. 'NAADP mobilizes Ca2+ from a thapsigargin-sensitive store in the nuclear envelope by activating ryanodine receptors', *J Cell Biol*, 163: 271-82.
Gilabert-Oriol, R., K. Mergel, M. Thakur, B. von Mallinckrodt, M. F. Melzig, H. Fuchs, and A. Weng. 2013. 'Real-time analysis of membrane permeabilizing effects of oleanane saponins', *Bioorg Med Chem*, 21: 2387-95.
Gomez-Suaga, P., and S. Hilfiker. 2012. 'LRRK2 as a modulator of lysosomal calcium homeostasis with downstream effects on autophagy', *Autophagy*, 8: 692-3.
Goodrich, S. P., H. Muller-Steffner, A. Osman, M. J. Moutin, K. Kusser, A. Roberts, D. L. Woodland, T. D. Randall, E. Kellenberger, P. T. LoVerde, F. Schuber, and F. E. Lund. 2005. 'Production of calcium-mobilizing metabolites by a novel member of the ADP-ribosyl cyclase family expressed in Schistosoma mansoni', *Biochemistry*, 44: 11082-97.
Graeff, R., and H. C. Lee. 2002. 'A novel cycling assay for nicotinic acid-adenine dinucleotide phosphate with nanomolar sensitivity', *Biochem J*, 367: 163-8.
Graeff, R., Q. Liu, I. A. Kriksunov, Q. Hao, and H. C. Lee. 2006. 'Acidic residues at the active sites of CD38 and ADP-ribosyl cyclase determine nicotinic acid adenine dinucleotide phosphate (NAADP) synthesis and hydrolysis activities', *J Biol Chem*, 281: 28951-7.
Graeff, R. M., T. F. Walseth, K. Fryxell, W. D. Branton, and H. C. Lee. 1994. 'Enzymatic synthesis and characterizations of cyclic GDP-ribose. A procedure for distinguishing enzymes with ADP-ribosyl cyclase activity', *J Biol Chem*, 269: 30260-7.
Guan, X. H., X. Hong, N. Zhao, X. H. Liu, Y. F. Xiao, T. T. Chen, L. B. Deng, X. L. Wang, J. B. Wang, G. J. Ji, M. Fu, K. Y. Deng, and H. B. Xin. 2017. 'CD38 promotes angiotensin II-induced cardiac hypertrophy', *J Cell Mol Med*, 21: 1492-502.
Guan, X. H., X. H. Liu, X. Hong, N. Zhao, Y. F. Xiao, L. F. Wang, L. Tang, K. Jiang, Y. S. Qian, K. Y. Deng, G. Ji, M. Fu, and H. B. Xin. 2016. 'CD38 Deficiency Protects the Heart from Ischemia/Reperfusion Injury through Activating SIRT1/FOXOs-Mediated Antioxidative Stress Pathway', *Oxid Med Cell Longev*, 2016: 7410257.
Guida, L., L. Franco, E. Zocchi, and A. De Flora. 1995. 'Structural role of disulfide bridges in the cyclic ADP-ribose related bifunctional ectoenzyme CD38', *FEBS Lett*, 368: 481-4.
Gul, R., S. Y. Kim, K. H. Park, B. J. Kim, S. J. Kim, M. J. Im, and U. H. Kim. 2008. 'A novel signaling pathway of ADP-ribosyl cyclase activation by angiotensin II in adult rat cardiomyocytes', *Am J Physiol Heart Circ Physiol*, 295: H77-88.
Gul, R., D. R. Park, A. I. Shawl, S. Y. Im, T. S. Nam, S. H. Lee, J. K. Ko, K. Y. Jang, D. Kim, and U. H. Kim. 2016. 'Nicotinic Acid Adenine Dinucleotide Phosphate

(NAADP) and Cyclic ADP-Ribose (cADPR) Mediate Ca2+ Signaling in Cardiac Hypertrophy Induced by beta-Adrenergic Stimulation', *PLoS One*, 11: e0149125.

Gul, R., J. H. Park, S. Y. Kim, K. Y. Jang, J. K. Chae, J. K. Ko, and U. H. Kim. 2009. 'Inhibition of ADP-ribosyl cyclase attenuates angiotensin II-induced cardiac hypertrophy', *Cardiovasc Res*, 81: 582-91.

Guse, A. H., C. P. da Silva, I. Berg, A. L. Skapenko, K. Weber, P. Heyer, M. Hohenegger, G. A. Ashamu, H. Schulze-Koops, B. V. Potter, and G. W. Mayr. 1999. 'Regulation of calcium signalling in T lymphocytes by the second messenger cyclic ADP-ribose', *Nature*, 398: 70-3.

Guse, A. H., and I. M. Wolf. 2016. 'Ca(2+) microdomains, NAADP and type 1 ryanodine receptor in cell activation', *Biochim Biophys Acta*, 1863: 1379-84.

Gustafsson, A. B., and R. A. Gottlieb. 2008. 'Heart mitochondria: gates of life and death', *Cardiovasc Res*, 77: 334-43.

Gyorke, I., and S. Gyorke. 1998. 'Regulation of the cardiac ryanodine receptor channel by luminal Ca2+ involves luminal Ca2+ sensing sites', *Biophys J*, 75: 2801-10.

Hara-Yokoyama, M., M. Kukimoto-Niino, K. Terasawa, S. Harumiya, K. A. Podyma-Inoue, N. Hino, K. Sakamoto, S. Itoh, N. Hashii, Y. Hiruta, N. Kawasaki, C. Mishima-Tsumagari, Y. Kaitsu, T. Matsumoto, M. Wakiyama, M. Shirouzu, T. Kasama, H. Takayanagi, N. Utsunomiya-Tate, K. Takatsu, T. Katada, Y. Hirabayashi, S. Yokoyama, and M. Yanagishita. 2012. 'Tetrameric interaction of the ectoenzyme CD38 on the cell surface enables its catalytic and raft-association activities', *Structure*, 20: 1585-95.

Harzheim, D., M. Movassagh, R. S. Foo, O. Ritter, A. Tashfeen, S. J. Conway, M. D. Bootman, and H. L. Roderick. 2009. 'Increased InsP3Rs in the junctional sarcoplasmic reticulum augment Ca2+ transients and arrhythmias associated with cardiac hypertrophy', *Proc Natl Acad Sci U S A*, 106: 11406-11.

Heidemann, A. C., C. G. Schipke, and H. Kettenmann. 2005. 'Extracellular application of nicotinic acid adenine dinucleotide phosphate induces Ca2+ signaling in astrocytes in situ', *J Biol Chem*, 280: 35630-40.

Higashida, H., M. Liang, T. Yoshihara, S. Akther, A. Fakhrul, C. Stanislav, T. S. Nam, U. H. Kim, S. Kasai, T. Nishimura, N. Al Mahmuda, S. Yokoyama, K. Ishihara, M. Gerasimenko, A. Salmina, J. Zhong, T. Tsuji, C. Tsuji, and O. Lopatina. 2017. 'An immunohistochemical, enzymatic, and behavioral study of CD157/BST-1 as a neuroregulator', *BMC Neurosci*, 18: 35.

Hohenegger, M., J. Suko, R. Gscheidlinger, H. Drobny, and A. Zidar. 2002. 'Nicotinic acid-adenine dinucleotide phosphate activates the skeletal muscle ryanodine receptor', *Biochem J*, 367: 423-31.

Holmberg, S. R., and A. J. Williams. 1990. 'The cardiac sarcoplasmic reticulum calcium-release channel: modulation of ryanodine binding and single-channel activity', *Biochim Biophys Acta*, 1022: 187-93.

Hong, T., and R. M. Shaw. 2017. 'Cardiac T-Tubule Microanatomy and Function', *Physiol Rev*, 97: 227-52.

Horenstein, A. L., V. Quarona, D. Toscani, F. Costa, A. Chillemi, V. Pistoia, N. Giuliani, and F. Malavasi. 2016. 'Adenosine Generated in the Bone Marrow Niche Through a CD38-Mediated Pathway Correlates with Progression of Human Myeloma', *Mol Med*, 22: 694-704.

Huang, M. H., D. S. Friend, M. E. Sunday, K. Singh, K. Haley, K. F. Austen, R. A. Kelly, and T. W. Smith. 1996. 'An intrinsic adrenergic system in mammalian heart', *J Clin Invest*, 98: 1298-303.

Iino, S., Y. Cui, A. Galione, and D. A. Terrar. 1997. 'Actions of cADP-ribose and its antagonists on contraction in guinea pig isolated ventricular myocytes. Influence of temperature', *Circ Res*, 81: 879-84.

Itoh, M., K. Ishihara, H. Tomizawa, H. Tanaka, Y. Kobune, J. Ishikawa, T. Kaisho, and T. Hirano. 1994. 'Molecular cloning of murine BST-1 having homology with

CD38 and Aplysia ADP-ribosyl cyclase', *Biochem Biophys Res Commun*, 203: 1309-17.

Jackson, D. G., and J. I. Bell. 1990. 'Isolation of a cDNA encoding the human CD38 (T10) molecule, a cell surface glycoprotein with an unusual discontinuous pattern of expression during lymphocyte differentiation', *J Immunol*, 144: 2811-5.

Jaimes, R., 3rd, R. D. Walton, P. Pasdois, O. Bernus, I. R. Efimov, and M. W. Kay. 2016. 'A technical review of optical mapping of intracellular calcium within myocardial tissue', *Am J Physiol Heart Circ Physiol*, 310: H1388-401.

Jha, A., M. Ahuja, S. Patel, E. Brailoiu, and S. Muallem. 2014. 'Convergent regulation of the lysosomal two-pore channel-2 by Mg(2)(+), NAADP, PI(3,5)P(2) and multiple protein kinases', *EMBO J*, 33: 501-11.

Jin, D., H. X. Liu, H. Hirai, T. Torashima, T. Nagai, O. Lopatina, N. A. Shnayder, K. Yamada, M. Noda, T. Seike, K. Fujita, S. Takasawa, S. Yokoyama, K. Koizumi, Y. Shiraishi, S. Tanaka, M. Hashii, T. Yoshihara, K. Higashida, M. S. Islam, N. Yamada, K. Hayashi, N. Noguchi, I. Kato, H. Okamoto, A. Matsushima, A. Salmina, T. Munesue, N. Shimizu, S. Mochida, M. Asano, and H. Higashida. 2007. 'CD38 is critical for social behaviour by regulating oxytocin secretion', *Nature*, 446: 41-5.

Johnson, D. M., and G. Antoons. 2018. 'Arrhythmogenic Mechanisms in Heart Failure: Linking beta-Adrenergic Stimulation, Stretch, and Calcium', *Front Physiol*, 9: 1453.

Johnson, D. M., J. Heijman, E. F. Bode, D. J. Greensmith, H. van der Linde, N. Abi-Gerges, D. A. Eisner, A. W. Trafford, and P. G. Volders. 2013. 'Diastolic spontaneous calcium release from the sarcoplasmic reticulum increases beat-to-beat variability of repolarization in canine ventricular myocytes after beta-adrenergic stimulation', *Circ Res*, 112: 246-56.

Ju, Y. K., J. Liu, B. H. Lee, D. Lai, E. A. Woodcock, M. Lei, M. B. Cannell, and D. G. Allen. 2011. 'Distribution and functional role of inositol 1,4,5-trisphosphate receptors in mouse sinoatrial node', *Circ Res*, 109: 848-57.

Kabbara, A. A., and D. G. Allen. 2001. 'The use of the indicator fluo-5N to measure sarcoplasmic reticulum calcium in single muscle fibres of the cane toad', *J Physiol*, 534: 87-97.

Kamp, T. J., and J. W. Hell. 2000. 'Regulation of cardiac L-type calcium channels by protein kinase A and protein kinase C', *Circ Res*, 87: 1095-102.

Kannt, A., K. Sicka, K. Kroll, D. Kadereit, and H. Gogelein. 2012. 'Selective inhibitors of cardiac ADPR cyclase as novel anti-arrhythmic compounds', *Naunyn Schmiedebergs Arch Pharmacol*, 385: 717-27.

Kato, I., Y. Yamamoto, M. Fujimura, N. Noguchi, S. Takasawa, and H. Okamoto. 1999. 'CD38 disruption impairs glucose-induced increases in cyclic ADP-ribose, [Ca2+]i, and insulin secretion', *J Biol Chem*, 274: 1869-72.

Katz, F., S. Povey, M. Parkar, C. Schneider, R. Sutherland, K. Stanley, E. Solomon, and M. Greaves. 1983. 'Chromosome assignment of monoclonal antibody-defined determinants on human leukemic cells', *Eur J Immunol*, 13: 1008-13.

Kellenberger, E., I. Kuhn, F. Schuber, and H. Muller-Steffner. 2011. 'Flavonoids as inhibitors of human CD38', *Bioorganic & Medicinal Chemistry Letters*, 21: 3841-4114.

Kim, H., E. L. Jacobson, and M. K. Jacobson. 1993. 'Synthesis and degradation of cyclic ADP-ribose by NAD glycohydrolases', *Science*, 261: 1330-3.

Kim, S. Y., B. H. Cho, and U. H. Kim. 2010. 'CD38-mediated Ca2+ signaling contributes to angiotensin II-induced activation of hepatic stellate cells: attenuation of hepatic fibrosis by CD38 ablation', *J Biol Chem*, 285: 576-82.

Kinnear, N. P., F. X. Boittin, J. M. Thomas, A. Galione, and A. M. Evans. 2004. 'Lysosome-sarcoplasmic reticulum junctions. A trigger zone for calcium signaling

by nicotinic acid adenine dinucleotide phosphate and endothelin-1', *J Biol Chem*, 279: 54319-26.

Kinnear, N. P., C. N. Wyatt, J. H. Clark, P. J. Calcraft, S. Fleischer, L. H. Jeyakumar, G. F. Nixon, and A. M. Evans. 2008. 'Lysosomes co-localize with ryanodine receptor subtype 3 to form a trigger zone for calcium signalling by NAADP in rat pulmonary arterial smooth muscle', *Cell Calcium*, 44: 190-201.

Kirchberger, M. A., M. Tada, and A. M. Katz. 1974. 'Adenosine 3':5'-monophosphate-dependent protein kinase-catalyzed phosphorylation reaction and its relationship to calcium transport in cardiac sarcoplasmic reticulum', *J Biol Chem*, 249: 6166-73.

Klabunde, R. E. 2012. *Cardiovascular Physiology Concepts* (Lippincott Williams & Wilkins).

Kohl, P., and R. G. Gourdie. 2014. 'Fibroblast-myocyte electrotonic coupling: does it occur in native cardiac tissue?', *J Mol Cell Cardiol*, 70: 37-46.

Kong, W., and V. G. Fast. 2014. 'The role of dye affinity in optical measurements of Cai(2+) transients in cardiac muscle', *Am J Physiol Heart Circ Physiol*, 307: H73-9.

Kowalczyk, A. P., and K. J. Green. 2013. 'Structure, function, and regulation of desmosomes', *Prog Mol Biol Transl Sci*, 116: 95-118.

Kukimoto, I., S. Hoshino, K. Kontani, K. Inageda, H. Nishina, K. Takahashi, and T. Katada. 1996. 'Stimulation of ADP-ribosyl cyclase activity of the cell surface antigen CD38 by zinc ions resulting from inhibition of its NAD+ glycohydrolase activity', *Eur J Biochem*, 239: 177-82.

Lahouratate, P., J. Guibert, and J. F. Faivre. 1997. 'cADP-ribose releases Ca2+ from cardiac sarcoplasmic reticulum independently of ryanodine receptor', *Am J Physiol*, 273: H1082-9.

Lam, A. K., and A. Galione. 2013. 'The endoplasmic reticulum and junctional membrane communication during calcium signaling', *Biochim Biophys Acta*, 1833: 2542-59.

Landstrom, A. P., D. Dobrev, and X. H. T. Wehrens. 2017. 'Calcium Signaling and Cardiac Arrhythmias', *Circ Res*, 120: 1969-93.

Lange, I., R. Penner, A. Fleig, and A. Beck. 2008. 'Synergistic regulation of endogenous TRPM2 channels by adenine dinucleotides in primary human neutrophils', *Cell Calcium*, 44: 604-15.

Langhorst, M. F., N. Schwarzmann, and A. H. Guse. 2004. 'Ca2+ release via ryanodine receptors and Ca2+ entry: major mechanisms in NAADP-mediated Ca2+ signaling in T-lymphocytes', *Cell Signal*, 16: 1283-9.

Le Peuch, C. J., C. Ferraz, M. P. Walsh, J. G. Demaille, and E. H. Fischer. 1979. 'Calcium and cyclic nucleotide dependent regulatory mechanisms during development of chick embryo skeletal muscle', *Biochemistry*, 18: 5267-73.

Lee, H. C. 2001. 'Physiological functions of cyclic ADP-ribose and NAADP as calcium messengers', *Annu Rev Pharmacol Toxicol*, 41: 317-45.

———. 2006. 'Structure and enzymatic functions of human CD38', *Mol Med*, 12: 317-23.

Lee, H. C., and R. Aarhus. 1991. 'ADP-ribosyl cyclase: an enzyme that cyclizes NAD+ into a calcium-mobilizing metabolite', *Cell Regul*, 2: 203-9.

———. 1995. 'A derivative of NADP mobilizes calcium stores insensitive to inositol trisphosphate and cyclic ADP-ribose', *J Biol Chem*, 270: 2152-7.

———. 2000. 'Functional visualization of the separate but interacting calcium stores sensitive to NAADP and cyclic ADP-ribose', *J Cell Sci*, 113 Pt 24: 4413-20.

Lee, H. C., R. Aarhus, R. Graeff, M. E. Gurnack, and T. F. Walseth. 1994. 'Cyclic ADP ribose activation of the ryanodine receptor is mediated by calmodulin', *Nature*, 370: 307-9.

Lee, H.C; Zhao, Y.J. 2014. 'The Type III Calcium Signaling Mechanism of CD38', *Messenger*, 3.

Lee, Y. K., D. Y. Yuk, J. W. Lee, S. Y. Lee, T. Y. Ha, K. W. Oh, Y. P. Yun, and J. T. Hong. 2009. '(-)-Epigallocatechin-3-gallate prevents lipopolysaccharide-induced elevation of beta-amyloid generation and memory deficiency', *Brain Res*, 1250: 164-74.

Levick, J.R. 2010. *An introduction to cardiac physiology*.

Lewis, A. M., P. K. Aley, A. Roomi, J. M. Thomas, R. Masgrau, C. Garnham, K. Shipman, C. Paramore, D. Bloor-Young, L. E. Sanders, D. A. Terrar, A. Galione, and G. C. Churchill. 2012. 'beta-Adrenergic receptor signaling increases NAADP and cADPR levels in the heart', *Biochem Biophys Res Commun*, 427: 326-9.

Lewis, A. M., R. Masgrau, S. R. Vasudevan, M. Yamasaki, J. S. O'Neill, C. Garnham, K. James, A. Macdonald, M. Ziegler, A. Galione, and G. C. Churchill. 2007. 'Refinement of a radioreceptor binding assay for nicotinic acid adenine dinucleotide phosphate', *Anal Biochem*, 371: 26-36.

Li, L., S. Mirza, S. J. Richardson, E. M. Gallant, C. Thekkedam, S. M. Pace, F. Zorzato, D. Liu, N. A. Beard, and A. F. Dulhunty. 2015. 'A new cytoplasmic interaction between junctin and ryanodine receptor Ca2+ release channels', *J Cell Sci*, 128: 951-63.

Li, X., A. V. Zima, F. Sheikh, L. A. Blatter, and J. Chen. 2005. 'Endothelin-1-induced arrhythmogenic Ca2+ signaling is abolished in atrial myocytes of inositol-1,4,5-trisphosphate(IP3)-receptor type 2-deficient mice', *Circ Res*, 96: 1274-81.

Lin-Moshier, Y., T. F. Walseth, D. Churamani, S. M. Davidson, J. T. Slama, R. Hooper, E. Brailoiu, S. Patel, and J. S. Marchant. 2012. 'Photoaffinity labeling of nicotinic acid adenine dinucleotide phosphate (NAADP) targets in mammalian cells', *J Biol Chem*, 287: 2296-307.

Lin, W. K. 2017. 'The roles of CD38 and NAADP in cardiac tissue', University of Oxford.

Lin, W. K., E. L. Bolton, W. A. Cortopassi, Y. Wang, F. O'Brien, M. Maciejewska, M. P. Jacobson, C. Garnham, M. Ruas, J. Parrington, M. Lei, R. Sitsapesan, A. Galione, and D. A. Terrar. 2017. 'Synthesis of the Ca(2+)-mobilizing messengers NAADP and cADPR by intracellular CD38 enzyme in the mouse heart: Role in beta-adrenoceptor signaling', *J Biol Chem*, 292: 13243-57.

Lipp, P., M. Laine, S. C. Tovey, K. M. Burrell, M. J. Berridge, W. Li, and M. D. Bootman. 2000. 'Functional InsP3 receptors that may modulate excitation-contraction coupling in the heart', *Curr Biol*, 10: 939-42.

Liu, J., Y. J. Zhao, W. H. Li, Y. N. Hou, T. Li, Z. Y. Zhao, C. Fang, S. L. Li, and H. C. Lee. 2017. 'Cytosolic interaction of type III human CD38 with CIB1 modulates cellular cyclic ADP-ribose levels', *Proc Natl Acad Sci U S A*.

Liu, N., B. Colombi, M. Memmi, S. Zissimopoulos, N. Rizzi, S. Negri, M. Imbriani, C. Napolitano, F. A. Lai, and S. G. Priori. 2006. 'Arrhythmogenesis in catecholaminergic polymorphic ventricular tachycardia: insights from a RyR2 R4496C knock-in mouse model', *Circ Res*, 99: 292-8.

Liu, Q., R. Graeff, I. A. Kriksunov, C. M. Lam, H. C. Lee, and Q. Hao. 2008. 'Conformational Closure of the Catalytic Site of Human CD38 Induced by Calcium', *Biochemistry*, 47: 13966-73.

Lloyd-Evans, E., A. J. Morgan, X. He, D. A. Smith, E. Elliot-Smith, D. J. Sillence, G. C. Churchill, E. H. Schuchman, A. Galione, and F. M. Platt. 2008. 'Niemann-Pick disease type C1 is a sphingosine storage disease that causes deregulation of lysosomal calcium', *Nat Med*, 14: 1247-55.

Lukyanenko, V., I. Gyorke, T. F. Wiesner, and S. Gyorke. 2001. 'Potentiation of Ca(2+) release by cADP-ribose in the heart is mediated by enhanced SR Ca(2+) uptake into the sarcoplasmic reticulum', *Circ Res*, 89: 614-22.

Lukyanenko, V., and S. Gyorke. 1999. 'Ca2+ sparks and Ca2+ waves in saponin-permeabilized rat ventricular myocytes', *J Physiol*, 521 Pt 3: 575-85.

Luzio, J. P., P. R. Pryor, and N. A. Bright. 2007. 'Lysosomes: fusion and function', *Nat Rev Mol Cell Biol*, 8: 622-32.

MacDonald, M. R., M. C. Petrie, N. M. Hawkins, J. R. Petrie, M. Fisher, R. McKelvie, D. Aguilar, H. Krum, and J. J. McMurray. 2008. 'Diabetes, left ventricular systolic dysfunction, and chronic heart failure', *Eur Heart J*, 29: 1224-40.

Macgregor, A. T., S. Rakovic, A. Galione, and D. A. Terrar. 2007. 'Dual effects of cyclic ADP-ribose on sarcoplasmic reticulum Ca2+ release and storage in cardiac myocytes isolated from guinea-pig and rat ventricle', *Cell Calcium*, 41: 537-46.

Macgregor, A., M. Yamasaki, S. Rakovic, L. Sanders, R. Parkesh, G. C. Churchill, A. Galione, and D. A. Terrar. 2007. 'NAADP controls cross-talk between distinct Ca2+ stores in the heart', *J Biol Chem*, 282: 15302-11.

MacLennan, D. H., C. J. Brandl, B. Korczak, and N. M. Green. 1985. 'Amino-acid sequence of a Ca2+ + Mg2+-dependent ATPase from rabbit muscle sarcoplasmic reticulum, deduced from its complementary DNA sequence', *Nature*, 316: 696-700.

Maier, L. S., and D. M. Bers. 2007. 'Role of Ca2+/calmodulin-dependent protein kinase (CaMK) in excitation-contraction coupling in the heart', *Cardiovasc Res*, 73: 631-40.

Malavasi, F., S. Deaglio, A. Funaro, E. Ferrero, A. L. Horenstein, E. Ortolan, T. Vaisitti, and S. Aydin. 2008. 'Evolution and function of the ADP ribosyl cyclase/CD38 gene family in physiology and pathology', *Physiol Rev*, 88: 841-86.

Malavasi, F., A. Funaro, S. Roggero, A. Horenstein, L. Calosso, and K. Mehta. 1994. 'Human CD38: a glycoprotein in search of a function', *Immunol Today*, 15: 95-7.

Mallone, R., S. Ferrua, M. Morra, E. Zocchi, K. Mehta, L. D. Notarangelo, and F. Malavasi. 1998. 'Characterization of a CD38-like 78-kilodalton soluble protein released from B cell lines derived from patients with X-linked agammaglobulinemia', *J Clin Invest*, 101: 2821-30.

Matiukas, A., B. G. Mitrea, M. Qin, A. M. Pertsov, A. G. Shvedko, M. D. Warren, A. V. Zaitsev, J. P. Wuskell, M. D. Wei, J. Watras, and L. M. Loew. 2007. 'Near-infrared voltage-sensitive fluorescent dyes optimized for optical mapping in blood-perfused myocardium', *Heart Rhythm*, 4: 1441-51.

Mattiazzi, A., and E. G. Kranias. 2011. 'CaMKII regulation of phospholamban and SR Ca2+ load', *Heart Rhythm*, 8: 784-7.

Mattick, P., J. Parrington, E. Odia, A. Simpson, T. Collins, and D. Terrar. 2007. 'Ca2+-stimulated adenylyl cyclase isoform AC1 is preferentially expressed in guinea-pig sino-atrial node cells and modulates the I(f) pacemaker current', *J Physiol*, 582: 1195-203.

Maxwell, J. T., and L. A. Blatter. 2017. 'A novel mechanism of tandem activation of ryanodine receptors by cytosolic and SR luminal Ca(2+) during excitation-contraction coupling in atrial myocytes', *J Physiol*, 595: 3835-45.

McKinsey, T. A. 2007. 'Derepression of pathological cardiac genes by members of the CaM kinase superfamily', *Cardiovasc Res*, 73: 667-77.

Mellman, I., R. Fuchs, and A. Helenius. 1986. 'Acidification of the endocytic and exocytic pathways', *Annu Rev Biochem*, 55: 663-700.

Meszaros, L. G., J. Bak, and A. Chu. 1993. 'Cyclic ADP-ribose as an endogenous regulator of the non-skeletal type ryanodine receptor Ca2+ channel', *Nature*, 364: 76-9.

Meszaros, L. G., R. W. Wrenn, and G. Varadi. 1997. 'Sarcoplasmic reticulum-associated and protein kinase C-regulated ADP-ribosyl cyclase in cardiac muscle', *Biochem Biophys Res Commun*, 234: 252-6.

Mojzisova, A., O. Krizanova, L. Zacikova, V. Kominkova, and K. Ondrias. 2001. 'Effect of nicotinic acid adenine dinucleotide phosphate on ryanodine calcium release channel in heart', *Pflugers Arch*, 441: 674-7.

Molkentin, J. D., J. R. Lu, C. L. Antos, B. Markham, J. Richardson, J. Robbins, S. R. Grant, and E. N. Olson. 1998. 'A calcineurin-dependent transcriptional pathway for cardiac hypertrophy', *Cell*, 93: 215-28.

Morandi, F., B. Morandi, A. L. Horenstein, A. Chillemi, V. Quarona, G. Zaccarello, P. Carrega, G. Ferlazzo, M. C. Mingari, L. Moretta, V. Pistoia, and F. Malavasi. 2015. 'A non-canonical adenosinergic pathway led by CD38 in human melanoma cells induces suppression of T cell proliferation', *Oncotarget*, 6: 25602-18.

Moreschi, I., S. Bruzzone, N. Bodrato, C. Usai, L. Guida, R. A. Nicholas, M. U. Kassack, E. Zocchi, and A. De Flora. 2008. 'NAADP+ is an agonist of the human P2Y11 purinergic receptor', *Cell Calcium*, 43: 344-55.

Morgan, A. J., L. C. Davis, S. K. Wagner, A. M. Lewis, J. Parrington, G. C. Churchill, and A. Galione. 2013. 'Bidirectional Ca(2)(+) signaling occurs between the endoplasmic reticulum and acidic organelles', *J Cell Biol*, 200: 789-805.

Morgan, A. J., and A. Galione. 2007. 'NAADP induces pH changes in the lumen of acidic Ca2+ stores', *Biochem J*, 402: 301-10.

———. 2008. 'Investigating cADPR and NAADP in intact and broken cell preparations', *Methods*, 46: 194-203.

———. 2014. 'Two-pore channels (TPCs): current controversies', *Bioessays*, 36: 173-83.

Morgan, A. J., F. M. Platt, E. Lloyd-Evans, and A. Galione. 2011. 'Molecular mechanisms of endolysosomal Ca2+ signalling in health and disease', *Biochem J*, 439: 349-74.

Mottahedeh, J., M. C. Haffner, T. R. Grogan, T. Hashimoto, P. D. Crowell, H. Beltran, A. Sboner, R. Bareja, D. Esopi, W. B. Isaacs, S. Yegnasubramanian, M. B. Rettig, D. A. Elashoff, E. A. Platz, A. M. De Marzo, M. A. Teitell, and A. S. Goldstein. 2018. 'CD38 is methylated in prostate cancer and regulates extracellular NAD()', *Cancer Metab*, 6: 13.

Muller-Steffner, H., I. Kuhn, M. Argentini, and F. Schuber. 2010. 'Identification of the N-glycosylation sites on recombinant bovine CD38 expressed in Pichia pastoris: their impact on enzyme stability and catalytic activity', *Protein Expr Purif*, 70: 151-7.

Munshi, C., R. Aarhus, R. Graeff, T. F. Walseth, D. Levitt, and H. C. Lee. 2000. 'Identification of the enzymatic active site of CD38 by site-directed mutagenesis', *J Biol Chem*, 275: 21566-71.

Munshi, C., C. Baumann, D. Levitt, V. A. Bloomfield, and H. C. Lee. 1998. 'The homo-dimeric form of ADP-ribosyl cyclase in solution', *Biochim Biophys Acta*, 1388: 428-36.

Mutafova-Yambolieva, V. N., S. J. Hwang, X. Hao, H. Chen, M. X. Zhu, J. D. Wood, S. M. Ward, and K. M. Sanders. 2007. 'Beta-nicotinamide adenine dinucleotide is an inhibitory neurotransmitter in visceral smooth muscle', *Proc Natl Acad Sci U S A*, 104: 16359-64.

Nam, T. S., S. H. Choi, S. Y. Rah, S. Y. Kim, W. Jang, M. J. Im, H. J. Kwon, and U. H. Kim. 2006. 'Discovery of a small-molecule inhibitor for kidney ADP-ribosyl cyclase: Implication for intracellular calcium signal mediated by cyclic ADP-ribose', *Exp Mol Med*, 38: 718-26.

Nebel, M., A. P. Schwoerer, D. Warszta, C. C. Siebrands, A. C. Limbrock, J. M. Swarbrick, R. Fliegert, K. Weber, S. Bruhn, M. Hohenegger, A. Geisler, L. Herich, S. Schlegel, L. Carrier, T. Eschenhagen, B. V. Potter, H. Ehmke, and A. H. Guse. 2013. 'Nicotinic acid adenine dinucleotide phosphate (NAADP)-mediated calcium signaling and arrhythmias in the heart evoked by beta-adrenergic stimulation', *J Biol Chem*, 288: 16017-30.

Neely Kayala, K. M., G. D. Dickinson, A. Minassian, K. C. Walls, K. N. Green, and F. M. Laferla. 2012. 'Presenilin-null cells have altered two-pore calcium channel expression and lysosomal calcium: implications for lysosomal function', *Brain Res*, 1489: 8-16.

Nerbonne, J. M., and R. S. Kass. 2005. 'Molecular physiology of cardiac repolarization', *Physiol Rev*, 85: 1205-53.

Noguchi, N., S. Takasawa, K. Nata, A. Tohgo, I. Kato, F. Ikehata, H. Yonekura, and H. Okamoto. 1997. 'Cyclic ADP-ribose binds to FK506-binding protein 12.6 to release Ca2+ from islet microsomes', *J Biol Chem*, 272: 3133-6.

Notomi, T., Y. Ezura, and M. Noda. 2012. 'Identification of two-pore channel 2 as a novel regulator of osteoclastogenesis', *J Biol Chem*, 287: 35057-64.

Nussinovitch, U., and L. Gepstein. 2015. 'Optogenetics for in vivo cardiac pacing and resynchronization therapies', *Nat Biotechnol*, 33: 750-4.

O'Brien, F., D. Eberhardt, K. Witschas, S. El-Ajouz, T. Iida, M. Nishi, H. Takeshima, R. Sitsapesan, and E. Venturi. 2019. 'Enhanced activity of multiple TRIC-B channels; an ER/SR mechanism to boost counterion currents', *J Physiol*.

O'Shea, C., A. P. Holmes, T. Y. Yu, J. Winter, S. P. Wells, J. Correia, B. J. Boukens, J. R. De Groot, G. S. Chu, X. Li, G. A. Ng, P. Kirchhof, L. Fabritz, K. Rajpoot, and D. Pavlovic. 2019. 'ElectroMap: High-throughput open-source software for analysis and mapping of cardiac electrophysiology', *Sci Rep*, 9: 1389.

Ogunbayo, O. A., Y. Zhu, D. Rossi, V. Sorrentino, J. Ma, M. X. Zhu, and A. M. Evans. 2011. 'Cyclic adenosine diphosphate ribose activates ryanodine receptors, whereas NAADP activates two-pore domain channels', *J Biol Chem*, 286: 9136-40.

Osuala, K., K. Telusma, S. M. Khan, S. Wu, M. Shah, C. Baker, S. Alam, I. Abukenda, A. Fuentes, H. B. Seifein, and S. N. Ebert. 2011. 'Distinctive left-sided distribution of adrenergic-derived cells in the adult mouse heart', *PLoS One*, 6: e22811.

Otsu, K., H. F. Willard, V. K. Khanna, F. Zorzato, N. M. Green, and D. H. MacLennan. 1990. 'Molecular cloning of cDNA encoding the Ca2+ release channel (ryanodine receptor) of rabbit cardiac muscle sarcoplasmic reticulum', *J Biol Chem*, 265: 13472-83.

Ovacik, A. M., J. Li, M. Lemper, D. Danilenko, N. Stagg, M. Mathieu, D. Ellerman, V. Gupta, N. Kalia, T. Nguy, V. Plaks, C. David Johnson, W. Wang, J. Brumm, B. Fine, T. Junttila, K. Lin, P. J. Carter, S. Prabhu, C. Spiess, and A. V. Kamath. 2019. 'Single cell-produced and in vitro-assembled anti-FcRH5/CD3 T-cell dependent bispecific antibodies have similar in vitro and in vivo properties', *MAbs*, 11: 422-33.

Owji, A., N. Varudkar, and S. N. Ebert. 2013. 'Therapeutic potential of Pnmt+ primer cells for neuro/myocardial regeneration', *Am J Stem Cells*, 2: 137-54.

Panche, A. N., A. D. Diwan, and S. R. Chandra. 2016. 'Flavonoids: an overview', *J Nutr Sci*, 5: e47.

Pandey, V., C. C. Chuang, A. M. Lewis, P. K. Aley, E. Brailoiu, N. J. Dun, G. C. Churchill, and S. Patel. 2009. 'Recruitment of NAADP-sensitive acidic Ca2+ stores by glutamate', *Biochem J*, 422: 503-12.

Paredes, R. M., J. C. Etzler, L. T. Watts, W. Zheng, and J. D. Lechleiter. 2008. 'Chemical calcium indicators', *Methods*, 46: 143-51.

Partida-Sanchez, S., D. A. Cockayne, S. Monard, E. L. Jacobson, N. Oppenheimer, B. Garvy, K. Kusser, S. Goodrich, M. Howard, A. Harmsen, T. D. Randall, and F. E. Lund. 2001. 'Cyclic ADP-ribose production by CD38 regulates intracellular calcium release, extracellular calcium influx and chemotaxis in neutrophils and is required for bacterial clearance in vivo', *Nat Med*, 7: 1209-16.

Patel, S., and S. Muallem. 2011. 'Acidic Ca(2+) stores come to the fore', *Cell Calcium*, 50: 109-12.

Penny, C. J., B. S. Kilpatrick, J. M. Han, J. Sneyd, and S. Patel. 2014. 'A computational model of lysosome-ER Ca2+ microdomains', *J Cell Sci*, 127: 2934-43.

Pereira, G. J., H. Hirata, L. G. do Carmo, R. S. Stilhano, R. P. Ureshino, N. C. Medaglia, S. W. Han, G. Churchill, C. Bincoletto, S. Patel, and S. S. Smaili. 2014. 'NAADP-sensitive two-pore channels are present and functional in gastric smooth muscle cells', *Cell Calcium*, 56: 51-8.

Pitt, S. J., T. M. Funnell, M. Sitsapesan, E. Venturi, K. Rietdorf, M. Ruas, A. Ganesan, R. Gosain, G. C. Churchill, M. X. Zhu, J. Parrington, A. Galione, and R. Sitsapesan. 2010. 'TPC2 is a novel NAADP-sensitive Ca2+ release channel, operating as a dual sensor of luminal pH and Ca2+', *J Biol Chem*, 285: 35039-46.

Pitt, S. J., A. K. Lam, K. Rietdorf, A. Galione, and R. Sitsapesan. 2014. 'Reconstituted human TPC1 is a proton-permeable ion channel and is activated by NAADP or Ca2+', *Sci Signal*, 7: ra46.

Pitt, S. J., B. Reilly-O'Donnell, and R. Sitsapesan. 2016. 'Exploring the biophysical evidence that mammalian two-pore channels are NAADP-activated calcium-permeable channels', *J Physiol*, 594: 4171-9.

Pogwizd, S. M., K. Schlotthauer, L. Li, W. Yuan, and D. M. Bers. 2001. 'Arrhythmogenesis and contractile dysfunction in heart failure: Roles of sodium-calcium exchange, inward rectifier potassium current, and residual beta-adrenergic responsiveness', *Circ Res*, 88: 1159-67.

Prakash, Y. S., M. S. Kannan, T. F. Walseth, and G. C. Sieck. 2000. 'cADP ribose and [Ca(2+)](i) regulation in rat cardiac myocytes', *Am J Physiol Heart Circ Physiol*, 279: H1482-9.

Prasad, G. S., D. E. McRee, E. A. Stura, D. G. Levitt, H. C. Lee, and C. D. Stout. 1996. 'Crystal structure of Aplysia ADP ribosyl cyclase, a homologue of the bifunctional ectozyme CD38', *Nat Struct Biol*, 3: 957-64.

Proven, A., H. L. Roderick, S. J. Conway, M. J. Berridge, J. K. Horton, S. J. Capper, and M. D. Bootman. 2006. 'Inositol 1,4,5-trisphosphate supports the arrhythmogenic action of endothelin-1 on ventricular cardiac myocytes', *J Cell Sci*, 119: 3363-75.

Pryor, P. R., F. Reimann, F. M. Gribble, and J. P. Luzio. 2006. 'Mucolipin-1 is a lysosomal membrane protein required for intracellular lactosylceramide traffic', *Traffic*, 7: 1388-98.

Puddu, P. E., R. Jouve, F. Langlet, J. C. Guillen, M. Lanti, and A. Reale. 1988. 'Prevention of postischemic ventricular fibrillation late after right or left stellate ganglionectomy in dogs', *Circulation*, 77: 935-46.

Rah, S. Y., M. Mushtaq, T. S. Nam, S. H. Kim, and U. H. Kim. 2010. 'Generation of cyclic ADP-ribose and nicotinic acid adenine dinucleotide phosphate by CD38 for Ca2+ signaling in interleukin-8-treated lymphokine-activated killer cells', *J Biol Chem*, 285: 21877-87.

Rajan, N., A. Tsarbopoulos, R. Kumarasamy, R. O'Donnell, S. S. Taremi, S. W. Baldwin, G. F. Seelig, X. Fan, B. Pramanik, and H. V. Le. 1995. 'Characterization of recombinant human interleukin 4 receptor from CHO cells: role of N-linked oligosaccharides', *Biochem Biophys Res Commun*, 206: 694-702.

Rakovic, S., Y. Cui, S. Iino, A. Galione, G. A. Ashamu, B. V. Potter, and D. A. Terrar. 1999. 'An antagonist of cADP-ribose inhibits arrhythmogenic oscillations of intracellular Ca2+ in heart cells', *J Biol Chem*, 274: 17820-7.

Rakovic, S., A. Galione, G. A. Ashamu, B. V. Potter, and D. A. Terrar. 1996. 'A specific cyclic ADP-ribose antagonist inhibits cardiac excitation-contraction coupling', *Curr Biol*, 6: 989-96.

Reddy, L. G., L. R. Jones, R. C. Pace, and D. L. Stokes. 1996. 'Purified, reconstituted cardiac Ca2+-ATPase is regulated by phospholamban but not by direct phosphorylation with Ca2+/calmodulin-dependent protein kinase', *J Biol Chem*, 271: 14964-70.

Reinherz, E. L., P. C. Kung, G. Goldstein, R. H. Levey, and S. F. Schlossman. 1980. 'Discrete stages of human intrathymic differentiation: analysis of normal thymocytes and leukemic lymphoblasts of T-cell lineage', *Proc Natl Acad Sci U S A*, 77: 1588-92.

Reuter, H., S. Kokubun, and B. Prod'hom. 1986. 'Properties and modulation of cardiac calcium channels', *J Exp Biol*, 124: 191-201.

Reyes-Harde, M., R. Empson, B. V. Potter, A. Galione, and P. K. Stanton. 1999. 'Evidence of a role for cyclic ADP-ribose in long-term synaptic depression in hippocampus', *Proc Natl Acad Sci U S A*, 96: 4061-6.

Reyes, L. A., J. Boslett, S. Varadharaj, F. De Pascali, C. Hemann, L. J. Druhan, G. Ambrosio, M. El-Mahdy, and J. L. Zweier. 2015. 'Depletion of NADP(H) due to CD38 activation triggers endothelial dysfunction in the postischemic heart', *Proc Natl Acad Sci U S A*, 112: 11648-53.

Rigg, L., B. M. Heath, Y. Cui, and D. A. Terrar. 2000. 'Localisation and functional significance of ryanodine receptors during beta-adrenoceptor stimulation in the guinea-pig sino-atrial node', *Cardiovasc Res*, 48: 254-64.

Rockman, H. A., W. J. Koch, and R. J. Lefkowitz. 2002. 'Seven-transmembrane-spanning receptors and heart function', *Nature*, 415: 206-12.

Roderick, H. L., and M. D. Bootman. 2003. 'Bi-directional signalling from the InsP3 receptor: regulation by calcium and accessory factors', *Biochem Soc Trans*, 31: 950-3.

Rohr, S. 2004. 'Role of gap junctions in the propagation of the cardiac action potential', *Cardiovasc Res*, 62: 309-22.

Ruas, M., L. C. Davis, C. C. Chen, A. J. Morgan, K. T. Chuang, T. F. Walseth, C. Grimm, C. Garnham, T. Powell, N. Platt, F. M. Platt, M. Biel, C. Wahl-Schott, J. Parrington, and A. Galione. 2015. 'Expression of Ca(2)(+)-permeable two-pore channels rescues NAADP signalling in TPC-deficient cells', *EMBO J*, 34: 1743-58.

Saito, A., S. Seiler, A. Chu, and S. Fleischer. 1984. 'Preparation and morphology of sarcoplasmic reticulum terminal cisternae from rabbit skeletal muscle', *J Cell Biol*, 99: 875-85.

Sanchez-Tusie, A. A., S. R. Vasudevan, G. C. Churchill, T. Nishigaki, and C. L. Trevino. 2014. 'Characterization of NAADP-mediated calcium signaling in human spermatozoa', *Biochem Biophys Res Commun*, 443: 531-6.

Santella, L., K. Kyozuka, A. A. Genazzani, L. De Riso, and E. Carafoli. 2000. 'Nicotinic acid adenine dinucleotide phosphate-induced Ca(2+) release. Interactions among distinct Ca(2+) mobilizing mechanisms in starfish oocytes', *J Biol Chem*, 275: 8301-6.

Sato, A., S. Yamamoto, N. Kajimura, M. Oda, J. Usukura, and H. Jingami. 1999. 'Inhibitor peptide SNP-1 binds to a soluble form of BST-1/CD157 at a 2:2 stoichiometry', *Eur J Biochem*, 264: 439-45.

Schiavoni, I., C. Scagnolari, A. L. Horenstein, P. Leone, A. Pierangeli, F. Malavasi, C. M. Ausiello, and G. Fedele. 2018. 'CD38 modulates respiratory syncytial virus-driven proinflammatory processes in human monocyte-derived dendritic cells', *Immunology*, 154: 122-31.

Singal, T., N. S. Dhalla, and P. S. Tappia. 2004. 'Phospholipase C may be involved in norepinephrine-induced cardiac hypertrophy', *Biochem Biophys Res Commun*, 320: 1015-9.

Singaravelu, K., and J. W. Deitmer. 2006. 'Calcium mobilization by nicotinic acid adenine dinucleotide phosphate (NAADP) in rat astrocytes', *Cell Calcium*, 39: 143-53.

Sitsapesan, R., S. J. McGarry, and A. J. Williams. 1994. 'Cyclic ADP-ribose competes with ATP for the adenine nucleotide binding site on the cardiac ryanodine receptor Ca(2+)-release channel', *Circ Res*, 75: 596-600.

Sitsapesan, R., R. A. Montgomery, K. T. MacLeod, and A. J. Williams. 1991. 'Sheep cardiac sarcoplasmic reticulum calcium-release channels: modification of conductance and gating by temperature', *J Physiol*, 434: 469-88.

Soares, S., M. Thompson, T. White, A. Isbell, M. Yamasaki, Y. Prakash, F. E. Lund, A. Galione, and E. N. Chini. 2007. 'NAADP as a second messenger: neither CD38

nor base-exchange reaction are necessary for in vivo generation of NAADP in myometrial cells', *Am J Physiol Cell Physiol*, 292: C227-39.

Spiess, M. 1995. 'Heads or tails--what determines the orientation of proteins in the membrane', *FEBS Lett*, 369: 76-9.

States, D. J., T. F. Walseth, and H. C. Lee. 1992. 'Similarities in amino acid sequences of Aplysia ADP-ribosyl cyclase and human lymphocyte antigen CD38', *Trends Biochem Sci*, 17: 495.

Stockigt, F., K. Brixius, L. Lickfett, R. Andrie, M. Linhart, G. Nickenig, and J. W. Schrickel. 2012. 'Total beta-adrenoceptor knockout slows conduction and reduces inducible arrhythmias in the mouse heart', *PLoS One*, 7: e49203.

Sugden, P. H., and A. Clerk. 2005. 'Endothelin signalling in the cardiac myocyte and its pathophysiological relevance', *Curr Vasc Pharmacol*, 3: 343-51.

Sun, L., O. A. Adebanjo, A. Koval, H. K. Anandatheerthavarada, J. Iqbal, X. Y. Wu, B. S. Moonga, X. B. Wu, G. Biswas, P. J. Bevis, M. Kumegawa, S. Epstein, C. L. Huang, N. G. Avadhani, E. Abe, and M. Zaidi. 2002. 'A novel mechanism for coupling cellular intermediary metabolism to cytosolic Ca2+ signaling via CD38/ADP-ribosyl cyclase, a putative intracellular NAD+ sensor', *FASEB J*, 16: 302-14.

Tada, M., M. Yamada, M. Kadoma, M. Inui, and F. Ohmori. 1982. 'Calcium transport by cardiac sarcoplasmic reticulum and phosphorylation of phospholamban', *Mol Cell Biochem*, 46: 73-95.

Takahashi, J., Y. Kagaya, I. Kato, J. Ohta, S. Isoyama, M. Miura, Y. Sugai, M. Hirose, Y. Wakayama, M. Ninomiya, J. Watanabe, S. Takasawa, H. Okamoto, and K. Shirato. 2003. 'Deficit of CD38/cyclic ADP-ribose is differentially compensated in hearts by gender', *Biochem Biophys Res Commun*, 312: 434-40.

Tang, W. X., Y. F. Chen, A. P. Zou, W. B. Campbell, and P. L. Li. 2002. 'Role of FKBP12.6 in cADPR-induced activation of reconstituted ryanodine receptors from arterial smooth muscle', *Am J Physiol Heart Circ Physiol*, 282: H1304-10.

Tifft, C. J., R. L. Proia, and R. D. Camerini-Otero. 1992. 'The folding and cell surface expression of CD4 requires glycosylation', *J Biol Chem*, 267: 3268-73.

Togashi, K., Y. Hara, T. Tominaga, T. Higashi, Y. Konishi, Y. Mori, and M. Tominaga. 2006. 'TRPM2 activation by cyclic ADP-ribose at body temperature is involved in insulin secretion', *EMBO J*, 25: 1804-15.

Tohgo, A., S. Takasawa, N. Noguchi, T. Koguma, K. Nata, T. Sugimoto, Y. Furuya, H. Yonekura, and H. Okamoto. 1994. 'Essential cysteine residues for cyclic ADP-ribose synthesis and hydrolysis by CD38', *J Biol Chem*, 269: 28555-7.

Touchberry, C. D., I. K. Bales, J. K. Stone, T. J. Rohrberg, N. K. Parelkar, T. Nguyen, O. Fuentes, X. Liu, C. K. Qu, J. J. Andresen, H. H. Valdivia, M. Brotto, and M. J. Wacker. 2010. 'Phosphatidylinositol 3,5-bisphosphate (PI(3,5)P2) potentiates cardiac contractility via activation of the ryanodine receptor', *J Biol Chem*, 285: 40312-21.

Tugba Durlu-Kandilci, N., M. Ruas, K. T. Chuang, A. Brading, J. Parrington, and A. Galione. 2010. 'TPC2 proteins mediate nicotinic acid adenine dinucleotide phosphate (NAADP)- and agonist-evoked contractions of smooth muscle', *J Biol Chem*, 285: 24925-32.

Umar, S., F. Malavasi, and K. Mehta. 1996. 'Post-translational modification of CD38 protein into a high molecular weight form alters its catalytic properties', *J Biol Chem*, 271: 15922-7.

Vaisitti, T., V. Audrito, S. Serra, R. Buonincontri, G. Sociali, E. Mannino, A. Pagnani, A. Zucchetto, E. Tissino, C. Vitale, M. Coscia, C. Usai, C. Pepper, V. Gattei, S. Bruzzone, and S. Deaglio. 2015. 'The enzymatic activities of CD38 enhance CLL growth and trafficking: implications for therapeutic targeting', *Leukemia*, 29: 356-68.

Vasudevan, S. R., A. Galione, and G. C. Churchill. 2008. 'Sperm express a Ca2+-regulated NAADP synthase', *Biochem J*, 411: 63-70.

Venturi, E., S. Pitt, E. Galfre, and R. Sitsapesan. 2012. 'From eggs to hearts: what is the link between cyclic ADP-ribose and ryanodine receptors?', *Cardiovasc Ther*, 30: 109-16.

von Heijne, G. 1989. 'Control of topology and mode of assembly of a polytopic membrane protein by positively charged residues', *Nature*, 341: 456-8.

———. 2006. 'Membrane-protein topology', *Nat Rev Mol Cell Biol*, 7: 909-18.

Wagner, L. E., 2nd, L. A. Groom, R. T. Dirksen, and D. I. Yule. 2014. 'Characterization of ryanodine receptor type 1 single channel activity using "on-nucleus" patch clamp', *Cell Calcium*, 56: 96-107.

Walseth, T. F., Y. Lin-Moshier, P. Jain, M. Ruas, J. Parrington, A. Galione, J. S. Marchant, and J. T. Slama. 2012. 'Photoaffinity labeling of high affinity nicotinic acid adenine dinucleotide phosphate (NAADP)-binding proteins in sea urchin egg', *J Biol Chem*, 287: 2308-15.

Wang, K., D. Terrar, D. J. Gavaghan, U. Min R. Mu, P. Kohl, and C. Bollensdorff. 2014. 'Living cardiac tissue slices: an organotypic pseudo two-dimensional model for cardiac biophysics research', *Prog Biophys Mol Biol*, 115: 314-27.

Wang, L., N. M. De Jesus, and C. M. Ripplinger. 2015. 'Optical Mapping of Intra-Sarcoplasmic Reticulum Ca2+ and Transmembrane Potential in the Langendorff-perfused Rabbit Heart', *J Vis Exp*.

Wang, X., X. Zhang, X. P. Dong, M. Samie, X. Li, X. Cheng, A. Goschka, D. Shen, Y. Zhou, J. Harlow, M. X. Zhu, D. E. Clapham, D. Ren, and H. Xu. 2012. 'TPC proteins are phosphoinositide- activated sodium-selective ion channels in endosomes and lysosomes', *Cell*, 151: 372-83.

Wang, Y. G., E. N. Dedkova, X. Ji, L. A. Blatter, and S. L. Lipsius. 2005. 'Phenylephrine acts via IP3-dependent intracellular NO release to stimulate L-type Ca2+ current in cat atrial myocytes', *J Physiol*, 567: 143-57.

Wang, Y., W. K. Lin, W. Crawford, H. Ni, E. L. Bolton, H. Khan, J. Shanks, G. Bub, X. Wang, D. J. Paterson, H. Zhang, A. Galione, S. N. Ebert, D. A. Terrar, and M. Lei. 2017. 'Optogenetic Control of Heart Rhythm by Selective Stimulation of Cardiomyocytes Derived from Pnmt(+) Cells in Murine Heart', *Sci Rep*, 7: 40687.

Warszta, D., M. Nebel, R. Fliegert, and A. H. Guse. 2014. 'NAD derived second messengers: Role in spontaneous diastolic Ca(2+) transients in murine cardiac myocytes', *DNA Repair (Amst)*, 23: 69-78.

Wei, W. J., H. Y. Sun, K. Y. Ting, L. H. Zhang, H. C. Lee, G. R. Li, and J. Yue. 2012. 'Inhibition of cardiomyocytes differentiation of mouse embryonic stem cells by CD38/cADPR/Ca2+ signaling pathway', *J Biol Chem*, 287: 35599-611.

Whalley, D. W., D. J. Wendt, and A. O. Grant. 1995. 'Basic concepts in cellular cardiac electrophysiology: Part I: Ion channels, membrane currents, and the action potential', *Pacing Clin Electrophysiol*, 18: 1556-74.

Wojcikiewicz, R. J. 1995. 'Type I, II, and III inositol 1,4,5-trisphosphate receptors are unequally susceptible to down-regulation and are expressed in markedly different proportions in different cell types', *J Biol Chem*, 270: 11678-83.

Wolf, I. M., B. P. Diercks, E. Gattkowski, F. Czarniak, J. Kempski, R. Werner, D. Schetelig, H. W. Mittrucker, V. Schumacher, M. von Osten, D. Lodygin, A. Flugel, R. Fliegert, and A. H. Guse. 2015. 'Frontrunners of T cell activation: Initial, localized Ca2+ signals mediated by NAADP and the type 1 ryanodine receptor', *Sci Signal*, 8: ra102.

Xie, G. H., S. Y. Rah, S. J. Kim, T. S. Nam, K. C. Ha, S. W. Chae, M. J. Im, and U. H. Kim. 2005. 'ADP-ribosyl cyclase couples to cyclic AMP signaling in the cardiomyocytes', *Biochem Biophys Res Commun*, 330: 1290-8.

Xie, G. H., S. Y. Rah, K. S. Yi, M. K. Han, S. W. Chae, M. J. Im, and U. H. Kim. 2003. 'Increase of intracellular Ca(2+) during ischemia/reperfusion injury of heart is mediated by cyclic ADP-ribose', *Biochem Biophys Res Commun*, 307: 713-8.

Yalcintepe, L., I. Albeniz, S. Adin-Cinar, D. Tiryaki, E. Bermek, R. M. Graeff, and H. C. Lee. 2005. 'Nuclear CD38 in retinoic acid-induced HL-60 cells', *Exp Cell Res*, 303: 14-21.

Yamada, M., M. Mizuguchi, N. Otsuka, K. Ikeda, and H. Takahashi. 1997. 'Ultrastructural localization of CD38 immunoreactivity in rat brain', *Brain Res*, 756: 52-60.

Yamaguchi, S., A. Jha, Q. Li, A. A. Soyombo, G. D. Dickinson, D. Churamani, E. Brailoiu, S. Patel, and S. Muallem. 2011. 'Transient receptor potential mucolipin 1 (TRPML1) and two-pore channels are functionally independent organellar ion channels', *J Biol Chem*, 286: 22934-42.

Yamamoto, M., H. Honjo, R. Niwa, and I. Kodama. 1998. 'Low-frequency extracellular potentials recorded from the sinoatrial node', *Cardiovasc Res*, 39: 360-72.

Yamasaki, M., R. Masgrau, A. J. Morgan, G. C. Churchill, S. Patel, S. J. Ashcroft, and A. Galione. 2004. 'Organelle selection determines agonist-specific Ca2+ signals in pancreatic acinar and beta cells', *J Biol Chem*, 279: 7234-40.

Young, L. J. 2007. 'Regulating the social brain: a new role for CD38', *Neuron*, 54: 353-6.

Yu, L., L. Zhou, G. Cao, S. S. Po, B. Huang, X. Zhou, M. Wang, S. Yuan, Z. Wang, S. Wang, and H. Jiang. 2017. 'Optogenetic Modulation of Cardiac Sympathetic Nerve Activity to Prevent Ventricular Arrhythmias', *J Am Coll Cardiol*, 70: 2778-90.

Yuan, W., and D. M. Bers. 1994. 'Ca-dependent facilitation of cardiac Ca current is due to Ca-calmodulin-dependent protein kinase', *Am J Physiol*, 267: H982-93.

Zaglia, T., N. Pianca, G. Borile, F. Da Broi, C. Richter, M. Campione, S. E. Lehnart, S. Luther, D. Corrado, L. Miquerol, and M. Mongillo. 2015. 'Optogenetic determination of the myocardial requirements for extrasystoles by cell type-specific targeting of ChannelRhodopsin-2', *Proc Natl Acad Sci U S A*, 112: E4495-504.

Zhang, F., S. Jin, F. Yi, and P. L. Li. 2009. 'TRP-ML1 functions as a lysosomal NAADP-sensitive Ca2+ release channel in coronary arterial myocytes', *J Cell Mol Med*, 13: 3174-85.

Zhang, F., M. Xu, W. Q. Han, and P. L. Li. 2011. 'Reconstitution of lysosomal NAADP-TRP-ML1 signaling pathway and its function in TRP-ML1(-/-) cells', *Am J Physiol Cell Physiol*, 301: C421-30.

Zhang, Z., Y. Xu, H. Song, J. Rodriguez, D. Tuteja, Y. Namkung, H. S. Shin, and N. Chiamvimonvat. 2002. 'Functional Roles of Ca(v)1.3 (alpha(1D)) calcium channel in sinoatrial nodes: insight gained using gene-targeted null mutant mice', *Circ Res*, 90: 981-7.

Zhao, Y. J., C. M. Lam, and H. C. Lee. 2012. 'The membrane-bound enzyme CD38 exists in two opposing orientations', *Sci Signal*, 5: ra67.

Zhao, Y. J., H. M. Zhang, C. M. Lam, Q. Hao, and H. C. Lee. 2011. 'Cytosolic CD38 protein forms intact disulfides and is active in elevating intracellular cyclic ADP-ribose', *J Biol Chem*, 286: 22170-7.

Zhao, Y. J., W. J. Zhu, X. W. Wang, L. H. Zhang, and H. C. Lee. 2015. 'Determinants of the membrane orientation of a calcium signaling enzyme CD38', *Biochim Biophys Acta*, 1853: 2095-103.

Zhu, M. X., J. Ma, J. Parrington, P. J. Calcraft, A. Galione, and A. M. Evans. 2010. 'Calcium signaling via two-pore channels: local or global, that is the question', *Am J Physiol Cell Physiol*, 298: C430-41.

Zhu, W., A. Y. Woo, Y. Zhang, C. M. Cao, and R. P. Xiao. 2011. 'beta-adrenergic receptor subtype signaling in the heart: from bench to the bedside', *Curr Top Membr*, 67: 191-204.

Zima, A. V., D. J. Bare, G. A. Mignery, and L. A. Blatter. 2007. 'IP3-dependent nuclear Ca2+ signalling in the mammalian heart', *J Physiol*, 584: 601-11.

Zima, A. V., and L. A. Blatter. 2004. 'Inositol-1,4,5-trisphosphate-dependent Ca(2+) signalling in cat atrial excitation-contraction coupling and arrhythmias', *J Physiol*, 555: 607-15.

Zocchi, E., L. Franco, L. Guida, L. Calder, and A. De Flora. 1995. 'Self-aggregation of purified and membrane-bound erythrocyte CD38 induces extensive decrease of its ADP-ribosyl cyclase activity', *FEBS Lett*, 359: 35-40.

Zong, X., M. Schieder, H. Cuny, S. Fenske, C. Gruner, K. Rotzer, O. Griesbeck, H. Harz, M. Biel, and C. Wahl-Schott. 2009. 'The two-pore channel TPCN2 mediates NAADP-dependent Ca(2+)-release from lysosomal stores', *Pflugers Arch*, 458: 891-9.

Zuhlke, R. D., G. S. Pitt, K. Deisseroth, R. W. Tsien, and H. Reuter. 1999. 'Calmodulin supports both inactivation and facilitation of L-type calcium channels', *Nature*, 399: 159-62.